TECHNISCHE UNIVERSITÄT KAISERSLAUTERN

Alexandros Sklavos

Service Area Based OFDM Air Interface for Beyond 3G Mobile Radio Systems

HS

Alexandros Sklavos
Ifigeneias Str. 48
17672 Kallithea
Griechenland
Geburtsort: Griechenland

Service Area Based OFDM Air Interface for Beyond 3G Mobile Radio Systems

deutscher Titel:

OFDM-Luftschnittstelle für Mobilfunksysteme jenseits der dritten Generation auf der Basis von Service Gebieten

Vom Fachbereich Elektrotechnik und Informationstechnik

der Technischen Universität Kaiserslautern

zur Verleihung des akademischen Grades

Doktor der Ingenieurwissenschaften (Dr.–Ing.)

genehmigte Dissertation

von

Dipl.–Ing. Alexandros Sklavos,

D 386

Vorwort

Contents

1 Introduction

1.1 Demands on future mobile radio systems

The target of a mobile radio system is the provision of communication services to multiple mobile terminals (MTs). Due to the demand for mobility of the MTs, each MT in a mobile radio system communicates with at least one fixed access point (AP) by means of transmission of electromagnetic waves with frequencies in the radio frequency band [Gib99, Ste92, DB96, Wes02]. Each AP communicates either directly or indirectly with other fixed entities of the mobile radio system such as mobile switching centers [GSM98], which perform tasks related to the proper forwarding of information to and from the APs. Such fixed entities are collectively described by the term core network of the mobile radio system. The wireless interface between the MTs and the fixed APs is called the air interface of the mobile radio system. Concerning the air interface one can discern between uplink (UL) and downlink (DL) transmission [Gib99, Ste92, DB96], depending on whether information is sent from the MTs to the APs or vice versa. Performance measures of high importance to mobile radio system operators such as the quality of service [Ste92, HT02] or the number of MTs which can be simultaneously supported in a given bandwidth B and area A [Lee89, Vit91, Ste92] are essentially determined by the air interface. Hence, the design of the air interface of future mobile radio systems is of paramount importance and forms the main focus of the present thesis.

As the following considerations of this Section are valid for the UL as well as for the DL, the more general terms transmitters and receivers will be used in this Section instead of the terms MTs and APs in order to describe the air interface independently of the direction of information flow in the air interface, i.e., independently of whether the UL or the DL is considered. Setting out from a group of antennas which are jointly available, a transmitter in a mobile radio system is an entity generating transmit signals for a group of antennas and a receiver corresponds to an entity obtaining the signals received by a group of antennas. Hence, the MTs are the transmitters in the UL and the receivers in the DL. On the other hand, in the general case no direct relation between APs and receivers in the UL and between APs and transmitters in the DL can be postulated. However, in the special case that only the antennas of each AP are jointly available the APs correspond to the receivers in the UL and to the transmitters in the DL.

If a linear transmission scheme is employed at each transmitter in the mobile radio system, then the signal at the location of each receiver consists of a superposition of a number of information bearing partial signals, each corresponding to a different MT, along with signals stemming from sources other than the transmitters of the considered mobile radio system, such as other mobile radio systems, or thermal and cosmic noise sources. Considering the detection of the information of a particular MT, the corresponding partial received signal is termed useful received

signal. The remaining partial received signals corresponding to other MTs disturb the useful received signal, and therefore act as multiple access interference [Gib99, Ste92, DB96, Wes02]. However, if nonlinear transmission schemes are employed, the signal at a specific receiver in general cannot be viewed as a superposition of partial received signals, each corresponding to an MT. For this reason, the definition of multiple access interference in the case of nonlinear transmission schemes is an open problem. Moreover, although the term interference is often used in a more general context to collectively describe all received signals not related to the detection of a particular data symbol, it is used in the following to denote only multiple access interference, which forms the main focus of the present thesis.

In state-of-the-art mobile radio systems, which are characterized by a high density of transmitters and receivers and high transmit powers, interference dominates the nonuseful part of the received signal in such a way that the effect of other noise signal sources, such as thermal or cosmic noise, can be safely neglected in the design of a mobile radio system. Therefore, mobile radio systems are interference limited [Cal88, Lee82]. The number K of MTs which can be supported with a given quality of service [Ste92, HT02], normalized to the system bandwidth B and the area A which is covered by the mobile radio system, is the spectrum capacity

$$\eta_{\mathrm{c}} = \frac{K}{B\,A} \tag{1.1}$$

of the mobile radio system [Lee89, Vit91, Ste92]. The spectrum capacity η_{c} of (1.1) is a measure for the efficiency of the use of the available frequency bandwidth B of a mobile radio system. An efficient use of the available frequency bandwidth B is of great importance to mobile radio system operators as it has been demonstrated above all by the outcome of auctions for the 3G mobile radio system spectrum, e.g., in Germany, where nearly 50 billion Euros were spent for the corresponding licenses by the mobile radio system operators [ntz00a, ntz00b]. In an interference limited system, the interference present at the antennas of the receivers limits the achievable spectrum capacity η_{c} of (1.1) [Sha48, CT91, Roh95]. Therefore, considering future mobile radio systems, an air interface should be developed, in which the adverse effects of the interfering signals are kept at a low level.

In what follows the radio channel of the air interface of mobile radio systems is dealt with. Mobile radio system operators use multiple APs to support a large number of MTs. However, for the purpose of modelling the air interface of a mobile radio system, instead of the total air interface with the usually very large number of transmitters and receivers, an excerpt of the mobile radio system is considered containing transmitters and receivers of a cohesive geographical area. Moreover, the said excerpt is chosen to be self-contained, i.e., no wireless communication takes place across its borders. Therefore, all signals stemming from transmitters outside the considered excerpt act as interference and are modelled as additive noise to the received signals in the considered excerpt. Hence, due to the fact that the modelling of the interference, e.g., as

Gaussian noise, is merely an approximation, the larger the excerpt of the mobile radio system is chosen, the more precise the resulting air interface model is.

In the considered excerpt of the mobile radio system, if special cases of obstructed radio channels, e.g., due to physical obstacles are not considered, signals radiated from each of the transmit antennas impinge at all the receive antennas. Hence, the radio channel of the considered excerpt of a mobile radio system in the UL as well in the DL is modelled as a multiple-input-multiple-output (MIMO) channel [Fos96, FG98, Tel99], in which the inputs are the multiple transmit antennas in which the transmit signals are fed and the outputs are the multiple receive antennas from which the received signals are obtained. Moreover, systems in which the channel is modelled as a MIMO channel, such as the chosen excerpt of a mobile radio system, are known as MIMO systems [Ala98, DCGV02, CS00, Ahl73, CT91, FCG$^+$03, GFVW98, GFVW99, Hug00, JVG01, JVG02, TSC98, VJG02, YC01, YRBC01]. If neighboring MIMO systems use the same frequency bands, then signals corresponding to MTs of neighboring MIMO systems are received by the receivers of a certain MIMO system and such signals act as interference to the useful received signals of the considered MIMO system. To mitigate the aforementioned performance degrading interference, the bandwidth B available to the mobile radio system operator is partitioned into disjoint frequency subbands and different subbands are allocated to neighboring MIMO systems. This way, transmissions in a MIMO system do not interfere with transmissions in directly neighboring MIMO systems. However, if the concept of bandwidth partitioning would be strictly applied as described, given the large number of MIMO systems in a mobile radio system, a very large system bandwidth B would be required to totally avoid interferences in a mobile radio system. Therefore, the subband allocated to a reference MIMO system is reused after a certain distance large enough so that the attenuation of the electromagnetic waves received in the reference MIMO system stemming from MIMO systems using the same frequency subband is sufficiently large and the induced interference by the reuse of the same frequency subband is acceptable [McD79]. The number of disjoint subbands in which the system bandwidth B is partitioned is called reuse factor of the mobile radio system [McD79].

In terms of achievable channel capacity [Sha48], the best case for a MIMO system is that all inputs and outputs of the MIMO channel are jointly available for joint processing and that perfect knowledge of the MIMO channel is present at both transmit and receive side [Tel99]. But in the case of the MIMO channel of the considered excerpt of a mobile radio system in general not all the inputs and outputs of the MIMO channel are jointly available, due to the spatial separation of the transmitters and receivers. For example, it is not possible to perform signal processing tasks jointly for different MTs, at least with a reasonable overhead, due to the fact that different MTs are spatially separated. Fig. 1.1 depicts the MIMO channel of a mobile radio system with N transmit and M receive antennas in total. Transmit and receive antennas of the MIMO channel in Fig. 1.1 form N_{B} and M_{B} groups corresponding to the N_{B} and M_{B}

transmitters and receivers, respectively, to indicate that only the antennas of each of the groups, i.e., of each of the transmitters or receivers, are jointly available.
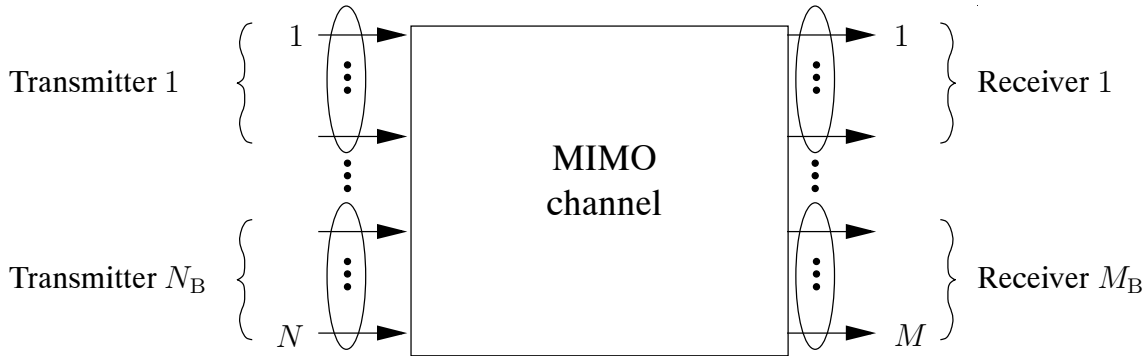
Figure 1.1. MIMO channel of an excerpt of a mobile radio system with N_B transmitters and M_B receivers

Depending on the value of N_B and M_B, different special cases of MIMO channel structures can be distinguished, as Table 1.1 shows.

Table 1.1. Classification of MIMO channel structures depending on the number N_B of transmit antennas and the number M_B of receive antennas

case number	N_B	M_B	MIMO structure
1	1	1	point-to-point channel
2	1	>1	broadcast channel
3	>1	1	multiple access channel
4	>1	>1	multipoint-to-multipoint channel

The first case corresponds to a point-to-point MIMO channel which means that all N inputs and M outputs of the MIMO channel are jointly available. Pioneering work on the point-to-point MIMO channel in [Tel99, Fos96, FG98] shows that in the presence of rich scattering and if perfect channel knowledge is available at least at the receiver, impressive gains in terms of channel capacity [Sha48] and spectrum efficiency [BBS97, Bla98] are achievable as compared to single antenna systems using signals of the same transmit energy. These high gains, almost for free, only at the cost of some increased hardware complexity, initiated a worldwide research on MIMO systems [Ala98, DCGV02, CS00, Ahl73, CT91, FCG$^+$03, GFVW98, GFVW99, Hug00, JVG01, JVG02, TSC98, VJG02, YC01, YRBC01]. The point-to-point MIMO channel corresponds to the case where the considered excerpt of the mobile radio system consists of a single transmitter communicating with a single receiver.

In the MIMO channel structure of the second case of Table 1.1 all inputs of the MIMO chan-

nel are jointly available whereas not all outputs are jointly available. This second case corresponds to the case where in the considered excerpt of the mobile radio system a single transmitter communicates with multiple receivers. In literature, such MIMO channels are known as broadcast channels [CS00, CT91]. Assuming that the transmitter disposes of channel knowledge a joint transmit signal processing could aim at reducing interference at the receivers [MBW$^+$00, WMS$^+$02].

The third case of Table 1.1 represents a MIMO channel structure, dual to the second case, where all outputs are jointly available whereas not all inputs of the MIMO channel are jointly available. Such MIMO channels are known as multiple access channels. Multiple access channels correspond to the case where multiple transmitters communicate with a single receiver in the considered excerpt of the mobile radio system. A joint signal processing at the receiver could aim at reducing interferences among the multiple transmitters [Kle96, WMS$^+$02].

In the most general last case of Table 1.1 of multipoint-to-multipoint MIMO channels, neither all the inputs nor all the outputs of the MIMO channel are jointly available. This corresponds to the case where multiple transmitters and multiple receivers exist in the considered excerpt of the mobile radio system. Due to the said dislocation between the transmitters and between the receivers interference suppression in multipoint-to-multipoint MIMO channels is a difficult task.

According to the author, the research towards future mobile radio systems should aim at an efficient utilization of the available frequency bandwidth B, i.e., high spectrum capacities η_c should be strived for. As high system capacities can be achieved by mitigating the adverse effects of interference, the demand for the development of air interface architectures targeted at the suppression of the interference between the useful signals of the active MTs follows. Given the MIMO nature of the radio channel of an excerpt of a mobile radio system, shown in Fig. 1.1, it is shown that such a goal can be approached by employing an air interface in which all inputs to the MIMO channel in the DL and all outputs of the MIMO channel in the UL are jointly available. Hence, the cases of multiple access channels and broadcast channels shown in Table 1.1 are of special interest as far as the design of the air interface of future mobile radio systems is concerned. The present thesis deals with such an air interface proposal for future mobile radio systems.

1.2 Service area based architectures versus cellular architectures

As demonstrated in the previous Section, there exists the demand for future mobile radio system air interfaces to yield high spectrum capacities η_c. The objective of this Section is to introduce a

novel air interface architecture by the employment of which the adverse effects of interference between the useful signals of the simultaneously active MTs in a MIMO system can be mitigated and therefore high spectral capacities η_c can be achieved. In order to better illuminate the basic characteristics of the novel air interface architecture, a brief overview of the characteristics of the cellular architecture, employed in state-of-the-art mobile radio systems, is performed.

The cellular architecture [McD79] is employed in mobile radio systems of the first-, second- and third generation. The fundamental concept of cellular systems is the cell, which is the geographical area of responsibility of an AP, i.e., the area in which the MTs associated with the particular AP reside [McD79, Gib99, DB96, Wes02]. In a cellular mobile radio system, the association of MTs to APs is performed according to criteria such as the quality of the propagation conditions, and is based on the premise that from the viewpoint of a certain MT there exists typically one AP to which the propagation conditions are most favorable. Due to this association of MTs to APs a partitioning of the whole geographical area of the mobile radio system into cells follows naturally.

In cellular mobile radio systems it can be discerned between two basic types of interference, depending on whether the signals of MTs of the same cell or of MTs of different cells interfere. In the case of interference between the signals of MTs of the same cell, the interference is called intracell interference. Intracell interference can be combated by techniques such as joint detection [Kle96, KB92] or joint transmission [MBW$^+$00, TWMB01]. On the other hand, if the useful signals of MTs of neighboring cells interfere, the interference is called intercell interference. The effects of intercell interference are mitigated in 2G mobile radio systems by means of partitioning of the bandwidth B, as explained in Section 1.1. However, due to the said partitioning of the bandwidth B an inefficient use of the system bandwidth B results.

Fig. 1.2 shows an excerpt of a mobile radio system based on the cellular concept consisting of twelve cells grouped in three clusters of four cells. As can be seen from Fig. 1.2, each cell has an AP. The APs in turn are connected to the core network of the mobile radio system which is the data source and data sink for the information sent to and received from the MTs, respectively.

Following the argumentation of Section 1.1, higher spectral capacities η_c of (1.1) can be achieved if a larger number of inputs of the MIMO channel in the DL or of outputs of the MIMO channel at the UL at the fixed side of the wireless communication channel are jointly available than in cellular mobile radio systems. The transition from the cellular architecture to the novel air interface architecture can be visualized as the result of merging of a group of neighboring cells. The merging of the neighboring cells consists in establishing a communication link between each of the APs and a central unit (CU), which is in turn connected to the core network of the mobile radio system. Each such group of APs defines a service area (SA) and the resulting
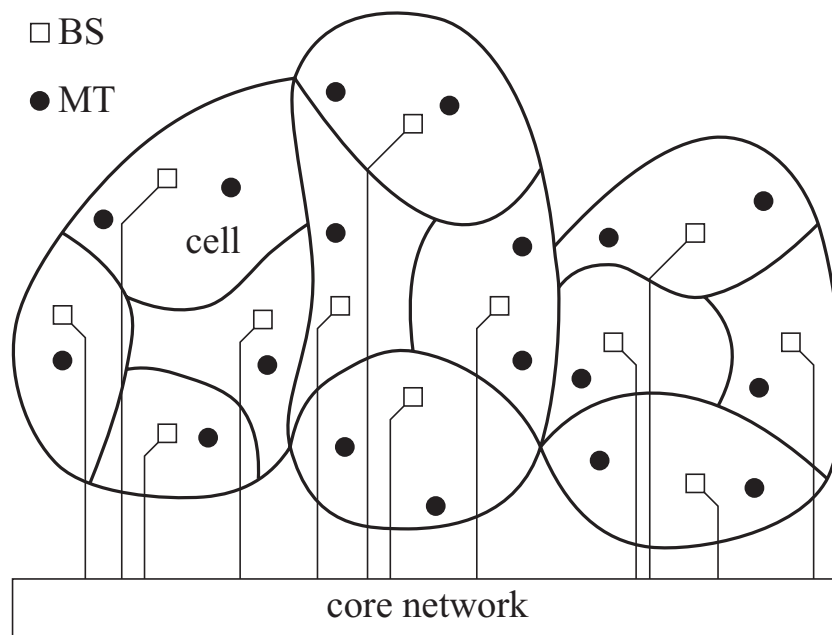
Figure 1.2. Excerpt of a cellular mobile radio system, consisting of 12 cells
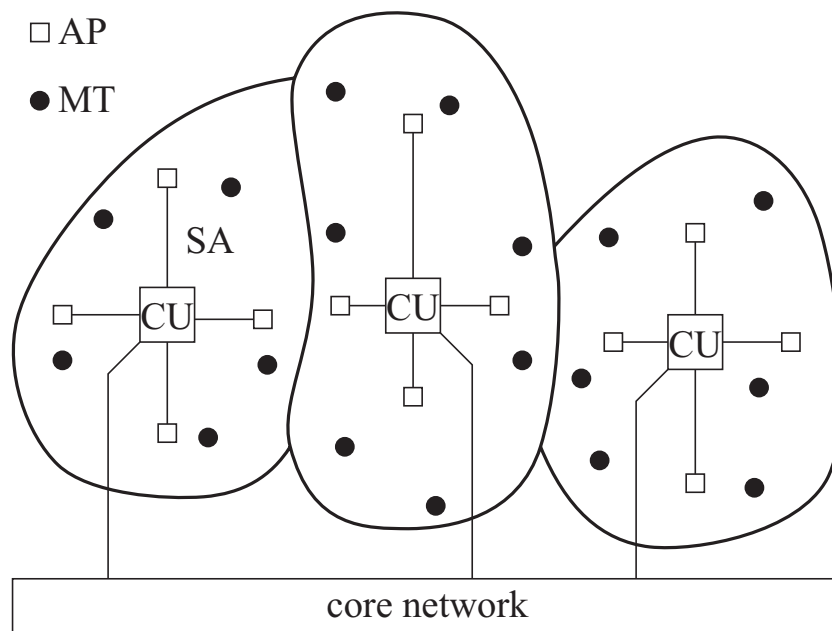
Figure 1.3. Excerpt of a mobile radio system employing the SA-based architecture, consisting of 3 SAs

mobile radio system air interface architecture is called service area based (SA-based) architecture [WMS$^+$02, SWC$^+$02, SWBC02, MWS$^+$02]. The crux of the novel SA-based air interface architecture consists in the fact that as a result of the merge of a number of cells in a single SA, the intercell interference between the useful signals corresponding to the MTs active in the said cells becomes intra-SA interference in the case of SA-based systems and can be easily combated by interference suppression techniques [Kle96, MBW$^+$00, WMS$^+$02]. Fig. 1.3 illustrates an excerpt from a mobile radio system employing the SA-based air interface architecture with three SAs, each consisting of four APs. Comparing Fig. 1.2 to Fig. 1.3, in the exemplary excerpt of the considered mobile radio system, each SA can be thought of as a union of four cells in terms of cellular architectures.

In the UL transmission in a SA, the signals transmitted from each MT are received by all APs of the SA and fed to the CU, which performs the signal processing tasks. If the SA is chosen to be the MIMO system of Fig. 1.1, all the outputs of the SA MIMO wireless channel are jointly available to the CU and therefore the MIMO channel in the UL of a SA-based air interface architecture is modelled as a multiple access channel [Ahl73], in which the MTs are the multiple transmitters and the CU is the receiver. If not all the outputs of the MIMO channel were jointly available, i.e., if the signals received by each of the APs were considered separately, as it is the case in the APs in cellular architectures, the mitigation of the interference from the partial received signals stemming from the other MTs of the SA caused to the useful received signal of a specific MT would be possible only in a limited extent at a certain AP [Ost01].

However, as in the UL of SA-based architectures all outputs of the MIMO channel are jointly available and given that the CU disposes of knowledge concerning the transmission properties of the MIMO channel of the SA, which is the result of a channel estimation procedure in the UL [SMW$^+$01, MWS$^+$02], the structure of each of the partial received signals at the APs is known at the CU. In the exemplary case of linear JD, the CU has knowledge of the vector subspace to which each of the partial received signals belongs and can therefore minimize the interference caused to the partial received signal of a desired MT by the partial received signals corresponding to the other MTs of the SA. This means that the CU can combine the received signals from the APs in an optimum way in terms of suppression of interference between the various simultaneously active MTs, i.e., the CU in the UL transmission in a SA-based architecture performs joint detection (JD) [WMS$^+$02, Kle96, KB92, SWC$^+$02, SWBC02].

In the DL transmission, information is sent from the core network to the MTs. For this purpose the CU generates AP-specific signals and each MT in the DL transmission receives the signals from all APs. Therefore, the channel valid for the DL in SA-based air interface architectures is modelled as a MIMO broadcast channel [CS00], in which the CU is the transmitter and the MTs are the multiple receivers. As it is the case with the UL transmission, if the transmit signals were

generated independently for each of the MTs, as is the case in cellular mobile radio systems, then each MT would also receive signals intended for the other MTs of the SA, i.e., signals which cannot be constructively utilized and act as interference to each of the MTs.

In SA-based architectures, the CU has knowledge concerning the MIMO broadcast channel valid for the DL transmission in the SA. Such a fact can hold, for example, if time division duplexing (TDD) [Pro95] is used and the time elapsing between UL and DL transmission is sufficiently smaller than the coherence time of the channel. In this case, channel knowledge resulting from a channel estimation process in the UL can be assumed to be valid also for the DL transmission. This reciprocity between UL and DL channels is known as channel reciprocity and given the parametrization of state-of-the-art mobile radio systems [ENS97, MBW$^+$00], the said channel reciprocity is a major advantage of TDD systems as compared to frequency division duplexing (FDD) systems in which the coherence bandwidth of the mobile radio channel [Par92] is typically smaller than the bandwidth of the frequency bands of UL and DL transmission.

Additionally to the channel knowledge, the receiver algorithms employed in the MTs active in a SA are known to the CU and this knowledge is exploited for the generation of the AP-specific transmit signals in the DL transmission. Transmission schemes which utilize knowledge concerning the structure of the receiver and of the mobile radio channel in order to generate the transmit signals are known as receiver oriented schemes, in contrast to transmitter oriented schemes, which adjust the receiver according to the structure of the transmitter. The advantage of receiver oriented schemes if applied on the DL is that no resources have to be spent for channel estimation in the DL and that a variety of MT structures, even very simple MTs, can be supported [MBW$^+$00, TWMB01, WMS$^+$02].

As all inputs to the MIMO broadcast channel are jointly available and the characteristics of the mobile radio channel valid for the DL transmission are known, the CU has a priori knowledge of the structure of the received signal at each MT for given transmit signals. Moreover, by exploiting the knowledge concerning the structure of the MTs, the CU can design transmit signals for the APs in such a way that the estimates of the sent data symbols at each of the MTs satisfy given criteria, e.g., are free from intra-SA interference. In a SA-based architecture the CU can design transmit signals jointly for all MTs of the SA in order to mitigate the effects of intra-SA interference, i.e., the CU in the DL transmission in a SA performs joint transmission (JT) [WMS$^+$02, MBW$^+$00, TWMB01, TWMB01].

It follows that the crux of the SA-based architectures consists in the availability of all the antennas of the APs to the CU, i.e., in the availability of all outputs to the multiple access channel in the UL and of all inputs of the broadcast channel in the DL. The CU can then employ JD and

JT in the UL and DL transmission, respectively, to minimize the interference between the MTs. Hence, in SA-based systems by means of JD and JT a significant portion of the intercell interference, which would be present in a cellular system, is combated. In the present thesis a variety of algorithms for JD and JT is investigated, such as linear, nonlinear and iterative algorithms.

1.3   OFDM transmission technique

At the transmitter side in a mobile radio system multiple data carrying signals are merged into a single transmit signal which is fed into one of the inputs of the time-continuous MIMO mobile radio channel. At the receiver side the multiple data carrying received signals are extracted from the received signal. The techniques of transmission of multiple data carrying signals using a single signal for each input and output of the MIMO mobile radio channel are called multiplexing techniques, the choice of which is an important aspect in the design of a mobile radio system. Orthogonal frequency division multiplexing (OFDM) is a multiplexing technique gaining considerable interest the last years. Moreover, OFDM is applied in numerous communications systems over the world [ETS97a, ETS97b, RCLF89, RS95, TL97, Cim85, Bin91, CTC91, Jon95, IEE99, CWKS97, vNAM$^+$99, ETS96, ETS99], is contained in a proposal for 3G systems in Europe [ETS98] and is considered to be the leading candidate multiplexing technique for beyond 3G mobile radio systems [RGG01b, Roh00, RGG01a]. In what follows, after describing the principles of some basic multiplexing techniques, an outline of the characteristics of an OFDM system is performed. Blockwise transmission is assumed and each block is called symbol slot.

A first choice regarding multiplexing is time division multiplexing where each symbol slot contains a serial concatenation in time of the data carrying signals. However, due to the multipath propagation in the wireless channel [Par92], in a mobile radio system employing time division multiplexing the part of the received signal corresponding to a particular data carrying signal contains apart from the desired data carrying signal signal portions caused by time delayed echoes of previously sent data carrying signals, an effect known as intersymbol interference. Future mobile radio systems are characterized by a demand for higher data rates, which translates in the case of time division multiplexing systems into shorter time durations of the data carrying signals and therefore a larger impact of intersymbol interference. In time division multiplexing systems a guard interval can be employed to combat intersymbol interference the use of which however introduces an overhead in the data transmission especially undesired in the case of high data rates.

In a system in which frequency division multiplexing is employed, the data carrying signals are sent in parallel, i.e., each of the data carrying signals modulates a sinusoidal signal of a

specific subcarrier frequency, called a subcarrier. Multiplexing techniques characterized by the modulation of multiple subcarriers with the data carrying signals are also known as multicarrier modulation techniques [GW00]. A decisive advantage offered by the frequency division multiplexing techniques and by multicarrier modulation techniques in general is the possibility to accommodate high data rates, as higher data rates require solely a larger number of subcarriers [vNP00] and are not limited by the amount of time dispersiveness of the mobile radio channel. If subcarrier spacings are chosen to be large enough so that spectra of different subcarriers do not overlap significantly, the available frequency bandwidth B is inefficiently used in frequency division multiplexing systems. Hence, as far as multicarrier modulation techniques are concerned, it is imperative to realize a tight subcarrier spacing and at the same time mitigate the effects of the undesired crosstalk between different subcarriers.

Much research has been conducted in the development of a multicarrier modulation system with a tight subcarrier spacing [FL61, Sal67]. OFDM [WE71, KZ89] is a multicarrier modulation technique in which the spectra of different subcarriers overlap without causing intercarrier interference. The interference free overlap of different subcarriers in OFDM systems is achieved by choosing subcarrier frequencies which satisfy an orthogonality relationship, thanks to which the signals corresponding to different subcarriers in an OFDM system are orthogonal to each other. The receiver in an OFDM system considers only a part of the total received signal, during which the aforementioned orthogonality of the signals is preserved. Hence, an OFDM system achieves an efficient use of the available bandwidth B, as a tight spacing of the subcarriers becomes possible. The physical transmission model of OFDM-based MIMO systems is treated in detail in Chapter 3.

The fundamentals of the OFDM technique are first presented in the paper of Weinstein and Erbert in 1971 [WE71], where a DFT structure is presented to realize the OFDM technique. But it was not until the realization of an OFDM system by highly efficient FFT structures in combination with its appealing simplicity when intensive research in OFDM was sparkled regarding, e.g., the application of different multiple access algorithms in OFDM systems [GRC+01, RG97, RGG01b, GRC+02], or the employment of adaptive modulation at each of the OFDM subcarriers [HH, CCB95, FH96, GR00].

OFDM is part of the digital video broadcasting (DVB) and digital audio broadcasting (DAB) systems in Europe [ETS97a, ETS97b, RCLF89, RS95, TL97, Cim85] and is applied in the digital subscriber line (DSL) standards in the USA [Bin91, CTC91, Jon95]. Moreover, many wireless local area network (WLAN) systems are based on OFDM, such as the IEEE 802.11a [IEE99, CWKS97, vNAM+99], the IEEE 802.11g [IEE03] and the HIPERLAN and HIPERLAN/2 systems [ETS96, ETS99].

1.4   State of the art and open questions

Two dominating characteristics of the SA-based air interface architecture are the MIMO nature
of the wireless channel of the SA and the employment of the multiuser algorithms of JD and JT
in order to mitigate the interference between MTs in the SA. Literature on mobile radio systems
abides in investigations concerning MIMO channels and in multiuser algorithms. In particular,
since the initial ground breaking discovery of the potential of MIMO systems, an explosion
of the number of investigations on MIMO systems is observed. On the other hand, multiuser
algorithms are continuously a topic of investigation since the early 80s and therefore a variety of
relevant publications is available. In this Section, the most important, according to the author,
literature citations on MIMO systems and on multiuser algorithms are listed and the citations
relevant to the considerations in the present thesis are highlighted. At the end of this Section,
open questions regarding the air interface of future mobile radio systems are pointed out.

Table 1.2 lists the most important contributions in the field of MIMO systems, dealing with the
achievable capacity of MIMO channels and with specific algorithms targeted at the achievement
of significant portions of the available MIMO capacity. In order to provide a more comprehen-
sive overview, the publications in Table 1.2 are grouped in the two categories:

   I: theoretical investigations on the capacity of MIMO systems, and
   II: near capacity-achieving MIMO algorithms for point-to-point MIMO channels.

Category I contains publications regarding the derivation of the capacity formulas for the MIMO
point-to-point wireless link, and for the MIMO multiple access channel and the MIMO broad-
cast channel for various cases regarding, e.g., whether channel state information is available
at the transmitter or at the receiver or neither at the receiver and the transmitter. Complemen-
tary to the theoretical considerations concerning the capacity of MIMO channels of Category
I, investigations of two practical algorithms for MIMO systems targeted at achieving at least
a significant portion of the theoretically available capacity of the MIMO channel, space time
coding and Bell Labs layered space time (BLAST), are listed in Category II.

[Tel99] and [Fos96] are two seminal works on the capacity of point-to-point MIMO channels
which unveil the large capacity potential of MIMO systems and sparkled a worldwide research
activity. In [Tel99] and [Fos96] a $N \times M$ point-to-point MIMO channel is investigated. If
a rich scattering environment provides independent channels between each pair of transmit
and receive antennas and the channel can be accurately tracked at the receiver, it is shown in
[Tel99] and [Fos96] that the use of a fraction of the total available transmit energy in each of
the equivalent $\min\{N, M\}$ independent single-input-single-output channels is counterbalanced
by the exploitation of the cross-couplings of the MIMO channel, resulting in a MIMO channel

Table 1.2. Contributions on MIMO systems

category	reference	remarks
I	[Tel99],[Fos96],[FG98],[VM01], [JVG01],[JG04],[MH99]	capacity of point-to-point MIMO channels
	[YRBC01],[Ahl73],[CT91], [VTA01],[JVG02]	capacity of multiple access channels
	[CT91],[CS00],[YC01], [VT03],[VJG02],[JVG02]	capacity of broadcast channels
II	[Wit93],[SW94],[TSC98], [Ala98],[TJC99]	space time coding
	[Fos96],[FG98], [GFVW98],[GFVW99]	D-BLAST, V-BLAST

capacity which scales linearly with $\min\{N, M\}$. However, it is not always possible to track the channel accurately, e.g., in the case that rapid motion of the receiver or the transmitter results in a fast variation of the channel. The case of partial channel state information is treated in [VM01, JVG01, JG04, MH99].

MIMO multiple access channels were first dealt with in [Ahl73] and in [CT91]. Considering the distributions of the input signals to the MIMO multiple access channel achieving the capacity regions, in [YRBC01] a modified iterative version of the waterfilling technique [CT91] is introduced and a numerical technique is employed to find the capacity region achieving covariance matrices of the input signals to the MIMO multiple access channel.

Concerning the capacity regions of the MIMO broadcast channel, the work of Costa [Cos83] attracted a lot of attention. Given that the transmitter for a single-input-single-output channel has knowledge of the interference at the receiver, Costa in [Cos83] shows that the capacity of the point-to-point single-input-single-output channel with additive Gaussian interference is the same as if interference was not present. In [CT91] an initial work on the capacity regions of the broadcast channel for the case that the transmitter has a single antenna is carried out and in [CS00] some first results on the broadcast channel with multiple antennas at the transmitter are presented. Yu and Cioffi in [YC01] introduce the Trellis precoding scheme and extend the considerations on the broadcast channel to the multi-antenna receiver case. Despite of serious efforts, the derivation of a closed capacity formula directly for the generalized broadcast channel remained a complex problem, until Jafar and Goldsmith in [JG04] revealed a duality in the rate regions between the broadcast channel and the multiple access channel, by the use of which the optimum covariance matrices can be found for the multiple access channel case using standard optimization techniques and then can be transformed to obtain the optimum covariance matrices for the dual broadcast channel, according to [JG04].

The quality of the estimation of a particular data symbol in terms of signal to noise ratio (SNR), after transmission through a distorting wireless channel can be greatly improved by providing an additional replica of the transmitted signal to the receiver via another channel. A system providing more than one independent channel from the transmitter to the receiver is said to provide diversity. For instance, in a SA-based system spatial diversity is provided by the employment of multiple APs in the SA. The transmit diversity scheme dominating in the literature is space time coding [Wit93, SW94, TSC98, Ala98], according to which each data symbol to be transmitted is encoded in time and in space, i.e., in time and along the various transmit antennas jointly available to the transmitter. Space time coding algorithms primarily focus on point-to-point MIMO channels as all inputs and outputs of the MIMO channel must be jointly available to implement joint space-time coding and decoding, respectively. The first space time coding proposal is considered to be from Winters [SW94], who was inspired by the multipath diversity scheme introduced by Wittneben in [Wit93]. The first decisive contribution however in the field of space time coding is considered to be the introduction of the space time trellis coding scheme by Tarokh et. al [TSC98], in which convolutional codes are employed for the temporal and spatial coding. Considering the application of block codes instead of convolutional codes, an important representative of the block space time coding approaches is the space time block coding algorithm by Alamouti [Ala98], which offers the same diversity benefit as space time trellis coding while having a decisively smaller decoding complexity. The space time block coding scheme by Alamouti has gained worldwide attention and is also adopted in the wideband CDMA and cdma2000 standards [w3G99, TIA00].

Instead of introducing redundancy, as it is the case in space time coding, in the case of the BLAST architecture [Fos96, FG98, GFVW98, GFVW99] independent data streams are transmitted from each transmit antenna. In this way, spatial diversity is sacrificed for an increased spectrum efficiency of the MIMO system. BLAST as well as space time coding, is an architecture for point-to-point MIMO channels as it requires joint availability of the inputs and outputs of the MIMO channel.

The support of multiple MTs in a SA-based system is achieved by the application of JD [Kle96] in the UL and JT [MBW+00] in the DL, as described in Section 1.2. JD and JT are algorithms belonging to the category of multiuser algorithms, the most important literature for which is contained in Table 1.3. As can be seen from Table 1.3, literature on multiuser algorithms can be classified into two main Categories:

I: transmitter oriented multiuser algorithms and
II: receiver oriented multiuser algorithms.

In wireless channels where transmitter oriented multiuser algorithms are applied, the receiver is designed according to the structure of the transmitter. Because literature on transmitter oriented

multiuser algorithms, which are also known as multiuser detection or multiuser estimation algorithms, is quite extensive, Category I contains only the most representative, according to the author, publications on transmitter oriented multiuser algorithms. Dual to transmitter oriented multiuser algorithms, in receiver oriented multiuser algorithms the transmitter adapts itself to the receiver, as for example in JT. In Category II the most important publications related to receiver oriented multiuser algorithms are listed.

Table 1.3. Contributions on multiuser systems

category	reference	remarks
Ia	[Ver98],[Ver86a],[Ver86b]	optimum multiuser detection
Ib	[LV89],[XSR90],[LV90], [KB92],[KB93],[Kle96], [Mil88],[BFKM93],[FKB94],[KKKB94], [KKKB96],[MH94],[Gra81]	linear multiuser estimation - RxZF JD - MMSE
	[VA90],[PH94],[VA91], [Var95],[Lam00b],[Lam00a], [YKI93],[KIHP90],[HL98], [DSR98]	iterative multiuser detection - multistage detection - parallel interference cancellation
	[Hag97],[BG96],[BM96], [HOP96],[BDMP98],[BGT93], [ARAS99],[Moh98],[RSAA98], [Hag96],[AGR98],[VW98]	turbo multiuser detection
II	[Fis02],[WR01],[Bar02], [VJ98],[MBW$^+$00],[KM00], [BOS98],[JKG$^+$02]	receiver oriented algorithms - Joint precoding/Joint Predistortion - TxZF JT - transmit Wiener Filter

Concerning transmitter oriented multiuser algorithms, it can be discerned among two main groups of algorithms:

- multiuser detection algorithms, producing discrete output values belonging to a predefined alphabet, and

- multiuser estimation algorithms, producing continuous output values, which are quantized with respect to the predefined alphabet in a separate step.

It follows that the concatenation of a multiuser estimator with the quantizer can be also seen as a multiuser detector.

The optimum multiuser detector in terms of the probability of erroneous detection is described in [Ver86a, Ver86b, Ver98]. Such an optimum detector yields estimates of the transmitted data

symbols in a nonlinear fashion, according to the maximum a posteriori (MAP) or maximum likelihood (ML) criterion using a priori knowledge concerning the transmitted data symbols. However, given the parametrization of state-of-the-art multiuser mobile radio systems, the optimum multiuser detector is highly complex and hence not realizable. Suboptimum multiuser detectors present a tradeoff between performance in terms of erroneous decision and implementation complexity and yield the estimates of the transmitted data symbols either linearly or in an iterative fashion.

Linear multiuser estimators yield continuous valued estimates of the transmitted data symbols by performing a linear operation on the received signal. Various linear multiuser estimators exist, which differ in the performance criterion which the estimates of the data symbols satisfy. In [KB92, KB93, Kle96, BFKM93, FKB94, LV90] receive zero-forcing JD (RxZF JD) is investigated, which delivers interference free estimates of the sent data symbols. The estimator applying the minimum mean square error (MMSE) principle investigated in [MH94, Gra81, LV89, XSR90, LV90, BFKM93, KKKB94, KKKB96] trades off interference suppression for an improved SNR of the estimated data symbols as compared to RxZF JD.

Alternatively to linear estimation, detection of the multiple transmitted data symbols can be performed in an iterative fashion. If convergent, iterative multiuser algorithms yield estimates of the transmitted data symbols in multiple iterations or stages, being at the same time less complex than linear multiuser algorithms. To the category of iterative multiuser detection algorithms belong multistage detection [VA90, VA91, YKI93, HL98] and parallel interference cancellation [Lam00b, Lam00a, DSR98, PH94, Var95, KIHP90], which are governed by the same general principles. An iterative data detection algorithm gaining considerable attention is turbo multiuser detection [DJB$^+$95, Moh98, RSAA98, WP99], which is based on the turbo principle [Hag96, Hag97, BG96, BGT93] originally designed for decoding concatenated forward error correcting (FEC) codes.

In receiver oriented multiuser algorithms, the transmitter generates transmit signals based on the knowledge of the structure of the receiver and of the wireless MIMO channel. The process of generation of transmit signals in receiver oriented algorithms is known as precoding or predistortion [Fis02, Bar02, YC01, Tom71, HM72]. A special case of predcoding algorithms are algorithms in which the transmit signals are generated by performing a linear operation on the data symbols [MBW$^+$00, TWMB01, KM00, JUN01, JKG$^+$02, VJ98]. Common to all precoding and predistortion algorithms is that the wireless channel is pre-equalized at the transmitter side. As in receiver oriented multiuser algorithms the signal processing tasks related to channel equalization are performed by the transmitter, multiuser precoding and predistortion algorithms are especially attractive for the application in the broadcast channel where multiple low complexity MTs are served.

The first precoding algorithm is considered to be the Tomlinson-Harashima precoding algorithm [Tom71, HM72]. According to the Tomlinson-Harashima precoding algorithm, the channel is pre-equalized at the transmitter by means of an inversion of the channel matrix and in order to avoid the peaks in the transmit power which would result at frequencies coinciding with channel fades, the amplitude of the transmit signal is restricted to a specific interval by means of a modulo-2 addition of the data symbols with a precoding sequence, which depends on the modulation used. Though the Tomlinson-Harashima precoding algorithm as described in [Tom71, HM72] is not a multiuser algorithm in its nature, Yu and Cioffi in [YC01] extend the Tomlinson-Harashima algorithm to the broadcast channel.

Linear predistortion and precoding algorithms differ in the way the linear transformation matrix is applied to the data symbols to be transmitted. In the predistortion method proposed for CDMA systems by Vojčić and Jang [VJ98], the linearly transformed data symbols are spread and then fed into the channel, whereas in the Joint Predistortion algorithm proposed by Kowalewski and Mangold [KM00, BOS98], the linear transformation is applied on the spread signals. On the other hand, in the case of JT [MBW$^+$00], the spreading process in the transmitter is not performed separately from the linear transformation. Given the structure of the receiver and of the wireless MIMO channel, the linear transformation matrix in JT is chosen in such a way that interference free estimates of the data symbols are obtained at the receivers and that the transmit signals are of minimum energy. Due to the interference free transmission, linear JT is also known as transmit ZF JT (TxZF JT) demonstrating the duality to RxZF JD in transmitter oriented multiuser algorithms. The search for the analogon of MMSE for the case of receiver oriented multiuser algorithms led to the derivation of the transmit Wiener filter by Joham et al. in [JKG$^+$02], which represents a trade-off between receive energy exploitation and interference suppression achieved by the transmit matched filtering (TxMF) and the TxZF JT algorithms, respectively, just as MMSE JD represents a trade-off between matched filter (MF) and RxZF JD in transmitter oriented multiuser algorithms.

As stated in Section 1.1, high spectrum capacities η_c should characterize future mobile radio systems. Due to the fact that mobile radio systems are interference limited, the high spectrum capacities can be achieved mainly by combatting interference. However, in cellular architectures intercell interference limits the achievable spectrum capacity η_c. According to the knowledge of the author, proposals regarding future mobile radio systems [AMAS02, WWR], as well as the contributions in Tables 1.2 and 1.3, refer to cell-based architectures. As such, they fail to address the issue of the suppression of interference, as shown in Section 1.2, and are thus inherently suboptimum with respect to the provision of high spectrum capacities η_c.

Hence, the need for the development of an alternative air interface architecture for future mobile radio systems is evident. The design of such an air interface architecture should be aimed at the

provision of high spectrum capacities, i.e., interference suppression should be the main focus of the novel air interface architecture. The SA-based air interface architecture described in Section 1.2 fulfills the aforementioned requirement as the suppression of interference between the simultaneously active MTs is the crux of the SA-base air interface architecture proposal. The investigation of a SA-based air interface architecture combined with the OFDM transmission technique is the topic of the present thesis.

1.5   Structure of the thesis

Apart from the Introduction, the present thesis is comprised of eight chapters, the contents of which are outlined in this Section.

For the purposes of the design and of the performance assessment of a mobile radio system, assumptions have to be made regarding the underlying wireless channel. In Chapter 2 the fundamental principles of mobile radio propagation are briefly recapitulated and the channel models used in the thesis are described.

In Chapter 3 a novel approach for the modelling of the data transmission in OFDM-based MIMO systems is performed. The novelty of the model for the data transmission in OFDM-based MIMO systems presented in Chapter 3 consists in taking into account the time-continuous nature of the MIMO channel. The developed model consists of a physical transmission model complemented with pre- and post-processing stages.

The mathematical modelling of the UL with JD in SA-based systems is performed in Chapter 4. For a single SA, the transmission model is derived, i.e., the mathematical expression of the received signals at the antennas of the APs as a function of the transmitted signals and of the channel matrix is derived. It is shown how JD is employed in SA-based systems to mitigate intra-SA interference by the joint detection of data symbols sent by each of the MTs, which are active simultaneously in the SA and in the same frequency band. Regarding JD algorithms for the UL, the cases of optimum nonlinear JD in the sense of MAP and ML JD, linear JD in the sense of RxZF JD and MMSE JD, and iterative JD with transparent, hard, soft and optimum data estimate refinement are investigated.

The DL with JT in a SA-based system is the topic of Chapter 5. First, the transmission model for the DL is derived, i.e., the complex amplitudes of the signals received by the MTs are expressed using matrix-vector notation as a function of the transmitted signals and of the channel matrix of the SA. The crux of Chapter 5 consists in showing how, with the aid of JT, interference between multiple MTs is suppressed and the need for channel estimation at the MTs is eliminated in

the DL of SA-based systems. With regard to JT schemes, a novel JT scheme optimum with respect to the average bit error probability is firstly investigated. Moreover, the application of TxZF JT is investigated, with the aid of which interference free estimates of the data symbols are available at the active MTs. Chapter 5 is concluded with the introduction of an iterative JT scheme, according to which the total transmit vector is designed in an iterative fashion in a way analog to iterative JD with transparent data estimate refinement presented in Chapter 4.

Chapter 6 covers the performance investigation of JD in the UL. In a first step, the performance measures asymptotic multiuser efficiency and bit error probability are defined, which are used in the context of UL transmission in SA-based systems to assess the efficiency with which JD uses the receive energy. Using the defined performance measures, the performance of optimum JD is analyzed. As the superior performance of optimum JD in comparison to linear JD is trivial, the target of the simulations is to quantify the performance gains achievable with optimum JD in comparison to linear JD in a SA-based system. Furthermore, using the geometric indoor channel model, RxZF JD is investigated by means of the calculation of the spatial distribution and of statistical results for the asymptotic multiuser efficiency. Finally, iterative JD with transparent, hard, soft and optimum data estimate refinement is investigated.

Performance investigations for the DL of SA-based systems with JT are the topic of Chapter 7. Two performance measures for JT, namely transmission efficiency and bit error probability are introduced. In the case of optimum JT, the average bit error probability at the MTs is determined for fixed and variable energy transmit signal vectors. Finally, TxZF JT and iterative JT are investigated in terms of transmission efficiency and bit error probability.

Chapter 8 presents an approach for the unified investigation of UL and DL in SA-based systems for the case of linear pre- and post processing. Moreover, the energy efficiency of a SA-based mobile radio system is defined as a performance measure. Chapter 8 is concluded with system level investigations of a SA-based mobile radio system.

Chapter 9 concludes the thesis by summarizing the results of Chapters 2 to 8 in English and in German.

2   Channel modelling

2.1   Introduction

The design of a SA-based air interface architecture, as of any air interface architecture, is considerably aided by computer simulations. Profound knowledge concerning the characteristics of the mobile radio channel of the SA is essential in order to be able to model the wireless channel of the SA in computer simulations as accurately as possible. Target of the present Chapter is to give an overview of the three channel models used in the simulations in this thesis. To this end, theoretical aspects of mobile radio propagation relevant to the radio transmissions in a SA-based air interface architecture are first briefly treated with.

2.2   Theory of mobile radio propagation

In a wireless transmission in a mobile radio system, signals emitted by a transmitter reach the receiver not only via direct line of sight (LOS) paths between transmitter and receiver. Transmitted signals often impinge at the antennas of each receiver after reflection, scattering or diffraction on physical obstacles. Only seldom does a direct LOS path exist [Par92, BARY95, FL96], especially in dense urban areas. Given the usually large number of surfaces interacting with the emitted electromagnetic waves, a multitude of paths exist along which indirect wireless transmissions take place. It follows that a multitude of signals with different amplitudes, phases and delays superimpose at the receiver.

In a static environment the mobile radio channel is described in the equivalent lowpass domain as a linear time invariant filter having the complex transfer function $\underline{H}(f)$. The superposition of the signals which reach the receiver each with a different delay τ [BBS97], varies for different frequencies f from destructive to constructive. Therefore, the mobile radio channel is said to be frequency selective, i.e., its transfer function $\underline{H}(f)$ fluctuates throughout the bandwidth B used for the wireless transmission. On the other hand, if the mobile radio channel has one dominant path and negligible signal energy is received via multipath propagation, then it is said to be frequency nonselective or flat fading channel and the corresponding transfer function $\underline{H}(f)$ is considered to be constant throughout the entire bandwidth B.

In a dynamic environment in which the movement of the MT and of its surroundings is taken into account, the way the signals from multiple paths superpose at the receiver is time variant. Depending on the relation of the movement of the MT to the system wavelength λ, it can be discerned between small- and large scale movement [BARY95, FL96].

If the MT covers a distance of fractions of λ, then small but rapid variations of the amplitude of the received signal occur. In particular, the small scale movement of the MT has a rather negligible effect on the attenuation but a large impact on the phase of each of the superposed signals. Therefore, the superposition of a large number of signals each with a rapidly changing phase results in an also rapidly varying envelope of the total received signal and the effect is called fast fading [Par92]. Large scale movement of the MT occurs if the movement of the MT is in the order of magnitude of tens of λ. In such a case, the dominant effect is shadowing, i.e., the limited lifetime of the individual paths. As the MT moves, some paths disappear and new paths are created. The resulting variation of the amplitude of the received signal is slow relative to the case of small scale movement, and is called slow fading [Par92]. However, the variation of the amplitude of the received signal caused by slow fading has a larger dynamic range as compared to the case of fast fading [BARY95]. Hence, in the case of the dynamic propagation environment, the time-variant transfer function $\underline{H}(f, t)$ is used to describe the mobile radio channel [BBS97, Par92].

2.3 Channel models used in the thesis

2.3.1 COST 207 channel models

The most widely used channel models are stochastic channel models, i.e., models in which the mobile radio channel is modelled as a bandlimited stochastic process. In the modelling procedure it is assumed that the stochastic process describing the channel is stationary in the wide sense at least in a small area and that the modelled wireless channel exhibits uncorrelated dispersiveness in time delays τ_w, $w = 1 \ldots W$, and Doppler shifts $f_{\mathrm{D},w}$, $w = 1 \ldots W$, of the W superposed paths, i.e., in stochastic models radio channels are modelled as wide sense stationary uncorrelated scattering (WSSUS) channels [Bel63, Sch88a, Hoe92]. Hence, in WSSUS channels, the scattering function $S(\tau, f_{\mathrm{D}})$ can be expressed as the product of the Doppler power spectrum $S_{\mathrm{c}}(0, f_{\mathrm{D}})$ and the power delay spectrum $\rho_{\mathrm{T}}(\tau, 0)$ as

$$S(\tau, f_{\mathrm{D}}) = S_{\mathrm{c}}(0, f_{\mathrm{D}}) \, \rho_{\mathrm{T}}(\tau, 0). \tag{2.1}$$

The most widely used stochastic channel models are the channel models of the COST 207 study [COS88]. According to the COST 207 channel modelling, the mobile radio channel consists of a superposition of a number W of uncorrelated paths, which have uniformly distributed null phases θ_w, $w = 1 \ldots W$, Doppler shifts $f_{\mathrm{D},w}$, $w = 1 \ldots W$, and unit amplitude.

The delays τ_w for each path w are taken from an interval $[\tau_{w,\min}, \tau_{w,\max}]$ according to an exponential-type power delay spectrum $a \exp(-b\tau_w)$, a, $b \in \mathbb{R}^+$. For different values of

$\tau_{w,\min}, \tau_{w,\max}, a$ and b four different propagation conditions are modelled, bad urban (BU), hilly terrain (HT), rural area (RA) and typical urban (TU), as Table 2.1 shows.

Table 2.1. Parameters for the channel models of the four different propagation conditions of the COST 207 study

environment	$\tau/\mu\mathrm{s}$	$\rho_{\mathrm{T}}(\tau)$
bad urban (BU)	$[0, 5]$	$\propto \ \exp(-\tau)$
	$[5, 10]$	$\propto \ 0.5 \exp(5 - \tau)$
hilly terrain (HT)	$[0, 2]$	$\propto \ \exp(-3.5\tau)$
	$[15, 20]$	$\propto \ 0.1 \exp(15 - \tau)$
rural area (RU)	$[0, 0.7]$	$\propto \ \exp(-9.2\tau)$
typical urban (TU)	$[0, 7]$	$\propto \ \exp(-\tau)$

If the motion of the MTs is not taken into account, i.e., if for each path w, $w = 1 \ldots W$, the Doppler shift $f_{\mathrm{D,w}}$ is not taken into account, with the uniformly distributed null phase θ_w and the delay τ_w taken from Table 2.1, the channel transfer function

$$\underline{H}(f) = \frac{1}{\sqrt{W}} \sum_{w=1}^{W} \exp(\mathrm{j}\theta_w) \exp(-\mathrm{j}2\pi f \tau_w) \tag{2.2}$$

of the mobile radio channel according to the COST 207 channel models is derived. In the simulation of SA-based mobile radio systems, (2.2) is used $K K_{\mathrm{B}}$ times to get the transfer functions $\underline{H}^{(k,k_{\mathrm{B}})}(f)$ of the wireless channels between each pair of MT k, $k = 1 \ldots K$, and AP k_{B}, $k_{\mathrm{B}} = 1 \ldots K_{\mathrm{B}}$.

2.3.2   Indoor geometric channel model

In order to perform simulations of a SA-based system in which OFDM is used, for each channel snapshot $K K_{\mathrm{B}}$ transfer functions $\underline{H}^{(k,k_{\mathrm{B}})}(f)$, for the $K K_{\mathrm{B}}$ channels between each MT and each AP have to be generated by means of a channel model. In order to take into account interdependencies between the wireless channels of the SA resulting from the geometrical structure of the SA, a geometric MIMO indoor channel model is developed specifically for the simulation needs of the thesis and it is described in the present Section. In contrast to the COST 207 channel models, which generate transfer functions $\underline{H}^{(k,k_{\mathrm{B}})}(f)$ as samples of a stochastic process, the geometric indoor channel model described in this Section is deterministic, i.e., the same transfer functions $\underline{H}^{(k,k_{\mathrm{B}})}(f)$ are generated given fixed positions of the MTs and geometry of the SA.

In the geometric channel model, the SA is a rectangular room of dimensions $x_{\max} \times y_{\max}$, as Fig. 2.1 shows. In the SA, a single CU, K MTs and K_{B} APs exist, each equipped with single element

antennas. The K MTs with coordinates $(x_{\mathrm{MT}}^{(k)}, y_{\mathrm{MT}}^{(k)})$, $k = 1 \ldots K$, are randomly positioned in the room and their positions are kept fixed once chosen. The K_{B} APs are uniformly deployed on a circular periphery of radius r_{B}, having its center at the origin of the cartesian coordinate system, which coincides with the center of the rectangular room of the SA. Their coordinates in the chosen system will be denoted by $(x_{\mathrm{AP}}^{(k_{\mathrm{B}})}, y_{\mathrm{AP}}^{(k_{\mathrm{B}})})$, $k_{\mathrm{B}} = 1 \ldots K_{\mathrm{B}}$.
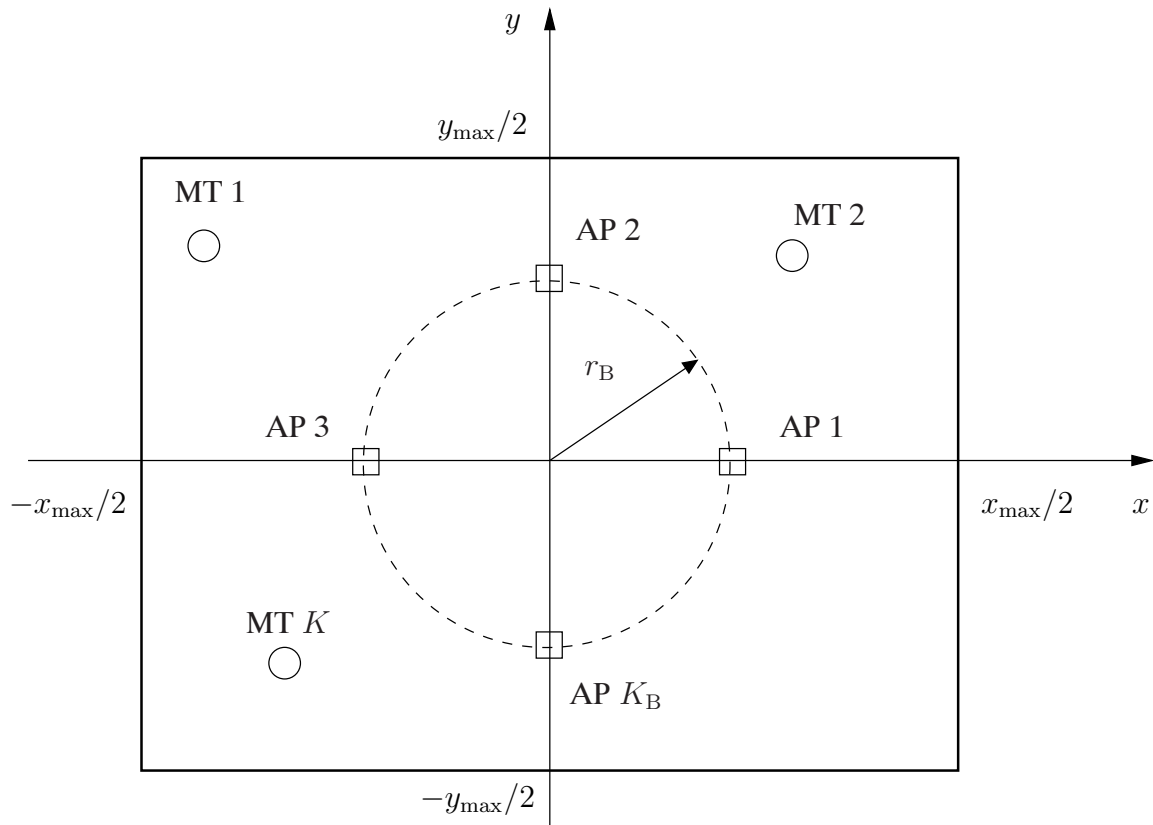
Figure 2.1. SA of dimensions $x_{\mathrm{max}} \times y_{\mathrm{max}}$ with K MTs with coordinates $(x_{\mathrm{MT}}^{(k)}, y_{\mathrm{MT}}^{(k)})$, randomly positioned in the SA and K_{B} APs with coordinates $(x_{\mathrm{AP}}^{(k_{\mathrm{B}})}, y_{\mathrm{AP}}^{(k_{\mathrm{B}})})$, deployed on a circular periphery of radius r_{B}

Reflection on the walls forming the borders of the SA is not taken into account. It is assumed that each wireless link between an AP k_{B} and an MT k consists approximately of one path, the one corresponding to the direct LOS transmission, and that such a LOS connection exists between all pairs of APs and MTs. Usually radio wave propagation in real life environments cannot be approximated with a LOS channel model. Nevertheless, the use of the geometric channel model permits the efficient study of special characteristics of SA-based systems, as it is shown in Chapter 6, and does not target at the modelling of a real life scenario.

With the distance

$$r^{(k,k_{\mathrm{B}})} = \sqrt{\left(y_{\mathrm{MT}}^{(k)} - y_{\mathrm{AP}}^{(k_{\mathrm{B}})}\right)^2 + \left(x_{\mathrm{AP}}^{(k_{\mathrm{B}})} - x_{\mathrm{MT}}^{(k)}\right)^2} \tag{2.3}$$

between MT k and AP k_{B}, for the considered subcarrier n_{F} and frequency f and the speed c_0 of propagation of electromagnetic waves in vacuum, the attenuation factor $1 \left/ r^{(k,k_{\mathrm{B}})^2}\right.$, and the phase rotation factor $\exp\left(-\mathrm{j}2\pi f r^{(k,k_{\mathrm{B}})}/c_0\right)$ of the direct path from MT k to AP k_{B} is calculated. Hence, the transfer function $\underline{H}^{(k,k_{\mathrm{B}})}(f)$ between MT k, AP k_{B} at frequency f can be expressed as

$$\underline{H}^{(k,k_{\mathrm{B}})}(f) = \frac{1}{r^{(k,k_{\mathrm{B}})}} \exp\left(-\mathrm{j}2\pi f \frac{r^{(k,k_{\mathrm{B}})}}{c_0}\right). \tag{2.4}$$

2.3.3 Multiple-input-multiple-output parametric channel model

In the SA-based air interface architecture the system performance is in many cases a function of the degree by which channels of different MTs are correlated, as will be shown in Chapter 6. For this reason, a deterministic MIMO parametric channel model is developed with which the degree of correlation between the channels of the various MTs is parameterized.

Given full system load, i.e.,

$$K_{\mathrm{B}} = K, \tag{2.5}$$

and with the variable $\underline{\rho} \in \mathbb{C}$, the output of the MIMO parametric channel model are the transfer functions

$$\underline{H}^{(k,k_{\mathrm{B}})}(f) = \begin{cases} 1 & k = k_{\mathrm{B}}, \\ \underline{\rho} & \text{else,} \end{cases} \quad k = 1 \ldots K, \ k_{\mathrm{B}} = 1 \ldots K_{\mathrm{B}}, \tag{2.6}$$

which are frequency nonselective. Using the variables $\underline{\rho}_{kk_{\mathrm{B}}} \in \mathbb{C}$, $k = 1 \ldots K$, $k_{\mathrm{B}} = 1 \ldots K_{\mathrm{B}}$, the MIMO parametric channel model can be extended to include more degrees of freedom, yielding the transfer functions

$$\underline{H}^{(k,k_{\mathrm{B}})}(f) = \begin{cases} 1 & k = k_{\mathrm{B}}, \\ \underline{\rho}_{kk_{\mathrm{B}}} & \text{else,} \end{cases} \quad k = 1 \ldots K, \ k_{\mathrm{B}} = 1 \ldots K_{\mathrm{B}}, \tag{2.7}$$

as output.

3 Modelling of OFDM-based MIMO systems

3.1 Introduction

Until now, OFDM-based systems are described by the use of a model based on IFFT, FFT, cyclic prefix addition and cyclic prefix removal operations [vNP00, FK03]. However, such approaches fail to address the fact that OFDM-based systems are just special cases of a more general class of multiuser systems in which a time-continuous signature is assigned to each discrete transmit value, i.e., of multiuser systems employing linear modulation.

Target of this Chapter is the development of a novel model for the data transmission in an OFDM-based system employing transmission over a MIMO channel with K_I inputs and K_O outputs. In a first step data transmission in a general multiuser system employing transmission over a time-continuous $K_\mathrm{O} \times K_\mathrm{I}$ MIMO channel is modelled and then the data transmission model for OFDM-based MIMO systems is derived as a special case.

Bandpass signal transmissions in multiuser systems can be efficiently described by the use of the equivalent low pass domain representation of signals, in which signals are represented by their complex envelopes [Pro95]. Moreover, the model for the data transmission can be decomposed into

- a physical transmission model and

- pre- and post-processing stages,

as Fig. 3.1 shows.

It is assumed that L bits $u_l^{(k)}$, $l = 1 \ldots L$, compiled into the bit vector

$$\mathbf{u}^{(k)} = \left(u_1^{(k)} \ldots u_L^{(k)} \right)^\mathrm{T},$$

(3.1)

are transmitted per MT k, $k = 1 \ldots K$. As shown in Fig. 3.1, the K_I transmit vectors

$$\underline{\mathbf{s}}^{(k_\mathrm{I})} = \left(\underline{s}^{(k_\mathrm{I},1,1)} \ldots \underline{s}^{(k_\mathrm{I},n_\mathrm{F},n_\mathrm{S})} \ldots \underline{s}^{(k_\mathrm{I},N_\mathrm{F},N_\mathrm{S})} \right)^\mathrm{T}, \; k_\mathrm{I} = 1 \ldots K_\mathrm{I},$$

(3.2)

of dimension $N_\mathrm{F} N_\mathrm{S}$ are generated from the K vectors $\mathbf{u}^{(k)}$, $k = 1 \ldots K$, of (3.1) by the pre-processing stage.
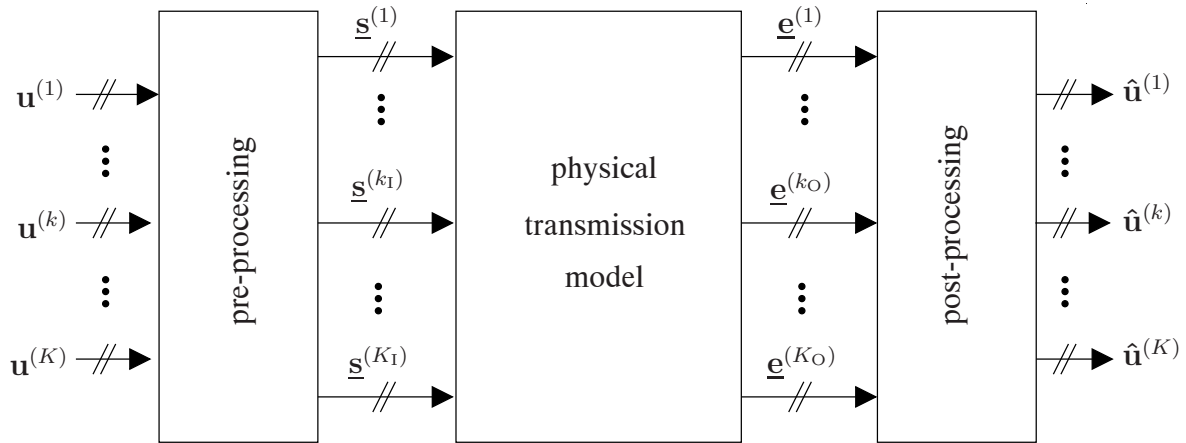
Figure 3.1. Model of the data transmission in a multiuser system with K MTs, in which the physical transmission takes place over a time-continuous MIMO channel with K_I inputs and K_O outputs, consisting of a model for the physical transmission with K_I vector inputs and K_O vector outputs, complemented with pre- and post- processing stages

The physical transmission model of the investigated multiuser system is used to describe each of the K_O received vectors

$$\underline{\mathbf{e}}^{(k_\mathrm{O})} = \left(\underline{e}^{(k_\mathrm{O},1,1)} \ldots \underline{e}^{(k_\mathrm{O},n_\mathrm{F},n_\mathrm{S})} \ldots \underline{e}^{(k_\mathrm{O},N_\mathrm{F},N_\mathrm{S})} \right)^{\mathrm{T}}, \; k_\mathrm{O} = 1 \ldots K_\mathrm{O}, \tag{3.3}$$

of dimension $N_\mathrm{F}N_\mathrm{S}$ as a function of the K_I transmit vectors $\underline{\mathbf{s}}^{(k_\mathrm{I})}$, $k_\mathrm{I} = 1 \ldots K_\mathrm{I}$, of (3.2). As the mobile radio channel itself is time-continuous the physical transmission model consists of an inner time-continuous part and an outer part which describes the synthesis and analysis of the time-continuous transmit and received signals, respectively.

At the receiver side, a post-processing of each received vector $\underline{\mathbf{e}}^{(k_\mathrm{O})}$ of (3.3) is performed, in order to yield the estimates

$$\hat{\mathbf{u}}^{(k)} = \left(\hat{u}_1^{(k)} \ldots \hat{u}_L^{(k)} \right)^{\mathrm{T}}, \; k = 1 \ldots K, \tag{3.4}$$

of the bit vectors $\mathbf{u}^{(k)}$, $k = 1 \ldots K$, of (3.1).

Due to the fact that the investigation of the impact of synchronization errors on the performance of OFDM-based MIMO systems is beyond the scope of this thesis, it is assumed hereafter that the investigated OFDM system is perfectly synchronized in the time and in the frequency domain [vSB97, HE97, BR98].
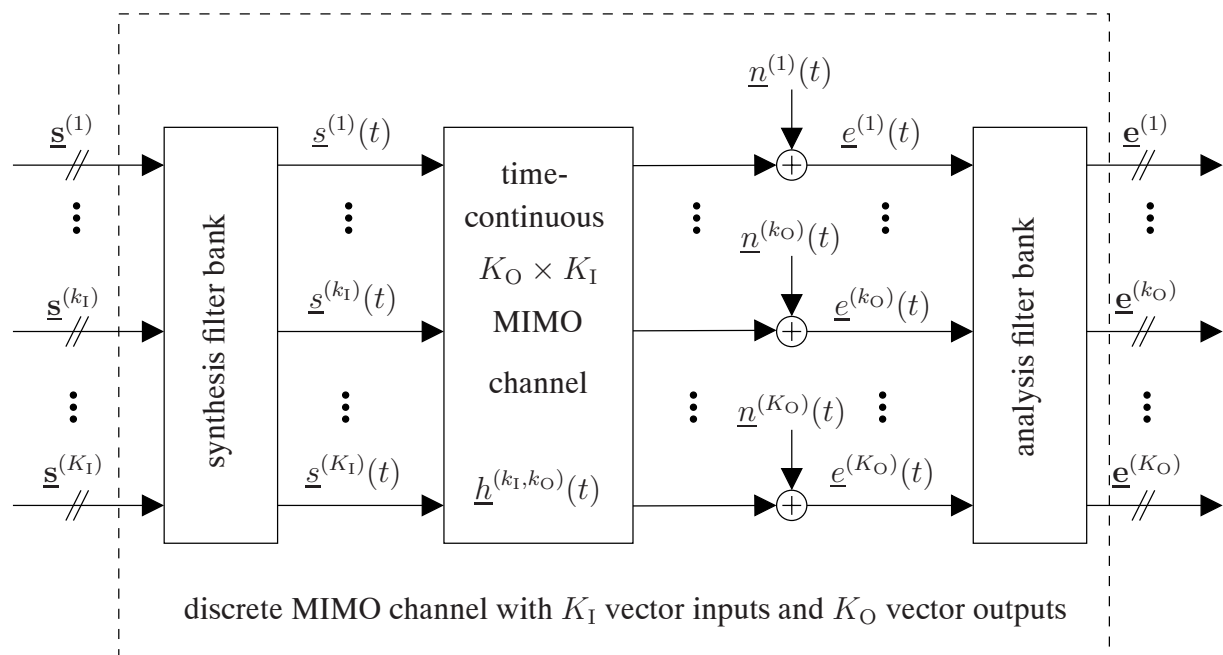
Figure 3.2. Physical transmission model with K_I vector inputs and K_O vector outputs of a multiuser system employing transmission over a time-continuous MIMO channel with K_I inputs and K_O outputs

3.2 Physical transmission model

3.2.1 General description of the physical transmission

Fig. 3.2 shows the physical transmission model of the considered multiuser system. The K_I transmit vectors $\underline{s}^{(k_I)}$, $k_I = 1 \ldots K_I$, of (3.2) are processed by the synthesis filter bank to produce the K_I corresponding time-continuous signals $\underline{s}^{(k_I)}(t)$, $k_I = 1 \ldots K_I$, which are transmitted through the time-continuous $K_O \times K_I$ MIMO channel, characterized by the $K_I K_O$ impulse responses $\underline{h}^{(k_I,k_O)}(t)$, $k_I = 1 \ldots K_I$, $k_O = 1 \ldots K_O$. It is assumed that each impulse response $\underline{h}^{(k_I,k_O)}(t)$ has a maximum duration of T_h.

The K_O time-continuous received signals $\underline{e}^{(k_O)}(t)$, $k_O = 1 \ldots K_O$, containing also noise $\underline{n}^{(k_O)}(t)$, $k_O = 1 \ldots K_O$, are processed by the analysis filter bank to yield the K_O received vectors $\underline{e}^{(k_O)}$, $k_O = 1 \ldots K_O$, of (3.3).

Due to the application of the synthesis and analysis filter banks, the $K_O \times K_I$ time-continuous MIMO channel is transformed into a discrete MIMO channel with K_I vector inputs and K_O vector outputs, as Fig. 3.2 shows.

3.2.2   Transmitter

The task of the synthesis filter bank in Fig. 3.2 is the synthesis of each time-continuous transmit signal $\underline{s}^{(k_{\mathrm{I}})}(t)$ from the transmit vector $\underline{s}^{(k_{\mathrm{I}})}$. The signature $\underline{c}_{\mathrm{t},n_{\mathrm{F}},n_{\mathrm{S}}}(t)$ is weighted by the transmit value $\underline{s}^{(k_{\mathrm{I}},n_{\mathrm{F}},n_{\mathrm{S}})}$ to produce the transmit-value-specific partial transmit signal

$$\underline{s}^{(k_{\mathrm{I}})}_{n_{\mathrm{F}},n_{\mathrm{S}}}(t) = \underline{s}^{(k_{\mathrm{I}},n_{\mathrm{F}},n_{\mathrm{S}})}\underline{c}_{\mathrm{t},n_{\mathrm{F}},n_{\mathrm{S}}}(t). \tag{3.5}$$

With the transmit-value-specific partial transmit signals $\underline{s}^{(k_{\mathrm{I}})}_{n_{\mathrm{F}},n_{\mathrm{S}}}(t)$, $n_{\mathrm{F}} = 1 \ldots N_{\mathrm{F}}$, $n_{\mathrm{S}} = 1 \ldots N_{\mathrm{S}}$, of (3.5), the transmit signal

$$\underline{s}^{(k_{\mathrm{I}})}(t) = \sum_{n_{\mathrm{F}}=1}^{N_{\mathrm{F}}} \sum_{n_{\mathrm{S}}=1}^{N_{\mathrm{S}}} \underline{s}^{(k_{\mathrm{I}})}_{n_{\mathrm{F}},n_{\mathrm{S}}}(t) \tag{3.6}$$

is calculated which is fed in the input k_{I} of the time-continuous $K_{\mathrm{O}} \times K_{\mathrm{I}}$ MIMO channel. In the following multicarrier systems are considered [vNP00, FK03], in which each signature $\underline{c}_{\mathrm{t},n_{\mathrm{F}},n_{\mathrm{S}}}(t)$ is a time- and frequency shifted replica of a basic transmit signature $\underline{c}_{\mathrm{t}}(t)$. With the symbol slot duration T_{s} and the subcarrier spacing F, the input-specific signature $\underline{c}_{\mathrm{t},n_{\mathrm{F}},n_{\mathrm{S}}}(t)$ at subcarrier n_{F} and symbol slot n_{S} is expressed as

$$\underline{c}_{\mathrm{t},n_{\mathrm{F}},n_{\mathrm{S}}}(t) = \underline{c}_{\mathrm{t}}\left(t - (n_{\mathrm{S}} - 1)T_{\mathrm{s}}\right) \exp\left(\mathrm{j}2\pi(n_{\mathrm{F}} - 1)Ft\right). \tag{3.7}$$

In the following the symbol slot duration T_{s} is chosen to be larger than the impulse response duration T_{h}, i.e., $T_{\mathrm{s}} > T_{\mathrm{h}}$ holds. In the specific case of OFDM systems the subcarrier spacing

$$F = \frac{1}{T_{\mathrm{s}} - T_{\mathrm{h}}} \tag{3.8}$$

and the basic transmit signature

$$\underline{c}_{\mathrm{t}}(t) = \frac{1}{\sqrt{T_{\mathrm{s}}}}\mathrm{rect}\left(\frac{t}{T_{\mathrm{s}}} - \frac{1}{2}\right) \tag{3.9}$$

are used and with the basic transmit signature $\underline{c}_{\mathrm{t}}(t)$ of (3.9), (3.7) becomes

$$\underline{c}_{\mathrm{t},n_{\mathrm{F}},n_{\mathrm{S}}}(t) = \frac{1}{\sqrt{T_{\mathrm{s}}}}\mathrm{rect}\left(\frac{t - (n_{\mathrm{S}} - 1)T_{\mathrm{s}}}{T_{\mathrm{s}}} - \frac{1}{2}\right) \exp\left(\mathrm{j}2\pi\frac{n_{\mathrm{F}} - 1}{T_{\mathrm{s}} - T_{\mathrm{h}}}t\right). \tag{3.10}$$

Due to (3.5), (3.6) and (3.10), in a specific OFDM symbol slot n_{S} the weighted sum of N_{F} sinusoidal signals $\underline{c}_{\mathrm{t},n_{\mathrm{F}},n_{\mathrm{S}}}(t)$, $n_{\mathrm{F}} = 1 \ldots N_{\mathrm{F}}$, of (3.10) is fed in the input K_{I} of the time-continuous MIMO channel. The transmitter defined by (3.5), (3.6) and (3.10) corresponds to a conventional OFDM transmitter [vNP00].

3.2.3 MIMO channel

Each time-continuous transmit signal $\underline{s}^{(k_I)}(t)$ of (3.6) passes through the time-continuous $K_O \times K_I$ MIMO channel, characterized by the impulse responses $\underline{h}^{(k_I,k_O)}(t)$, $k_I = 1 \ldots K_I$, $k_O = 1 \ldots K_O$. Hence, with the K_I time-continuous transmit signals $\underline{s}^{(k_I)}(t)$, $k_I = 1 \ldots K_I$, of (3.6), the K_I impulse responses $\underline{h}^{(k_I,k_O)}(t)$, $k_I = 1 \ldots K_I$, and the additive noise $\underline{n}^{(k_O)}(t)$, for the time-continuous received signal $\underline{e}^{(k_O)}(t)$ at output k_O of the time-continuous MIMO channel

$$
\begin{aligned}
\underline{e}^{(k_O)}(t) &= \sum_{k_I=1}^{K_I} \int_{-\infty}^{\infty} \underline{s}^{(k_I)}(t-\tau)\underline{h}^{(k_I,k_O)}(\tau)\mathrm{d}\tau \; + \; \underline{n}^{(k_O)}(t) \\
&= \sum_{k_I=1}^{K_I} \sum_{n_F=1}^{N_F} \sum_{n_S=1}^{N_S} \int_0^{T_h} \underline{s}^{(k_I,n_F,n_S)} \underline{c}_{t,n_F,n_S}(t-\tau)\underline{h}^{(k_I,k_O)}(\tau)\mathrm{d}\tau \; + \; \underline{n}^{(k_O)}(t) \quad (3.11)
\end{aligned}
$$

holds. From (3.11) it can be seen that the combined effect of the input-specific signature $\underline{c}_{t,n_F,n_S}(t)$ and of the impulse response $\underline{h}^{(k_I,k_O)}(t)$ on each transmit value $\underline{s}^{(k_I,n_F,n_S)}$ is characterized by the combined impulse response

$$
\underline{b}_{n_F,n_S}^{(k_I,k_O)}(t) = \int_0^{T_h} \underline{c}_{t,n_F,n_S}(t-\tau)\underline{h}^{(k_I,k_O)}(\tau)\mathrm{d}\tau, \tag{3.12}
$$

with which the expression (3.11) for the time-continuous received signal $\underline{e}^{(k_O)}(t)$ becomes

$$
\underline{e}^{(k_O)}(t) = \sum_{k_I=1}^{K_I} \sum_{n_F=1}^{N_F} \sum_{n_S=1}^{N_S} \underline{s}^{(k_I,n_F,n_S)} \underline{b}_{n_F,n_S}^{(k_I,k_O)}(t) \; + \; \underline{n}^{(k_O)}(t). \tag{3.13}
$$

The additive noise $\underline{n}^{(k_O)}(t)$ in (3.13) is considered to be zero-mean white noise with the two-sided spectral power density $N_0/2$, i.e., the variance

$$
\sigma^2 = N_0 \tag{3.14}
$$

characterizes each of the real and imaginary parts of the noise $\underline{n}^{(k_O)}(t)$ in the following. Moreover, it is assumed that the noise $\underline{n}^{(k_O)}(t)$ and $\underline{n}^{(k'_O)}(t)$ at different outputs $k_O \neq k'_O$ of the time-continuous MIMO channel is uncorrelated, i.e.,

$$
\mathrm{E}\left\{\underline{n}^{(k_O)}(t+\tau)\underline{n}^{*(k'_O)}(t)\right\} = \begin{cases} N_0\delta(\tau) & k_O = k'_O, \\ 0 & \text{else,} \end{cases} \tag{3.15}
$$

holds.

3.2.4 Receiver

At the receiver side of the considered multiuser system, an analysis filter bank is employed, as shown in Fig. 3.2. The task of the analysis filter bank is the filtering of each time-continuous received signal $\underline{e}^{(k_O)}(t)$ in order to yield the $N_F N_S$ received values $\underline{e}^{(k_O,n_F,n_S)}$, $n_F = 1 \ldots N_F$, $n_S = 1 \ldots N_S$. To perform this task, a bank of K_O filters is employed in the analysis filter bank. Each filter in the analysis filter bank has the impulse response $\underline{c}_{r,n_F,n_S}(t)$ and its output is sampled. In multicarrier systems, with a basic receive signature $\underline{c}_r(t)$, each impulse response $\underline{c}_{r,n_F,n_S}(t)$ is chosen as

$$\underline{c}_{r,n_F,n_S}(t) = \underline{c}_r\left(t - (n_S - 1)T_s\right) \exp\left(j2\pi\left(n_F - 1\right) Ft\right), \tag{3.16}$$

in analogy to (3.7). In the special case of OFDM

$$\underline{c}_r(t) = \frac{1}{\sqrt{T_s - T_h}}\mathrm{rect}\left(\frac{-t - T_h}{T_s - T_h} - \frac{1}{2}\right) \tag{3.17}$$

holds. With the basic receive signature $\underline{c}_r(t)$ of (3.17) and the subcarrier spacing F of (3.8), (3.16) becomes

$$\underline{c}_{r,n_F,n_S}(t) = \frac{1}{\sqrt{T_s - T_h}}\mathrm{rect}\left(\frac{-t - T_h - (n_S - 1)T_s}{T_s - T_h} - \frac{1}{2}\right) \exp\left(j2\pi\frac{n_F - 1}{T_s - T_h}t\right). \tag{3.18}$$

In OFDM systems each impulse response $\underline{c}_{r,n_F,n_S}(t)$ of (3.18) is matched to the part $(n_S - 1)T_s - T_h \leq t \leq n_S T_s$ of the combined impulse response $\underline{b}_{n_F,n_S}^{(k_I,k_O)}$ of (3.12) of duration $T_s - T_h$. As it will be shown in what follows, during the aforementioned time interval, for a given input k_I, the combined impulse responses $\underline{b}_{n_F,n_S}^{(k_I,k_O)}$, $n_F = 1 \ldots N_F$, $n_S = 1 \ldots N_S$, of (3.18) are orthogonal.

With the time-continuous received signal $\underline{e}^{(k_O)}(t)$ of (3.13), the impulse responses

$$\underline{c}_{r,n_F,n_S}(t), \ n_F = 1 \ldots N_F, \ n_S = 1 \ldots N_S, \tag{3.19}$$

of (3.16) and the combined impulse responses

$$\underline{b}_{n_F,n_S}^{(k_I,k_O)}(t), \ n_F = 1 \ldots N_F, \ n_S = 1 \ldots N_S, \ k_I = 1 \ldots K_I, \tag{3.20}$$

of (3.12), for the vector output k_O of the analysis filter bank

$$
\begin{aligned}
\underline{e}^{(k_O,n_F,n_S)} &= \int\limits_{-\infty}^{\infty} \underline{e}^{(k_O)}(t)\underline{c}_{r,n_F,n_S}(-t)\mathrm{d}t \\
&= \sum_{k_I=1}^{K_I}\sum_{n_F'=1}^{N_F}\sum_{n_S'=1}^{N_S} \underline{s}^{(k_I,n_F',n_S')} \int\limits_{-\infty}^{\infty} \underline{b}_{n_F',n_S'}^{(k_I,k_O)}(t)\underline{c}_{r,n_F,n_S}(-t)\mathrm{d}t \ + \ \underline{n}^{(k_O,n_F,n_S)}, \\
&\quad n_F = 1 \ldots N_F, \ n_S = 1 \ldots N_S,
\end{aligned}
\tag{3.21}
$$

holds. In (3.21)

$$n^{(k_O,n_F,n_S)} = \int_{-\infty}^{\infty} \underline{n}^{(k_O)}(t)\underline{c}_{r,n_F,n_S}(-t)\mathrm{d}t, \; n_F = 1\ldots N_F, \; n_S = 1\ldots N_S, \tag{3.22}$$

are the $N_F N_S$ noise values $\underline{n}^{(k_O,n_F,n_S)}$, $n_F = 1\ldots N_F$, $n_S = 1\ldots N_S$, at vector output k_O of the physical transmission model, which follow after filtering and sampling of the noise $\underline{n}^{(k_O)}(t)$ of the output k_O of the time-continuous MIMO channel.

From (3.12), for the combined impulse response $\underline{b}^{(k_I,k_O)}_{n_F,n'_S}(t)$ in (3.21), follows

$$\underline{b}^{(k_I,k_O)}_{n_F,n'_S}(t) = 0, \;\; \text{for} \;\; t \notin [(n'_S - 1)T_s, \; n'_S T_s + T_h]. \tag{3.23}$$

Moreover, in the case of OFDM follows for the impulse response $\underline{c}_{r,n_F,n_S}(t)$ of (3.18)

$$\underline{c}_{r,n_F,n_S}(t) = 0, \;\; \text{for} \;\; t \notin [-(n_S - 1)T_s - T_h, \; -n_S T_s]. \tag{3.24}$$

Hence, as a consequence of (3.23) and (3.24),

$$\int_{-\infty}^{\infty} \underline{b}^{(k_I,k_O)}_{n_F,n'_S}(t)\underline{c}_{r,n_F,n_S}(-t)\mathrm{d}t = 0, \; \text{for } n_S \neq n'_S, \tag{3.25}$$

i.e., the received value $\underline{e}^{(k_O,n_F,n_S)}$ has no contributions from the transmit value $\underline{s}^{(k_I,n_F,n'_S)}$ for $n_S \neq n'_S$, which means that transmissions in different symbol slots in OFDM-based MIMO systems are totally independent.

With the matrix $\underline{H}^{(k_I,k_O)}(f)$ being the result of the Fourier transformation of the impulse response $\underline{h}^{(k_I,k_O)}(t)$, the discrete transfer coefficients

$$\begin{aligned}
\underline{h}^{(k_I,k_O,n_F)} &= \int_{-\infty}^{\infty} \underline{b}^{(k_I,k_O)}_{n_F,n_S}(t)\underline{c}_{r,n_F,n_S}(-t)\mathrm{d}t \\
&= \sqrt{\frac{T_s - T_h}{T_s}} \int_0^{T_h} \exp\left(-\mathrm{j}2\pi(n_F - 1)F\tau\right) \underline{h}^{(k_I,k_O)}(\tau)\mathrm{d}\tau, \\
&= \sqrt{\frac{T_s - T_h}{T_s}} \, \underline{H}^{(k_I,k_O)}\left((n_F - 1)F\right).
\end{aligned} \tag{3.26}$$

are defined and using (3.8), (3.10), (3.12), (3.18) and (3.26), it follows

$$
\begin{aligned}
\int_{-\infty}^{\infty} \underline{b}_{n_{\mathrm{F}}',n_{\mathrm{S}}}^{(k_{\mathrm{I}},k_{\mathrm{O}})}(t)\underline{c}_{\mathrm{r},n_{\mathrm{F}},n_{\mathrm{S}}}(-t)\mathrm{d}t \; = \; & \frac{1}{\sqrt{T_{\mathrm{s}}-T_{\mathrm{h}}}\sqrt{T_{\mathrm{s}}}} \int_{T_{\mathrm{h}}}^{T_{\mathrm{s}}}\int_{0}^{T_{\mathrm{h}}} \exp\left(\mathrm{j}2\pi(n_{\mathrm{F}}'-1)F(t-\tau)\right)\underline{h}^{(k_{\mathrm{I}},k_{\mathrm{O}})}(\tau)\mathrm{d}\tau \\
& \cdot \exp\left(-\mathrm{j}2\pi(n_{\mathrm{F}}-1)Ft\right)\mathrm{d}t \\
= \; & \frac{1}{\sqrt{T_{\mathrm{s}}-T_{\mathrm{h}}}\sqrt{T_{\mathrm{s}}}} \int_{T_{\mathrm{h}}}^{T_{\mathrm{s}}} \exp\left(\mathrm{j}2\pi\frac{n_{\mathrm{F}}'-n_{\mathrm{F}}}{T_{\mathrm{s}}-T_{\mathrm{h}}}t\right)\mathrm{d}t \\
& \cdot \int_{0}^{T_{\mathrm{h}}} \exp\left(-\mathrm{j}2\pi\frac{n_{\mathrm{F}}'-1}{T_{\mathrm{s}}-T_{\mathrm{h}}}\tau\right)\underline{h}^{(k_{\mathrm{I}},k_{\mathrm{O}})}(\tau)\mathrm{d}\tau \\
= \; & \begin{cases} \underline{h}^{(k_{\mathrm{I}},k_{\mathrm{O}},n_{\mathrm{F}})} & n_{\mathrm{F}}=n_{\mathrm{F}}', \\ 0 & \text{else,} \end{cases}
\end{aligned} \tag{3.27}
$$

i.e., the transmissions in different subcarriers n_{F}' and n_{F} in OFDM-based MIMO systems are also totally independent.

With the independence of transmissions in different symbol slots of (3.25) and different subcarriers of (3.27), the expression of (3.21) for the received value $\underline{e}^{(k_{\mathrm{O}},n_{\mathrm{F}},n_{\mathrm{S}})}$ of the vector output k_{O} of the discrete MIMO channel at subcarrier n_{F} and symbol slot n_{S} using the discrete transfer coefficients $\underline{h}^{(k_{\mathrm{I}},k_{\mathrm{O}},n_{\mathrm{F}})}$, $k_{\mathrm{I}}=1\ldots K_{\mathrm{I}}$, of (3.26) is simplified to

$$
\begin{aligned}
\underline{e}^{(k_{\mathrm{O}},n_{\mathrm{F}},n_{\mathrm{S}})} \; = \; & \sum_{k_{\mathrm{I}}=1}^{K_{\mathrm{I}}} \underline{s}^{(k_{\mathrm{I}},n_{\mathrm{F}},n_{\mathrm{S}})} \int_{-\infty}^{\infty} \underline{b}_{n_{\mathrm{F}},n_{\mathrm{S}}}^{(k_{\mathrm{I}},k_{\mathrm{O}})}(t)\underline{c}_{\mathrm{r},n_{\mathrm{F}},n_{\mathrm{S}}}(-t)\mathrm{d}t \; + \; \underline{n}^{(k_{\mathrm{O}},n_{\mathrm{F}},n_{\mathrm{S}})}, \\
= \; & \sum_{k_{\mathrm{I}}=1}^{K_{\mathrm{I}}} \underline{s}^{(k_{\mathrm{I}},n_{\mathrm{F}},n_{\mathrm{S}})} \underline{h}^{(k_{\mathrm{I}},k_{\mathrm{O}},n_{\mathrm{F}})} \; + \; \underline{n}^{(k_{\mathrm{O}},n_{\mathrm{F}},n_{\mathrm{S}})}.
\end{aligned} \tag{3.28}
$$

demonstrating that each received value $\underline{e}^{(k_{\mathrm{O}},n_{\mathrm{F}},n_{\mathrm{S}})}$ depends solely on the K_{I} transmit values $\underline{s}^{(k_{\mathrm{I}},n_{\mathrm{F}},n_{\mathrm{S}})}$, $k_{\mathrm{I}}=1\ldots K_{\mathrm{I}}$, at the same subcarrier n_{F} and symbol slot n_{S} and the said dependence is quantified by the discrete transfer coefficients $\underline{h}^{(k_{\mathrm{I}},k_{\mathrm{O}},n_{\mathrm{F}})}$ of (3.26). Because at a specific OFDM symbol slot n_{S} each impulse response $\underline{c}_{\mathrm{r},n_{\mathrm{F}},n_{\mathrm{S}}}(t)$ of (3.18) is matched to a section of the combined impulse response $\underline{b}_{n_{\mathrm{F}},n_{\mathrm{S}}}^{(k_{\mathrm{I}},k_{\mathrm{O}})}$ of duration $T_{\mathrm{s}}-T_{\mathrm{h}}$, rather than to the whole combined impulse response $\underline{b}_{n_{\mathrm{F}},n_{\mathrm{S}}}^{(k_{\mathrm{I}},k_{\mathrm{O}})}$ of length $T_{\mathrm{s}}+T_{\mathrm{h}}$, the operation of the analysis filter bank is suboptimum with respect to the exploitation of the energy of the time-continuous received signal $\underline{e}^{(k_{\mathrm{O}})}(t)$ of (3.13) at output k_{O}. This suboptimality is quantified by the energy loss factor

$$
\frac{T_{\mathrm{s}}-T_{\mathrm{h}}}{T_{\mathrm{s}}} < 1. \tag{3.29}
$$

Moreover, with (3.22), the noise values $\underline{n}^{(k_{\mathrm{O}},n_{\mathrm{F}},n_{\mathrm{S}})}$ of (3.28) have the correlation

$$
\begin{aligned}
\mathrm{E}\left\{\underline{n}^{(k_{\mathrm{O}},n_{\mathrm{F}},n_{\mathrm{S}})}\underline{n}^{*(k'_{\mathrm{O}},n'_{\mathrm{F}},n'_{\mathrm{S}})}\right\} &= \mathrm{E}\left\{\int_{-\infty}^{\infty}\underline{n}^{(k_{\mathrm{O}})}(t_1)\underline{c}_{\mathrm{r},n_{\mathrm{F}},n_{\mathrm{S}}}(-t_1)\mathrm{d}t_1\int_{-\infty}^{\infty}\underline{n}^{*(k'_{\mathrm{O}})}(t_2)\underline{c}_{\mathrm{r},n'_{\mathrm{F}},n'_{\mathrm{S}}}(-t_2)\mathrm{d}t_2\right\} \\[2mm]
&= \int_{-\infty}^{\infty}\int_{-\infty}^{\infty}\mathrm{E}\left\{\underline{n}^{(k_{\mathrm{O}})}(t_1)\underline{n}^{*(k'_{\mathrm{O}})}(t_2)\right\}\underline{c}_{\mathrm{r},n_{\mathrm{F}},n_{\mathrm{S}}}(-t_1)\underline{c}_{\mathrm{r},n'_{\mathrm{F}},n'_{\mathrm{S}}}(-t_2)\mathrm{d}t_1\mathrm{d}t_2 \\[2mm]
&= N_0\int_{-\infty}^{\infty}\underline{c}_{\mathrm{r},n_{\mathrm{F}},n_{\mathrm{S}}}(t)\underline{c}_{\mathrm{r},n'_{\mathrm{F}},n'_{\mathrm{S}}}(t)\mathrm{d}t \\[2mm]
&= \begin{cases} N_0 & k_{\mathrm{O}}=k'_{\mathrm{O}},\ n_{\mathrm{F}}=n'_{\mathrm{F}},\ n_{\mathrm{S}}=n'_{\mathrm{S}} \\[2mm] 0 & \text{else} \end{cases}.
\end{aligned} \tag{3.30}
$$

The receiver described by (3.18) and (3.21) corresponds to a conventional OFDM receiver [vNP00].

3.2.5 Matrix-vector transmission model

Due to the independence of transmissions at different subcarriers and symbol slots, a compact subcarrier- and symbol slot wise discrete physical transmission model for OFDM-based MIMO systems is derived. Due to the subcarrier- and symbol slot wise investigation, the transmission over each of the $N_{\mathrm{F}}N_{\mathrm{S}}$ independent $K_{\mathrm{O}}\times K_{\mathrm{I}}$ discrete MIMO channels is modelled separately. To this end, the transmit vector

$$
\underline{\mathbf{s}}^{(n_{\mathrm{F}},n_{\mathrm{S}})} = \left(\underline{s}^{(1,n_{\mathrm{F}},n_{\mathrm{S}})}\dots\underline{s}^{(K_{\mathrm{I}},n_{\mathrm{F}},n_{\mathrm{S}})}\right)^{\mathrm{T}} \tag{3.31}
$$

of dimension K_{I} is formed, containing the K_{I} transmit values $\underline{s}^{(k_{\mathrm{I}},n_{\mathrm{F}},n_{\mathrm{S}})}$, $k_{\mathrm{I}}=1\dots K_{\mathrm{I}}$. Moreover, the received vector

$$
\underline{\mathbf{e}}^{(n_{\mathrm{F}},n_{\mathrm{S}})} = \left(\underline{e}^{(1,n_{\mathrm{F}},n_{\mathrm{S}})}\dots\underline{e}^{(K_{\mathrm{O}},n_{\mathrm{F}},n_{\mathrm{S}})}\right)^{\mathrm{T}} \tag{3.32}
$$

of dimension K_{O}, and the noise vector

$$
\underline{\mathbf{n}}^{(n_{\mathrm{F}},n_{\mathrm{S}})} = \left(\underline{n}^{(1,n_{\mathrm{F}},n_{\mathrm{S}})}\dots\underline{n}^{(K_{\mathrm{O}},n_{\mathrm{F}},n_{\mathrm{S}})}\right)^{\mathrm{T}} \tag{3.33}
$$

of dimension K_{O}, with the autocorrelation matrix

$$
\underline{\mathbf{R}}_{\mathrm{n}} = \mathrm{E}\left\{\underline{\mathbf{n}}^{(n_{\mathrm{F}},n_{\mathrm{S}})}\underline{\mathbf{n}}^{(n_{\mathrm{F}},n_{\mathrm{S}})*\mathrm{T}}\right\} = N_0\,\mathbf{I}_{K_{\mathrm{O}}} \tag{3.34}
$$

are defined, containing the K_O received values $\underline{e}^{(k_O, n_F, n_S)}$, $k_O = 1 \ldots K_O$, and the K_O noise values $\underline{n}^{(k_O, n_F, n_S)}$, $k_O = 1 \ldots K_O$, at subcarrier n_F and symbol slot n_S, respectively. Moreover, the $K_I K_O$ transfer coefficients $\underline{h}^{(k_I, k_O, n_F)}$, $k_I = 1 \ldots K_I$, $k_O = 1 \ldots K_O$, of (3.26) are compiled in the $K_O \times K_I$ channel matrix

$$\underline{\mathbf{H}}^{(n_S, n_F)} = \begin{pmatrix} \underline{h}^{(1,1,n_F)} & \cdots & \underline{h}^{(K_I,1,n_F)} \\ \underline{h}^{(1,2,n_F)} & \cdots & \underline{h}^{(K_I,2,n_F)} \\ \vdots & \ddots & \vdots \\ \underline{h}^{(1,K_O,n_F)} & \cdots & \underline{h}^{(K_I,K_O,n_F)} \end{pmatrix}. \tag{3.35}$$

With $\underline{\mathbf{e}}^{(n_F, n_S)}$ of (3.32), $\underline{\mathbf{H}}^{(n_F)}$ of (3.35), $\underline{\mathbf{s}}^{(n_F, n_S)}$ of (3.31) and $\underline{\mathbf{n}}^{(n_F, n_S)}$ of (3.33), the transmission model

$$\underline{\mathbf{e}}^{(n_F, n_S)} = \underline{\mathbf{H}}^{(n_F)} \underline{\mathbf{s}}^{(n_F, n_S)} + \underline{\mathbf{n}}^{(n_F, n_S)} \tag{3.36}$$

for subcarrier n_F and symbol slot n_S for OFDM-based MIMO systems is derived.

3.3 Pre- and post-processing stages

3.3.1 Optimum and suboptimum approaches

In what follows, transmissions at an isolated OFDM symbol slot n_S are considered, i.e.,

$$N_S = 1 \tag{3.37}$$

holds and consequently the index n_S is hereafter dropped for the sake of simplicity.

In terms of the probability of erroneous detection of $\mathbf{u}^{(k)}$, the optimum strategy regarding pre- and post-processing in Fig. 3.1, is the generation of $\underline{\mathbf{s}}^{(k_I)}$ directly from all $\mathbf{u}^{(k)}$, $k = 1 \ldots K$, and the detection of $\mathbf{u}^{(k)}$ from all $\underline{\mathbf{e}}^{(k_O)}$, $k_O = 1 \ldots K_O$, in one step, respectively [Mas02].

However, such a strategy may not be followed for reasons such as the high complexity. One important class of suboptimum approaches for the pre-processing stages is characterized by a two-step approach. In a first step, after FEC coding and modulation of the bit vectors $\mathbf{u}^{(k)}$ of (3.1), the complex data symbols

$$\underline{d}^{(k, n_F)} \in \mathbb{D}, \; n_F = 1 \ldots N_F, \; k = 1 \ldots K, \tag{3.38}$$

taken from the data symbol alphabet

$$\mathbb{D} = \{\underline{d}_1, \ldots, \underline{d}_D\} \tag{3.39}$$

of cardinality D result. The K data symbols $\underline{d}^{(k,n_\mathrm{F})}$, $k = 1 \ldots K$, of (3.38) corresponding to a single subcarrier n_F are compiled into the data vector

$$\mathbf{d}^{(n_\mathrm{F})} = \left(\underline{d}^{(1,n_\mathrm{F})} \ldots \underline{d}^{(K,n_\mathrm{F})}\right)^\mathrm{T} \tag{3.40}$$

of dimension K, and the N_F data vectors $\mathbf{d}^{(n_\mathrm{F})}$, $n_\mathrm{F} = 1 \ldots N_\mathrm{F}$, of (3.40) are stacked to form the total data vector

$$\mathbf{d} = \left(\mathbf{d}^{(1)\,\mathrm{T}} \ldots \mathbf{d}^{(N_\mathrm{F})\,\mathrm{T}}\right)^\mathrm{T}. \tag{3.41}$$

In a second step, the transmit vectors $\mathbf{s}^{(n_\mathrm{F})}$, $n_\mathrm{F} = 1 \ldots N_\mathrm{F}$, of (3.31) are generated from the total data vector $\mathbf{d}$ of (3.41). In the corresponding class of suboptimum post-processing stages, the estimates

$$\hat{\mathbf{d}}^{(n_\mathrm{F})} = \left(\hat{\underline{d}}^{(1,n_\mathrm{F})} \ldots \hat{\underline{d}}^{(K,n_\mathrm{F})}\right)^\mathrm{T}, \ n_\mathrm{F} = 1 \ldots N_\mathrm{F}, \tag{3.42}$$

of the data vectors $\mathbf{d}^{(n_\mathrm{F})}$, $n_\mathrm{F} = 1 \ldots N_\mathrm{F}$, of (3.40), which can be compiled to the total estimated data vector

$$\hat{\mathbf{d}} = \left(\hat{\mathbf{d}}^{(1)\,\mathrm{T}} \ldots \hat{\mathbf{d}}^{(N_\mathrm{F})\,\mathrm{T}}\right)^\mathrm{T}, \tag{3.43}$$

are obtained from the received vectors $\underline{e}^{(n_\mathrm{F})}$, $n_\mathrm{F} = 1 \ldots N_\mathrm{F}$, of (3.32). In a second step the estimated data symbols $\hat{\underline{d}}^{(k,n_\mathrm{F})}$, $k = 1 \ldots K$, $n_\mathrm{F} = 1 \ldots N_\mathrm{F}$, contained in the estimated data vectors $\hat{\underline{\mathbf{d}}}^{(n_\mathrm{F})}$, $n_\mathrm{F} = 1 \ldots N_\mathrm{F}$, of (3.42) are demodulated and FEC decoded to yield the estimated bit vectors $\hat{\mathbf{u}}^{(k)}$, $k = 1 \ldots K$, of (3.4).

3.3.2 Subcarrierwise pre- and post-processing

In Section 3.2 it is shown that a subcarrierwise model can be used to model the physical transmission in an OFDM-based MIMO system. As transmissions at different subcarriers are independent of each other [vNP00], the subcarrierwise investigation followed in the physical transmission model, under certain circumstances can be extended to the pre- and post processing stages. In particular, if the post-processing stage in an OFDM-based MIMO system operates in a subcarrierwise fashion, then also the pre-processing stage can be implemented in a subcarrierwise manner, without loss of performance. Equivalently, if subcarrierwise pre-processing is applied at the pre-processing stage then the post-processing stage can operate in a subcarrierwise fashion.

In the case that both pre- and post-processing can be performed in a subcarrierwise fashion, an OFDM-based MIMO system employing transmission over N_F subcarriers can be considered as N_F independent smaller multiuser OFDM-based MIMO systems. Moreover, given the usually large number of subcarriers to be used in future mobile radio systems [vNP00], subcarrierwise pre- and post-processing techniques, if applicable, prove to be especially attractive in terms of computational complexity [SWBC02].

4   Uplink transmission in the service area concept

4.1   Transmission model

In this Chapter, the model of the UL with JD in a SA-based mobile radio system employing OFDM is described. Fig. 4.1 illustrates a SA in the UL transmission.
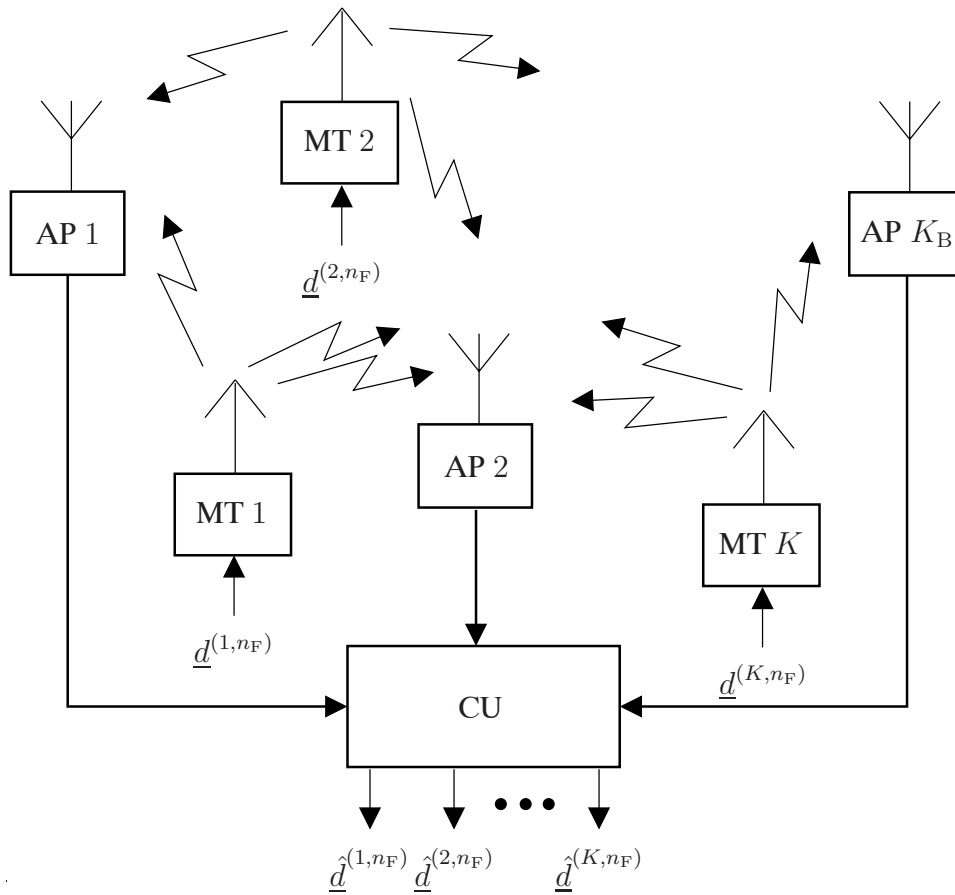
Figure 4.1. SA in UL transmission at subcarrier n_F, consisting of a CU, K MTs and K_B APs

The SA of Fig. 4.1 consists of K MTs, K_B APs and one CU. The K MTs and the K_B APs are equipped each with a single omnidirectional antenna. As stated in Chapter 3, a subcarrierwise physical transmission model can be used. At a certain subcarrier n_F, UL transmission in a SA-based system takes place over a MIMO channel with

$$K_\mathrm{I} = K \qquad (4.1)$$

inputs and

$$K_\mathrm{O} = K_\mathrm{B} \qquad (4.2)$$

outputs. It is assumed that all transfer factors $\underline{h}^{(k,k_\mathrm{B},n_\mathrm{F})}$, $k = 1 \ldots K$, $k_\mathrm{B} = 1 \ldots K_\mathrm{B}$, and hence the $K_\mathrm{B} \times K$ transfer matrix $\underline{\mathbf{H}}^{(n_\mathrm{F})}$ of (3.35), are exactly known at the CU.

Each MT k applies FEC coding on the bit vector $\mathbf{u}^{(k)}$ of (3.1) to yield the coded bit vector

$$\mathbf{d}^{(k)} = \left(d_1^{(k)} \ldots d_M^{(k)} \right)^\mathrm{T} \tag{4.3}$$

of dimension M. After modulation of the coded bit vector $\mathbf{d}^{(k)}$ of (4.3), N_F complex data symbols $\underline{d}^{(k,n_\mathrm{F})}$, $n_\mathrm{F} = 1 \ldots N_\mathrm{F}$, result per MT k. The K complex data symbols $\underline{d}^{(k,n_\mathrm{F})}$, $k = 1 \ldots K$, sent by all the K active MTs at the considered subcarrier n_F, are compiled in the data vector $\underline{\mathbf{d}}^{(n_\mathrm{F})}$ of (3.40) of dimension K. The MTs are simple OFDM transmitters, employing no pre-processing, i.e.,

$$\underline{\mathbf{s}}^{(n_\mathrm{F})} = \underline{\mathbf{d}}^{(n_\mathrm{F})} \tag{4.4}$$

holds for the transmit signal vector $\underline{\mathbf{s}}^{(n_\mathrm{F})}$ of (3.31). With (4.4) and using the $K_\mathrm{B} \times K$ transfer matrix $\underline{\mathbf{H}}^{(n_\mathrm{F})}$ of (3.35), the noise vector $\underline{\mathbf{n}}^{(n_\mathrm{F})}$ of (3.33) of dimension K_B representing inter-SA interference, the expression (3.36) for the received vector $\underline{\mathbf{e}}^{(n_\mathrm{F})}$ of dimension K_B containing the K_B received values $\underline{e}^{(k_\mathrm{B},n_\mathrm{F})}$, $k_\mathrm{B} = 1 \ldots K_\mathrm{B}$, at the K_B APs at subcarrier n_F, becomes

$$\underline{\mathbf{e}}^{(n_\mathrm{F})} = \underline{\mathbf{H}}^{(n_\mathrm{F})} \, \underline{\mathbf{d}}^{(n_\mathrm{F})} + \underline{\mathbf{n}}^{(n_\mathrm{F})} \tag{4.5}$$

for the case of the UL in a SA-based system employing OFDM. With the total data vector

$$\underline{\mathbf{d}} = \left(\underline{\mathbf{d}}^{(1)\,\mathrm{T}} \ldots \underline{\mathbf{d}}^{(N_\mathrm{F})\,\mathrm{T}} \right)^\mathrm{T} \tag{4.6}$$

of dimension $K N_\mathrm{F}$, the $K_\mathrm{B} N_\mathrm{F} \times K N_\mathrm{F}$ total transfer matrix

$$\underline{\mathbf{H}} = \begin{pmatrix} \underline{\mathbf{H}}^{(1)} & \mathbf{0} & \ldots & \mathbf{0} \\ \mathbf{0} & \underline{\mathbf{H}}^{(2)} & \ldots & \mathbf{0} \\ \vdots & \vdots & \ldots & \vdots \\ \mathbf{0} & \mathbf{0} & \ldots & \underline{\mathbf{H}}^{(N_\mathrm{F})} \end{pmatrix}, \tag{4.7}$$

and the total noise vector

$$\underline{\mathbf{n}} = \left(\underline{\mathbf{n}}^{(1)\,\mathrm{T}} \ldots \underline{\mathbf{n}}^{(N_\mathrm{F})\,\mathrm{T}} \right)^\mathrm{T} \tag{4.8}$$

of dimension $K_\mathrm{B} N_\mathrm{F}$, the expression for the total received vector

$$\underline{\mathbf{e}} = \left(\underline{\mathbf{e}}^{(1)\,\mathrm{T}} \ldots \underline{\mathbf{e}}^{(N_\mathrm{F})\,\mathrm{T}} \right)^\mathrm{T} \tag{4.9}$$

of dimension $K_\mathrm{B} N_\mathrm{F}$ becomes

$$\underline{\mathbf{e}} = \underline{\mathbf{H}} \, \underline{\mathbf{d}} + \underline{\mathbf{n}}. \tag{4.10}$$

The expression of (4.10) represents the total transmission model for the UL in a SA-based system.

As can be seen from (4.5) and (4.10), each received value $\underline{e}^{(k_\mathrm{B},n_\mathrm{F})}$ contains contributions from all K data symbols $\underline{d}^{(k,n_\mathrm{F})}$, $k = 1 \ldots K$, sent at the corresponding subcarrier n_F. In SA-based systems, JD is the post-processing algorithm in the CU and the task of JD is to obtain an estimate $\underline{\hat{d}}^{(k,n_\mathrm{F})}$ for each data symbol $\underline{d}^{(k,n_\mathrm{F})}$. From the viewpoint of JD, (4.10) represents N_F independent linear systems of equations, each with K_B equations and K unknowns. In other words, in each of the N_F linear equation systems, K data symbols $\underline{d}^{(k,n_\mathrm{F})}$, $k = 1 \ldots K$, have to be jointly detected from the K_B received values $\underline{e}^{(k_\mathrm{B},n_\mathrm{F})}$, $k_\mathrm{B} = 1 \ldots K_\mathrm{B}$, of (4.5) available to the CU. Such a detection becomes feasible only if

$$K_\mathrm{B} \geq K \tag{4.11}$$

holds, i.e., only if each of the N_F systems of equations is not underdetermined.

In the following algorithms for JD are presented, with the aid of which the spatial receive diversity inherent in the UL transmission of SA-based systems is exploited, i.e., the signals received at the K_B APs are combined targeting at the suppression of the interference between the useful received signals of the active MTs.

4.2 Optimum joint detection

4.2.1 Approaches to optimum post-processing

The approach regarding the post-processing stage at the CU which is optimum with respect to the erroneous decision for the bit $u_l^{(k)}$, is a JD algorithm which, given the total received vector $\underline{e}$ of (4.10), yields the estimate $\hat{u}_l^{(k)}$ with the maximum a posteriori probability $\mathrm{P}\left(\hat{u}_l^{(k)}|\underline{e}\right)$ under consideration of the modulation constellation $\mathbb{D}$ and the FEC code, i.e.,

$$\hat{u}_l^{(k)} = \underset{\hat{u}_l^{(k)} \in \{+1,-1\}}{\arg\max} \left\{ \mathrm{P}\left(\hat{u}_l^{(k)}|\underline{e}\right) \right\}, \; k = 1 \ldots K, \; l = 1 \ldots L, \tag{4.12}$$

holds [Ver86a, Ver86b, Ver98]. However, given practical parametrization of multiuser mobile radio systems, the detector described by (4.12) is not realizable in multiuser scenarios due the high complexity.

In what follows, only JD algorithms are considered which correspond to suboptimum, relative to (4.12), approaches, in which estimates $\underline{\hat{d}}^{(k,n_\mathrm{F})}$ of the data symbols $\underline{d}^{(k,n_\mathrm{F})}$ are obtained in an intermediate step in the JD process, as described in Section 3.3.1. Hence, the term optimum JD is used hereafter to refer to JD algorithms which are optimum with respect to the probability of erroneous detection of the total data vector $\underline{d}$ of (3.41). As described in Section 3.2, each

received value $\underline{e}^{(k_{\mathrm{B}},n_{\mathrm{F}})}$ contains no contributions from data symbols $\underline{d}^{(k,n_{\mathrm{F}}')}$ sent at subcarrier $n_{\mathrm{F}}' \neq n_{\mathrm{F}}$, and therefore optimum JD in a SA-based system can be performed in a subcarrierwise fashion, i.e., optimum JD of the data vector $\underline{\mathbf{d}}^{(n_{\mathrm{F}})}$ of (3.40) from the received vector $\underline{\mathbf{e}}^{(n_{\mathrm{F}})}$ of (3.32) can be performed for each subcarrier n_{F}, $n_{\mathrm{F}} = 1 \dots N_{\mathrm{F}}$, separately [SWBC02].

4.2.2   Maximum a posteriori joint detection

The optimum approach for JD with respect to the probability of erroneous detection of the data vector $\underline{\mathbf{d}}^{(n_{\mathrm{F}})}$ of (3.40) is JD performed according to the MAP principle [Ver86a]. Given the received vector $\underline{\mathbf{e}}^{(n_{\mathrm{F}})}$ of (4.5) and the cardinality D of the data symbol alphabet $\mathbb{D}$ of (3.39), from the D^K possible data vectors $\underline{\hat{\mathbf{d}}}^{(n_{\mathrm{F}})} \in \mathbb{D}^K$ the data vector $\underline{\hat{\mathbf{d}}}^{(n_{\mathrm{F}})}$ yielding the maximum a posteriori probability $\mathrm{P}\left(\underline{\hat{\mathbf{d}}}^{(n_{\mathrm{F}})}|\underline{\mathbf{e}}^{(n_{\mathrm{F}})}\right)$ is chosen as the estimate

$$\underline{\hat{\mathbf{d}}}^{(n_{\mathrm{F}})} = \arg\max_{\underline{\hat{\mathbf{d}}}^{(n_{\mathrm{F}})} \in \mathbb{D}^K} \left\{ \mathrm{P}\left(\underline{\hat{\mathbf{d}}}^{(n_{\mathrm{F}})}|\underline{\mathbf{e}}^{(n_{\mathrm{F}})}\right) \right\} \tag{4.13}$$

according to optimum JD.

4.2.3   Maximum likelihood joint detection

With the conditional probability density function $\mathrm{p}\left(\underline{\mathbf{e}}^{(n_{\mathrm{F}})} \mid \underline{\hat{\mathbf{d}}}^{(n_{\mathrm{F}})}\right)$ of the received vector $\underline{\mathbf{e}}^{(n_{\mathrm{F}})}$ of (4.5), the probability density function $\mathrm{p}\left(\underline{\mathbf{e}}^{(n_{\mathrm{F}})}\right)$ of the received vector $\underline{\mathbf{e}}^{(n_{\mathrm{F}})}$ of (4.5) and the a priori probability $\mathrm{P}\left(\underline{\hat{\mathbf{d}}}^{(n_{\mathrm{F}})}\right)$ of the data vector $\underline{\hat{\mathbf{d}}}^{(n_{\mathrm{F}})}$, the Bayes rule [Pap00] can be applied on the a posteriori probability $\mathrm{P}\left(\underline{\hat{\mathbf{d}}}^{(n_{\mathrm{F}})}|\underline{\mathbf{e}}^{(n_{\mathrm{F}})}\right)$ of the data vector $\underline{\hat{\mathbf{d}}}^{(n_{\mathrm{F}})}$ of (3.40), to yield

$$\mathrm{P}\left(\underline{\hat{\mathbf{d}}}^{(n_{\mathrm{F}})}|\underline{\mathbf{e}}^{(n_{\mathrm{F}})}\right) = \frac{1}{\mathrm{p}\left(\underline{\mathbf{e}}^{(n_{\mathrm{F}})}\right)} \mathrm{p}\left(\underline{\mathbf{e}}^{(n_{\mathrm{F}})} \mid \underline{\hat{\mathbf{d}}}^{(n_{\mathrm{F}})}\right) \mathrm{P}\left(\underline{\hat{\mathbf{d}}}^{(n_{\mathrm{F}})}\right). \tag{4.14}$$

If the data vectors $\underline{\hat{\mathbf{d}}}^{(n_{\mathrm{F}})}$ in (4.14) are equiprobable, the probability $\mathrm{P}\left(\underline{\hat{\mathbf{d}}}^{(n_{\mathrm{F}})}\right)$ plays no role in the maximization process of (4.13). Moreover, the probability density function $\mathrm{p}\left(\underline{\mathbf{e}}^{(n_{\mathrm{F}})}\right)$ of the received vector $\underline{\mathbf{e}}^{(n_{\mathrm{F}})}$ in (4.14) is independent of the considered vector $\underline{\mathbf{d}}^{(n_{\mathrm{F}})}$ and can therefore be omitted in the maximization process. Hence, in the case of equiprobable data vectors $\underline{\hat{\mathbf{d}}}^{(n_{\mathrm{F}})}$ the maximization of the a posteriori probability $\mathrm{P}\left(\underline{\hat{\mathbf{d}}}^{(n_{\mathrm{F}})}|\underline{\mathbf{e}}^{(n_{\mathrm{F}})}\right)$ in (4.13) is equivalent with the maximization of the likelihood function $\mathrm{p}\left(\underline{\mathbf{e}}^{(n_{\mathrm{F}})} \mid \underline{\hat{\mathbf{d}}}^{(n_{\mathrm{F}})}\right)$ due to (4.14), and the MAP detector of (4.13) becomes the ML detector [Ver98]

$$\underline{\hat{\mathbf{d}}}^{(n_{\mathrm{F}})} = \arg\max_{\underline{\hat{\mathbf{d}}}^{(n_{\mathrm{F}})} \in \mathbb{D}^K} \left\{ \mathrm{p}\left(\underline{\mathbf{e}}^{(n_{\mathrm{F}})} \mid \underline{\hat{\mathbf{d}}}^{(n_{\mathrm{F}})}\right) \right\}. \tag{4.15}$$

For the case of zero-mean, Gaussian distributed and uncorrelated noise values $\underline{n}^{(k_\mathrm{B},n_\mathrm{F})}$, $k_\mathrm{B} = 1 \ldots K_\mathrm{B}$, with variance σ^2 of real and imaginary parts, for the likelihood function

$$\mathrm{p}\left(\underline{\mathbf{e}}^{(n_\mathrm{F})}|\underline{\hat{\mathbf{d}}}^{(n_\mathrm{F})}\right) = \frac{1}{(\pi\sigma^2)^{K_\mathrm{B}}} \exp\left\{-\frac{1}{\sigma^2}\left\|\underline{\mathbf{e}}^{(n_\mathrm{F})} - \underline{\mathbf{H}}^{(n_\mathrm{F})}\underline{\hat{\mathbf{d}}}^{(n_\mathrm{F})}\right\|^2\right\} \tag{4.16}$$

follows and ML JD of (4.15) takes the simplified form

$$\underline{\hat{\mathbf{d}}}^{(n_\mathrm{F})} = \underset{\underline{\hat{\mathbf{d}}}^{(n_\mathrm{F})}\in\mathbb{D}^K}{\arg\min}\left\{\left\|\underline{\mathbf{e}}^{(n_\mathrm{F})} - \underline{\mathbf{H}}^{(n_\mathrm{F})}\underline{\hat{\mathbf{d}}}^{(n_\mathrm{F})}\right\|^2\right\}. \tag{4.17}$$

4.2.4 Complexity of optimum joint detection

In order to detect all N_F data vectors $\underline{\mathbf{d}}^{(n_\mathrm{F})}$, $n_\mathrm{F} = 1 \ldots N_\mathrm{F}$, both MAP JD of (4.13) and ML JD of (4.15) involve in total N_F exhaustive search processes among the set $\mathbb{D}^K$ of cardinality D^K. As the aforementioned search is the complexity dominating process, the computational complexity of subcarrierwise optimum JD is $\mathcal{O}\left(N_\mathrm{F}\,D^K\right)$.

If subcarrierwise optimum JD were not possible, exhaustive search among all elements of the set $\mathbb{D}^{KN_\mathrm{F}}$ of cardinality D^{KN_F} would have to be performed in order to detect the total data vector $\underline{\mathbf{d}} \in \mathbb{D}^{KN_\mathrm{F}}$ and the complexity of such a detection would be $\mathcal{O}\left(D^{KN_\mathrm{F}}\right)$. Hence,

$$\mathcal{O}\left(N_\mathrm{F}\,D^K\right) \ll \mathcal{O}\left(D^{KN_\mathrm{F}}\right) \tag{4.18}$$

readily holds. The decisive reduction in computational complexity needed to perform optimum JD in OFDM-based MIMO systems is clear. Hence, from (4.18), the application of optimum JD in the form of MAP or ML JD can be considered in OFDM-based MIMO systems, e.g., in SA-based systems.

4.3 Linear joint detection

4.3.1 General model of linear joint detection

Despite of the reduction in the computational complexity of optimum JD achieved thanks to the subcarrierwise detection in SA-based systems, the computational complexity due to the exhaustive search involved in both MAP and ML JD may still be undesired. Representing a trade-off between probability of erroneous decision for $\underline{\mathbf{d}}^{(n_\mathrm{F})}$ and complexity, linear JD algorithms yield

the estimate $\hat{\underline{\mathbf{d}}}^{(n_{\mathrm{F}})}$ of $\underline{\mathbf{d}}^{(n_{\mathrm{F}})}$ through a linear transformation of the received vector $\underline{\mathbf{e}}^{(n_{\mathrm{F}})}$. There-fore, linear JD algorithms can be described by a $K \times K_{\mathrm{B}}$ demodulator matrix $\underline{\mathbf{D}}^{(n_{\mathrm{F}})}$ as

$$\hat{\underline{\mathbf{d}}}^{(n_{\mathrm{F}})} = \underline{\mathbf{D}}^{(n_{\mathrm{F}})} \underline{\mathbf{e}}^{(n_{\mathrm{F}})}. \tag{4.19}$$

As (4.19) shows, in contrast to MAP JD of (4.13) and ML JD of (4.15) in linear JD the knowledge concerning the modulation constellation $\mathbb{D}$ is not exploited, i.e., $\hat{\underline{\mathbf{d}}}^{(n_{\mathrm{F}})} \in \mathbb{C}^K$ follows for the estimated data vector $\hat{\underline{\mathbf{d}}}^{(n_{\mathrm{F}})}$ obtained by linear JD as shown in (4.19).

Depending on the criterion which $\hat{\underline{\mathbf{d}}}^{(n_{\mathrm{F}})}$ of (4.19) should satisfy, there exist numerous possibilities for the choice of the demodulator matrix $\underline{\mathbf{D}}^{(n_{\mathrm{F}})}$. In the following, the cases of RxZF JD and MMSE JD are considered.

4.3.2   Receive zero-forcing joint detection

According to the RxZF criterion, with the received vector $\underline{\mathbf{e}}^{(n_{\mathrm{F}})}$ of (3.36) and the transfer matrix $\underline{\mathbf{H}}^{(n_{\mathrm{F}})}$ of (3.35), the estimate $\hat{\underline{\mathbf{d}}}^{(n_{\mathrm{F}})}$ of the data vector $\underline{\mathbf{d}}^{(n_{\mathrm{F}})}$ minimizes the Euclidean distance $\left\| \underline{\mathbf{e}}^{(n_{\mathrm{F}})} - \underline{\mathbf{H}}^{(n_{\mathrm{F}})} \hat{\underline{\mathbf{d}}}^{(n_{\mathrm{F}})} \right\|^2$, or in other words, the estimated data vector $\hat{\underline{\mathbf{d}}}^{(n_{\mathrm{F}})}$ is chosen, from which the reconstructed received vector $\underline{\mathbf{H}}^{(n_{\mathrm{F}})} \hat{\underline{\mathbf{d}}}^{(n_{\mathrm{F}})}$ with the minimum Euclidean distance to the received vector $\underline{\mathbf{e}}^{(n_{\mathrm{F}})}$ results. The criterion of RxZF JD is expressed as [KB92, KB93, Kle96, BFKM93, FKB94, LV90]

$$\hat{\underline{\mathbf{d}}}^{(n_{\mathrm{F}})} = \underset{\hat{\underline{\mathbf{d}}}^{(n_{\mathrm{F}})'} \in \mathbb{C}^K}{\arg \min} \left\{ \left\| \underline{\mathbf{e}}^{(n_{\mathrm{F}})} - \underline{\mathbf{H}}^{(n_{\mathrm{F}})} \hat{\underline{\mathbf{d}}}^{(n_{\mathrm{F}})'} \right\|^2 \right\}. \tag{4.20}$$

Comparing (4.17) and (4.20) it follows that in the case of zero-mean Gaussian noise, ML JD and the RxZF JD have similar criteria. The difference between ML JD and the RxZF JD is that the estimated data symbols $\hat{\underline{d}}^{(k,n_{\mathrm{F}})}$, $k = 1 \ldots K$, of (4.20) of RxZF JD can take any continuous value from $\mathbb{C}$, whereas the estimates $\hat{\underline{d}}^{(k,n_{\mathrm{F}})}$, $k = 1 \ldots K$, of ML JD of (4.17) can only take the D discrete values of $\mathbb{D}$.

With the received vector $\underline{\mathbf{e}}^{(n_{\mathrm{F}})}$ of (3.36), the transfer matrix $\underline{\mathbf{H}}^{(n_{\mathrm{F}})}$ of (3.35), the expression

$$\hat{\underline{\mathbf{d}}}^{(n_{\mathrm{F}})} = \underbrace{\left(\underline{\mathbf{H}}^{(n_{\mathrm{F}})*\mathrm{T}} \underline{\mathbf{H}}^{(n_{\mathrm{F}})} \right)^{-1} \underline{\mathbf{H}}^{(n_{\mathrm{F}})*\mathrm{T}}}_{\underline{\mathbf{D}}_{\mathrm{RxZF}}^{(n_{\mathrm{F}})}} \underline{\mathbf{e}}^{(n_{\mathrm{F}})} \tag{4.21}$$

for the estimated data vector $\hat{\underline{\mathbf{d}}}^{(n_{\mathrm{F}})}$ of RxZF JD follows from (4.20). As (4.21) shows, $\underline{\mathbf{D}}_{\mathrm{RxZF}}^{(n_{\mathrm{F}})}$ is the left side pseudoinverse of the channel matrix $\underline{\mathbf{H}}^{(n_{\mathrm{F}})}$. Moreover, for deterministic $\underline{\mathbf{H}}^{(n_{\mathrm{F}})}$ and random $\underline{\mathbf{n}}^{(n_{\mathrm{F}})}$, the estimated data vector $\hat{\underline{\mathbf{d}}}^{(n_{\mathrm{F}})}$ of (4.21) of RxZF JD satisfies

$$\mathrm{E}\left\{ \hat{\underline{\mathbf{d}}}^{(n_{\mathrm{F}})} \right\} = \underline{\mathbf{d}}^{(n_{\mathrm{F}})}, \tag{4.22}$$

i.e., RxZF JD delivers unbiased estimates $\hat{\underline{d}}^{(k,n_{\mathrm{F}})}$, $k = 1 \ldots K$, of the data symbols $\underline{d}^{(k,n_{\mathrm{F}})}$, $k = 1 \ldots K$, eliminating all intra-SA interference.

As opposed to RxZF JD for CDMA systems [KB92, KB93, Kle96, BFKM93] by which MTs in a cell are separated based on their channel signatures and CDMA codes, RxZF JD in SA-based systems eliminates intra-SA interference using only the channel signatures of the K MTs inherent in the transfer matrix $\underline{\mathbf{H}}^{(n_{\mathrm{F}})}$. Due to the spatial separation of the APs the transfer matrix $\underline{\mathbf{H}}^{(n_{\mathrm{F}})}$ has, if special cases are not considered, full rank and can be used for the spatial separation of the MTs.

4.3.3   Minimum mean square error joint detection

The criterion which the estimated data vector $\hat{\underline{\mathbf{d}}}^{(n_{\mathrm{F}})}$ of MMSE JD satisfies is the MMSE error $\min \left\{ \mathrm{E} \left\{ \left\| \underline{\mathbf{d}}^{(n_{\mathrm{F}})} - \hat{\underline{\mathbf{d}}}^{(n_{\mathrm{F}})'} \right\|^{2} \right\} \right\}$, hence for deterministic $\underline{\mathbf{H}}^{(n_{\mathrm{F}})}$ and random $\underline{\mathbf{n}}^{(n_{\mathrm{F}})}$, the MMSE JD criterion is expressed as [MH94, Gra81, LV89, XSR90, LV90, BFKM93, KKKB94, KKKB96]

$$\hat{\underline{\mathbf{d}}}^{(n_{\mathrm{F}})} = \underset{\hat{\underline{\mathbf{d}}}^{(n_{\mathrm{F}})'} \in \mathbb{C}^{K}}{\arg \min} \left\{ \mathrm{E} \left\{ \left\| \underline{\mathbf{d}}^{(n_{\mathrm{F}})} - \hat{\underline{\mathbf{d}}}^{(n_{\mathrm{F}})'} \right\|^{2} \right\} \right\}. \tag{4.23}$$

With the correlation matrix

$$\underline{\mathbf{R}}_{\mathrm{dd}}^{(n_{\mathrm{F}})} = \mathrm{E} \left\{ \underline{\mathbf{d}}^{(n_{\mathrm{F}})} \underline{\mathbf{d}}^{(n_{\mathrm{F}})*\mathrm{T}} \right\} \tag{4.24}$$

of the data vector $\underline{\mathbf{d}}^{(n_{\mathrm{F}})}$, the received vector $\underline{\mathbf{e}}^{(n_{\mathrm{F}})}$ of (3.36), the transfer matrix $\underline{\mathbf{H}}^{(n_{\mathrm{F}})}$ of (3.35) and the variance σ^{2} of real and imaginary parts of the noise values $\underline{n}^{(k_{\mathrm{B}},n_{\mathrm{F}})}$, $k_{\mathrm{B}} = 1 \ldots K_{\mathrm{B}}$, MMSE JD is expressed as

$$\hat{\underline{\mathbf{d}}}^{(n_{\mathrm{F}})} = \underbrace{\left(\underline{\mathbf{H}}^{(n_{\mathrm{F}})*\mathrm{T}} \underline{\mathbf{H}}^{(n_{\mathrm{F}})} + \sigma^{2} \underline{\mathbf{R}}_{\mathrm{dd}}^{(n_{\mathrm{F}})-1} \right)^{-1} \underline{\mathbf{H}}^{(n_{\mathrm{F}})*\mathrm{T}}}_{\underline{\mathbf{D}}_{\mathrm{MMSE}}^{(n_{\mathrm{F}})}} \underline{\mathbf{e}}^{(n_{\mathrm{F}})}. \tag{4.25}$$

From (4.25) it can be seen that MMSE JD of (4.25), unlike RxZF JD of (4.21), does not deliver unbiased estimates. Instead, in the case of the the MMSE JD, as compared to RxZF JD, information concerning the reliability of the estimated data symbols $\hat{\underline{d}}^{(k,n_{\mathrm{F}})}$ is additionally taken into account. In particular, for a low noise power σ^{2}, the MMSE JD demodulator matrix $\underline{\mathbf{D}}_{\mathrm{MMSE}}^{(n_{\mathrm{F}})}$ of (4.25) converges towards the demodulator matrix $\underline{\mathbf{D}}_{\mathrm{RxZF}}^{(n_{\mathrm{F}})}$ of (4.21) of RxZF JD but for high noise levels an all-zero estimated vector $\hat{\underline{\mathbf{d}}}^{(n_{\mathrm{F}})}$ is obtained.

In comparison to MMSE JD for CDMA systems [MH94, Gra81, LV89, XSR90, LV90, BFKM93, KKKB94, KKKB96], in which the MMSE criterion of (4.23) is applied in each cell using the channel matrix and the CDMA component, in the case of MMSE JD for SA-based systems only the transfer matrix $\underline{\mathbf{H}}^{(n_{\mathrm{F}})}$ is used to suppress the intra-SA interference.

4.4 Iterative joint detection

4.4.1 General model of iterative joint detection

JD can also be realized in an iterative fashion [Lam00b, Lam00a, DSR98, PH94, Var95, KIHP90]. The data detection model according to iterative JD is illustrated in Fig. 4.2. As shown in Fig. 4.2,
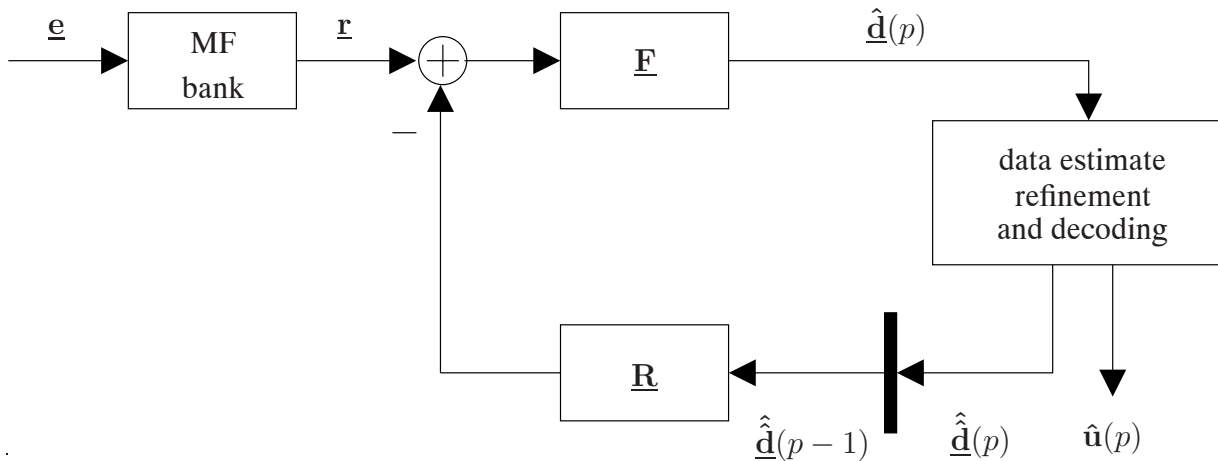
Figure 4.2. Iterative JD model with data estimate refinement

in iterative JD the estimate $\hat{\mathbf{u}}(p)$ of the bit vector $\mathbf{u}$ is the output of each iteration p, $p = 1 \ldots P$. In order to yield the estimated bit vector $\hat{\mathbf{u}}(p)$ in each iteration p, a refined version $\hat{\underline{\hat{\mathbf{d}}}}(p-1)$ of the total estimated data vector $\underline{\hat{\mathbf{d}}}(p-1)$ of iteration $p-1$ is used to reconstruct the intra-SA interference by the aid of the reverse path matrix $\underline{\mathbf{R}}$. The reconstructed intra-SA interference $\underline{\mathbf{R}}\,\hat{\underline{\hat{\mathbf{d}}}}(p-1)$ is then subtracted from the output

$$\underline{\mathbf{r}} = \underline{\mathbf{H}}^{*\mathrm{T}}\underline{\mathbf{e}} \tag{4.26}$$

of a MF bank, and after multiplication with the forward path matrix $\underline{\mathbf{F}}$, the total data vector estimate $\underline{\hat{\mathbf{d}}}(p)$ results from which the estimated bit vector $\hat{\mathbf{u}}(p)$ follows by means of demodulation and FEC decoding.

Due to the iterative character of JD, intra-SA interference is removed by means of subtraction rather than by exhaustive search as in optimum JD in Section 4.2, or by matrix inversion as in linear JD in Section 4.3. As no significant advantage regarding complexity is gained by performing iterative JD in a subcarrierwise fashion, nonsubcarrierwise iterative JD is considered.

The forward path matrix $\underline{\mathbf{F}}$ and reverse path matrix $\underline{\mathbf{R}}$ used in iterative JD are chosen based on the criteria described in Section 4.4.2. For given forward path matrix $\underline{\mathbf{F}}$ and reverse path matrix

$\underline{\mathbf{R}}$, iterative JD variants differ in the choice of the data estimate refinement and decoding block. In what follows, four cases of data estimate refinement techniques, by which also decoding is performed, are considered. In cases in which the operation of the described block does not depend on the iteration index p, p is omitted for the sake of simplicity in the following. Finally, considerations are performed for the case of BPSK modulation and can also be directly extended to QPSK modulated data symbols.

4.4.2 Transparent data estimate refinement

The most trivial data estimate refinement technique for iterative JD is to perform transparent data estimate refinement as Fig. 4.3 shows, i.e.,

$$\hat{\hat{\underline{\mathbf{d}}}} = \hat{\underline{\mathbf{d}}}. \tag{4.27}$$

holds. In the case of transparent data estimate refinement, issues regarding the convergence of iterative JD can be analytically investigated. If iterative JD with transparent data estimate refinement converges, then after an infinitely large number of iterations the limiting value of the total estimated data vector $\hat{\underline{\mathbf{d}}}(\infty)$ is obtained. With the forward path matrix $\underline{\mathbf{F}}$ and the reverse path matrix $\underline{\mathbf{R}}$ follows for the limiting value $\hat{\underline{\mathbf{d}}}(\infty)$ of the total estimated data vector

$$\begin{aligned} \hat{\underline{\mathbf{d}}}(\infty) &= \underline{\mathbf{F}}\,\underline{\mathbf{r}} - \underline{\mathbf{F}}\,\underline{\mathbf{R}}\,\hat{\underline{\mathbf{d}}}(\infty) \\ &= \left(\underline{\mathbf{F}}^{-1} + \underline{\mathbf{R}}\right)^{-1}\underline{\mathbf{r}}. \end{aligned} \tag{4.28}$$

Hence, if iterative JD with transparent data estimate refinement converges, then the limiting value $\hat{\underline{\mathbf{d}}}(\infty)$ of the total estimated data vector is equal to the total estimated data vector $\hat{\underline{\mathbf{d}}}$ of a linear estimator characterized by the demodulator matrix

$$\underline{\mathbf{D}}_\infty = \left(\underline{\mathbf{F}}^{-1} + \underline{\mathbf{R}}\right)^{-1}\underline{\mathbf{H}}^{*\mathrm{T}}. \tag{4.29}$$

From (4.29) it can be seen that depending on $\underline{\mathbf{F}}$ and $\underline{\mathbf{R}}$ the convergence of iterative JD with transparent data estimate refinement to any desired linear JD scheme can be achieved. For example, with the matrix operator $\mathrm{diag}\,(\cdot)$ returning a matrix with the elements on the main diagonal of its matrix argument, and the operator $\overline{\mathrm{diag}}\,(\cdot)$ returning a matrix with the offdiagonal elements of its matrix argument, choosing

$$\underline{\mathbf{F}} = \left(\mathrm{diag}\left(\underline{\mathbf{H}}^{*\mathrm{T}}\underline{\mathbf{H}}\right)\right)^{-1} \tag{4.30}$$

and

$$\underline{\mathbf{R}} = \overline{\mathrm{diag}}\left(\underline{\mathbf{H}}^{*\mathrm{T}}\underline{\mathbf{H}}\right) \tag{4.31}$$

it can be achieved that iterative JD with transparent data estimate refinement, if convergent, converges towards RxZF JD.
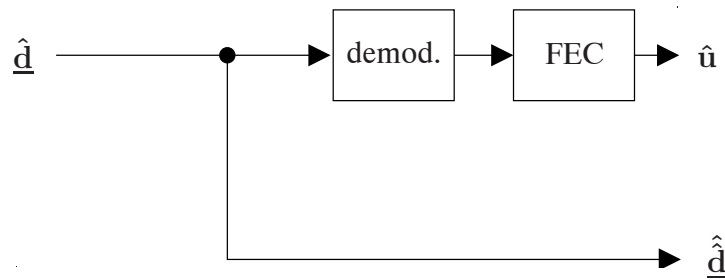
Figure 4.3. Data estimate refinement and decoding block of iterative JD with transparent data estimate refinement

Until now, the limiting value of iterative JD with transparent data estimate refinement is dealt with. Regarding the criterion of convergence, the spectral radius [Sch88b] $\lambda_{\max}(\underline{\mathbf{X}})$ of a complex matrix $\underline{\mathbf{X}}$ with Q eigenvalues $\underline{\lambda}_q$, $q = 1 \ldots Q$, is introduced. The spectral radius $\lambda_{\max}(\underline{\mathbf{X}})$ of $\underline{\mathbf{X}}$ is defined as [Sch88b]

$$\lambda_{\max}(\underline{\mathbf{X}}) = \max\left\{|\underline{\lambda}_1|, \ldots, |\underline{\lambda}_Q|\right\}. \tag{4.32}$$

With the $KN_{\mathrm{F}} \times KN_{\mathrm{F}}$ product $\underline{\mathbf{F}}\,\underline{\mathbf{R}}$ of the forward path matrix $\underline{\mathbf{R}}$ and reverse path matrix $\underline{\mathbf{F}}$, it has been shown [TR00] that iterative JD with transparent data estimate refinement converges if

$$\lambda_{\max}(\underline{\mathbf{F}}\,\underline{\mathbf{R}}) \leq 1 \tag{4.33}$$

holds, i.e., if all Q eigenvalues $\underline{\lambda}_q$, $q = 1 \ldots Q$, of $\underline{\mathbf{F}}\,\underline{\mathbf{R}}$ lie within the bounds of the unity circle around the origin of the complex plane.

4.4.3 Data estimate refinement by hard quantization

A first step towards the refinement of the total estimated data vector $\hat{\underline{\mathbf{d}}}$ is to exploit the knowledge of the modulation constellation $\mathbb{D}^{KN_{\mathrm{F}}}$ in the data estimate refinement process, as Fig. 4.4 shows.

In this case, data estimate refinement consists in quantizing the continuous valued elements $\hat{\underline{d}}^{(k,n_{\mathrm{F}})}$ of the total estimated data vector $\hat{\underline{\mathbf{d}}}$ with respect to the modulation constellation $\mathbb{D}$, to yield the total refined estimate

$$\hat{\hat{\underline{\mathbf{d}}}} = \arg\min_{\underline{\mathbf{d}} \in \mathbb{D}^{KN_{\mathrm{F}}}}\left\{\left\|\hat{\underline{\mathbf{d}}} - \underline{\mathbf{d}}\right\|^2\right\}. \tag{4.34}$$

of the data vector $\underline{\mathbf{d}}$.
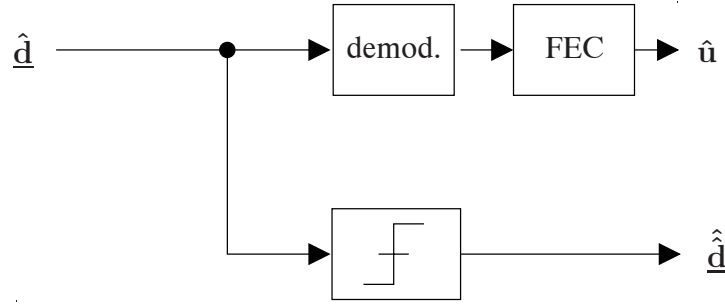
Figure 4.4. Data estimate refinement and decoding block of iterative JD with data estimate refinement by hard quantization

4.4.4 Data estimate refinement by soft quantization

Data estimate refinement by soft quantization is an improvement of the data estimate refinement by hard quantization, in which the reliability of each estimated coded bit $\hat{d}_m^{(k)}$ is taken into account. Fig. 4.5 shows the model for iterative JD with data estimate refinement by soft quantization.
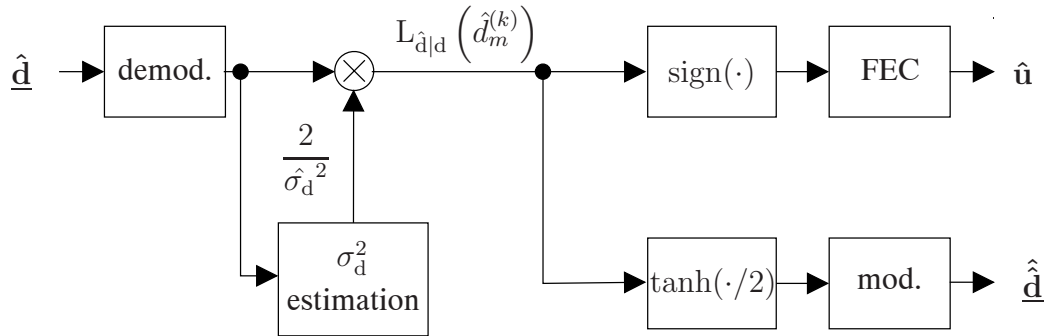
Figure 4.5. Data estimate refinement and decoding block of iterative JD with data estimate refinement by soft quantization

Soft quantization is the data estimate refinement technique which minimizes the error [MH97, Lam00b, INF01, WOWB02, MW03]

$$E\left\{\left(\hat{\hat{d}}_m^{(k)} - d_m^{(k)}\right)^2 \bigg| \hat{d}_m^{(k)}\right\} = \left(\hat{\hat{d}}_m^{(k)} - E\left\{d_m^{(k)} | \hat{d}_m^{(k)}\right\}\right)^2 + \text{var}\left\{d_m^{(k)} | \hat{d}_m^{(k)}\right\}. \tag{4.35}$$

The error $E\left\{\left(\hat{\hat{d}}_m^{(k)} - d_m^{(k)}\right)^2 \bigg| \hat{d}_m^{(k)}\right\}$ of (4.35) becomes minimal if the refined estimate

$$\hat{\hat{d}}_m^{(k)} = E\left\{d_m^{(k)} | \hat{d}_m^{(k)}\right\} \tag{4.36}$$

is chosen. In the case of BPSK, the log-likelihood ratio [Hag97]

$$L_{d|\hat{d}}\left(\hat{d}_m^{(k)}\right) = \ln\left(\frac{P\left(d_m^{(k)} = +1|\hat{d}_m^{(k)}\right)}{P\left(d_m^{(k)} = -1|\hat{d}_m^{(k)}\right)}\right) \tag{4.37}$$

of the a posteriori probabilities $P\left(d_m^{(k)} = \pm 1|\hat{d}_m^{(k)}\right)$ of the coded bit $d_m^{(k)}$ is used to complement the hard decision for $d_m^{(k)}$, expressed by the sign of $L_{d|\hat{d}}\left(\hat{d}_m^{(k)}\right)$ with reliability information expressed by the magnitude of $L_{d|\hat{d}}\left(\hat{d}_m^{(k)}\right)$ [Hag97].

The log-likelihood ratio $L_{d|\hat{d}}\left(\hat{d}_m^{(k)}\right)$ of (4.37) can be expressed depending on the conditional probabilities $P\left(\hat{d}_m^{(k)}|d_m^{(k)} \pm 1\right)$ of the estimated coded bit $\hat{d}_m^{(k)}$ and on the a priori probabilities $P\left(d_m^{(k)} = \pm 1\right)$ of the coded bit $d_m^{(k)}$ as

$$L_{d|\hat{d}}\left(\hat{d}_m^{(k)}\right) = \underbrace{\ln\left(\frac{P\left(\hat{d}_m^{(k)}|d_m^{(k)} = +1\right)}{P\left(\hat{d}_m^{(k)}|d_m^{(k)} = -1\right)}\right)}_{L_{\hat{d}|d}\left(\hat{d}_m^{(k)}\right)} + \ln\left(\frac{P\left(d_m^{(k)} = +1\right)}{P\left(d_m^{(k)} = -1\right)}\right). \tag{4.38}$$

With (4.37), and assuming that all coded bits $d_m^{(k)}$, $k = 1\ldots K$, $m = 1\ldots M$, are equiprobable, i.e.

$$\ln\left(\frac{P\left(d_m^{(k)} = +1\right)}{P\left(d_m^{(k)} = -1\right)}\right) = 0, \; k = 1\ldots K, \; m = 1\ldots M, \tag{4.39}$$

holds,

$$P\left(\hat{d}_m^{(k)}|d_m^{(k)} = +1\right) = \frac{\exp\left\{L_{\hat{d}|d}\left(\hat{d}_m^{(k)}\right)\big/2\right\}}{\exp\left\{L_{\hat{d}|d}\left(\hat{d}_m^{(k)}\right)\big/2\right\} + \exp\left\{-L_{\hat{d}|d}\left(\hat{d}_m^{(k)}\right)\big/2\right\}} \tag{4.40}$$

and

$$P\left(\hat{d}_m^{(k)}|d_m^{(k)} = -1\right) = \frac{\exp\left\{-L_{\hat{d}|d}\left(\hat{d}_m^{(k)}\right)\big/2\right\}}{\exp\left\{L_{\hat{d}|d}\left(\hat{d}_m^{(k)}\right)\big/2\right\} + \exp\left\{-L_{\hat{d}|d}\left(\hat{d}_m^{(k)}\right)\big/2\right\}} \tag{4.41}$$

follow and using (4.40) and (4.41), (4.36) becomes

$$\hat{\hat{d}}_m^{(k)} = \tanh\left(\frac{L_{\hat{d}|d}\left(\hat{d}_m^{(k)}\right)}{2}\right). \tag{4.42}$$

To calculate the refined estimate $\hat{\hat{d}}_m^{(k)}$ as in (4.42), the log-likelihood ratio $L_{\hat{d}|d}\left(\hat{d}_m^{(k)}\right)$, i.e., the probabilities $P\left(\hat{d}_m^{(k)}|d_m^{(k)} = \pm 1\right)$, need to be calculated. To accomplish this task, it is assumed that zero-mean additive white Gaussian noise $\tilde{n}_\mathrm{d}$ with variance σ_d^2 disturbes the estimated coded bits

$$\hat{d}_m^{(k)} = d_m^{(k)} + \tilde{n}_\mathrm{d}. \tag{4.43}$$

Hence, with the probability density function

$$p_{\hat{d}}\left(\hat{d}_m^{(k)}|d_m^{(k)} = \pm 1\right) = \frac{1}{\sqrt{2\pi}\sigma_\mathrm{d}} \exp\left(-\frac{1}{2\sigma_\mathrm{d}^2}\left(\hat{d}_m^{(k)} \mp 1\right)^2\right) \tag{4.44}$$

of $\hat{d}_m^{(k)}$ and the corresponding log-likelihood ratio

$$L_{\hat{d}|d}\left(\hat{d}_m^{(k)}\right) = \frac{2\hat{d}_m^{(k)}}{\sigma_\mathrm{d}^2}, \tag{4.45}$$

the refined estimate

$$\hat{\hat{d}}_m^{(k)} = \tanh\left(\frac{\hat{d}_m^{(k)}}{\sigma_\mathrm{d}^2}\right) \tag{4.46}$$

of the coded bit $d_m^{(k)}$ can be calculated from (4.42).

Therefore by iterative JD with data estimate refinement by soft quantization, in each iteration intra-SA interference is reconstructed using the refined estimates $\hat{\hat{d}}_m^{(k)}$, $k = 1 \ldots K$, $m = 1 \ldots M$, of (4.46) of the coded bits $d_m^{(k)}$, $k = 1 \ldots K$, $m = 1 \ldots M$ and subsequently subtracted from the output $\underline{r}$ of the MF bank of (4.26). In the present Section it is shown that the data estimate refinement error $E\left\{\left(\hat{\hat{d}}_m^{(k)} - d_m^{(k)}\right)^2 \Big| \hat{d}_m^{(k)}\right\}$ of (4.35) is minimized if the continuous valued refined estimate $\hat{\hat{d}}_m^{(k)}$ of (4.46) is used for the discrete valued coded bit $d_m^{(k)} \in \{-1, +1\}$.

4.4.5 Optimum data estimate refinement — turbo multiuser data detection

The data estimate refinement techniques described in Sections 4.4.3 and 4.4.4 are based on quantization, i.e., on the exploitation of information regarding the modulation alphabet $\mathbb{D}$. As by means of FEC coding, information concerning one bit $u_l^{(k)}$, is spread over more than one coded bit estimate $\hat{d}_m^{(k)}$, any approach not exploiting this knowledge is in its nature suboptimum. A data estimate refinement and decoding block in which the refined estimated vector $\hat{\underline{\hat{d}}}$ is gained by means of optimum MAP evaluation of the FEC code is shown in Fig. 4.6.
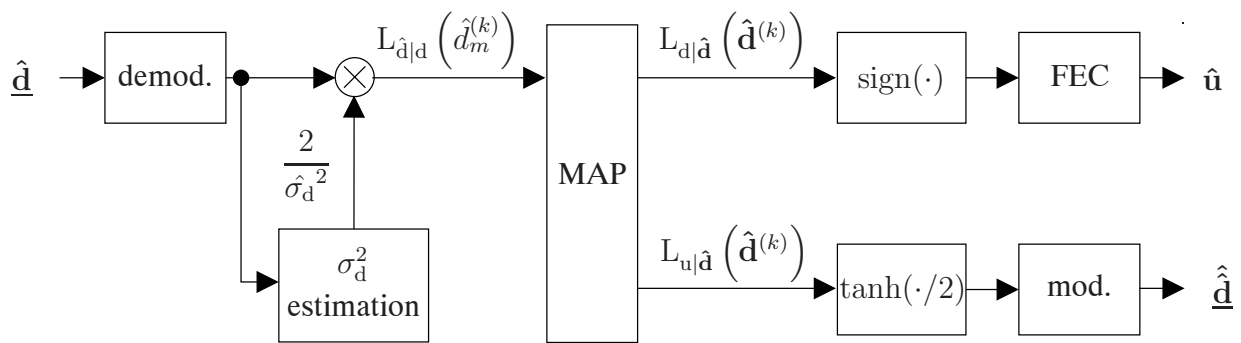
Figure 4.6. Data estimate refinement and decoding block of iterative JD with optimum data estimate refinement

The criterion of optimum data estimate refinement is similar to the criterion of (4.35) of data estimate refinement with soft quantization. In particular, using the estimate

$$\hat{\mathbf{d}}^{(k)} = \left(\hat{d}_1^{(k)} \dots \hat{d}_M^{(k)} \right)^{\mathrm{T}}, \qquad (4.47)$$

of the coded bit vector $\mathbf{d}^{(k)}$ of (4.3), the exploitation of the FEC code knowledge in the case of optimum data estimate refinement alters (4.35) to the criterion [WOWB02]

$$\mathrm{E}\left\{ \left(\hat{\hat{d}}_m^{(k)} - d_m^{(k)} \right)^2 \Big| \hat{\mathbf{d}}^{(k)} \right\} = \left(\hat{\hat{d}}_m^{(k)} - \mathrm{E}\left\{ d_m^{(k)} | \hat{\mathbf{d}}^{(k)} \right\} \right)^2 + \mathrm{var}\left\{ d_m^{(k)} | \hat{\mathbf{d}}^{(k)} \right\} \qquad (4.48)$$

of optimum data estimate refinement. By exploiting knowledge concerning FEC coding, not just a single estimated coded bit $\hat{d}_m^{(k)}$ as in (4.35), but the whole coded estimated bit vector $\hat{\mathbf{d}}^{(k)}$ of (4.47) is taken into account. The error $\mathrm{E}\left\{ \left(\hat{\hat{d}}_m^{(k)} - d_m^{(k)} \right)^2 \Big| \hat{\mathbf{d}}^{(k)} \right\}$ of (4.48) becomes minimum if the refined estimates

$$\hat{\hat{d}}_m^{(k)} = \mathrm{E}\left\{ d_m^{(k)} | \hat{\mathbf{d}}^{(k)} \right\}, \ k = 1 \dots K, \ m = 1 \dots M, \qquad (4.49)$$

of the coded bits $\hat{\hat{d}}_m^{(k)}$, $k = 1 \dots K$, $m = 1 \dots M$, are chosen by the refinement procedure. If BPSK is used, the log-likelihood ratio

$$\mathrm{L}_{\mathrm{d}|\hat{\mathbf{d}}}\left(\hat{\mathbf{d}}^{(k)} \right) = \ln \left(\frac{\mathrm{P}\left(d_m^{(k)} = +1 | \hat{\mathbf{d}}^{(k)} \right)}{\mathrm{P}\left(d_m^{(k)} = -1 | \hat{\mathbf{d}}^{(k)} \right)} \right) \qquad (4.50)$$

of the a posteriori probabilities

$$\mathrm{P}\left(d_m^{(k)} = \pm 1 | \hat{\mathbf{d}}^{(k)} \right) = \sum_{\mathbf{d}^{(k)} | \mathbf{d}^{(k)} \in \mathbb{D}^K \wedge d_m^{(k)} = \pm 1} \mathrm{P}\left(\hat{\mathbf{d}}^{(k)} | \mathbf{d}^{(k)} \right) \qquad (4.51)$$

can be used, from which with (4.50), the refined estimate

$$\hat{\hat{d}}_m^{(k)} = \tanh \left(\frac{\mathrm{L}_{\mathrm{d}|\hat{\mathbf{d}}}\left(\hat{\mathbf{d}}^{(k)} \right)}{2} \right) \qquad (4.52)$$

of each coded bit $d_m^{(k)}$ can be calculated.

An algorithm with the aid of which the log-likelihood ratios $L_{d|\hat{d}}\left(\hat{\mathbf{d}}^{(k)}\right)$, $k = 1 \ldots K$, $m = 1 \ldots M$, of (4.50) can be calculated is the Bahl Cocke Jelinek Raviv (BCJR) algorithm [BCJR74]. The BCJR algorithm is a soft-input-soft-output MAP symbol by symbol detector, which takes the log-likelihood ratios $L_{\hat{d}|d}\left(\hat{d}_m^{(k)}\right)$, $k = 1 \ldots K$, $m = 1 \ldots M$, as inputs. At its output the BCJR algorithm provides the log-likelihood ratios $L_{d|\hat{d}}\left(\hat{\mathbf{d}}^{(k)}\right)$, $k = 1 \ldots K$, $m = 1 \ldots M$, of (4.50) from which the refined estimates $\hat{\hat{d}}_m^{(k)}$, $k = 1 \ldots K$, $m = 1 \ldots M$, of the coded bits $d_m^{(k)}$, $m = 1 \ldots M$, $k = 1 \ldots K$, can be calculated according to (4.52), and $L_{u|\hat{d}}\left(\hat{\mathbf{d}}^{(k)}\right)$, $k = 1 \ldots K$, from which the estimates

$$\hat{u}_l^{(k)} = \text{sign}\left(L_{u|\hat{d}}\left(\hat{\mathbf{d}}^{(k)}\right)\right), \, l = 1 \ldots L, \, k = 1 \ldots K, \tag{4.53}$$

of the bits $u_l^{(k)}$, $l = 1 \ldots L$, $k = 1 \ldots K$, can be calculated by means of hard quantization as Fig. 4.6 shows, i.e., the BCJR algorithm also performs FEC decoding [BCJR74].

With a closer look at Figs. 4.2 and 4.6, one can see that the iterative JD detector with optimum data estimate refinement by means of FEC coding evaluation is comprised of two parts. The part evaluating the FEC code, see Fig. 4.6, and the remaining part performing multiuser detection, see Fig. 4.2. In contrast to serial multiuser detection schemes, the two parts of the iterative JD detector of 4.2 and Fig. 4.6 exchange soft information. Hence, iterative JD with optimum data estimate refinement by means of FEC coding evaluation is a multiuser detector following the turbo principle [Hag97, Poo00].

It is therefore shown how turbo multiuser detection [Hag97, Poo00] can be used as an iterative JD algorithm in the CU in SA-based systems. From the said employment of iterative JD with optimum data estimate refinement, knowledge concerning the FEC code additionally to the knowledge of the spatial signatures of the MTs, contained in the total transfer matrix $\underline{\mathbf{H}}$, is exploited to combat intra-SA interference in an efficient way and to provide a high spectrum capacity η_c of (1.1) in SA-based systems.

5 Downlink transmission in the service area concept

5.1 Transmission model

After having dealt with the UL with JD in Chapter 4, the modelling of the DL with JT forms the topic of the present Chapter. In Fig. 5.1 a SA with a CU, K_B APs and K MTs in DL transmission is illustrated.
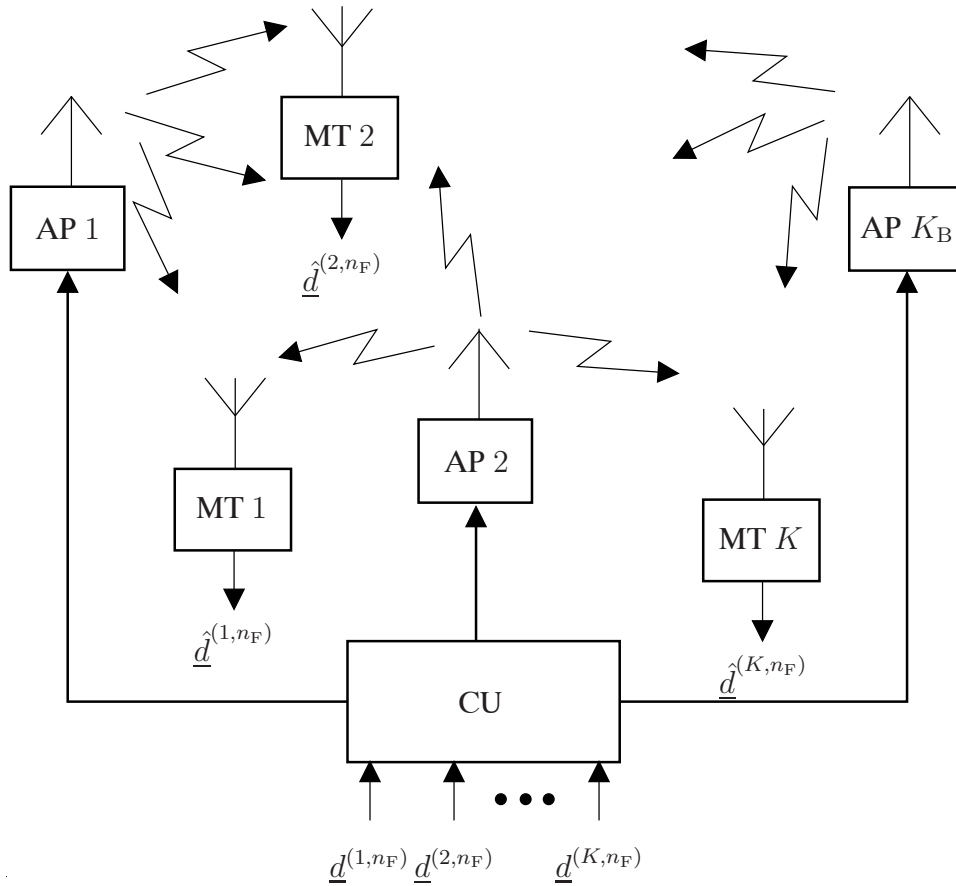
Figure 5.1. SA in DL transmission at subcarrier n_F, consisting of a CU, K MTs and K_B APs

The transmission model for the DL can be derived in a subcarrierwise fashion, following the argumentation of Chapter 3. At a specific subcarrier n_F, K data symbols $\underline{d}^{(k,n_F)}$, $k = 1 \ldots K$, have to be sent from the core network to the K MTs. From the K data symbols $\underline{d}^{(k,n_F)}$, $k = 1 \ldots K$, contained in the data vector $\underline{\mathbf{d}}^{(n_F)}$ of (3.40), K_B AP-specific transmit values $\underline{s}^{(k_B,n_F)}$, $k_B = 1 \ldots K_B$, contained in the transmit vector $\underline{\mathbf{s}}^{(n_F)}$ of (3.31) are generated by the CU, and are fed into the MIMO channel of the SA with

$$K_I = K_B \tag{5.1}$$

inputs and

$$K_{\mathrm{O}} = K \tag{5.2}$$

outputs.

If TDD is employed and the time elapsing between UL and DL transmission is sufficiently smaller than the coherence time of the wireless channel of the SA, reciprocity characterizes the channels of UL and DL. Therefore, as the $K_{\mathrm{B}} \times K$ transfer matrix $\underline{\mathbf{H}}^{(n_{\mathrm{F}})}$ is used in the physical transmission model for the UL of (4.10), the $K \times K_{\mathrm{B}}$ transfer matrix $\underline{\mathbf{H}}^{(n_{\mathrm{F}})\mathrm{T}}$ is used to model the physical transmission in the DL. Furthermore, it is assumed that all transfer factors $\underline{h}^{(k,k_{\mathrm{B}},n_{\mathrm{F}})}$, $k = 1 \ldots K$, $k_{\mathrm{B}} = 1 \ldots K_{\mathrm{B}}$, and hence the $K \times K_{\mathrm{B}}$ transfer matrix $\underline{\mathbf{H}}^{(n_{\mathrm{F}})\mathrm{T}}$ are exactly known to the CU.

With the transmit vector $\underline{\mathbf{s}}^{(n_{\mathrm{F}})}$ of (3.31) of dimension K_{B}, the $K \times K_{\mathrm{B}}$ transfer matrix $\underline{\mathbf{H}}^{(n_{\mathrm{F}})\mathrm{T}}$ and the noise vector $\underline{\mathbf{n}}^{(n_{\mathrm{F}})}$ of (3.33) of dimension K, the expression for the received vector

$$\underline{\mathbf{e}}^{(n_{\mathrm{F}})} = \underline{\mathbf{H}}^{(n_{\mathrm{F}})\mathrm{T}}\, \underline{\mathbf{s}}^{(n_{\mathrm{F}})} + \underline{\mathbf{n}}^{(n_{\mathrm{F}})} \tag{5.3}$$

of (3.32) of dimension K at subcarrier n_{F} follows. Furthermore, using the total transmit vector

$$\underline{\mathbf{s}} = \left(\underline{\mathbf{s}}^{(1)\mathrm{T}} \ldots \underline{\mathbf{s}}^{(N_{\mathrm{F}})\mathrm{T}}\right)^{\mathrm{T}} \tag{5.4}$$

of dimension $K_{\mathrm{B}}N_{\mathrm{F}}$, the $KN_{\mathrm{F}} \times K_{\mathrm{B}}N_{\mathrm{F}}$ total transfer matrix $\underline{\mathbf{H}}^{\mathrm{T}}$ and the total noise vector

$$\underline{\mathbf{n}} = \left(\underline{\mathbf{n}}^{(1)\mathrm{T}} \ldots \underline{\mathbf{n}}^{(N_{\mathrm{F}})\mathrm{T}}\right)^{\mathrm{T}} \tag{5.5}$$

of dimension KN_{F}, (5.3) can be extended to include transmissions at all N_{F} subcarriers yielding the total received vector

$$\underline{\mathbf{e}} = \underline{\mathbf{H}}^{\mathrm{T}}\, \underline{\mathbf{s}} + \underline{\mathbf{n}} \tag{5.6}$$

of dimension KN_{F}.

Each MT k, $k = 1 \ldots K$, contains a simple OFDM receiver employing no post-processing, taking the received value $\underline{e}^{(k,n_{\mathrm{F}})}$ as the estimated data symbol $\hat{\underline{d}}^{(k,n_{\mathrm{F}})}$, i.e., the expression

$$\hat{\underline{\mathbf{d}}}^{(n_{\mathrm{F}})} = \underline{\mathbf{e}}^{(n_{\mathrm{F}})} \tag{5.7}$$

describes the function of the K MTs as receivers. Under consideration of (5.7), the crux of JT consists in generating at each subcarrier n_{F} the K_{B} transmit values $\underline{s}^{(k_{\mathrm{B}},n_{\mathrm{F}})}$, $k_{\mathrm{B}} = 1 \ldots K_{\mathrm{B}}$, jointly for all K MTs. As is the case in the UL transmission, it is assumed that

$$K_{\mathrm{B}} \geq K \tag{5.8}$$

holds, i.e., each of the N_F systems of equations for determining the K_B transmit values $\underline{s}^{(k_\mathrm{B},n_\mathrm{F})}$, $k_\mathrm{B} = 1 \ldots K_\mathrm{B}$, from the K data symbols $\underline{d}^{(k,n_\mathrm{F})}$, $k = 1 \ldots K$, is underdetermined.

By the employment of the JT algorithms presented in the following, the spatial transmit diversity in the DL transmission of SA-based systems is exploited and such transmit signals are generated by JT by the transmission of which interference between the active MTs is suppressed.

5.2   Optimum joint transmission

5.2.1   Introduction

In the present Section, a novel nonlinear JT scheme is presented, which is optimum with respect to the average bit error probability $\overline{P}_\mathrm{b}^{(n_\mathrm{F})}$ at the MTs. In contrast to approaches to a minimum BER transmission for the DL of state-of-the-art CDMA mobile radio systems, see, e.g., [IRF03], a flexible and compact model characterizes the optimum nonlinear JT scheme for SA-based systems, due to the fact that optimum JT can be performed in a subcarrierwise fashion. In what follows, the term optimum JT is used to denote JT which is optimum in the sense of the average bit error probability $\overline{P}_\mathrm{b}^{(n_\mathrm{F})}$ at the MTs. For the sake of simplicity, investigations are carried out using real signals. The extension to complex valued signals is straightforward and can be performed by considering the real valued equivalent isomorphic form of the complex signals [ZF86].

With respect to the average bit error probability $\overline{P}_\mathrm{b}^{(n_\mathrm{F})}$ the transmission of data vectors $\underline{\mathbf{d}}^{(n_\mathrm{F})}, \underline{\mathbf{d}}^{(n_\mathrm{F})'} \in \mathbb{D}^K$, where the data vector $\underline{\mathbf{d}}^{(n_\mathrm{F})'}$ is a rotated version of the data vector $\underline{\mathbf{d}}^{(n_\mathrm{F})}$, is equivalent, which means that the investigation of both data vectors $\underline{\mathbf{d}}^{(n_\mathrm{F})'}$ and $\underline{\mathbf{d}}^{(n_\mathrm{F})}$ in terms of the average bit error probability $\overline{P}_\mathrm{b}^{(n_\mathrm{F})}$ is redundant. Equivalently, the set $\mathbb{D}^K$ of the data vectors contains V effective data vectors $\underline{\mathbf{d}}_v^{(n_\mathrm{F})}$, $v = 1 \ldots V$, which contribute to the average bit error probability $\overline{P}_\mathrm{b}^{(n_\mathrm{F})}$ and $D^K - V$ data vectors which result from the V effective data vectors $\underline{\mathbf{d}}_v^{(n_\mathrm{F})}$, $v = 1 \ldots V$, by means of a rotation operation and do not contribute to the average bit error probability $\overline{P}_\mathrm{b}^{(n_\mathrm{F})}$. Hence, for the purposes of investigation of the average bit error probability $\overline{P}_\mathrm{b}^{(n_\mathrm{F})}$, it suffices to consider the set

$$\mathbb{D}_\mathrm{eff}^K = \left\{ \underline{\mathbf{d}}_1^{(n_\mathrm{F})}, \ldots, \underline{\mathbf{d}}_V^{(n_\mathrm{F})} \right\} \subset \mathbb{D}^K \tag{5.9}$$

of effective data vectors $\underline{\mathbf{d}}_v^{(n_\mathrm{F})}$, $v = 1 \ldots V$, of cardinality V instead of the set $\mathbb{D}^K$ of cardinality D^K. For a given modulation scheme the choice of the effective data vectors $\underline{\mathbf{d}}_v^{(n_\mathrm{F})} \in \mathbb{D}_\mathrm{eff}^K$ is not unique, whereas the cardinality V of the set $\mathbb{D}_\mathrm{eff}^K$ of (5.9) of effective data vectors is fixed. In this thesis, optimum JT with BPSK is investigated, i.e.,

$$\mathbb{D} = \{+1, -1\} \tag{5.10}$$

holds, and the set $\mathbb{D}_{\text{eff}}^K$ of (5.9) of effective data vectors has the cardinality

$$\left| \mathbb{D}_{\text{eff}}^K \right| = V = 2^{K-1}. \tag{5.11}$$

The task of optimum JT is to determine for each subcarrier n_{F} an effective transmit vector $\underline{\mathbf{s}}_v^{(n_{\text{F}})}$ of dimension K_{B} for each effective data vector $\underline{\mathbf{d}}_v^{(n_{\text{F}})}$ of (5.9) of dimension K which, given a specific scenario, results in the minimum possible average bit error probability $\overline{P}_{\text{b}}^{(n_{\text{F}})}$ at the MTs. With the set

$$\mathbb{S}_{\text{eff}}^{(n_{\text{F}})} = \left\{ \underline{\mathbf{s}}_1^{(n_{\text{F}})}, \ldots, \underline{\mathbf{s}}_V^{(n_{\text{F}})} \right\} \tag{5.12}$$

of effective transmit vectors $\underline{\mathbf{s}}_v^{(n_{\text{F}})}$, $v = 1 \ldots V$, of cardinality V and the set $\mathbb{D}_{\text{eff}}^K$ of (5.9) of effective data vectors, JT is described with a mapping function

$$f^{(n_{\text{F}})} : \mathbb{D}_{\text{eff}}^K \longrightarrow \mathbb{S}_{\text{eff}}^{(n_{\text{F}})} \tag{5.13}$$

with which the set $\mathbb{D}_{\text{eff}}^K$ of (5.9) of effective data vectors is mapped to the set $\mathbb{S}_{\text{eff}}^{(n_{\text{F}})}$ of (5.12) of effective transmit vectors. In the case of optimum JT, the mapping function $f^{(n_{\text{F}})}$ of (5.13) is nonlinear in contrast to linear JT schemes in the case of which $f^{(n_{\text{F}})}$ is linear.

In order to investigate optimum JT, a novel parameterized representation of JT transmit signals for the case of BPSK is developed and presented in this Chapter. It is shown that in the considered model, the average bit error probability $\overline{P}_{\text{b}}^{(n_{\text{F}})}$ is a function of the parameters describing the transmitted signal and that the parameter set corresponding to optimum JT results after numerical minimization. For the considerations concerning optimum JT, DL transmission without FEC coding is considered and therefore optimum JT is derived in a subcarrierwise fashion.

5.2.2 Transmit energy strategies

Two different strategies concerning the transmit energy

$$T_{\text{tot},v}^{(n_{\text{F}})} = \frac{1}{2} \underline{\mathbf{s}}_v^{(n_{\text{F}})*\text{T}} \underline{\mathbf{s}}_v^{(n_{\text{F}})} \tag{5.14}$$

of each effective transmit vector $\underline{\mathbf{s}}_v^{(n_{\text{F}})}$ can be followed, namely

- fixed transmit energy $T_{\text{tot},v}^{(n_{\text{F}})}$ and

- variable transmit energy $T_{\text{tot},v}^{(n_{\text{F}})}$.

With the V transmit energies $T_{\text{tot},v}^{(n_{\text{F}})}$, $v = 1 \ldots V$, of (5.14), the transmit energy T per data symbol and the number K of MTs, it is assumed that the average energy

$$\overline{T}_{\text{tot},v}^{(n_{\text{F}})} = \frac{1}{V} \sum_{v=1}^{V} T_{\text{tot},v}^{(n_{\text{F}})} = KT \tag{5.15}$$

is fixed.

According to the fixed transmit energy strategy, each effective transmit vector $\underline{\mathbf{s}}_v^{(n_{\text{F}})}$ has a fixed given transmit energy

$$T_{\text{tot},v}^{(n_{\text{F}})} = KT. \tag{5.16}$$

On the other hand, in the case of the variable transmit energy strategy, the transmit energy $T_{\text{tot},v}^{(n_{\text{F}})}$
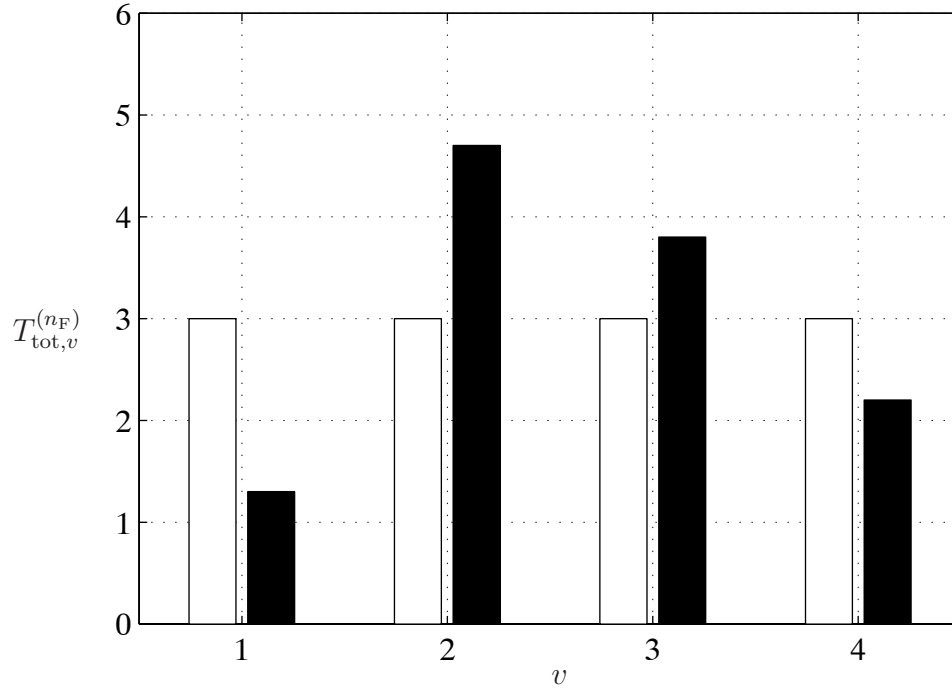
Figure 5.2. Exemplary case for the energy $T_{\text{tot},v}^{(n_{\text{F}})}$ of each effective transmit vector $\underline{\mathbf{s}}_v^{(n_{\text{F}})}$, $v = 1 \ldots V$, as a function of v, according to the variable transmit energy strategy (black bars) and fixed transmit energy strategy (white bars); Parameters: $K = 3$, $T = 1$

is fixed only at the average, i.e., the average value $\overline{T}_{\text{tot},v}^{(n_{\text{F}})}$ of (5.15) is given. Fig. 5.2 illustrates the two strategies for $T_{\text{tot},v}^{(n_{\text{F}})}$ of (5.14) for the case of $K = 3$ and $T = 1$.

With the vector

$$\underline{\mathbf{s}}_{0,v}^{(n_{\text{F}})} = \left(\underline{s}_{0,v}^{(1,n_{\text{F}})} \ldots \underline{s}_{0,v}^{(K_{\text{B}},n_{\text{F}})} \right)^{\text{T}} \tag{5.17}$$

of dimension K_{B}, which is normalized as

$$
\frac{1}{2} \underline{\mathbf{s}}_{0,v}^{(n_{\mathrm{F}})*\mathrm{T}} \underline{\mathbf{s}}_{0,v}^{(n_{\mathrm{F}})} = KT, \tag{5.18}
$$

and with the energy factor $t_v^{(n_{\mathrm{F}})}$, the effective transmit vector $\underline{\mathbf{s}}_v^{(n_{\mathrm{F}})}$ is expressed as

$$
\underline{\mathbf{s}}_v^{(n_{\mathrm{F}})} = t_v^{(n_{\mathrm{F}})} \underline{\mathbf{s}}_{0,v}^{(n_{\mathrm{F}})}. \tag{5.19}
$$

Using (5.14) and (5.18), it can be seen from (5.19) that the energy

$$
T_{\mathrm{tot},v}^{(n_{\mathrm{F}})} = t_v^{(n_{\mathrm{F}})2} KT \tag{5.20}
$$

of each effective transmit vector $\underline{\mathbf{s}}_v^{(n_{\mathrm{F}})}$, $v = 1 \ldots V$, is completely determined by the energy factor $t_v^{(n_{\mathrm{F}})}$. For example, it can be deduced from (5.16) and (5.20) that the fixed transmit energy strategy can be realized by setting

$$
t_v^{(n_{\mathrm{F}})} = 1, \ v = 1 \ldots V. \tag{5.21}
$$

5.2.3 Parameterized representation of JT transmit signals

The crux of the parameterized representation of JT signals consists in the expression of the vector $\mathbf{s}_{0,v}^{(n_{\mathrm{F}})}$ of (5.17) and the energy factor $t_v^{(n_{\mathrm{F}})}$ in a coordinate system, which is an extension of the spherical coordinate system in multidimensional spaces. The used coordinates are denoted as generalized spherical coordinates.

With the $K_{\mathrm{B}} - 1$ angles $\varphi_v^{(k_{\mathrm{B}},n_{\mathrm{F}})} \in [-\pi, \pi]$, $k_{\mathrm{B}} = 1 \ldots K_{\mathrm{B}} - 1$, and with the dummy angle

$$
\varphi_v^{(K_{\mathrm{B}},n_{\mathrm{F}})} = 0, \tag{5.22}
$$

the K_{B} elements $s_{0,v}^{(k_{\mathrm{B}},n_{\mathrm{F}})}$, $k_{\mathrm{B}} = 1 \ldots K_{\mathrm{B}}$, of the vector $\mathbf{s}_{0,v}^{(n_{\mathrm{F}})}$ of (5.17) can be expressed with the aid of generalized spherical coordinates as

$$
s_{0,v}^{(k_{\mathrm{B}},n_{\mathrm{F}})} = \sqrt{2KT} \prod_{k_{\mathrm{B}}'=1}^{k_{\mathrm{B}}-1} \sin\left(\varphi_v^{(k_{\mathrm{B}}',n_{\mathrm{F}})}\right) \cos\left(\varphi_v^{(k_{\mathrm{B}},n_{\mathrm{F}})}\right), \ k_{\mathrm{B}} = 1 \ldots K_{\mathrm{B}}. \tag{5.23}
$$

Moreover, with the $V - 1$ angles $\vartheta_v^{(n_{\mathrm{F}})} \in [0, \pi/2]$, $v = 1 \ldots V - 1$, and the dummy angle

$$
\vartheta_V^{(n_{\mathrm{F}})} = 0, \tag{5.24}
$$

follows for the energy factor

$$
t_v^{(n_{\mathrm{F}})} = \sqrt{V} \prod_{v'=1}^{v-1} \sin\left(\vartheta_{v'}^{(n_{\mathrm{F}})}\right) \cos\left(\vartheta_v^{(n_{\mathrm{F}})}\right). \tag{5.25}
$$

Using $s_{0,v}^{(k_\mathrm{B},n_\mathrm{F})}$ of (5.23) and $t_v^{(n_\mathrm{F})}$ of (5.25) follows from (5.19) that the set $\mathbb{S}_{\mathrm{eff}}^{(n_\mathrm{F})}$ of effective transmit vectors $\mathbf{s}_v^{(n_\mathrm{F})}$, $v = 1 \ldots V$, and hence a given JT scheme, is fully described by the $(K_\mathrm{B} - 1)V$ angles $\varphi_v^{(k_\mathrm{B},n_\mathrm{F})}$, $k_\mathrm{B} = 1 \ldots K_\mathrm{B} - 1$, $v = 1 \ldots V$, and the $V - 1$ angles $\vartheta_v^{(n_\mathrm{F})}$, $v = 1 \ldots V - 1$. For

$$K_\mathrm{B} = 2 \tag{5.26}$$

and

$$K_\mathrm{B} = 3 \tag{5.27}$$

the used generalized spherical coordinates are equivalent to polar and spherical coordinates, respectively. In the case of fixed transmit energy strategy, Figs. 5.3 and 5.4 and illustrate the constraint of (5.16) for the transmit energy $T_{\mathrm{tot},v}^{(n_\mathrm{F})}$ of the effective transmit signal vector $\mathbf{s}_v^{(n_\mathrm{F})}$ in a geometric fashion. In particular, Fig. 5.3 shows that in the case of (5.26) $\mathbf{s}_v^{(n_\mathrm{F})}$ lies on the periphery of the unity circle whereas according to Fig. 5.4, if (5.27) holds, $\mathbf{s}_v^{(n_\mathrm{F})}$ lies on the surface of the unity sphere.

Figure 5.3. Representation of the energy constraint for the effective transmit vector $\mathbf{s}_v^{(n_\mathrm{F})}$; Parameters: $K_\mathrm{B} = 2$, $K = 2$, fixed transmit energy strategy

Equivalently, the $(K_\mathrm{B} - 1)V$ angles $\varphi_v^{(k_\mathrm{B},n_\mathrm{F})}$, $k_\mathrm{B} = 1 \ldots K_\mathrm{B} - 1$, $v = 1 \ldots V$, and the $V - 1$ angles $\vartheta_v^{(n_\mathrm{F})}$, $v = 1 \ldots V - 1$, corresponding to a given JT scheme can be calculated from given

effective transmit signal vectors $\mathbf{s}_v^{(n_{\mathrm{F}})}$. Introducing the four-quadrant arcus tangent function

$$
\arctan2(x, y) = \begin{cases} \arctan\left(\dfrac{x}{y}\right) & \text{for } y \geq 0, \\[2mm] \arctan\left(\dfrac{x}{y}\right) + \pi & \text{for } y < 0, x > 0, \\[2mm] \arctan\left(\dfrac{x}{y}\right) - \pi & \text{for } y < 0, x < 0, \end{cases} \tag{5.28}
$$

using (5.19) and (5.23), the $(K_{\mathrm{B}} - 1)V$ angles

$$
\varphi_v^{(k_{\mathrm{B}}, n_{\mathrm{F}})} = \arctan2\left(s_v^{(k_{\mathrm{B}}+1, n_{\mathrm{F}})}, \cos\left(\varphi_v^{(k_{\mathrm{B}}+1, n_{\mathrm{F}})}\right) s_v^{(k_{\mathrm{B}}, n_{\mathrm{F}})}\right), \ k_{\mathrm{B}} = K_{\mathrm{B}} - 1 \ldots 1, \ v = 1 \ldots V,
$$
$$\tag{5.29}$$

and with $T_{\mathrm{tot}, v}^{(n_{\mathrm{F}})}$, $v = 1 \ldots V$, of (5.20) the $V - 1$ angles

$$
\vartheta_v^{(n_{\mathrm{F}})} = \arctan2\left(\sqrt{\sum_{v'=v+1}^{V} T_{\mathrm{tot}, v'}^{(n_{\mathrm{F}})}}, \sqrt{T_{\mathrm{tot}, v}^{(n_{\mathrm{F}})}}\right), \ v = 1 \ldots V - 1, \tag{5.30}
$$

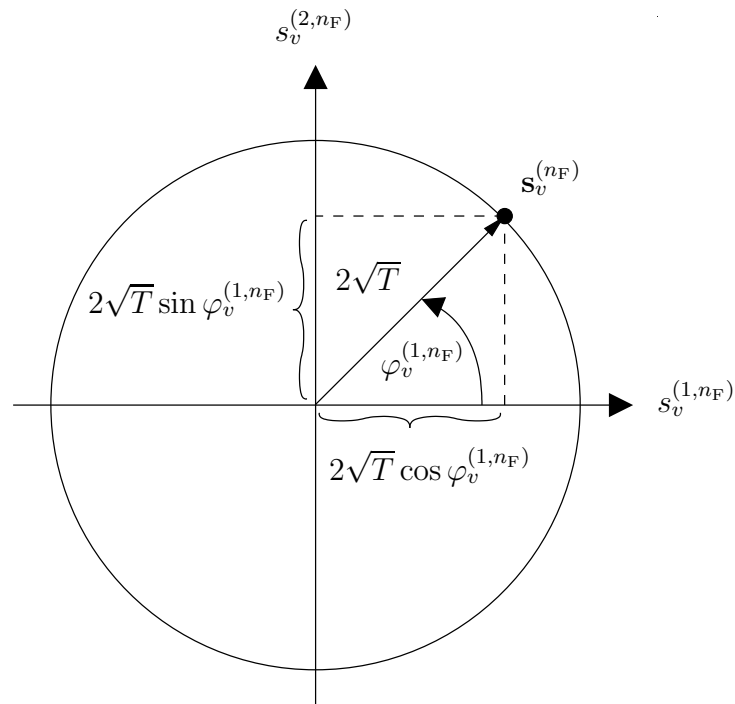can be calculated from given effective transmit signal vectors $\mathbf{s}_v^{(n_{\mathrm{F}})}$, $v = 1 \ldots V$.
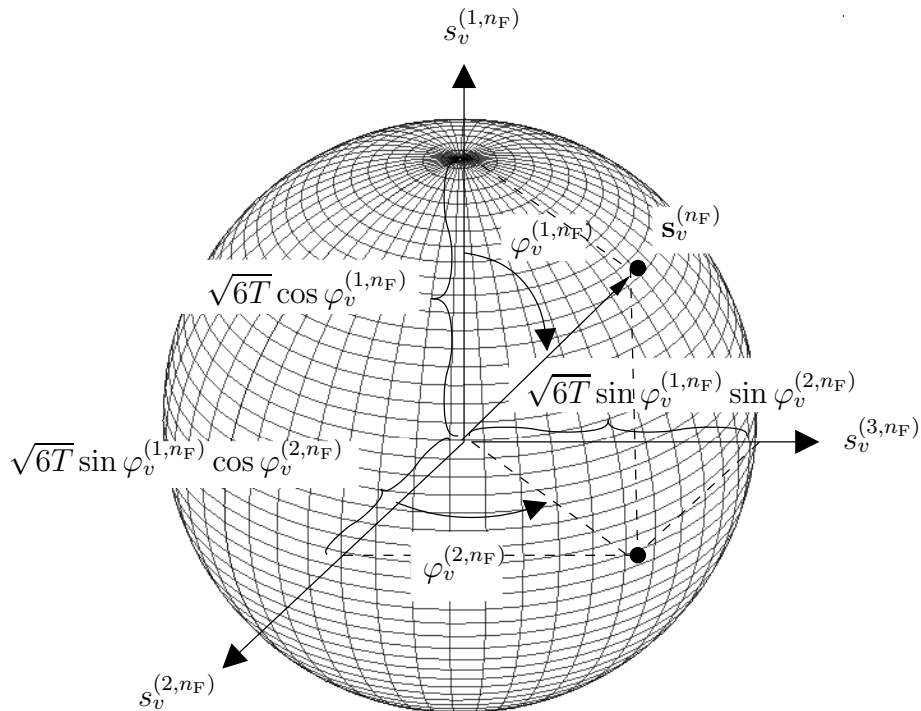
Figure 5.4. Representation of the energy constraint for the effective transmit vector $\mathbf{s}_v^{(n_{\mathrm{F}})}$; Parameters: $K_{\mathrm{B}} = 3$, $K = 3$, fixed transmit energy strategy

5.2.4 Optimization

The effective received vector

$$\mathbf{e}_v^{(n_{\mathrm{F}})} = \left(e_v^{(1,n_{\mathrm{F}})} \dots e_v^{(K,n_{\mathrm{F}})}\right)^{\mathrm{T}} \tag{5.31}$$

of dimension K is introduced, which contains the K effective received values $e_v^{(k,n_{\mathrm{F}})}$, $k = 1 \dots K$, received by each MT k, $k = 1 \dots K$. With the effective transmit vector $\mathbf{s}_v^{(n_{\mathrm{F}})}$ of dimension K_{B}, the $K \times K_{\mathrm{B}}$ channel transfer matrix $\mathbf{H}^{(n_{\mathrm{F}})\mathrm{T}}$, and the noise vector $\mathbf{n}^{(n_{\mathrm{F}})}$ of dimension K,

$$\mathbf{e}_v^{(n_{\mathrm{F}})} = \mathbf{H}^{(n_{\mathrm{F}})\mathrm{T}}\mathbf{s}_v^{(n_{\mathrm{F}})} + \mathbf{n}^{(n_{\mathrm{F}})} \tag{5.32}$$

follows for the effective received vector $\mathbf{e}_v^{(n_{\mathrm{F}})}$. In (5.32) it is assumed that the noise values $n^{(k,n_{\mathrm{F}})}$, $k = 1 \dots K$, are zero-mean Gaussian distributed random variables with variance σ^2.

In the case of BPSK, the MTs contain only quantizers, and therefore with the cardinality V of $\mathbb{D}_{\mathrm{eff}}^K$ of (5.9), the number K of MTs, and with the effective received value $e_v^{(k,n_{\mathrm{F}})}$, the bit error probability

$$P_{\mathrm{b},v}^{(k,n_{\mathrm{F}})} = \frac{1}{2}\mathrm{erfc}\left(\pm\frac{e_v^{(k,n_{\mathrm{F}})}}{\sqrt{2}\sigma}\right) \tag{5.33}$$

can be calculated for MT k in the case that the effective data vector $\mathbf{d}_v^{(n_{\mathrm{F}})}$ is transmitted. Moreover, the bit error probability

$$\overline{P}_{\mathrm{b},v}^{(n_{\mathrm{F}})} = \frac{1}{K}\sum_{k=1}^{K} P_{\mathrm{b},v}^{(k,n_{\mathrm{F}})} \tag{5.34}$$

results after averaging of $P_{\mathrm{b},v}^{(k,n_{\mathrm{F}})}$ of (5.33) over all K MTs, and the average bit error probability

$$\overline{P}_{\mathrm{b}}^{(n_{\mathrm{F}})} = \frac{1}{V}\sum_{v=1}^{V} \overline{P}_{\mathrm{b},v}^{(n_{\mathrm{F}})} \tag{5.35}$$

results after averaging of $\overline{P}_{\mathrm{b},v}^{(n_{\mathrm{F}})}$ of (5.35) over all V effective data vectors $\mathbf{d}_v^{(n_{\mathrm{F}})} \in \mathbb{D}_{\mathrm{eff}}^K$.

The average bit error probability $\overline{P}_{\mathrm{b}}^{(n_{\mathrm{F}})}$ of (5.35) of JT is a real function of the $(K_{\mathrm{B}} - 1)V$ angles $\varphi_v^{(k_{\mathrm{B}},n_{\mathrm{F}})}$, $k_{\mathrm{B}} = 1 \dots K_{\mathrm{B}} - 1$, $v = 1 \dots V$, and the $V - 1$ angles $\vartheta_v^{(K)}$, $v = 1 \dots V - 1$. Hence, for given $\mathbb{D}_{\mathrm{eff}}^K$, the mapping function $f^{(n_{\mathrm{F}})}$ leading to the minimum average bit error probability $\overline{P}_{\mathrm{b}}^{(n_{\mathrm{F}})}$ can be determined by means of numerical minimization of $\overline{P}_{\mathrm{b}}^{(n_{\mathrm{F}})}$ of (5.35) with respect to the $(K_{\mathrm{B}} - 1)V$ angles $\varphi_v^{(k_{\mathrm{B}},n_{\mathrm{F}})}$, $k_{\mathrm{B}} = 1 \dots K_{\mathrm{B}} - 1$, $v = 1 \dots V$, and the $V - 1$ angles $\vartheta_v^{(n_{\mathrm{F}})}$, $v = 1 \dots V - 1$. The resulting $\mathbf{s}_{v,\mathrm{opt}}^{(n_{\mathrm{F}})} \in \mathbb{S}_{\mathrm{eff,opt}}^{(n_{\mathrm{F}})}$ are the effective transmit vectors of optimum JT. The transmit vectors $\mathbf{s}_{\mathrm{opt}}^{(n_{\mathrm{F}})}$ comprising the total set $\mathbb{S}_{\mathrm{opt}}^{(n_{\mathrm{F}})}$ of transmit vectors $\mathbf{s}_{\mathrm{opt}}^{(n_{\mathrm{F}})}$ of optimum JT follow by corresponding rotation of the transmit vectors $\mathbf{s}_{v,\mathrm{opt}}^{(n_{\mathrm{F}})} \in \mathbb{S}_{\mathrm{eff,opt}}^{(n_{\mathrm{F}})}$.

Various numerical minimization algorithms can be applied in order to yield the effective transmit vectors $\mathbf{s}_{v,\mathrm{opt}}^{(n_{\mathrm{F}})}$ of optimum JT. A first approach is the use of methods based on gradient approaches, such as Newton methods [Sto83]. Such minimization algorithms use information concerning the gradient of the objective function to be minimized, and in each iteration the direction of steepest descent is followed to locate the minimum of the objective function. The inverse of the Hessian matrix, needed for the location of the minimum of the objective function, is numerically calculated by Newton methods. In order to avoid the large number of computations involved in the direct numerical calculation of the Hessian matrix, quasi-Newton methods [Bro70, Fle70, Gol70, Sha70] use the observed behavior of the objective function and of its gradient to make an approximation to the Hessian matrix using an appropriate updating technique such as the formula of Broyden [Bro70], Fletcher [Fle70], Goldfarb [Gol70], and Shanno [Sha70] (BFGS). Instead of approximating the Hessian matrix and performing the inversion in a second step, the inverse of the Hessian matrix can be approximated using the formula from Davidon [Dav59], Fletcher and Powell [FP63] (DFP).

5.3   Transmit zero-forcing joint transmission

In this Section, TxZF JT is dealt with. With regard to the considerations of Section 5.2, in the case of linear JT the mapping function $f^{(n_{\mathrm{F}})}$ of (5.13) is linear and can be therefore described by a $K_{\mathrm{B}} \times K$ modulator matrix $\underline{\mathbf{M}}^{(n_{\mathrm{F}})}$. According to TxZF JT for SA-based systems, the transmit vector $\underline{\mathbf{s}}^{(n_{\mathrm{F}})}$ of dimension K_{B} is generated from the data vector $\underline{\mathbf{d}}^{(n_{\mathrm{F}})}$ of dimension K under consideration of the structure of the K MTs given by (5.7), through a linear transformation [MBW$^+$00, Fis02]

$$\underline{\mathbf{s}}^{(n_{\mathrm{F}})} = \underline{\mathbf{M}}^{(n_{\mathrm{F}})} \underline{\mathbf{d}}^{(n_{\mathrm{F}})}. \tag{5.36}$$

In the present thesis, linear JT in the sense of TxZF JT [WMS$^+$02, MBW$^+$00, WSLW03] is considered. By TxZF JT, intra-SA interference in the DL of SA-based systems is completely eliminated, i.e., using (5.7), in the absence of noise the requirement of an interference free estimate reads

$$\hat{\underline{\mathbf{d}}}^{(n_{\mathrm{F}})} = \underline{\mathbf{d}}^{(n_{\mathrm{F}})} \tag{5.37}$$

and with (5.6) follows

$$\underline{\mathbf{H}}^{(n_{\mathrm{F}})\mathrm{T}} \underline{\mathbf{s}} = \underline{\mathbf{d}}^{(n_{\mathrm{F}})}. \tag{5.38}$$

By posing the requirement of (5.38) on the transmit vector $\underline{\mathbf{s}}^{(n_{\mathrm{F}})}$ of (5.36), given that $K_{\mathrm{B}} \geq K$, an underdetermined system of K equations and K_{B} unknowns results, which means that there exist infinitely many transmit vectors $\underline{\mathbf{s}}^{(n_{\mathrm{F}})}$ which fulfill the requirement of (5.38), and that an additional requirement should be posed on the transmit vector $\underline{\mathbf{s}}^{(n_{\mathrm{F}})}$.

With respect to the inter-SA interference in the DL, it is desirable to minimize the total transmit energy

$$T_{\text{tot}}^{(n_{\text{F}})} = \frac{1}{2} \underline{\mathbf{s}}^{(n_{\text{F}})*\text{T}} \underline{\mathbf{s}}^{(n_{\text{F}})},$$ (5.39)

which is radiated from the investigated SA. Therefore, among all transmit vectors $\underline{\mathbf{s}}^{(n_{\text{F}})}$ which fulfill (5.38), the transmit vector [MBW+00, WMS+02]

$$\underline{\mathbf{s}}^{(n_{\text{F}})} = \underbrace{\underline{\mathbf{H}}^{(n_{\text{F}})*} \left(\underline{\mathbf{H}}^{(n_{\text{F}})\text{T}} \underline{\mathbf{H}}^{(n_{\text{F}})*} \right)^{-1}}_{\underline{\mathbf{M}}_{\text{TxZF}}^{(n_{\text{F}})}} \underline{\mathbf{d}}^{(n_{\text{F}})}$$ (5.40)

is used in TxZF JT, which has the least energy $T_{\text{tot}}^{(n_{\text{F}})}$ of (5.39) and consequently causes the minimum possible inter-SA interference.

As is the case with RxZF JD in the UL transmission, see Section 4.3.2, by TxZF JT intra-SA interference in the DL transmission of SA-based systems is eliminated using only the channel signatures of the MTs in the transfer matrix $\underline{\mathbf{H}}^{(n_{\text{F}})\text{T}}$ of the DL transmission, as compared to TxZF JT in CDMA systems by which also the CDMA components are used to eliminate interference in each cell [MBW+00, WMS+02].

5.4   Iterative joint transmission

Drawing an analogy to iterative JD of Section 4.4, in this Section an iterative JT algorithm is presented. Unlike TxZF JT of Section 5.3, in iterative JT intra-SA interference is mitigated in an iterative fashion, rather than with a direct matrix inversion. Fig. 5.5 shows the model for iterative JT.

As shown in Fig. 5.5, using the $KN_{\text{F}} \times KN_{\text{F}}$ forward path matrix $\underline{\mathbf{F}}$ and the $KN_{\text{F}} \times KN_{\text{F}}$ reverse path matrix $\underline{\mathbf{R}}$, the data vector $\underline{\mathbf{d}}$ of dimension KN_{F} is pre-processed in an iterative way. With the initial value

$$\underline{\mathbf{t}}(0) = \mathbf{0},$$ (5.41)

in each iteration p, $p = 1 \ldots P$, the transformed total data vector

$$\underline{\mathbf{t}}(p) = \underline{\mathbf{F}} \ (\underline{\mathbf{d}} - \underline{\mathbf{R}} \ \underline{\mathbf{t}}(p-1))$$ (5.42)

of dimension KN_{F} is produced, from which the total transmit vector

$$\underline{\mathbf{s}}(p) = \underline{\mathbf{H}}^* \ \underline{\mathbf{t}}(p)$$ (5.43)

of dimension $K_{\text{B}}N_{\text{F}}$ is generated.
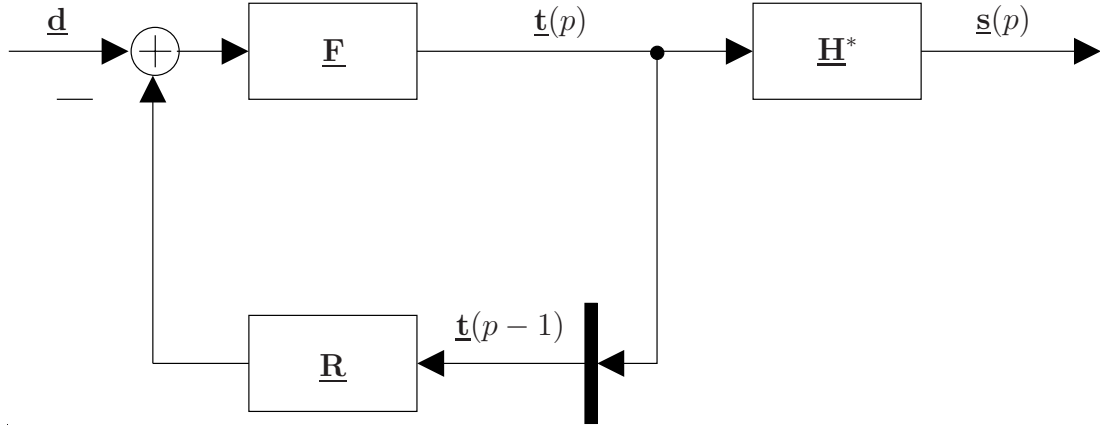
Figure 5.5. Iterative JT model

If iterative JT converges, then for the limiting value of the transformed data vector

$$
\begin{aligned}
\underline{t}(\infty) &= \underline{F}\,(\underline{d} - \underline{R}\,\underline{t}(\infty)) \\
&= \left(\underline{F}^{-1} + \underline{R}\right)^{-1}\underline{d}.
\end{aligned}
\tag{5.44}
$$

holds. Comparing the expression for the convergence value of the transformed data vector $\underline{t}(\infty)$ of (5.44) to the expression (4.28) for the limiting value of the estimated data vector $\underline{\hat{d}}(\infty)$ of iterative JD, it can be deduced that iterative JT and iterative JD with transparent data estimate refinement are described by the formally equivalent expressions (4.28) and (5.44). Hence, using the results of 4.4.2, with the the forward path matrix $\underline{F}$ and the reverse path matrix $\underline{R}$, it follows that iterative JT converges if and only if for the spectral radius [Sch88b] $\lambda_{\max}(\underline{F}\,\underline{R})$ of the matrix product $\underline{F}\,\underline{R}$ of dimension $K N_{\mathrm{F}} \times K N_{\mathrm{F}}$

$$
\lambda_{\max}(\underline{F}\,\underline{R}) \leq 1
\tag{5.45}
$$

holds. In the case of convergence, with $\underline{t}(\infty)$ of (5.44) and with the matrix

$$
\underline{M}_{\infty} = \underline{H}^{*}\left(\underline{F}^{-1} + \underline{R}\right)^{-1}
\tag{5.46}
$$

of dimension $K_{\mathrm{B}} N_{\mathrm{F}} \times K N_{\mathrm{F}}$, the limiting value of the total transmit vector

$$
\underline{s}(\infty) = \underline{H}^{*}\left(\underline{F}^{-1} + \underline{R}\right)^{-1}\underline{d}
\tag{5.47}
$$

is equal to the total transmit vector

$$
\underline{s} = \underline{M}_{\infty}\,\underline{d}
\tag{5.48}
$$

of a linear JT scheme characterized by the total modulator matrix $\underline{M}_{\infty}$ of (5.46). For example, choosing

$$
\underline{F} = \left(\mathrm{diag}\left(\underline{H}^{\mathrm{T}}\underline{H}^{*}\right)\right)^{-1}
\tag{5.49}
$$

and

$$\underline{\mathbf{R}} = \overline{\mathrm{diag}} \left(\underline{\mathbf{H}}^{\mathrm{T}} \underline{\mathbf{H}}^* \right) \tag{5.50}$$

$\underline{\mathbf{M}}_\infty$ of (5.46) becomes

$$\underline{\mathbf{M}}_\infty = \underline{\mathbf{H}}^* \left(\underline{\mathbf{H}}^{\mathrm{T}} \underline{\mathbf{H}}^* \right)^{-1} \tag{5.51}$$

and therefore the convergence of the transmit vector $\underline{\mathbf{s}}(p)$ of iterative JT towards the transmit vector $\underline{\mathbf{s}}$ of TxZF JT can be achieved.

6   Performance investigation of uplink transmission

6.1   Preliminary remarks

In Chapter 4 the transmission and detection model for the UL in SA-based air interface architectures employing OFDM is presented. The present Chapter deals with the assessment of the performance of the various JD algorithms which are described in Chapter 4. In particular, performance measures for JD are introduced and on the basis of these measures, the performance of the various JD algorithms is assessed in a number of different scenarios.

In a first step, assumptions are introduced which significantly simplify the expressions that follow. Aspects concerning the performance comparison of SA-based systems employing different modulation schemes are not dealt with in the present thesis. Therefore, without loss of generality it is assumed that QPSK modulation is employed. Furthermore, the data symbols $\underline{d}^{(k,n_{\mathrm{F}})}$, $k = 1 \ldots K$, transmitted at a specific subcarrier n_{F} in the UL are assumed to be uncorrelated. With the data vector $\underline{\mathbf{d}}^{(n_{\mathrm{F}})}$ of (3.40) and the $K \times K$ identity matrix $\mathbf{I}_K$, the aforementioned assumption is expressed by the data correlation matrix

$$\underline{\mathbf{R}}_{\mathrm{dd}}^{(n_{\mathrm{F}})} = \mathrm{E}\left\{\underline{\mathbf{d}}^{(n_{\mathrm{F}})}\underline{\mathbf{d}}^{(n_{\mathrm{F}})*\mathrm{T}}\right\} = 2\,\mathbf{I}_K \tag{6.1}$$

of dimension $K \times K$. Finally, Gaussian distributed noise values $\underline{n}^{(k_{\mathrm{B}},n_{\mathrm{F}})}$, $k_{\mathrm{B}} = 1 \ldots K_{\mathrm{B}}$, are assumed and with the variance σ^2 of the real and imaginary part of each noise value $\underline{n}^{(k_{\mathrm{B}},n_{\mathrm{F}})}$ and the $K_{\mathrm{B}} \times K_{\mathrm{B}}$ identity matrix $\mathbf{I}_{K_{\mathrm{B}}}$, the noise vector $\underline{\mathbf{n}}^{(n_{\mathrm{F}})}$ of (3.33) is characterized by the noise correlation matrix

$$\underline{\mathbf{R}}_{\mathrm{nn}}^{(n_{\mathrm{F}})} = \mathrm{E}\left\{\underline{\mathbf{n}}^{(n_{\mathrm{F}})}\underline{\mathbf{n}}^{(n_{\mathrm{F}})*\mathrm{T}}\right\} = 2\sigma^2\mathbf{I}_{K_{\mathrm{B}}} \tag{6.2}$$

of dimension $K_{\mathrm{B}} \times K_{\mathrm{B}}$.

Target of JD in the UL of SA-based systems is the suppression of the interference between the received signals from the K MTs active in the SA. As far as the detection of the data symbol $\underline{d}^{(k,n_{\mathrm{F}})}$ is concerned, using (6.1), the transfer matrix $\underline{\mathbf{H}}^{(n_{\mathrm{F}})}$ of (3.35), and introducing the operator $[\cdot]_{k,k}$ which is used on a quadratic matrix returning the k-th element of its main diagonal, the price to be paid for the suppression of the intra-SA interference disturbing the partial received signal from MT k at subcarrier n_{F}, is the suboptimum use of the receive energy

$$
\begin{aligned}
R^{(k,n_{\mathrm{F}})} &= \frac{1}{2}\mathrm{E}\left\{|\underline{d}^{(k,n_{\mathrm{F}})}|^2\right\}\left[\underline{\mathbf{H}}^{(n_{\mathrm{F}})*\mathrm{T}}\underline{\mathbf{H}}^{(n_{\mathrm{F}})}\right]_{k,k} \\
&= \left[\underline{\mathbf{H}}^{(n_{\mathrm{F}})*\mathrm{T}}\underline{\mathbf{H}}^{(n_{\mathrm{F}})}\right]_{k,k},
\end{aligned}
\tag{6.3}
$$

resulting from the transmission of data symbol $\underline{d}^{(k,n_{\mathrm{F}})}$, when compared to an optimum single user reference system based on matched filtering, in which only the data symbol $\underline{d}^{(k,n_{\mathrm{F}})}$ is transmitted and hence no need for interference suppression is present.

Common to all performance measures for JD introduced in this thesis is the assessment of the said suboptimum use of the receive energy $R^{(k,n_{\mathrm{F}})}$ of (6.3). In particular, with the performance measures for JD introduced in the present Chapter, the use of the receive energy $R^{(k,n_{\mathrm{F}})}$ of (6.3) by JD is assessed on the basis of the SNR of the estimate $\hat{\underline{d}}^{(k,n_{\mathrm{F}})}$ of the data symbol $\underline{d}^{(k,n_{\mathrm{F}})}$ and of the achieved bit error probability $P_{\mathrm{b}}^{(k,n_{\mathrm{F}})}$.

Using the matrix operator $[\cdot]_k$ which returns the k-th column of its argument as a column vector, in the reference system in which only the data symbol $\underline{d}^{(k,n_{\mathrm{F}})}$ is transmitted, transmission takes place over the mobile radio channel described by the transfer vector $\left[\underline{\mathbf{H}}^{(n_{\mathrm{F}})}\right]_k$ thus yielding the received vector

$$\underline{\mathbf{e}}^{(n_{\mathrm{F}})} = \left[\underline{\mathbf{H}}^{(n_{\mathrm{F}})}\right]_k \underline{d}^{(k,n_{\mathrm{F}})} + \underline{\mathbf{n}}^{(n_{\mathrm{F}})}. \tag{6.4}$$

In terms of the use of the receive energy $R^{(k,n_{\mathrm{F}})}$ of (6.3), in the reference system the optimum approach concerning data estimation is employed, being the use of a filter matched to the channel $\left[\underline{\mathbf{H}}^{(n_{\mathrm{F}})}\right]_k$ by which the estimated data symbol

$$\hat{\underline{d}}^{(k,n_{\mathrm{F}})} = \left(\left[\underline{\mathbf{H}}^{(n_{\mathrm{F}})}\right]_k\right)^{*\mathrm{T}} \underline{\mathbf{e}}^{(n_{\mathrm{F}})} \tag{6.5}$$

is obtained from the received vector $\underline{\mathbf{e}}^{(n_{\mathrm{F}})}$ of (6.4). In this case, with the variance σ^2 of real and imaginary parts of each noise value $\underline{n}^{(k_{\mathrm{B}},n_{\mathrm{F}})}$, the maximum possible SNR

$$\begin{aligned}
\gamma_{\mathrm{ref}}^{(k,n_{\mathrm{F}})} &= \frac{\mathrm{E}\left\{\left|\underline{d}^{(n_{\mathrm{F}})}\right|^2\right\}}{\mathrm{E}\left\{\left|\hat{\underline{d}}^{(n_{\mathrm{F}})} - \underline{d}^{(n_{\mathrm{F}})}\right|^2\right\}} \\
&= \frac{1}{\sigma^2}\left[\underline{\mathbf{H}}^{(n_{\mathrm{F}})*\mathrm{T}}\underline{\mathbf{H}}^{(n_{\mathrm{F}})}\right]_{k,k}
\end{aligned} \tag{6.6}$$

and the minimum possible bit error probability $P_{\mathrm{b,ref}}^{(k,n_{\mathrm{F}})}$ for given receive energy $R^{(k,n_{\mathrm{F}})}$ of (6.3) is obtained, which in the case of QPSK reads

$$P_{\mathrm{b,ref}}^{(k,n_{\mathrm{F}})} = \frac{1}{2}\,\mathrm{erfc}\left(\sqrt{\frac{1}{2\sigma^2}\left[\underline{\mathbf{H}}^{(n_{\mathrm{F}})*\mathrm{T}}\underline{\mathbf{H}}^{(n_{\mathrm{F}})}\right]_{k,k}}\right). \tag{6.7}$$

Due to the fact that in the reference system a single data symbol $\underline{d}^{(k,n_{\mathrm{F}})}$ is considered, the performance of the reference system in terms of the bit error probability $P_{\mathrm{b}}^{(k,n_{\mathrm{F}})}$ is also referred to as single user bound.

6.2   Bit error probability

6.2.1   The bit error probability as performance measure

In this thesis, the main performance measure used to assess the efficiency with which the receive energy $R^{(k,n_\mathrm{F})}$ of (6.3) is used in JD is the bit error probability $P_\mathrm{b}^{(k,n_\mathrm{F})}$. In particular, using the receive energy $R^{(k,n_\mathrm{F})}$, the receive energy per bit $E_\mathrm{b}^{(k,n_\mathrm{F})}$ corresponding to each of the information bits contained in the QPSK data symbol $\underline{d}^{(k,n_\mathrm{F})}$ is determined and, using the two-sided power spectral density $N_0/2$ of the noise, the corresponding bit error probability $P_\mathrm{b}^{(k,n_\mathrm{F})}$ is simulated for various values of $E_\mathrm{b}^{(k,n_\mathrm{F})}/N_0$. In the case that the performance of JD averaged over a large number of realizations of the mobile radio channel is investigated, the average bit error probability $\overline{P}_\mathrm{b}$ is simulated for various values of $\overline{E}_\mathrm{b}/N_0$.

The suboptimum use of the receive energy $R^{(k,n_\mathrm{F})}$ of (6.3) is expressed using simulations of the bit error probability $P_\mathrm{b}^{(k,n_\mathrm{F})}$ versus $E_\mathrm{b}^{(k,n_\mathrm{F})}/N_0$ through the fact that for a given $E_\mathrm{b}^{(k,n_\mathrm{F})}/N_0$ JD produces a bit error probability $P_\mathrm{b}^{(k,n_\mathrm{F})}$ larger than the bit error probability $P_\mathrm{b,ref}^{(k,n_\mathrm{F})}$ of the reference system. Equivalently, in order to achieve a given bit error probability $P_\mathrm{b}^{(k,n_\mathrm{F})}$, JD needs a larger $E_\mathrm{b}^{(k,n_\mathrm{F})}/N_0$ as compared to the single user reference system.

In the simulation results for the bit error probability $P_\mathrm{b}^{(k,n_\mathrm{F})}$ of JD presented in this Section, also the bit error probability $P_\mathrm{b}^{(k,n_\mathrm{F})}$ resulting from single user estimation in the sense of MF [Ver98] is included for reasons of comparison. With MF, the estimated data symbols

$$\hat{\underline{\mathbf{d}}}^{(n_\mathrm{F})} = \left(\mathrm{diag}\left(\underline{\mathbf{H}}^{(n_\mathrm{F})*\mathrm{T}} \underline{\mathbf{H}}^{(n_\mathrm{F})} \right) \right)^{-1} \underline{\mathbf{H}}^{(n_\mathrm{F})*\mathrm{T}} \underline{\mathbf{e}}^{(n_\mathrm{F})} \tag{6.8}$$

are obtained from the received vector $\underline{\mathbf{e}}^{(n_\mathrm{F})}$ of (4.5). In the case of single user estimation by MF, the estimated data symbols $\hat{\underline{\mathbf{d}}}^{(n_\mathrm{F})}$ of (6.8) contain intra-SA interference. As intra-SA interference is a systematic estimation error present even at high $E_\mathrm{b}^{(k,n_\mathrm{F})}/N_0$, the bit error probability $P_\mathrm{b}^{(k,n_\mathrm{F})}$ of MF single user estimation of (6.8) converges, in the majority of cases, to an error floor.

6.2.2   Bit error probability of optimum versus linear joint detection

As explained in Section 4.2, the fact that optimum JD can be performed in a subcarrierwise fashion in SA-based OFDM systems, makes the application of optimum JD feasible. Target of the present Section is to investigate the gains achievable with optimum JD as compared to linear JD in SA-based systems quantitatively, in terms of the average bit error probability $\overline{P}_\mathrm{b}$.

In Figs. 6.1 and 6.2 the average average bit error probability $\overline{P_{\mathrm{b}}}$ is plotted versus $\overline{E_{\mathrm{b}}}/N_0$ for the cases of ML JD, compared to RxZF JD and MMSE JD and single user detection in the sense of MF. Following parametrization characterizes the simulations of Figs. 6.1 and 6.2:

- $K_{\mathrm{B}} = 4$ APs,

- $N_{\mathrm{F}} = 32$ subcarriers,

- the COST 207 RA channel model,

- $W = 14$ paths,

- a bandwidth of $B = 20\,\mathrm{MHz}$,

- convolutional FEC code with rate $R = 1/2$,

- FEC code generator matrix $\begin{pmatrix} 1 & 0 & 0 & 1 & 1 \\ 1 & 1 & 1 & 0 & 1 \end{pmatrix}$, and

- hard FEC decoding.

The case of $K = 2$ MTs active in the SA is shown in Fig. 6.1. It can be seen from Fig. 6.1 that ZF JD and MMSE JD result in an average bit error probability $\overline{P_{\mathrm{b}}}$ very close to the single user bound. In particular, ZF JD and MMSE JD need a $2\,\mathrm{dB}$ and $1.4\,\mathrm{dB}$ larger $\overline{E_{\mathrm{b}}}/N_0$, respectively, in order to achieve an average bit error probability $\overline{P_{\mathrm{b}}} = 10^{-2}$ as compared to the single user reference system. Moreover, when employing single user detection in the sense of MF a $\overline{E_{\mathrm{b}}}/N_0$ increased by approximately $14.3\,\mathrm{dB}$ relative to the reference system is required to achieve a average average bit error probability $\overline{P_{\mathrm{b}}} = 10^{-2}$. Finally, by optimum JD in the sense of ML JD the increase in the $\overline{E_{\mathrm{b}}}/N_0$ as compared to the reference system required to obtain an average bit error probability $\overline{P_{\mathrm{b}}} = 10^{-2}$ is $0.9\,\mathrm{dB}$.

In the case of system load $K/K_{\mathrm{B}} = 1$, i.e., if $K = 4$ holds, the average bit error probability $\overline{P_{\mathrm{b}}}$ obtained by optimum JD as compared to linear JD is shown in Fig. 6.2. It can be seen from Fig. 6.2 that by single user detection an error floor is quickly reached and RxZF JD requires a $12.7\,\mathrm{dB}$ larger $\overline{E_{\mathrm{b}}}/N_0$ in order to obtain an average bit error probability $\overline{P_{\mathrm{b}}} = 10^{-2}$. On the other hand, MMSE JD achieves an average bit error probability $\overline{P_{\mathrm{b}}} = 10^{-2}$ with a $\overline{E_{\mathrm{b}}}/N_0$ which is by $6.6\,\mathrm{dB}$ larger than the $\overline{E_{\mathrm{b}}}/N_0$ required by the single user reference system. Finally, in the case of ML JD the increase of the required $\overline{E_{\mathrm{b}}}/N_0$ as compared to the reference system in order to obtain an average bit error probability $\overline{P_{\mathrm{b}}} = 10^{-2}$ is limited to $2.7\,\mathrm{dB}$.
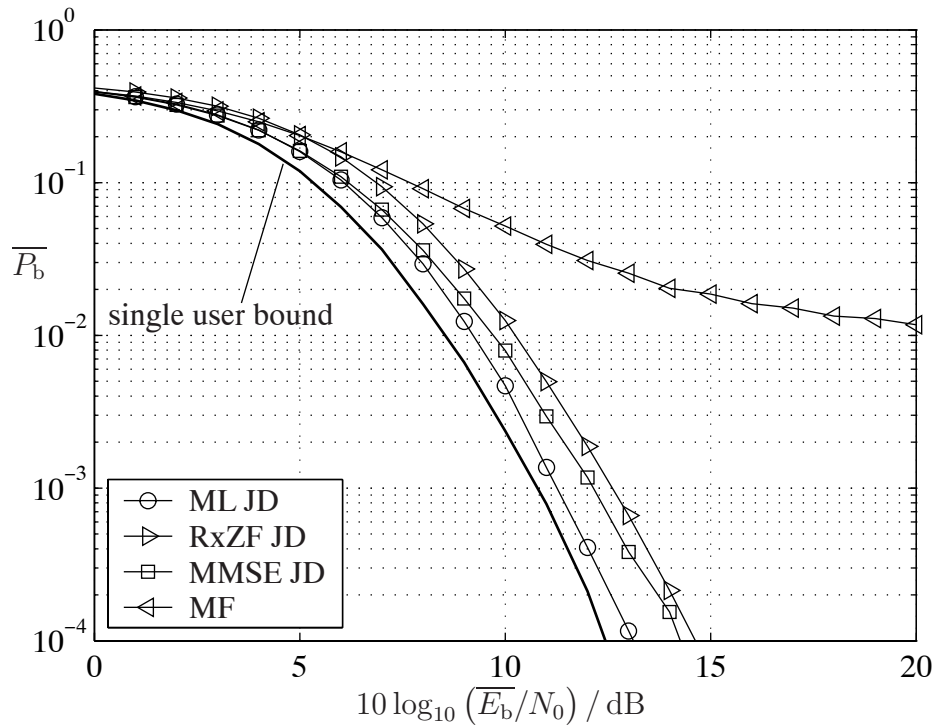
Figure 6.1. Average bit error probability $\overline{P}_\mathrm{b}$ of optimum JD in the sense of ML JD, MMSE JD and RxZF JD and single user detection by MF with the COST 207 RA channel model; Parameters: $K = 2$, $K_\mathrm{B} = 4$, $R = 1/2$, $N_\mathrm{F} = 32$, $W = 14$, $B = 20\,\mathrm{MHz}$
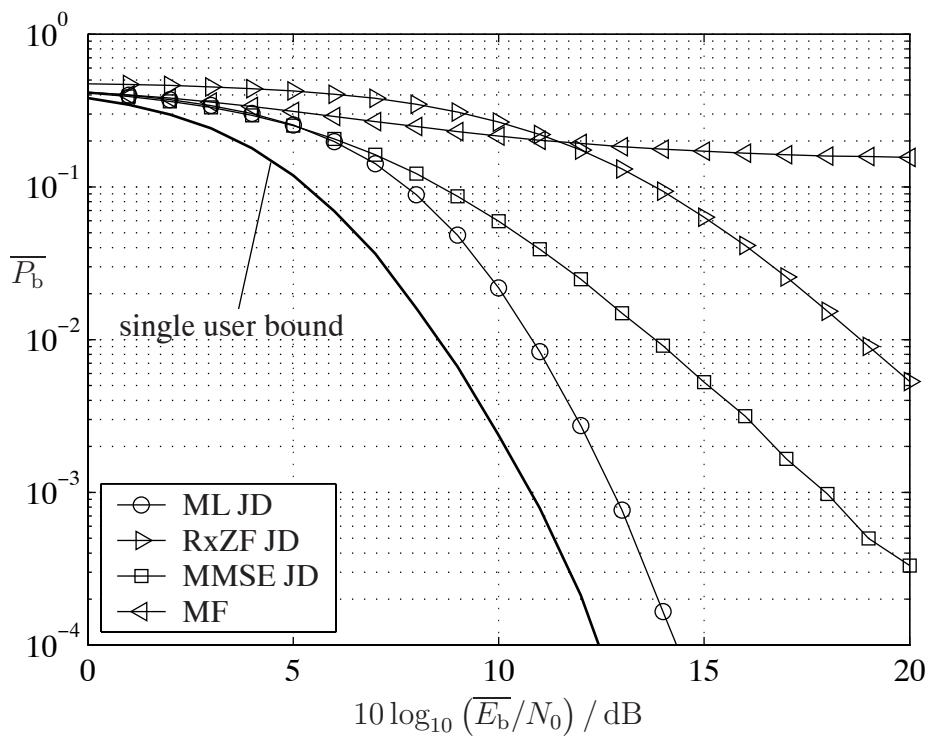
Figure 6.2. Average bit error probability $\overline{P}_\mathrm{b}$ of optimum JD in the sense of ML JD, MMSE JD and RxZF JD and single user detection by MF with the COST 207 RA channel model; Parameters: $K = 4$, $K_\mathrm{B} = 4$, $R = 1/2$, $N_\mathrm{F} = 32$, $W = 14$, $B = 20\,\mathrm{MHz}$

Summarizing the simulation results concerning the bit error probability performance of optimum JD as compared to linear JD shown in Figs. 6.1 and 6.1, in SA-based systems optimum JD is feasible and significant performance gains of up to $10\,\text{dB}$ in terms of the required $\overline{E}_\text{b}/N_0$ at a bit error probability $\overline{P}_\text{b} = 10^{-2}$ can be achieved as compared to RxZF JD and MMSE JD in the case of the considered scenarios. Moreover, by comparing Fig. 6.1 to Fig. 6.2, it follows that the application of optimum JD is especially favorable in SA-based systems characterized by high system loads K/K_B. For fixed K_B, as K increases the number $K-1$ of partial received signals interfering with the useful signal of a desired MT also increases. In such a case the exploitation of the knowledge concerning the data symbols $\underline{d}^{(k,n_\text{F})}$, $k = 1 \ldots K$, to be detected by JD, proves to be especially beneficial in terms of the average bit error probability $\overline{P}_\text{b}$.

Hence with the aid of ML JD, interference can be combated and a high spectrum capacity η_c of (1.1) can be offered in SA-based systems while a low price is paid in terms of the efficiency of the use of the receive energy $R^{(k,n_\text{F})}$ of (6.3), as compared to the case of linear JD in the sense of RxZF JD and MMSE JD.

6.2.3 Bit error probability of iterative joint detection

Intra-SA interference can be also mitigated by iterative JD, as shown in Section 4.4, and the target of the present Section is the assessment of the performance of iterative JD as compared to the performance of linear JD in terms of the achievable bit error probability $P_\text{b}^{(k,n_\text{F})}$. In all simulations concerning the bit error probability $P_\text{b}^{(k,n_\text{F})}$ of iterative JD in this Section, the forward path matrix

$$\underline{\mathbf{F}} = \left(\text{diag}\left(\underline{\mathbf{H}}^{*\text{T}}\underline{\mathbf{H}}\right)\right)^{-1} \tag{6.9}$$

and the reverse path matrix

$$\underline{\mathbf{R}} = \overline{\text{diag}}\left(\underline{\mathbf{H}}^{*\text{T}}\underline{\mathbf{H}}\right) \tag{6.10}$$

are chosen. As shown in Section 4.4, with $\underline{\mathbf{F}}$ of (6.9) and $\underline{\mathbf{R}}$ of (6.10), if iterative JD with transparent data estimate refinement converges, then it converges towards RxZF JD. For this reason, iterative JD is compared to RxZF JD in the following. Finally, the bit error probability performance of single user detection in the sense of MF is provided for reference, because irrespective of the applied data estimate refinement technique, the estimated data vector $\underline{\hat{\mathbf{d}}}(1)$ in the first iteration of iterative JD is the estimated data vector $\underline{\hat{\mathbf{d}}}$ of (6.8) obtained with single user detection by MF.

In a first step, Figs. 6.3 to 6.6 depict the simulation results of iterative JD in which the FEC code is not evaluated for the data estimate refinement procedure, i.e., iterative JD with transparent data estimate refinement, and iterative JD with data estimate refinement by hard and soft quantization is considered. In the simulations of Figs. 6.3-6.6 following parameters are used:

- $K = 4$ MTs,

- $K_{\mathrm{B}} = 4$ APs,

- single subcarrier,

- single snapshot of the MIMO parametric channel model,

- no FEC coding,

- $P = 5$ iterations,

- forward path matrix $\underline{\mathbf{F}} = \left(\mathrm{diag} \left(\underline{\mathbf{H}}^{*\mathrm{T}} \underline{\mathbf{H}} \right) \right)^{-1}$, and

- reverse path matrix $\underline{\mathbf{R}} = \overline{\mathrm{diag}} \left(\underline{\mathbf{H}}^{*\mathrm{T}} \underline{\mathbf{H}} \right)$.

Figs. 6.3 and 6.4 show the bit error probability $P_{\mathrm{b}}^{(1,1)}$ versus $E_{\mathrm{b}}^{(1,1)}/N_0$ of iterative JD with transparent data estimate refinement and of RxZF JD. With the parameter ρ of (2.6) of the MIMO parametric channel model, the cases of

$$\rho = 0.1, \tag{6.11}$$

and

$$\rho = 0.15, \tag{6.12}$$

are considered. If (6.11) holds, it can be seen from Fig. 6.3 that the bit error probability $P_{\mathrm{b}}^{(1,1)}$ obtained by iterative JD with transparent data estimate refinement converges to the bit error probability $P_{\mathrm{b}}^{(1,1)}$ obtained by RxZF JD. On the other hand, if (6.12) holds, Fig. 6.4 shows that $P_{\mathrm{b}}^{(1,1)}$ obtained by iterative JD with transparent data estimate refinement converges slower towards the bit error probability $P_{\mathrm{b}}^{(1,1)}$ obtained by RxZF JD as compared to the case of (6.11).
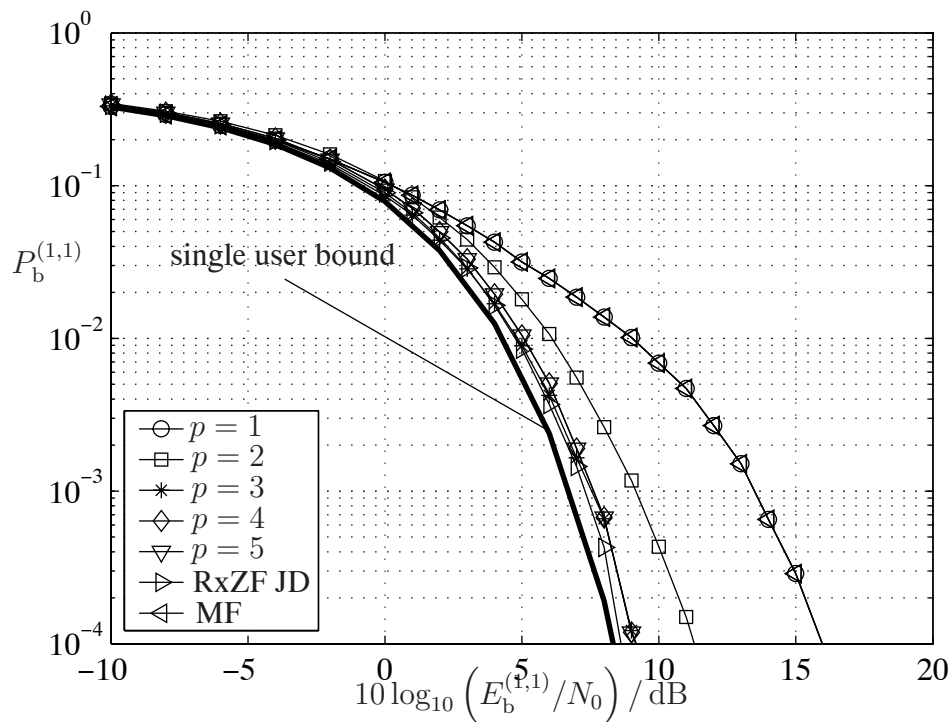
Figure 6.3. Bit error probability $P_{\mathrm{b}}^{(1,1)}$ of iterative JD with transparent data estimate refinement and of RxZF JD and single user detection by MF; Parameters: $K = 4$, $K_{\mathrm{B}} = 4$, $P = 5$, no FEC coding, MIMO parametric channel model with $\rho = 0.1$
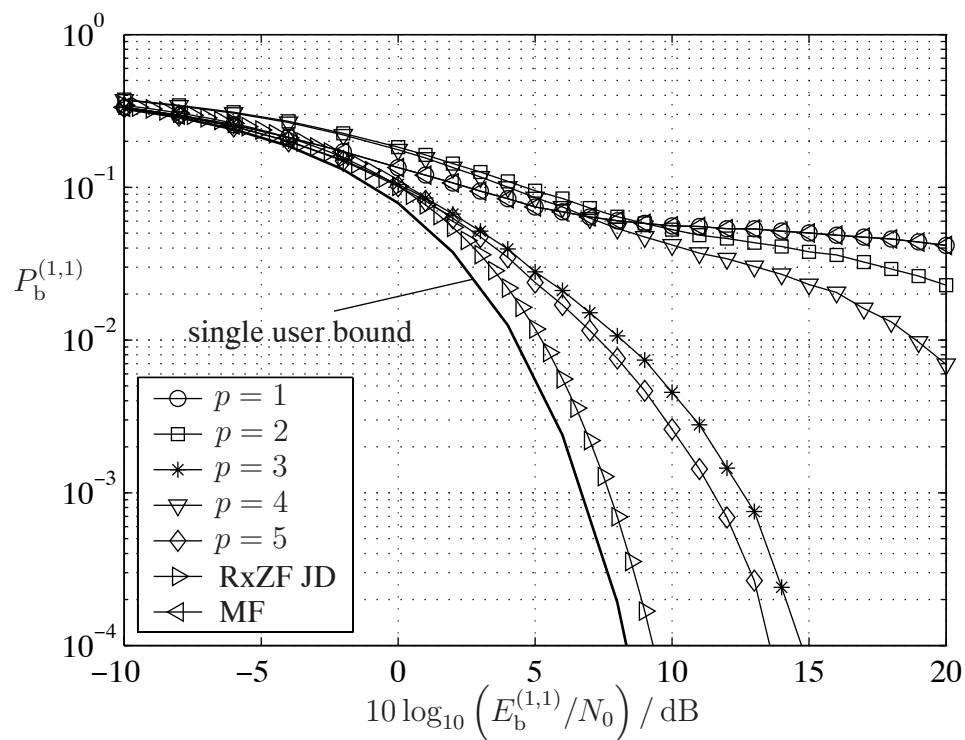
Figure 6.4. Bit error probability $P_{\mathrm{b}}^{(1,1)}$ of iterative JD with transparent data estimate refinement and of RxZF JD and single user detection by MF; Parameters: $K = 4$, $K_{\mathrm{B}} = 4$, $P = 5$, no FEC coding, MIMO parametric channel model with $\rho = 0.15$

Setting out from the results of Fig. 6.3, i.e., from the fact that RxZF JD requires only $0.4\,\mathrm{dB}$ larger $E_{\mathrm{b}}^{(1,1)}/N_0$ than the $E_{\mathrm{b}}^{(1,1)}/N_0$ required by the reference system in order to achieve a bit error probability $P_{\mathrm{b}}^{(1,1)} = 10^{-3}$, it can be deduced that in the case of (6.11), shown in Fig. 6.3, less interference disturbs the useful received signal corresponding to data symbol $\underline{d}^{(k,n_{\mathrm{F}})}$, as compared to the case of (6.12) shown in Fig. 6.4.

The condition (4.33) for the convergence of iterative JD with transparent data estimate refinement can be analytically computed as a function of ρ in the case of the MIMO parametric channel model. Setting

$$\beta = \frac{2\rho + (K-2)\rho^2}{1 + (K-1)\rho^2},\tag{6.13}$$

from the characteristic polynom

$$|\underline{\mathbf{F}}\,\underline{\mathbf{R}} - \lambda\mathbf{I}| = ((K-1)\beta - \lambda)^{N_{\mathrm{F}}} \, (-1)^{N_{\mathrm{F}}(K-1)} \, (\lambda + \beta)^{N_{\mathrm{F}}(K-1)}\tag{6.14}$$

follows the eigenvalue

$$\lambda_1 = (K-1)\frac{2\rho + (K-2)\rho^2}{1 + (K-1)\rho^2}\tag{6.15}$$

with multiplicity N_{F} and the eigenvalue

$$\lambda_2 = -\frac{2\rho + (K-2)\rho^2}{1 + (K-1)\rho^2}\tag{6.16}$$

with multiplicity $N_{\mathrm{F}}(K-1)$ of the $KN_{\mathrm{F}} \times KN_{\mathrm{F}}$ matrix product $\underline{\mathbf{F}}\,\underline{\mathbf{R}}$. From (6.15) and (6.16) the spectral radius

$$\lambda_{\max}\left(\underline{\mathbf{F}}\,\underline{\mathbf{R}}\right) = (K-1)\frac{2\rho + (K-2)\rho^2}{1 + (K-1)\rho^2}\tag{6.17}$$

of $\underline{\mathbf{F}}\,\underline{\mathbf{R}}$ is obtained and using (4.33), it follows from (6.17) that iterative JD with transparent data estimate refinement in the case of the MIMO parametric channel model converges if

$$\rho < \frac{1}{K-3}\left(\sqrt{2\frac{K-2}{K-1}} - 1\right)\tag{6.18}$$

holds. In the specific case of

$$K = 4\tag{6.19}$$

(6.18) yields

$$\rho < 0.155.\tag{6.20}$$
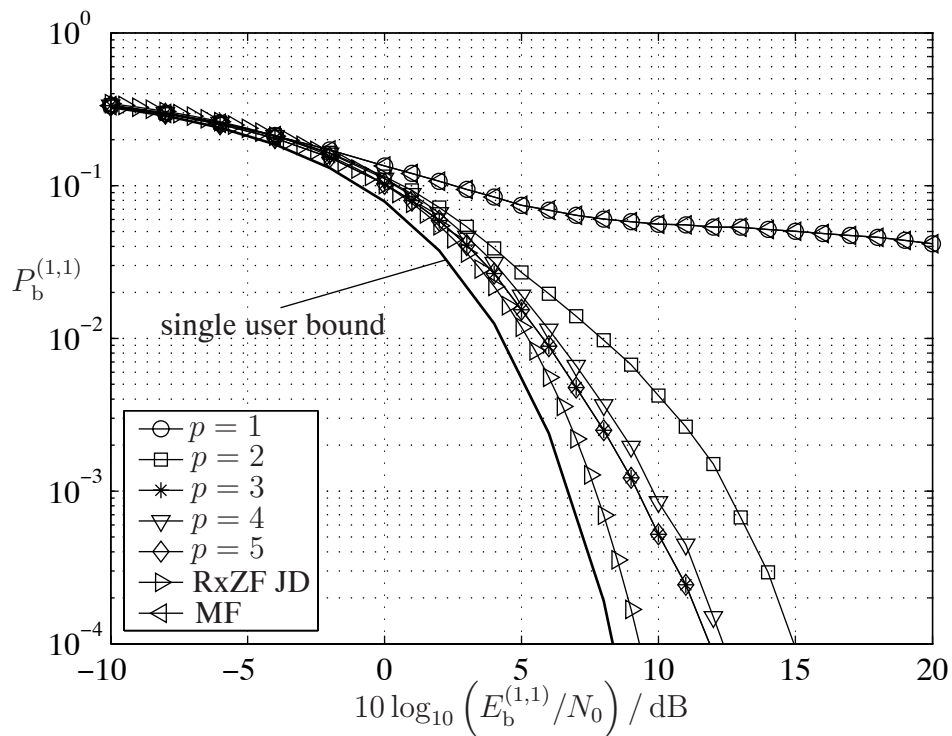
Figure 6.5. Bit error probability $P_{\mathrm{b}}^{(1,1)}$ of iterative JD with data estimate refinement by hard quantization and of RxZF JD and single user detection by MF; Parameters: $K = 4$, $K_{\mathrm{B}} = 4$, $P = 5$, no FEC coding, MIMO parametric channel model with $\rho = 0.15$
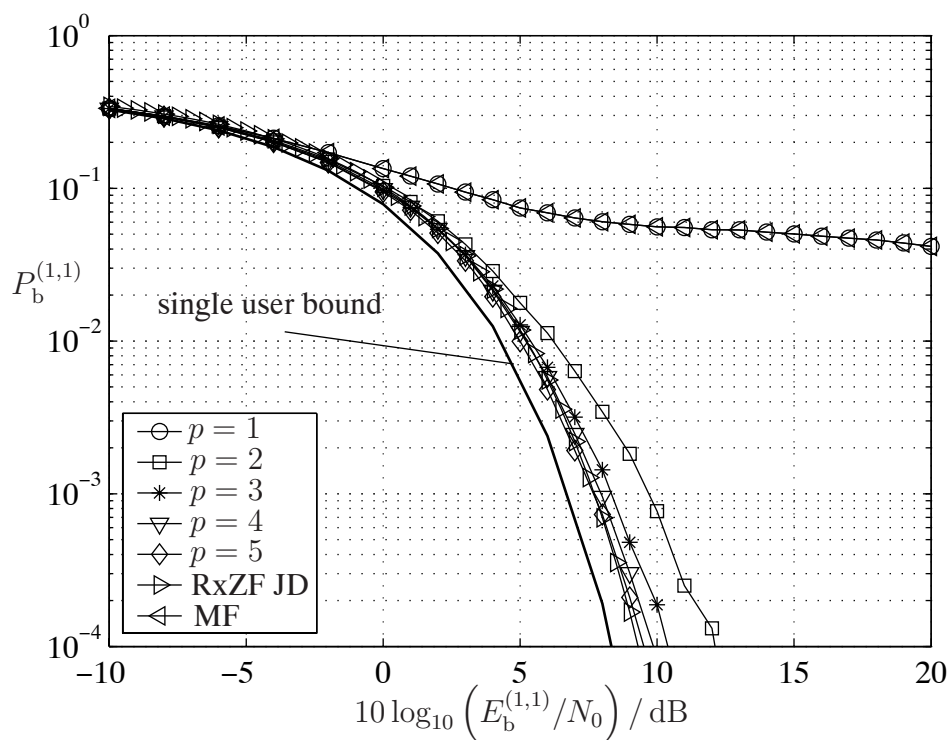
Figure 6.6. Bit error probability $P_{\mathrm{b}}^{(1,1)}$ of iterative JD with data estimate refinement by soft quantization and of RxZF JD and single user detection by MF; Parameters: $K = 4$, $K_{\mathrm{B}} = 4$, $P = 5$, no FEC coding, MIMO parametric channel model with $\rho = 0.15$

Figs. 6.5 and 6.6 show the performance of iterative JD with data estimate refinement by hard and soft quantization, respectively, in the case of the MIMO parametric channel model with

$$\rho = 0.15 \tag{6.21}$$

in terms of the bit error probability $P_b^{(1,1)}$. As shown in Figs. 6.5 and 6.6, convergence is reached by both data estimate refinement techniques and data estimate refinement with hard quantization converges slower than data estimate refinement by soft quantization. Moreover, comparing Figs. 6.5 and 6.6 it can be seen that given a target bit error probability $P_b^{(1,1)} = 10^{-3}$, the $E_b^{(1,1)}/N_0$ of iterative JD with data estimate refinement by soft quantization converges to a value of $0.7\,\mathrm{dB}$ larger than that required by the reference system, whereas in the case of hard quantization the required $E_b^{(1,1)}/N_0$ in the limiting case is $2.7\,\mathrm{dB}$ larger than that of the reference system.

The bit error probability performance of iterative JD with optimum data estimate refinement is illustrated in Figs. 6.7 and 6.8. As stated in Section 4.4.5, the crux of the optimum data estimate refinement consists in exploiting the knowledge of the employed FEC code for data estimate refinement. For this reason, the average bit error probability $\overline{P}_b$ in a coded transmission is investigated. In the simulations of Figs. 6.7-6.8 following parameters are used:

- $K_B = 4$ APs,

- $N_F = 32$ subcarriers,

- the COST 207 RA channel model,

- $W = 14$ paths,

- a bandwidth of $B = 20\,\mathrm{MHz}$,

- convolutional FEC code with rate $R = 1/2$,

- FEC code generator matrix $\begin{pmatrix} 1 & 0 & 0 & 1 & 1 \\ 1 & 1 & 1 & 0 & 1 \end{pmatrix}$,

- soft FEC decoding, and

- $P = 5$ iterations.

For the sake of simplicity iterative JD with optimum data estimate refinement is compared only to iterative JD with data estimate refinement by soft quantization and to RxZF JD.
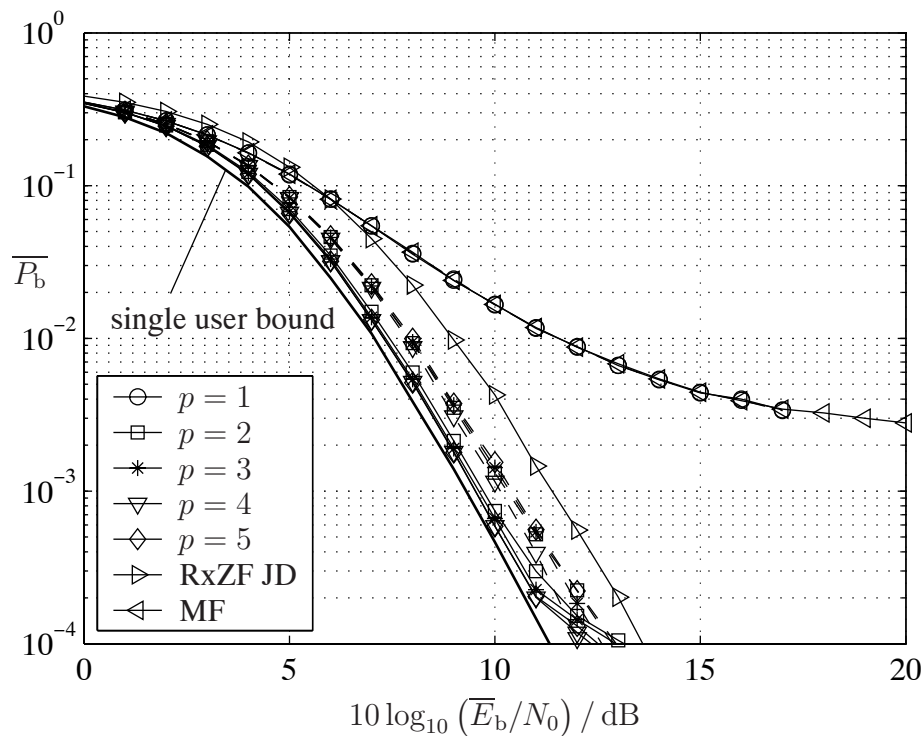
Figure 6.7. Average bit error probability $\overline{P}_{\mathrm{b}}$ of iterative JD with data estimate refinement by optimum data estimate refinement (solid lines), by soft quantization (dashed lines), of RxZF JD and of MF with the COST 207 RA channel model; Parameters: $K = 2$, $K_{\mathrm{B}} = 4$, $P = 5$, $R = 1/2$, $N_{\mathrm{F}} = 32$, $W = 14$, $B = 20\,\mathrm{MHz}$
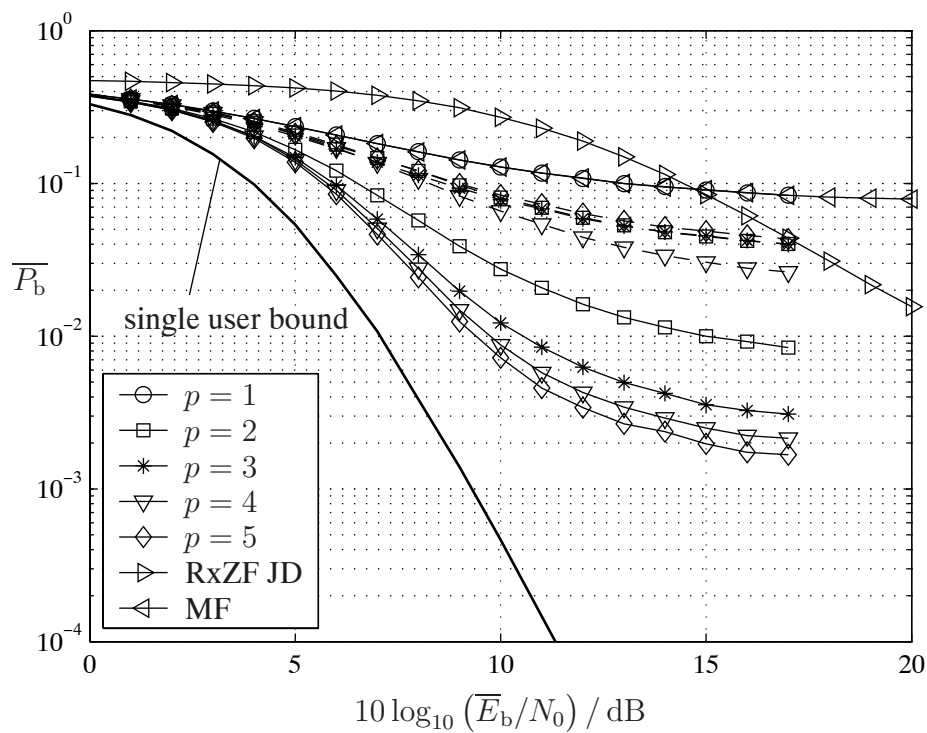
Figure 6.8. Average bit error probability $\overline{P}_{\mathrm{b}}$ of iterative JD with data estimate refinement by optimum data estimate refinement (solid lines), by soft quantization (dashed lines), of RxZF JD and of MF with the COST 207 RA channel model; Parameters: $K = 4$, $K_{\mathrm{B}} = 4$, $P = 5$, $R = 1/2$, $N_{\mathrm{F}} = 32$, $W = 14$, $B = 20\,\mathrm{MHz}$

Fig. 6.7 presents the average bit error probability $\overline{P}_b$ of iterative JD with optimum data estimate refinement and of iterative JD with data estimate refinement by soft quantization for

$$K = 2. \tag{6.22}$$

From Fig. 6.7 it can be seen that with RxZF JD a $2.3\,\mathrm{dB}$ larger $\overline{E}_b/N_0$ relative to the reference system is needed for an average bit error probability $\overline{P}_b = 10^{-2}$ whereas with iterative JD with data estimate refinement by soft quantization the corresponding required $\overline{E}_b/N_0$ is $1.1\,\mathrm{dB}$ larger than that of the reference system. By optimum data estimate refinement, an $\overline{E}_b/N_0$ larger than that in the reference system only by $0.2\,\mathrm{dB}$ is needed in iterative JD in order to achieve an average bit error probability $\overline{P}_b = 10^{-2}$.

If

$$K = 4 \tag{6.23}$$

holds, the average bit error probability $\overline{P}_b$ of iterative JD with optimum data estimate refinement and of data estimate refinement by soft quantization and of RxZF JD is shown in Fig. 6.8. In the case of (6.23), Fig. 6.8 shows that both RxZF JD and iterative JD with data estimate refinement by soft quantization need a $\overline{E}_b/N_0$ larger by $14.3\,\mathrm{dB}$ than the $\overline{E}_b/N_0$ required by the reference system in order to achieve an average bit error probability $\overline{P}_b = 10^{-2}$. On the other hand, if optimum data estimate refinement is applied in iterative JD, an $\overline{E}_b/N_0$ larger by $2.7\,\mathrm{dB}$ is needed to achieve an average bit error probability $\overline{P}_b = 10^{-2}$ as compared to the single user reference system.

Summarizing the results of Figs. 6.7 to 6.8, iterative JD with optimum data estimate refinement can bring substantial gains in terms of the bit error probability $\overline{P}_b$ over iterative JD with data estimate refinement by soft quantization and over RxZF JD. In particular, given a bit error probability $\overline{P}_b = 10^{-2}$, it is shown in Fig. 6.7 that iterative JD with optimum data estimate refinement can reduce the required $\overline{E}_b/N_0$ by $0.9\,\mathrm{dB}$ as compared to iterative JD with data estimate refinement by soft quantization and by $2.1\,\mathrm{dB}$ as compared to RxZF JD. However, the gains in the required $\overline{E}_b/N_0$ by iterative JD with optimum data estimate refinement become higher in a fully loaded system as it is shown in Fig. 6.8. In this case, in contrast to RxZF JD and iterative JD with data estimate refinement by soft quantization which both need a $\overline{E}_b/N_0$ larger by $14.3\,\mathrm{dB}$ than the $\overline{E}_b/N_0$ required by the reference system in order to achieve an average bit error probability $\overline{P}_b = 10^{-2}$, by the employment of iterative JD with optimum data estimate refinement the bit error probability $\overline{P}_b = 10^{-2}$ is obtained with a $2.7\,\mathrm{dB}$ higher $\overline{E}_b/N_0$.

6.3 Asymptotic multiuser efficiency

6.3.1 The asymptotic multiuser efficiency as performance measure

The fact that JD needs a higher $\left(E_{\mathrm{b}}^{(k,n_{\mathrm{F}})}/N_0\right)_{\mathrm{JD}}$ at its input than the $\left(E_{\mathrm{b}}^{(k,n_{\mathrm{F}})}/N_0\right)_{\mathrm{ref}}$ required by the reference system in order to achieve a given target bit error probability $P_{\mathrm{b}}^{(k,n_{\mathrm{F}})}$ is expressed by the multiuser efficiency [Ver98, LV89]

$$\eta_{\mathrm{e}}^{(k,n_{\mathrm{F}})}(\sigma^2) = \left.\frac{\left(E_{\mathrm{b}}^{(k,n_{\mathrm{F}})}/N_0\right)_{\mathrm{ref}}}{\left(E_{\mathrm{b}}^{(k,n_{\mathrm{F}})}/N_0\right)_{\mathrm{JD}}}\right|_{P_{\mathrm{b,JD}}^{(k,n_{\mathrm{F}})} = P_{\mathrm{b,ref}}^{(k,n_{\mathrm{F}})}} \in [0,1] \qquad (6.24)$$

of JD. The asymptotic value of the multiuser efficiency $\eta_{\mathrm{e}}^{(k,n_{\mathrm{F}})}(\sigma^2)$ of (6.24) for vanishing power σ^2 of the noise is termed asymptotic multiuser efficiency [Ver98, LV89]

$$\eta^{(k,n_{\mathrm{F}})} = \lim_{\sigma^2 \to 0} \eta_{\mathrm{e}}^{(k,n_{\mathrm{F}})}(\sigma^2). \qquad (6.25)$$

The use of the asymptotic multiuser efficiency $\eta^{(k,n_{\mathrm{F}})}$ of (6.25) instead of the multiuser efficiency $\eta_{\mathrm{e}}^{(k,n_{\mathrm{F}})}(\sigma^2)$ of (6.24) is advantageous when the description of the performance of JD by a single scalar value is desired. In the present thesis, the asymptotic multiuser efficiency $\eta^{(k,n_{\mathrm{F}})}$ of (6.25) is used to assess linear JD in the sense of RxZF JD without FEC coding.

Using (6.1), the variance σ^2 of real and imaginary parts of each noise value $\underline{n}^{(k_{\mathrm{B}},n_{\mathrm{F}})}$ and with the $K_{\mathrm{B}} \times K$ transfer matrix $\underline{\mathbf{H}}^{(n_{\mathrm{F}})}$, the SNR

$$\begin{aligned}
\gamma_{\mathrm{RxZF}}^{(k,n_{\mathrm{F}})} &= \frac{\left[\mathrm{E}\left\{\underline{\mathbf{d}}^{(n_{\mathrm{F}})}\underline{\mathbf{d}}^{(n_{\mathrm{F}})*\mathrm{T}}\right\}\right]_{k,k}}{\left[\mathrm{E}\left\{\left(\hat{\underline{\mathbf{d}}}^{(n_{\mathrm{F}})} - \underline{\mathbf{d}}^{(n_{\mathrm{F}})}\right)\left(\hat{\underline{\mathbf{d}}}^{(n_{\mathrm{F}})} - \underline{\mathbf{d}}^{(n_{\mathrm{F}})}\right)^{*\mathrm{T}}\right\}\right]_{k,k}} \\
&= \frac{1}{\sigma^2\left[\left(\underline{\mathbf{H}}^{(n_{\mathrm{F}})*\mathrm{T}}\underline{\mathbf{H}}^{(n_{\mathrm{F}})}\right)^{-1}\right]_{k,k}}
\end{aligned} \qquad (6.26)$$

of the estimated data symbol $\hat{\underline{d}}^{(k,n_{\mathrm{F}})}$ of RxZF JD according to (4.21) is calculated. Due to the fact that the estimated data symbol $\hat{\underline{d}}^{(k,n_{\mathrm{F}})}$ of (4.21) is unbiased, the estimation error $\hat{\underline{\mathbf{d}}}^{(n_{\mathrm{F}})} - \underline{\mathbf{d}}^{(n_{\mathrm{F}})}$ is Gaussian [XSR90, Ver98, LV89] and with the output SNR $\gamma_{\mathrm{RxZF}}^{(k,n_{\mathrm{F}})}$ of (6.26), the bit error probability

$$P_{\mathrm{b,RxZF}}^{(k,n_{\mathrm{F}})} = \frac{1}{2}\mathrm{erfc}\left(\sqrt{\frac{\gamma_{\mathrm{RxZF}}^{(k,n_{\mathrm{F}})}}{2}}\right) \qquad (6.27)$$

of each bit in the QPSK data symbol $\underline{d}^{(k,n_{\mathrm{F}})}$ results. Setting out from the fact that the bit error probability $P_{\mathrm{b,RxZF}}^{(k,n_{\mathrm{F}})}$ of (6.27) is a bijective and strictly monotonically decreasing function of the output SNR $\gamma_{\mathrm{RxZF}}^{(k,n_{\mathrm{F}})}$ of (6.26), $\eta_{\mathrm{e}}^{(k,n_{\mathrm{F}})}(\sigma^2)$ of (6.24) becomes

$$\eta_{\mathrm{e}}^{(k,n_{\mathrm{F}})}(\sigma^2) = \left. \frac{\left(E_{\mathrm{b}}^{(k,n_{\mathrm{F}})}/N_0 \right)_{\mathrm{ref}}}{\left(E_{\mathrm{b}}^{(k,n_{\mathrm{F}})}/N_0 \right)_{\mathrm{JD}}} \right|_{\gamma_{\mathrm{RxZF}}^{(k,n_{\mathrm{F}})} = \gamma_{\mathrm{ref}}^{(k,n_{\mathrm{F}})}} \in [0, 1]. \tag{6.28}$$

It can be shown with the receive energy $R^{(k,n_{\mathrm{F}})}$ of (6.3) and with σ^2 of (3.14) that in SA-based systems in the absence of FEC coding

$$\frac{E_{\mathrm{b}}^{(k,n_{\mathrm{F}})}}{N_0} = \left(\frac{E_{\mathrm{b}}^{(k,n_{\mathrm{F}})}}{N_0} \right)_{\mathrm{ref}} = \left(\frac{E_{\mathrm{b}}^{(k,n_{\mathrm{F}})}}{N_0} \right)_{\mathrm{JD}} = \frac{1}{2} \frac{R^{(k,n_{\mathrm{F}})}}{N_0} = \frac{1}{2\sigma^2} \left[\underline{\mathbf{H}}^{(n_{\mathrm{F}})*\mathrm{T}} \underline{\mathbf{H}}^{(n_{\mathrm{F}})} \right]_{k,k} \tag{6.29}$$

holds. Further, using (6.26) and (6.29), the SNR

$$\gamma_{\mathrm{RxZF}}^{(k,n_{\mathrm{F}})} = 2 \left(\left[\left(\underline{\mathbf{H}}^{(n_{\mathrm{F}})*\mathrm{T}} \underline{\mathbf{H}}^{(n_{\mathrm{F}})} \right)^{-1} \right]_{k,k} \left[\underline{\mathbf{H}}^{(n_{\mathrm{F}})*\mathrm{T}} \underline{\mathbf{H}}^{(n_{\mathrm{F}})} \right]_{k,k} \right)^{-1} \frac{E_{\mathrm{b}}^{(k,n_{\mathrm{F}})}}{N_0} \tag{6.30}$$

of the estimate of the data symbol $\underline{d}^{(k,n_{\mathrm{F}})}$ by RxZF JD and with (6.6) and (6.29), the SNR

$$\gamma_{\mathrm{ref}}^{(k,n_{\mathrm{F}})} = 2 \frac{E_{\mathrm{b}}^{(k,n_{\mathrm{F}})}}{N_0} \tag{6.31}$$

of the estimate of the data symbol $\underline{d}^{(k,n_{\mathrm{F}})}$ by the reference system are calculated. As (6.30) and (6.31) show, both $\gamma_{\mathrm{RxZF}}^{(k,n_{\mathrm{F}})}$ and $\gamma_{\mathrm{ref}}^{(k,n_{\mathrm{F}})}$ are linear functions of $E_{\mathrm{b}}^{(k,n_{\mathrm{F}})}/N_0$ of (6.29) and therefore the expression of the multiuser efficiency $\eta_{\mathrm{e}}^{(k,n_{\mathrm{F}})}(\sigma^2)$ of (6.28) is further simplified to

$$\eta_{\mathrm{e,RxZF}}^{(k,n_{\mathrm{F}})}(\sigma^2) = \frac{\gamma_{\mathrm{RxZF}}^{(k,n_{\mathrm{F}})}}{\gamma_{\mathrm{ref}}^{(k,n_{\mathrm{F}})}} = \left(\left[\left(\underline{\mathbf{H}}^{(n_{\mathrm{F}})*\mathrm{T}} \underline{\mathbf{H}}^{(n_{\mathrm{F}})} \right)^{-1} \right]_{k,k} \left[\underline{\mathbf{H}}^{(n_{\mathrm{F}})*\mathrm{T}} \underline{\mathbf{H}}^{(n_{\mathrm{F}})} \right]_{k,k} \right)^{-1} \tag{6.32}$$

According to (6.32), the multiuser efficiency $\eta_{\mathrm{e,RxZF}}^{(k,n_{\mathrm{F}})}(\sigma^2)$ of RxZF JD in SA-based systems does not depend on $E_{\mathrm{b}}^{(k,n_{\mathrm{F}})}/N_0$ and hence, with (6.25) a compact expression also for the asymptotic multiuser efficiency

$$\eta_{\mathrm{RxZF}}^{(k,n_{\mathrm{F}})} = \frac{\gamma_{\mathrm{RxZF}}^{(k,n_{\mathrm{F}})}}{\gamma_{\mathrm{ref}}^{(k,n_{\mathrm{F}})}} = \left(\left[\left(\underline{\mathbf{H}}^{(n_{\mathrm{F}})*\mathrm{T}} \underline{\mathbf{H}}^{(n_{\mathrm{F}})} \right)^{-1} \right]_{k,k} \left[\underline{\mathbf{H}}^{(n_{\mathrm{F}})*\mathrm{T}} \underline{\mathbf{H}}^{(n_{\mathrm{F}})} \right]_{k,k} \right)^{-1} \tag{6.33}$$

of RxZF JD without FEC coding is derived.

For the case of QPSK using the asymptotic multiuser efficiency $\eta_{\mathrm{RxZF}}^{(k,n_{\mathrm{F}})}$ of (6.33), for the bit error probability $P_{\mathrm{b,RxZF}}^{(k,n_{\mathrm{F}})}$ of (6.27)

$$P_{\mathrm{b,RxZF}}^{(k,n_{\mathrm{F}})} = \frac{1}{2}\mathrm{erfc}\left(\sqrt{\eta_{\mathrm{RxZF}}^{(k,n_{\mathrm{F}})} \frac{\gamma_{\mathrm{ref}}^{(k,n_{\mathrm{F}})}}{2}} \right) \tag{6.34}$$

follows.

Closely related to the asymptotic multiuser efficiency $\eta_{\mathrm{RxZF}}^{(k,n_{\mathrm{F}})}$ of (6.33) is the SNR degradation [Kle96, SWC$^+$02]

$$
\begin{aligned}
\delta_{\mathrm{RxZF}}^{(k,n_{\mathrm{F}})} &= \frac{\gamma_{\mathrm{ref}}^{(k,n_{\mathrm{F}})}}{\gamma_{\mathrm{RxZF}}^{(k,n_{\mathrm{F}})}} \\
&= \left[\left(\underline{\mathbf{H}}^{(n_{\mathrm{F}})*\mathrm{T}}\underline{\mathbf{H}}^{(n_{\mathrm{F}})}\right)^{-1}\right]_{k,k} \left[\underline{\mathbf{H}}^{(n_{\mathrm{F}})*\mathrm{T}}\underline{\mathbf{H}}^{(n_{\mathrm{F}})}\right]_{k,k}
\end{aligned}
\tag{6.35}
$$

of RxZF JD. From the comparison of (6.35) and (6.33) follows that in the case of RxZF JD of the data symbol $\underline{d}^{(k,n_{\mathrm{F}})}$ the SNR degradation $\delta_{\mathrm{RxZF}}^{(k,n_{\mathrm{F}})}$ is the inverse of the asymptotic multiuser efficiency $\eta_{\mathrm{RxZF}}^{(k,n_{\mathrm{F}})}$ and quantifies the decreased SNR $\gamma_{\mathrm{RxZF}}^{(k,n_{\mathrm{F}})}$ of RxZF JD as compared to the SNR $\gamma_{\mathrm{ref}}^{(k,n_{\mathrm{F}})}$ of the reference system. The said decrease of the SNR is the price to be paid for the elimination of intra-SA interference by RxZF JD. Moreover, in the case of RxZF JD, the SNR degradation $\delta_{\mathrm{RxZF}}^{(k,n_{\mathrm{F}})}$ of (6.35) and the asymptotic multiuser efficiency $\eta_{\mathrm{RxZF}}^{(k,n_{\mathrm{F}})}$ of (6.33) both express the fact that only the component of the useful received signal of MT k is used which is orthogonal to the received signals corresponding to the other $K-1$ MTs of the SA due to the need for elimination of the intra-SA interference. Hence, the SNR degradation $\delta_{\mathrm{RxZF}}^{(k,n_{\mathrm{F}})}$ of (6.35), and equivalently the inverse of the asymptotic multiuser efficiency $\eta_{\mathrm{RxZF}}^{(k,n_{\mathrm{F}})}$ of (6.33) are a measure for the amount of intra-SA interference disturbing the estimation of data symbol $\underline{d}^{(k,n_{\mathrm{F}})}$.

6.3.2 Statistics of the asymptotic multiuser efficiency of receive zero-forcing joint detection

Following the argumentation of Section 6.3.1, according to which the asymptotic multiuser efficiency $\eta_{\mathrm{RxZF}}^{(k,n_{\mathrm{F}})}$ of (6.33) of RxZF JD is a measure for the intra-SA interference, in the present Section the asymptotic multiuser efficiency $\eta_{\mathrm{RxZF}}^{(k,n_{\mathrm{F}})}$ is investigated by the aid of the indoor geometric channel model at a single subcarrier n_{F} in order to provide insight into characteristics of the intra-SA interference.

Using the indoor geometric channel model described in Section 2.3.2, with the distance $r^{(k,k_{\mathrm{B}})}$ between MT k and AP k_{B} and the wavelength λ, follows from (2.4) for the corresponding channel coefficient

$$
\underline{h}^{(k,k_{\mathrm{B}},n_{\mathrm{F}})} = \frac{1}{r^{(k,k_{\mathrm{B}})}} \exp\left(-\mathrm{j}\frac{2\pi}{\lambda}r^{(k,k_{\mathrm{B}})}\right).
\tag{6.36}
$$

In the considered scenario

$$
K = 2
\tag{6.37}
$$

MTs and

$$K_{\mathrm{B}} = 2 \tag{6.38}$$

APs are considered. If (6.38) holds, then the SA structure resulting from the geometric channel model of Section 2.3.2 is symmetrical. Due to the symmetry of the scenario, it suffices to consider only the space defined by $x \in [0, x_{\mathrm{max}}/2]$ and $y \in [0, y_{\mathrm{max}}/2]$. Without loss of generality, MT 1 is placed at the origin, i.e.,

$$r^{(1,1)} = r^{(1,2)} = r_{\mathrm{B}} \tag{6.39}$$

holds. MT 2 is randomly positioned in the considered scenario and the variable $\alpha \in \mathbb{R}$ is introduced to quantize the difference between $r^{(2,1)}$ and $r^{(2,2)}$ as

$$r^{(2,2)} = r^{(2,1)} + \alpha. \tag{6.40}$$

With the coefficients $\underline{h}^{(k,k_{\mathrm{B}},n_{\mathrm{F}})}$, $k = 1 \ldots K$, $k_{\mathrm{B}} = 1 \ldots K_{\mathrm{B}}$, of (6.36) and with the distances $r^{(k,k_{\mathrm{B}})}$, $k = 1 \ldots K$, $k_{\mathrm{B}} = 1 \ldots K_{\mathrm{B}}$, according to (6.39) and (6.40), the asymptotic multiuser efficiency

$$\overline{\eta}_{\mathrm{RxZF}}^{(n_{\mathrm{F}})} = \frac{1}{2} - \frac{\left(\alpha + r^{(2,1)}\right) \cos\left(\dfrac{2\pi}{\lambda}\alpha\right)}{2\, r^{(2,1)2} + 2\alpha\, r^{(2,1)} + \alpha^2} \tag{6.41}$$

averaged over the K data symbols $\underline{d}^{(k,n_{\mathrm{F}})}$, $k = 1 \ldots K$, can be calculated from (6.33). As can be seen from (6.41), the average asymptotic multiuser efficiency $\overline{\eta}_{\mathrm{RxZF}}^{(n_{\mathrm{F}})}$ depends on $r^{(2,1)}$ and α, or equivalently, $\overline{\eta}_{\mathrm{RxZF}}^{(n_{\mathrm{F}})}$ of (6.41) is a scalar function of the coordinates $\left(x_{\mathrm{MT}}^{(2)}, y_{\mathrm{MT}}^{(2)}\right)$ of MT 2. Hence, $\overline{\eta}_{\mathrm{RxZF}}^{(n_{\mathrm{F}})}$ of (6.41) at the considered scenario can be visualized with the aid of a three-dimensional plot of $\overline{\eta}_{\mathrm{RxZF}}^{(n_{\mathrm{F}})}$ of (6.41) with respect to the coordinates $\left(x_{\mathrm{MT}}^{(2)}, y_{\mathrm{MT}}^{(2)}\right)$ of MT 2. Fig. 6.9 contains the aforementioned three-dimensional plot.

As Fig. 6.9 shows, the spatial distribution of $\overline{\eta}_{\mathrm{RxZF}}^{(n_{\mathrm{F}})}$ is characterized by a periodical succession of maxima and minima. The expression of (6.41) for $\overline{\eta}_{\mathrm{RxZF}}^{(n_{\mathrm{F}})}$ can be rewritten as

$$\overline{\eta}_{\mathrm{RxZF}}^{(n_{\mathrm{F}})} = \frac{1}{2} - \frac{\left(\dfrac{\alpha}{r^{(2,1)}} + 1\right) \cos\left(\dfrac{2\pi}{\lambda}\alpha\right)}{2 + 2\left(\dfrac{\alpha}{r^{(2,1)}}\right) + \left(\dfrac{\alpha}{r^{(2,1)}}\right)^2}. \tag{6.42}$$

Given a fixed distance $r^{(2,1)}$ and if $\alpha/r^{(2,1)} \ll 1$, which holds, e.g., if the distances $r^{(2,k_{\mathrm{B}})}$, $k_{\mathrm{B}} = 1 \ldots K_{\mathrm{B}}$, of MT 2 to the APs of the SA are in the order of magnitude of tens of λ, the terms $\alpha/r^{(2,1)}$ in (6.42) vanish and the variation of $\overline{\eta}_{\mathrm{RxZF}}^{(n_{\mathrm{F}})}$ of (6.42) is dominated by the variation of the term $\cos\left(\dfrac{2\pi}{\lambda}\alpha\right)$. Hence, it follows from (6.42) that $\overline{\eta}_{\mathrm{RxZF}}^{(n_{\mathrm{F}})}$ of (6.42) has

- minima $\overline{\eta}_{\mathrm{RxZF}}^{(n_{\mathrm{F}})} = 0$ at $\alpha = \kappa\lambda$, $\kappa \in \mathbb{N}$, and
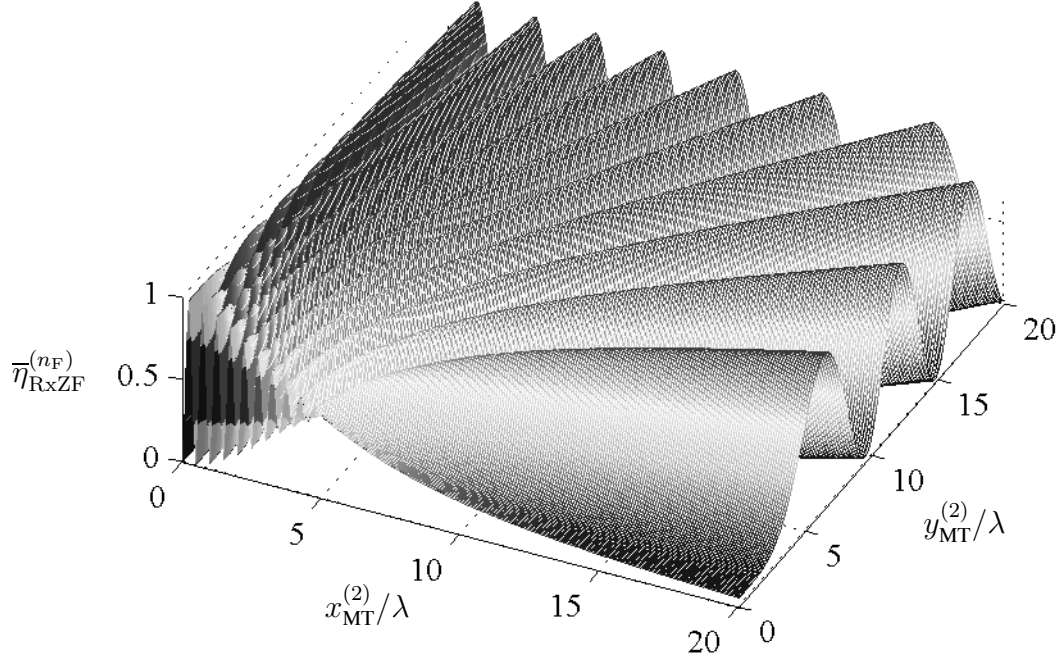
Figure 6.9. Average asymptotic multiuser efficiency $\overline{\eta}_{\mathrm{RxZF}}^{(n_{\mathrm{F}})}$ of RxZF JD as a function of $\left(x_{\mathrm{MT}}^{(2)}, y_{\mathrm{MT}}^{(2)} \right)$; Parameters: $K = 2$, $K_{\mathrm{B}} = 2$, geometric indoor channel model, $x_{\max} = 40\lambda$, $y_{\max} = 40\lambda$, $r_{\mathrm{B}} = 5\lambda$, $\lambda = 0.15\,\mathrm{m}$

- maxima $\overline{\eta}_{\mathrm{RxZF}}^{(n_{\mathrm{F}})} = 1$ at $\alpha = \dfrac{\kappa}{2}\lambda$, $\kappa \in \mathbb{N}$.

Moreover, due to the dependence of the minima and maxima of $\overline{\eta}_{\mathrm{RxZF}}^{(n_{\mathrm{F}})}$ on α, which according to (6.40) is the difference of the distances from MT2 to the APs of the SA, i.e., to two fixed points, the paths along which $\overline{\eta}_{\mathrm{RxZF}}^{(n_{\mathrm{F}})}$ presents maxima and minima have a hyperbolic form.

In order to provide a physical explanation for the maxima and minima of the asymptotic multiuser efficiency $\overline{\eta}_{\mathrm{RxZF}}^{(n_{\mathrm{F}})}$ of (6.42), the fact that the k-th column

$$\left[\underline{\mathbf{H}}^{(n_{\mathrm{F}})} \right]_k = \left(\underline{h}^{(k,1,n_{\mathrm{F}})} \dots \underline{h}^{(k,K_{\mathrm{B}},n_{\mathrm{F}})} \right)^{\mathrm{T}} \tag{6.43}$$

of the $K_{\mathrm{B}} \times K$ channel matrix $\underline{\mathbf{H}}^{(n_{\mathrm{F}})}$ describes the wireless channel between MT k and the K_{B} APs of the SA at subcarrier n_{F} is exploited. In the specific considered scenario, the wireless channel $\left[\underline{\mathbf{H}}^{(n_{\mathrm{F}})} \right]_1$ of MT 1 is a scaled all-ones vector, whereas if $\alpha/r^{(2,1)} \ll 1$ holds, the wireless channel $\left[\underline{\mathbf{H}}^{(n_{\mathrm{F}})} \right]_2$ of MT 2 is determined by the value of α:

- If $\alpha = \kappa\lambda$, $\kappa \in \mathbb{N}$, using (6.36), (6.40) and (6.43), it follows that the wireless channel $\left[\underline{\mathbf{H}}^{(n_{\mathrm{F}})} \right]_2$ of MT 2 is also a scaled all-ones vector. In this case, the wireless channels

$\left[\underline{\mathbf{H}}^{(n_{\mathrm{F}})}\right]_{k}$, $k = 1 \ldots K$, are up to a scaling factor identical, i.e., the vectors $\left[\underline{\mathbf{H}}^{(n_{\mathrm{F}})}\right]_{k}$, $k = 1 \ldots K$, have the same direction, and because RxZF JD uses only the orthogonal parts of each of the partial received signals, a poor use of the receive energy $R^{(k,n_{\mathrm{F}})}$ is made and a zero asymptotic multiuser efficiency $\overline{\eta}_{\mathrm{RxZF}}^{(n_{\mathrm{F}})}$ results.

- If $\alpha = \dfrac{\kappa}{2}\lambda$, $\kappa \in \mathbb{N}$, using (6.36), (6.40) and (6.43), it follows that the wireless channel $\left[\underline{\mathbf{H}}^{(n_{\mathrm{F}})}\right]_{2}$ of MT 2 consists of elements antipodal to each other. Equivalently, the vectors $\left[\underline{\mathbf{H}}^{(n_{\mathrm{F}})}\right]_{k}$, $k = 1 \ldots K$, are orthogonal which means that orthogonal partial signals comprise the received signal. Hence, RxZF JD makes optimum use of the receive energy $R^{(k,n_{\mathrm{F}})}$ and a unity $\overline{\eta}_{\mathrm{RxZF}}^{(n_{\mathrm{F}})}$ results.

Concluding, the dependence of the average asymptotic multiuser efficiency $\overline{\eta}_{\mathrm{RxZF}}^{(n_{\mathrm{F}})}$ of RxZF JD and equivalently, of the amount of intra-SA interference disturbing each of the partial received signals, on the correlation between the wireless channels $\left[\underline{\mathbf{H}}^{(n_{\mathrm{F}})}\right]_{k}$, $k = 1 \ldots K$, which is expected from theory, is visualized and analyzed with the aid of the geometrical indoor model.

A further interesting aspect concerning the intra-SA interference is the investigation of the statistical properties of the average asymptotic multiuser efficiency $\overline{\eta}_{\mathrm{RxZF}}^{(n_{\mathrm{F}})}$ of the data symbols $\underline{d}^{(k,n_{\mathrm{F}})}$, $k = 1 \ldots K$, of RxZF JD. For random positioning of the K MTs, Figs. 6.10 and 6.11 depict the complementary cumulative distribution function (CCDF) $\mathrm{Prob}\left\{\overline{\eta}_{\mathrm{RxZF}}^{(n_{\mathrm{F}})} \geq \Gamma\right\}$ of $\overline{\eta}_{\mathrm{RxZF}}^{(n_{\mathrm{F}})}$. Following parameters are common to Figs. 6.10 and 6.11:

- indoor geometric channel model,

- single subcarrier,

- $r_{\mathrm{B}} = 5\lambda$,

- $x_{\max} = 40\lambda$, and

- $y_{\max} = 40\lambda$.

For

$$K = 2 \tag{6.44}$$

Fig. 6.10 shows that by an equal number K_{B} of installed APs an average asymptotic multiuser efficiency $\overline{\eta}_{\mathrm{RxZF}}^{(n_{\mathrm{F}})}$ of at least 0.6 is achieved with probability 0.3. Increasing the number of APs to 3,4,5, and 6 results in a corresponding increase of the probability $\mathrm{Prob}\left\{\overline{\eta}_{\mathrm{RxZF}}^{(n_{\mathrm{F}})} \geq 0.6\right\}$ to 0.55, 0.65, 0.75, and 0.85, respectively.
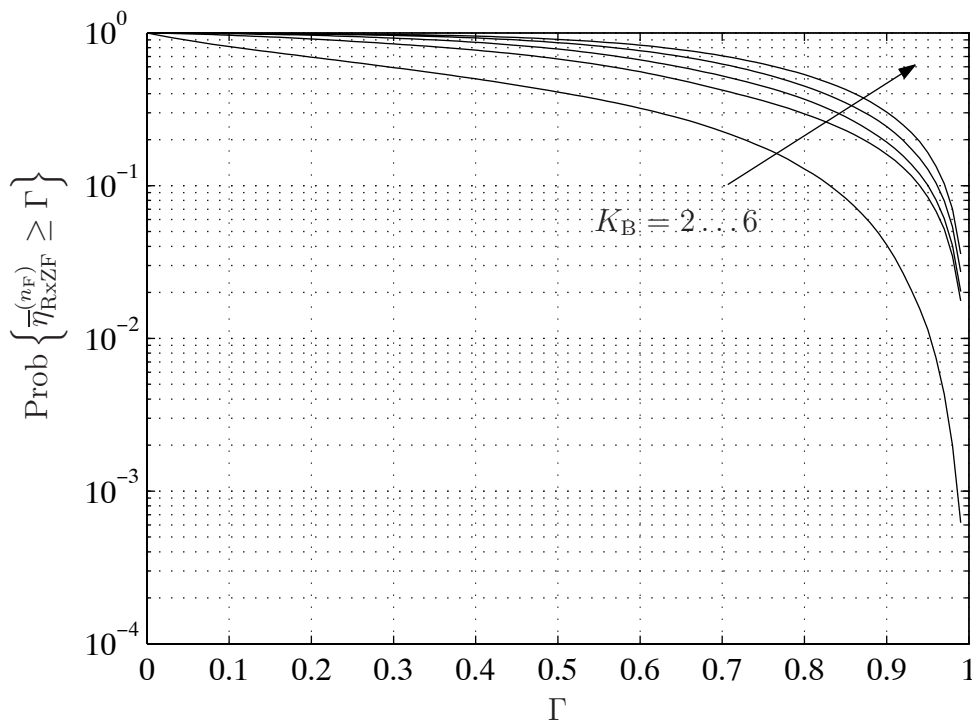
Figure 6.10. CCDF of $\overline{\eta}_{\mathrm{RxZF}}^{(n_{\mathrm{F}})}$; Parameters: $K = 2$, $K_{\mathrm{B}} = 2 \ldots 6$, single subcarrier, geometric indoor channel model, $r_{\mathrm{B}} = 5\lambda$, $x_{\max} = 40\lambda$, $y_{\max} = 40\lambda$
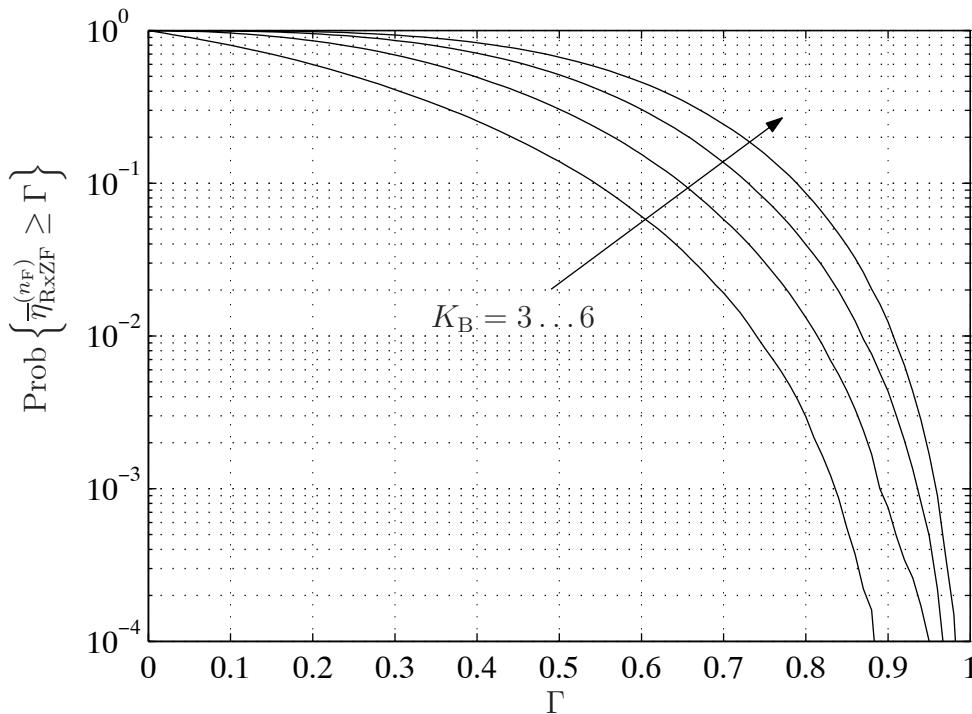
Figure 6.11. CCDF of $\overline{\eta}_{\mathrm{RxZF}}^{(n_{\mathrm{F}})}$; Parameters: $K = 3$, $K_{\mathrm{B}} = 3 \ldots 6$, single subcarrier, geometric indoor channel model, $r_{\mathrm{B}} = 5\lambda$, $x_{\max} = 40\lambda$, $y_{\max} = 40\lambda$

In the case of

$$K = 3 \tag{6.45}$$

it can be seen from Fig. 6.11 that by the use of a number $K_{\mathrm{B}} = K$ of APs, an $\overline{\eta}_{\mathrm{RxZF}}^{(n_{\mathrm{F}})}$ of 0.6 is achieved with probability 0.06. On the other hand, if 4, 5, or 6 APs are used, an average asymptotic multiuser efficiency $\overline{\eta}_{\mathrm{RxZF}}^{(n_{\mathrm{F}})}$ of at least 0.6 is obtained with probabilities 0.15, 0.3, and 0.45, respectively.

Comparing Figs. 6.10 and 6.11 the conclusion can be drawn that given a fixed number K of MTs in the SA, with an increasing number K_{B} of the employed APs an also increasing value of the minimum average asymptotic multiuser efficiency $\overline{\eta}_{\mathrm{RxZF}}^{(n_{\mathrm{F}})}$ which can be achieved with a given probability results. Equivalently, if K_{B} increases the degree by which the K wireless channels $\left[\underline{\mathbf{H}}^{(n_{\mathrm{F}})} \right]_{k}$, $k = 1 \ldots K$, are correlated decreases and intra-SA interference can be combated more efficiently. Moreover, Figs. 6.10 and 6.11 show that the cases of (6.44) and (6.45) are not equivalent in terms of the probability with which a given $\overline{\eta}_{\mathrm{RxZF}}^{(n_{\mathrm{F}})}$ can be obtained. In particular, if (6.45) holds, for a given ratio K/K_{B}, a desired value of $\overline{\eta}_{\mathrm{RxZF}}^{(n_{\mathrm{F}})}$ is achieved with a lower probability as compared to the case of (6.44).

7 Performance investigation of downlink transmission

7.1 Preliminary remarks

After having introduced the model for JT in the DL of SA-based systems in Chapter 5, the assessment of the performance of the various JT schemes forms the topic of the present Chapter. To this end, performance measures appropriate for the assessment of JT are introduced and with the aid of the said measures, the JT algorithms presented in Chapter 5 are assessed under different scenarios.

As it is the case in Chapter 6, it is assumed that each data symbol $\underline{d}^{(k,n_\mathrm{F})}$ intended for MT k at subcarrier n_F is the result of a QPSK modulation, if not explicitly stated otherwise. Moreover, data symbols intended for different MTs are assumed to be uncorrelated. Hence, with the $K \times K$ identity matrix $\mathbf{I}_K$, for the data correlation matrix $\underline{\mathbf{R}}_{\mathrm{dd}}^{(n_\mathrm{F})}$ of dimension $K \times K$ at subcarrier n_F

$$\underline{\mathbf{R}}_{\mathrm{dd}}^{(n_\mathrm{F})} = \mathrm{E}\left\{ \underline{\mathbf{d}}^{(n_\mathrm{F})} \underline{\mathbf{d}}^{(n_\mathrm{F})*\mathrm{T}} \right\} = 2\,\mathbf{I}_K \tag{7.1}$$

holds. It is also assumed that the noise value $\underline{n}^{(k,n_\mathrm{F})}$ present at the antenna of MT k at subcarrier n_F is a complex zero-mean Gaussian variable with variance σ^2 of real and imaginary parts. Moreover, due to the spatial separation of the MTs, noise values $\underline{n}^{(k,n_\mathrm{F})}$ and $\underline{n}^{(k',n_\mathrm{F})}$ at different MTs $k \neq k'$ are uncorrelated. As a result, with the $K \times K$ identity matrix $\mathbf{I}_K$, for the noise correlation matrix $\underline{\mathbf{R}}_{\mathrm{nn}}^{(n_\mathrm{F})}$ of dimension $K \times K$ at subcarrier n_F holds

$$\underline{\mathbf{R}}_{\mathrm{nn}}^{(n_\mathrm{F})} = \mathrm{E}\left\{ \underline{\mathbf{n}}^{(n_\mathrm{F})} \underline{\mathbf{n}}^{(n_\mathrm{F})*\mathrm{T}} \right\} = 2\sigma^2\mathbf{I}_K. \tag{7.2}$$

In JT, the transmit vector $\underline{\mathbf{s}}^{(n_\mathrm{F})}$ is generated by the CU jointly from all data symbols $\underline{d}^{(k,n_\mathrm{F})}$, $k = 1\ldots K$, as described in Chapter 5. Compared to a reference system, in which only the data symbol $\underline{d}^{(k,n_\mathrm{F})}$ is transmitted, in JT the additional task of suppressing the intra-SA interference exists. Therefore, with the partial transmit energy $T^{(k,n_\mathrm{F})}$ associated with data symbol $\underline{d}^{(k,n_\mathrm{F})}$, the price to be paid for the interference suppression in JT is the suboptimum use of the partial transmit energy $T^{(k,n_\mathrm{F})}$.

All performance measures for JT introduced in the following assess the said suboptimum use of the partial transmit energy $T^{(k,n_\mathrm{F})}$. In particular, the suboptimum use of the partial transmit energy $T^{(k,n_\mathrm{F})}$ is assessed in terms of the bit error probability measured at each MT, and by means of the efficiency with which JT converts the partial transmit energy $T^{(k,n_\mathrm{F})}$ into receive energy $R^{(k,n_\mathrm{F})}$.

The reference system is the system which optimally uses the transmit energy $T^{(k,n_{\mathrm{F}})}$. With the transfer matrix $\underline{\mathbf{H}}^{(n_{\mathrm{F}})\mathrm{T}}$ valid for the DL in a SA-based system, in the reference system a single data symbol $\underline{d}^{(k,n_{\mathrm{F}})}$ is transmitted from the core network over the mobile radio channel characterized by the row transfer vector $\left(\left[\underline{\mathbf{H}}^{(n_{\mathrm{F}})}\right]_k\right)^{\mathrm{T}}$. To this end the TxMF transmit vector [JKG$^+$02]

$$\underline{\mathbf{s}}^{(n_{\mathrm{F}})} = \left(\left[\underline{\mathbf{H}}^{(n_{\mathrm{F}})}\right]_k\right)^* \underline{d}^{(k,n_{\mathrm{F}})} \tag{7.3}$$

is used, the choice of which is optimum in terms of use of the corresponding transmit energy

$$\begin{aligned}
T_{\mathrm{ref}}^{(k,n_{\mathrm{F}})} &= \frac{1}{2}\mathrm{E}\left\{\underline{\mathbf{s}}^{(n_{\mathrm{F}})*\mathrm{T}}\underline{\mathbf{s}}^{(n_{\mathrm{F}})}\right\} \\
&= \frac{1}{2}\mathrm{E}\left\{|\underline{d}^{(k,n_{\mathrm{F}})}|^2\right\}\left(\left[\underline{\mathbf{H}}^{(n_{\mathrm{F}})}\right]_k\right)^{\mathrm{T}}\left(\left[\underline{\mathbf{H}}^{(n_{\mathrm{F}})}\right]_k\right)^* \\
&= \left[\underline{\mathbf{H}}^{(n_{\mathrm{F}})\mathrm{T}}\underline{\mathbf{H}}^{(n_{\mathrm{F}})*}\right]_{k,k}.
\end{aligned} \tag{7.4}$$

Given the transmit energy $T_{\mathrm{ref}}^{(k,n_{\mathrm{F}})}$ of (7.4), using (7.1), and with the transmit vector $\underline{\mathbf{s}}^{(n_{\mathrm{F}})}$ of (7.3), the received value

$$\underline{e}^{(k,n_{\mathrm{F}})} = \left(\left[\underline{\mathbf{H}}^{(n_{\mathrm{F}})}\right]_k\right)^{\mathrm{T}}\underline{\mathbf{s}}^{(n_{\mathrm{F}})} + \underline{n}^{(k,n_{\mathrm{F}})} \tag{7.5}$$

with the maximum possible receive energy

$$\begin{aligned}
R_{\mathrm{ref}}^{(k,n_{\mathrm{F}})} &= \frac{1}{2}\mathrm{E}\left\{\left|\underline{e}^{(k,n_{\mathrm{F}})}\right|^2\right\} \\
&= \frac{1}{2}\mathrm{E}\left\{\left(\left(\left[\underline{\mathbf{H}}^{(n_{\mathrm{F}})}\right]_k\right)^{\mathrm{T}}\underline{\mathbf{s}}^{(n_{\mathrm{F}})}\right)^{*\mathrm{T}}\left(\left[\underline{\mathbf{H}}^{(n_{\mathrm{F}})}\right]_k\right)^{\mathrm{T}}\underline{\mathbf{s}}^{(n_{\mathrm{F}})}\right\} \\
&= \left(\left[\underline{\mathbf{H}}^{(n_{\mathrm{F}})\mathrm{T}}\underline{\mathbf{H}}^{(n_{\mathrm{F}})*}\right]_{k,k}\right)^2
\end{aligned} \tag{7.6}$$

is produced. Due to the fact that, given the transmit energy $T_{\mathrm{ref}}^{(k,n_{\mathrm{F}})}$ of (7.4), the received energy $R_{\mathrm{ref}}^{(k,n_{\mathrm{F}})}$ of (7.6) is maximum, the reference system achieves also the minimum possible bit error probability $P_{\mathrm{b,ref}}^{(k,n_{\mathrm{F}})}$ [Pro95].

The resulting bit error probability $P_{\mathrm{b,ref}}^{(k,n_{\mathrm{F}})}$ of the reference system can be computed for the case of QPSK using the received energy $R_{\mathrm{ref}}^{(k,n_{\mathrm{F}})}$ of (7.6) and the variance σ^2 or the real and imaginary parts of each noise value $\underline{n}^{(k,n_{\mathrm{F}})}$, as

$$P_{\mathrm{b,ref}}^{(k,n_{\mathrm{F}})} = \frac{1}{2}\mathrm{erfc}\left(\sqrt{\frac{1}{2\sigma^2}\left[\underline{\mathbf{H}}^{(n_{\mathrm{F}})\mathrm{T}}\underline{\mathbf{H}}^{(n_{\mathrm{F}})*}\right]_{k,k}}\right). \tag{7.7}$$

As only the transmission of $\underline{d}^{(k,n_{\mathrm{F}})}$ is considered, the optimum performance of the reference system in terms of the considered performance measures is also referred to as single user bound.

7.2 Bit error probability

7.2.1 The bit error probability as performance measure

The bit error probability $P_{\mathrm{b}}^{(k,n_{\mathrm{F}})}$ associated with each bit in the QPSK data symbol $\underline{d}^{(k,n_{\mathrm{F}})}$ depends on the receive energy $R^{(k,n_{\mathrm{F}})}$ and on the variance σ^2 of the real and imaginary parts of the noise value $\underline{n}^{(k,n_{\mathrm{F}})}$ at the antenna of the considered MT k. The MTs in a SA-based system employ no multiuser detection, and therefore the receive energy $R^{(k,n_{\mathrm{F}})}$ is used in an optimum way by each MT k.

In order to investigate the suboptimum conversion of the transmit energy $T^{(k,n_{\mathrm{F}})}$ into receive energy $R^{(k,n_{\mathrm{F}})}$ in terms of the bit error probability $P_{\mathrm{b}}^{(k,n_{\mathrm{F}})}$, with the variance σ^2 or the real and imaginary parts of the noise value $\underline{n}^{(k,n_{\mathrm{F}})}$ the bit error probability $P_{\mathrm{b}}^{(k,n_{\mathrm{F}})}$ of each bit in the QPSK data symbol $\underline{d}^{(k,n_{\mathrm{F}})}$ is simulated versus $T^{(k,n_{\mathrm{F}})}/\sigma^2$. Given a value of $T^{(k,n_{\mathrm{F}})}/\sigma^2$, the increased bit error probability $P_{\mathrm{b}}^{(k,n_{\mathrm{F}})}$ of JT as compared to the bit error probability $P_{\mathrm{b,ref}}^{(k,n_{\mathrm{F}})}$ of the reference system reflects the suboptimum use of the transmit energy $T^{(k,n_{\mathrm{F}})}$.

7.2.2 Bit error probability of transmit zero-forcing joint transmission

In the present Section the performance of TxZF JT is assessed in terms of the bit error probability $P_{\mathrm{b}}^{(k,n_{\mathrm{F}})}$ of the data symbol $\underline{d}^{(k,n_{\mathrm{F}})}$. The target of the assessment is to quantify the effectiveness by which a given transmit energy $T^{(k,n_{\mathrm{F}})}$ is used in TxZF JT relative to the reference system which achieves an optimum use of the transmit energy $T^{(k,n_{\mathrm{F}})}$.

Due to the fact that TxZF JT in the DL transmission eliminates intra-SA interference just as RxZF JD eliminates intra-SA interference in the UL transmission, the bit error probability $P_{\mathrm{b}}^{(k,n_{\mathrm{F}})}$ of TxZF JT is investigated in comparison to the bit error probability $P_{\mathrm{b}}^{(k,n_{\mathrm{F}})}$ of RxZF JD. In order to perform the said comparison, in the case of RxZF JD each data symbol $\underline{d}^{(k,n_{\mathrm{F}})}$ is scaled with the factor $\sqrt{\left[\left(\underline{\mathbf{H}}^{*\mathrm{T}}\underline{\mathbf{H}}\right)^{-1}\right]_{k,k}}$ so that RxZF JD delivers the estimated data symbol $\hat{\underline{d}}^{(k,n_{\mathrm{F}})}$ with a fixed SNR $\gamma_{\mathrm{RxZF}}^{(k,n_{\mathrm{F}})} = 1/\sigma^2$, see (6.26), equal to the SNR of the estimated data symbol $\hat{\underline{d}}^{(k,n_{\mathrm{F}})}$ by TxZF JT.

Fig. 7.1 shows the bit error probability $P_{\mathrm{b}}^{(1,1)}$ of the data symbol $\underline{d}^{(1,1)}$ versus $T^{(1,1)}/\sigma^2$ obtained by TxZF JT for

- $K_{\mathrm{B}} = 4$ APs,

- a single subcarrier,

- a frozen channel with a transfer matrix $\underline{\mathbf{H}}^{(n_{\mathrm{F}})\mathrm{T}}$ comprised of all K_{B} columns and of the first K rows of the matrix

$$
\begin{pmatrix}
0.20 + 0.45\mathrm{j} & 0.20 - 0.32\mathrm{j} & 0.39 + 0.37\mathrm{j} & 0.20 - 0.22\mathrm{j} \\
-0.04 + 0.17\mathrm{j} & 0.08 + 0.12\mathrm{j} & -0.04 - 0.10\mathrm{j} & 0.10 + 0.34\mathrm{j} \\
0.06 + 0.74\mathrm{j} & 0.06 - 0.12\mathrm{j} & -0.10 + 0.71\mathrm{j} & 0.31 + 0.02\mathrm{j} \\
0.20 - 0.58\mathrm{j} & 0.20 - 0.59\mathrm{j} & 0.20 - 0.19\mathrm{j} & 0.20 - 0.72\mathrm{j}
\end{pmatrix}, \text{ and}
$$

- no FEC coding.

It is shown in Fig. 7.1 that the price to be paid for the elimination of intra-SA interference by TxZF JT with the considered parameters in the case of $K = 2$ MTs is that a $3.4\,\mathrm{dB}$ larger $T^{(1,1)}/\sigma^2$ is needed to achieve a bit error probability $P_{\mathrm{b}}^{(1,1)} = 10^{-2}$ as compared to the reference system. On the other hand, if $K = 4$ holds, i.e., under full system load $K/K_{\mathrm{B}} = 1$, the $T^{(1,1)}/\sigma^2$ needed by TxZF JT for a bit error probability $P_{\mathrm{b}}^{(1,1)} = 10^{-2}$ is $9\,\mathrm{dB}$ higher than in the case of the single user reference system. It can also be seen in Fig. 7.1 that the difference of $T^{(1,1)}/\sigma^2$ required by TxZF JT and by the single user reference system does not depend on the target bit error probability $P_{\mathrm{b}}^{(1,1)}$. Moreover, in both cases of $K = 2$ and $K = 4$ MTs the same $T^{(1,1)}/\sigma^2$ is needed by TxZF JT and by RxZF JD to achieve a given bit error probability $P_{\mathrm{b}}^{(1,1)}$.

Fig. 7.2 depicts the bit error probability P_{b} of TxZF JT averaged over many channel snapshots for

- $K_{\mathrm{B}} = 6$ APs,

- a single subcarrier, and

- random channel matrix $\underline{\mathbf{H}}^{(n_{\mathrm{F}})\mathrm{T}}$ with independent identically distributed complex elements $\underline{h}^{(k,k_{\mathrm{B}},n_{\mathrm{F}})}$, $\mathrm{Re}\left\{\underline{h}^{(k,k_{\mathrm{B}},n_{\mathrm{F}})}\right\}$ and $\mathrm{Im}\left\{\underline{h}^{(k,k_{\mathrm{B}},n_{\mathrm{F}})}\right\}$ being zero-mean random variables with unit variance.
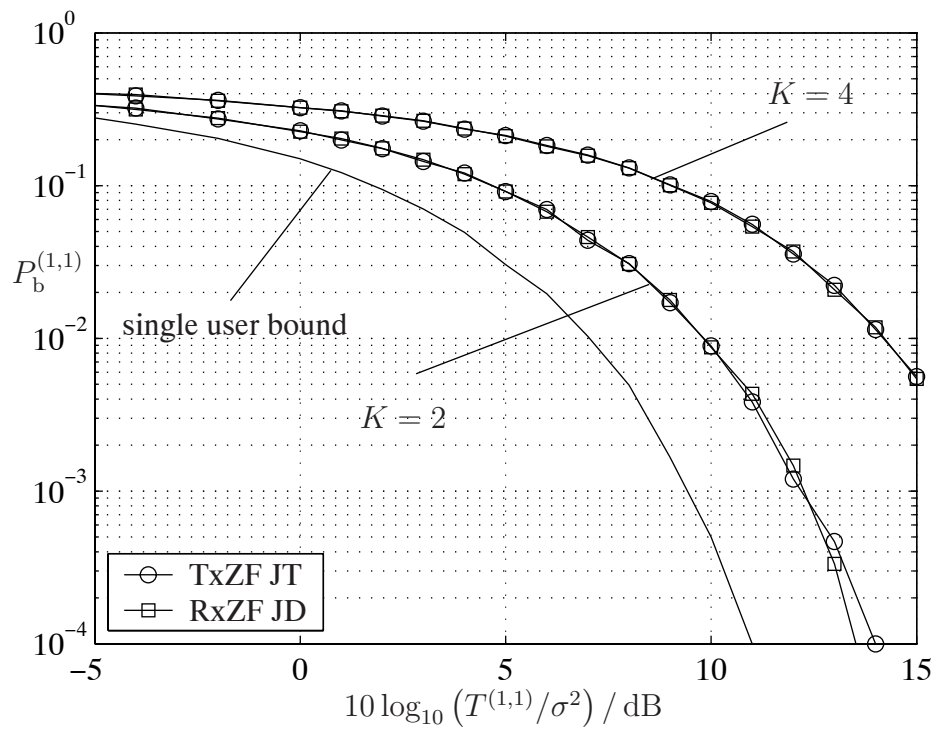
Figure 7.1. Bit error probability $P_{\mathrm{b}}^{(1,1)}$ of TxZF JT as compared to RxZF JD in a frozen channel; Parameters: $K_{\mathrm{B}} = 4$, single subcarrier, no FEC coding
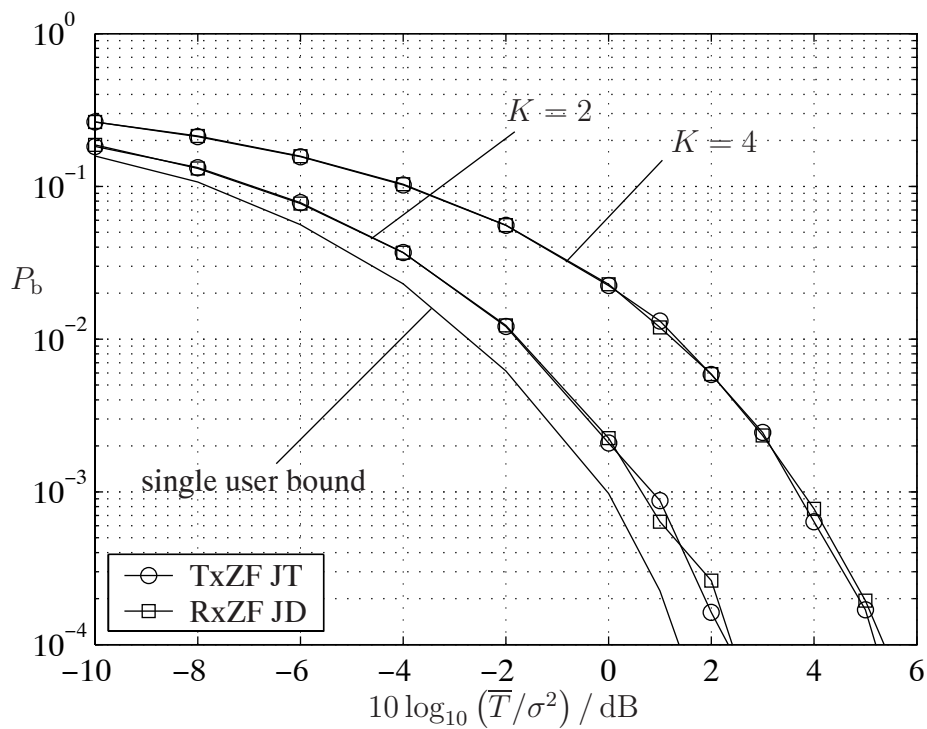
Figure 7.2. Bit error probability P_{b} of TxZF JT as compared to RxZF JD in a living channel; Parameters: $K_{\mathrm{B}} = 6$, single subcarrier, no FEC coding

As it is shown in Fig. 7.2, if $K = 2$ holds, TxZF JT requires a $\overline{T}/\sigma^2$ which is $0.6\,\text{dB}$ larger than the one required by the single user reference system, in order to obtain a bit error probability $P_\text{b} = 10^{-2}$. With $K = 4$ MTs the increase in the $\overline{T}/\sigma^2$ relative to the single user reference system, which is required to obtain a bit error probability $P_\text{b} = 10^{-2}$, is $2.4\,\text{dB}$. It is shown in Fig. 7.2 that the same $\overline{T}/\sigma^2$ is required by both TxZF JT in the DL transmission and RxZF JD in the UL transmission in order to obtain a given bit error probability P_b.

An interesting duality between RxZF JD and TxZF JT is revealed by the results of Figs. 7.1 and 7.2. In particular, it can be deduced from the said comparison that the same price has to be paid by both RxZF JD in the UL and TxZF JT in the DL for the elimination of the intra-SA interference. Moreover, the said duality between RxZF JD and TxZF JT holds in the case of a frozen channel, as Fig. 7.1 shows, as well as in the case of a living channel, shown in Fig. 7.2. The aforementioned duality between UL and DL in the case of intra-SA interference elimination by JD and JT is further investigated in Chapter 8.

7.2.3   Bit error probability of optimum versus transmit zero-forcing joint transmission

In Section 5.2 a novel JT scheme is introduced which is optimum with respect to the average bit error probability at the MTs. In particular, it is shown that for each effective BPSK data vector $\mathbf{d}_v^{(n_\text{F})}$, an effective transmit vector $\mathbf{s}_v^{(n_\text{F})}$ is determined by the transmission of which the minimum possible average bit error probability $\overline{P}_{\text{b},v}^{(n_\text{F})}$ results at the MTs. Target of the present Section is to assess the performance of optimum JT in comparison to the performance of linear JT in the sense of TxZF in terms of the average bit error probability $\overline{P}_{\text{b},v}^{(n_\text{F})}$ at the MTs. Moreover, the angles corresponding to the transmit signals of TxZF JT are taken as the initial values for the numerical minimization procedure for optimum JT.

It is shown in Section 5.2.4 that the average bit error probability $\overline{P}_\text{b}^{(n_\text{F})}$ of JT is a function of the $(K_\text{B} - 1)V$ angles $\varphi_v^{(k_\text{B},n_\text{F})}$, $k_\text{B} = 1 \ldots K_\text{B} - 1$, $v = 1 \ldots V$, and the $V - 1$ angles $\vartheta_v^{(n_\text{F})}$, $v = 1 \ldots V - 1$. For this reason, in a first step the dependence of $\overline{P}_\text{b}^{(n_\text{F})}$ on the $K_\text{B} - 1$ angles $\varphi_v^{(k_\text{B},n_\text{F})}$, $k_\text{B} = 1 \ldots K_\text{B} - 1$ for a fixed given v and for the case of fixed transmit energy strategy is investigated and the solutions corresponding to optimum JT and to TxZF JT are visualized in Figs. 7.3 and 7.4. Following parameters are common to Figs. 7.3 and 7.4:

- full system load $K/K_\text{B} = 1$,

- single subcarrier,

- extended MIMO parametric model,

- BPSK modulation,

- fixed transmit energy strategy,

- $v = 1$, with $\mathbf{d}_v^{(n_F)} = [1 \ \ldots \ 1]^T$, and

- $T/\sigma^2 = 1$.

In Fig. 7.3 the bit error probabilities $P_{b,v}^{(k,n_F)}$, $k = 1 \ldots K$, and the average bit error probability $\overline{P}_{b,v}^{(n_F)}$ for the case of

$$K = 2 \tag{7.8}$$

as a function of $\varphi_v^{(1,n_F)}$ are depicted. As can be seen from Fig. 7.3, there are intervals in which
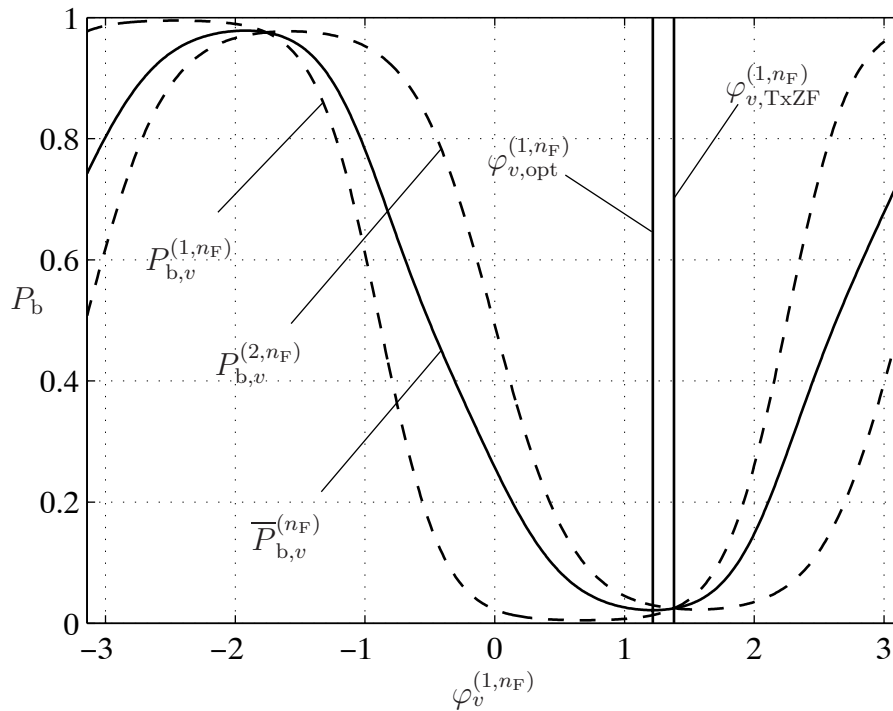
Figure 7.3. Bit error probabilities $P_{b,v}^{(k,n_F)}$, $k = 1 \ldots K$, and average bit error probability $\overline{P}_{b,v}^{(n_F)}$, as a function of $\varphi_v^{(1,n_F)}$; Parameters: $K = 2$, $K_B = 2$, $T/\sigma^2 = 1$, $v = 1$, $\mathbf{d}_v^{(n_F)} = [1 \ 1]^T$, extended MIMO parametric channel model, $\rho_{12} = 0.81$, $\rho_{21} = 0.01$.

the bit error probabilities $P_{b,v}^{(k,n_F)}$, $k = 1 \ldots K$, are greater than 0.5. This happens due to the fact that in the said intervals the corresponding transmit signals are not suited for the transmission of the data vector $\mathbf{d}_v^{(n_F)} = [1 \ 1]^T$. As an example, for the considered

$$\mathbf{d}_v^{(n_F)} = [1 \ 1]^T, \tag{7.9}$$

the received value

$$e_v^{(1,n_F)} = \cos\left(\varphi_v^{(1,n_F)}\right) + \rho_{12}\sin\left(\varphi_v^{(1,n_F)}\right) \tag{7.10}$$

at the absence of noise results in a correct decision after quantization only if

$$-\arctan\left(\frac{1}{\rho_{12}}\right) \leq \quad \varphi_v^{(1,n_F)} \quad \leq \pi - \arctan\left(\frac{1}{\rho_{12}}\right) \Rightarrow$$
$$-0.89 \leq \quad \varphi_v^{(1,n_F)} \quad \leq 2.25 \tag{7.11}$$

holds. Moreover, in Fig. 7.3, the angle

$$\varphi_{v,\text{TxZF}}^{(1,n_F)} = 1.38 \tag{7.12}$$

resulting in an average bit error probability

$$\overline{P}_{b,v,\text{TxZF}}^{(n_F)} = 0.025 \tag{7.13}$$

corresponding to TxZF JT, as well as the angle

$$\varphi_{v,\text{opt}}^{(1,n_F)} = 1.22 \tag{7.14}$$

yielding the minimum average bit error probability

$$\overline{P}_{b,v,\text{opt}}^{(n_F)} = 0.022 \tag{7.15}$$

corresponding to optimum JT are marked. From (7.12) and (7.14) it is deduced that the TxZF JT solution does not yield the minimum possible $\overline{P}_{b,v}^{(n_F)}$, hence, (7.12) and (7.14) suggest that there are gains over TxZF JT in terms of average bit error probability $\overline{P}_{b,v}^{(n_F)}$ which can be achieved by optimum JT. On the other hand, from (7.12) to (7.15) it turns out that for the considered channel the TxZF JT solution, although not optimum in terms of $\overline{P}_{b,v}^{(n_F)}$, is close to the optimum solution corresponding to optimum JT.

If

$$K = 3, \tag{7.16}$$

holds, the average bit error probability $\overline{P}_{b,v}^{(n_F)}$ is a function of two angles $\varphi_{v,\text{opt}}^{(k_B,n_F)}$, $k_B = 1 \ldots K_B -$ 1, and is illustrated in Fig. 7.4. In the case of (7.16), the search for the tuple $\left(\varphi_{v,\text{opt}}^{(1,n_F)}, \varphi_{v,\text{opt}}^{(2,n_F)}\right)$ corresponding to optimum JT is a two-dimensional minimization task. As Fig. 7.4 shows, the tuple

$$\left(\varphi_{v,\text{TxZF}}^{(1,n_F)}, \varphi_{v,\text{TxZF}}^{(2,n_F)}\right) = (2.12, 0.73) \tag{7.17}$$

corresponds to TxZF JT and leads to a bit error probability

$$\overline{P}_{b,v,\text{TxZF}}^{(n_F)} = 0.189, \tag{7.18}$$
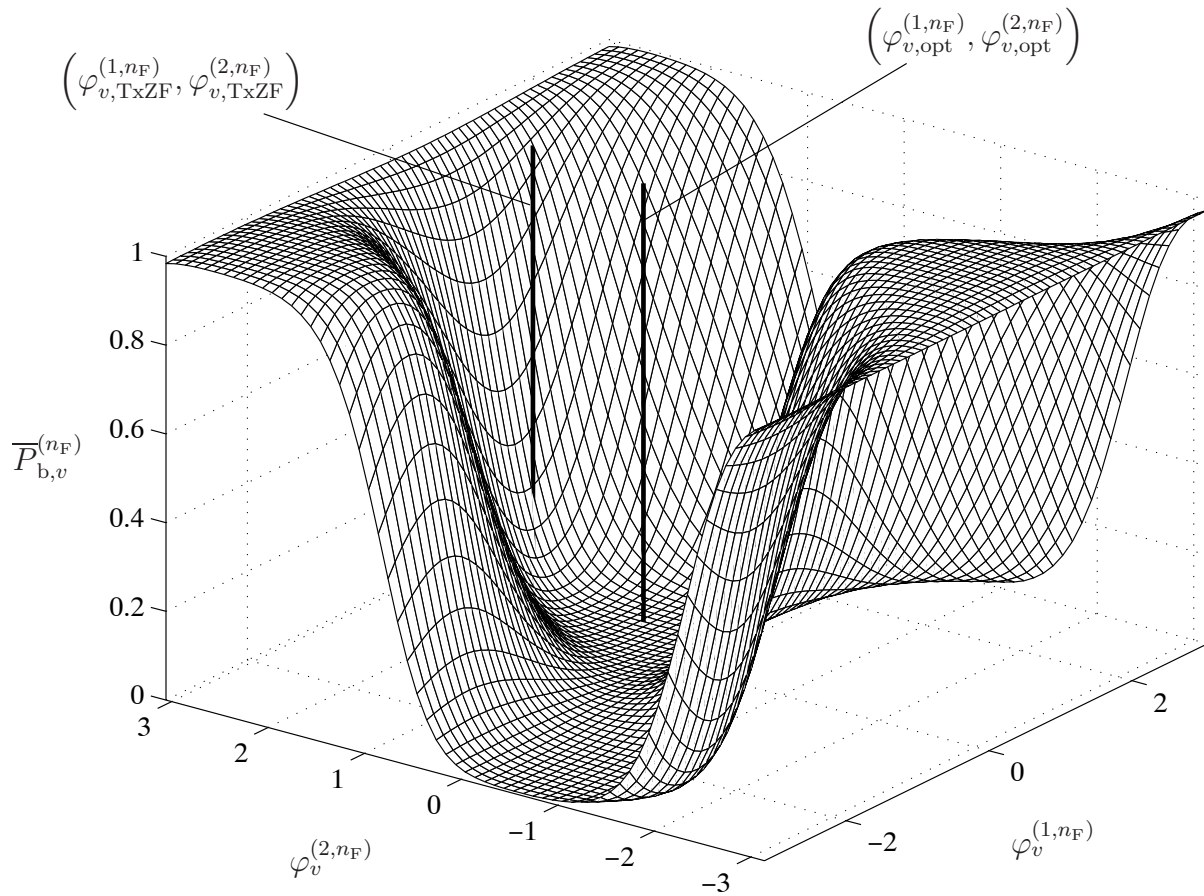
Figure 7.4. Average bit error probability $\overline{P}_{\mathrm{b},v}^{(n_\mathrm{F})}$, as a function of $\varphi_v^{(k_\mathrm{B},n_\mathrm{F})}$, $k_\mathrm{B} = 1 \ldots K_\mathrm{B} - 1$; Parameters: $K = 3$, $K_\mathrm{B} = 3$, $v = 1$, $\mathbf{d}_v^{(n_\mathrm{F})} = [1\ 1\ 1]^\mathrm{T}$, $T/\sigma^2 = 1$, extended MIMO parametric channel model, $\rho_{12} = 0.15$, $\rho_{13} = 0.70$, $\rho_{21} = 0.38$, $\rho_{23} = 0.86$, $\rho_{31} = 0.85$, $\rho_{32} = 0.59$.

whereas the solution for optimum JT

$$\left(\varphi_{v,\mathrm{opt}}^{(1,n_\mathrm{F})}, \varphi_{v,\mathrm{opt}}^{(2,n_\mathrm{F})} \right) = (0.86, 0.57) \tag{7.19}$$

yields the minimum possible bit error probability

$$\overline{P}_{\mathrm{b},v,\mathrm{opt}}^{(n_\mathrm{F})} = 0.001. \tag{7.20}$$

Comparing (7.17) and (7.19) to (7.12) and (7.14), it can be seen that the TxZF JT solution of (7.17) and the optimum JT solution of (7.19) have a larger Euclidean distance than the TxZF JT solution of (7.12) and the optimum JT solution of (7.15). Moreover, from the comparison of (7.18) and (7.20) to (7.13) and (7.15) follows that larger gains in terms of $\overline{P}_{\mathrm{b},v}^{(n_\mathrm{F})}$ are achievable in the case of higher K in the considered channel snapshots. In particular, optimum JT achieves

a reduction of 12% of $\overline{P}_{\mathrm{b},v}^{(n_{\mathrm{F}})}$ in the case of (7.8) and a reduction of 95% of $\overline{P}_{\mathrm{b},v}^{(n_{\mathrm{F}})}$ in the case of (7.16).

In Figs. 7.5-7.6, optimum JT is assessed in terms of the bit error probability $\overline{P}_{\mathrm{b}}^{(n_{\mathrm{F}})}$ averaged over all data vectors $\mathbf{d}^{(n_{\mathrm{F}})}$. Following parameters are common to Figs. 7.5-7.6:

- single subcarrier,

- BPSK modulation,

- $K_{\mathrm{B}} = 8$ APs,

- $K = 2 \ldots 6$ MTs, and

- transfer matrix $\underline{\mathbf{H}}^{(n_{\mathrm{F}})\mathrm{T}}$ comprised of all K_{B} columns and of the first K rows of the matrix

$$
\begin{pmatrix}
0.50 & 0.43 & 0.49 & 0.07 & 0.23 & 0.44 & 0.16 & 0.20 \\
0.14 & 0.27 & 0.55 & 0.12 & 0.56 & 0.01 & 0.11 & 0.52 \\
0.39 & 0.40 & 0.26 & 0.13 & 0.30 & 0.44 & 0.12 & 0.55 \\
0.27 & 0.45 & 0.50 & 0.34 & 0.24 & 0.21 & 0.38 & 0.33 \\
0.48 & 0.50 & 0.03 & 0.15 & 0.45 & 0.45 & 0.16 & 0.27 \\
0.45 & 0.43 & 0.21 & 0.12 & 0.31 & 0.29 & 0.32 & 0.53 \\
0.31 & 0.12 & 0.56 & 0.01 & 0.14 & 0.48 & 0.10 & 0.56 \\
0.01 & 0.27 & 0.01 & 0.50 & 0.45 & 0.29 & 0.46 & 0.43
\end{pmatrix}.
$$

Fig. 7.5 shows the performance of optimum JT and TxZF JT in terms of the bit error probability $\overline{P}_{\mathrm{b}}^{(n_{\mathrm{F}})}$ versus T/σ^2 for the case of fixed transmit energy strategy. It can be seen from Fig. 7.5 that no noticeable difference between optimum JT and TxZF JT exists in the case of 2 MTs. This fact is to be expected as follows from the discussions concerning Fig. 7.3. By a stepwise increase of the number of MTs from 2 to 6, the T/σ^2 gains of optimum JT as compared to TxZF JT increase to $0.3\,\mathrm{dB}$, $0.4\,\mathrm{dB}$, $0.5\,\mathrm{dB}$ and $0.9\,\mathrm{dB}$, respectively, at a bit error probability $\overline{P}_{\mathrm{b}}^{(n_{\mathrm{F}})} = 10^{-1}$. The bit error probability $\overline{P}_{\mathrm{b}}^{(n_{\mathrm{F}})}$ of optimum JT and TxZF JT in the case of variable transmit energy strategy is shown in Fig. 7.6. As Fig. 7.6 shows, by employing the variable transmit energy strategy, for $K = 2 \ldots 6$ optimum JT yields T/σ^2 gains of $0.8\,\mathrm{dB}, 0.8\,\mathrm{dB}, 0.8\,\mathrm{dB}$ and $1.2\,\mathrm{dB}$ over TxZF JT, respectively, at a bit error probability $\overline{P}_{\mathrm{b}}^{(n_{\mathrm{F}})} = 10^{-1}$.

Figure 7.5. Average bit error probability $\overline{P}_{\mathrm{b}}^{(n_{\mathrm{F}})}$ for optimum JT (solid lines), and TxZF JT (dashed lines); Parameters: $K_{\mathrm{B}} = 8$, $K = 2 \ldots 6$, fixed transmit energy
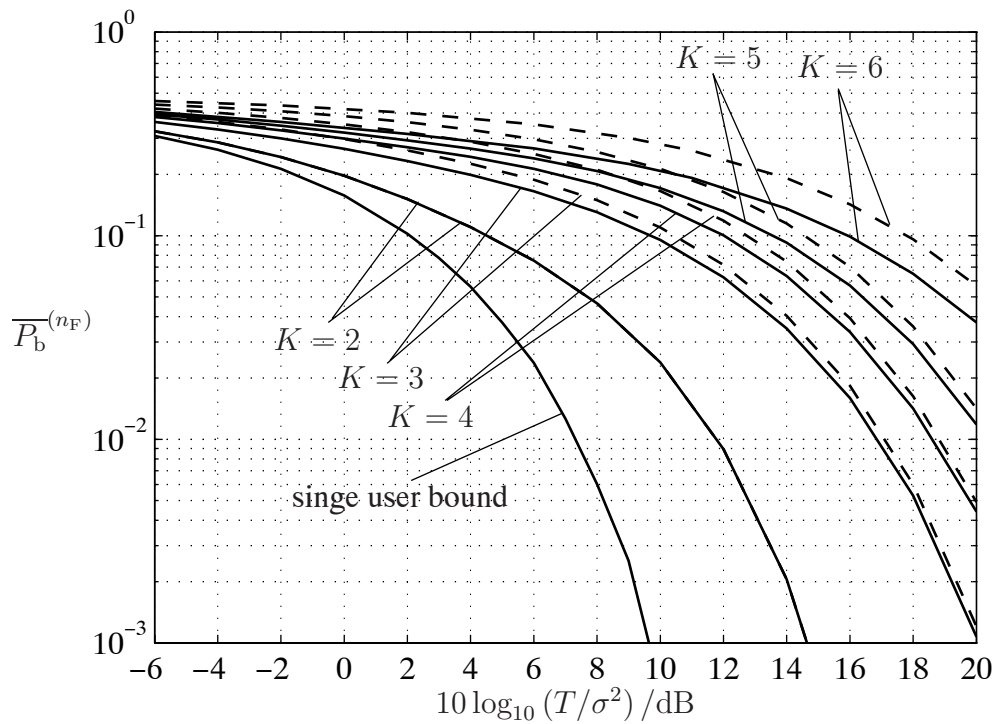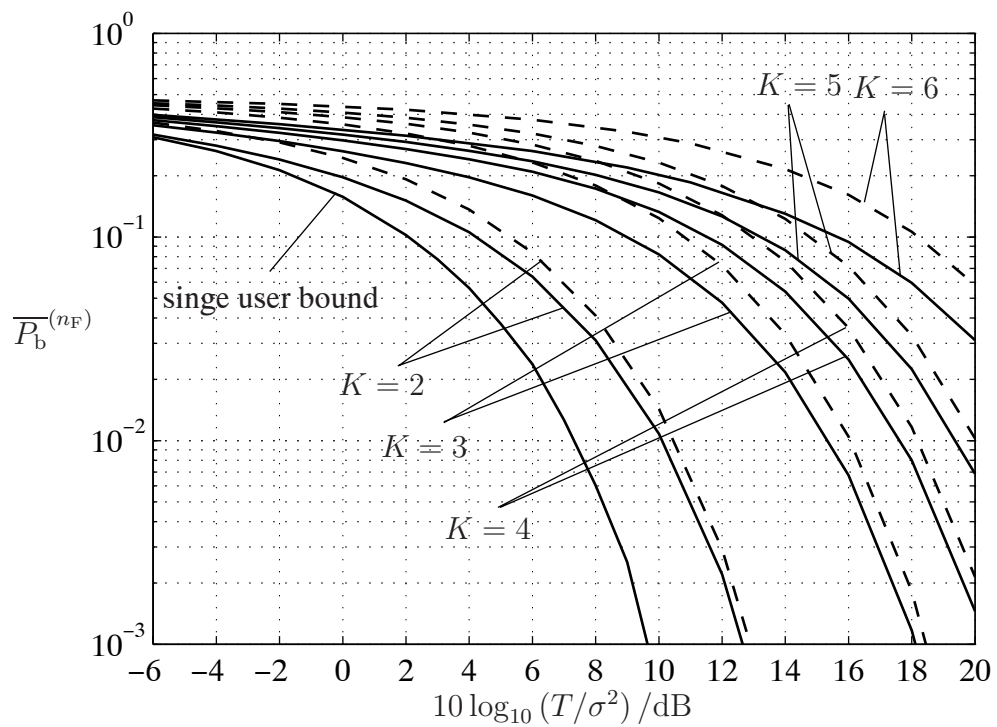

Figure 7.6. Average bit error probability $\overline{P}_{\mathrm{b}}^{(n_{\mathrm{F}})}$ for optimum JT (solid lines), and TxZF JT (dashed lines); Parameters: $K_{\mathrm{B}} = 8$, $K = 2 \ldots 6$, variable transmit energy

Summarizing the findings of the simulations of Figs. 7.5 and 7.6, up to $1.2\,\mathrm{dB}$ of T/σ^2 at a bit error probability $\overline{P}_\mathrm{b}^{(n_\mathrm{F})} = 10^{-1}$ can be gained by employing optimum JT as compared to TxZF JT. Moreover, higher gains in terms of bit error probability $\overline{P}_\mathrm{b}^{(n_\mathrm{F})}$ are possible by optimum JT over TxZF JT in the case of the variable transmit energy strategy than in the case of fixed transmit energy strategy. The minimization of $\overline{P}_\mathrm{b}^{(n_\mathrm{F})}$ not only with respect to the $(K_\mathrm{B} - 1)V$ angles $\varphi_v^{(k_\mathrm{B},n_\mathrm{F})}$, $k_\mathrm{B} = 1\ldots K_\mathrm{B} - 1$, $v = 1\ldots V$, but also with respect to the $V - 1$ angles $\vartheta_v^{(n_\mathrm{F})}$, $v = 1\ldots V-1$, in the case of optimum JT with variable transmit energy brings additional degrees of freedom, a fact which translates into higher gains in $\overline{P}_\mathrm{b}^{(n_\mathrm{F})}$ as compared to the case of fixed transmit energy strategy. In both cases of Figs. 7.5 and 7.6 the gains of optimum JT over TxZF JT decrease as the target bit error probability $\overline{P}_\mathrm{b}^{(n_\mathrm{F})}$ decreases. Hence, TxZF JT is the optimum approach in terms of bit error probability $\overline{P}_\mathrm{b}^{(n_\mathrm{F})}$ in the case of high T/σ^2.
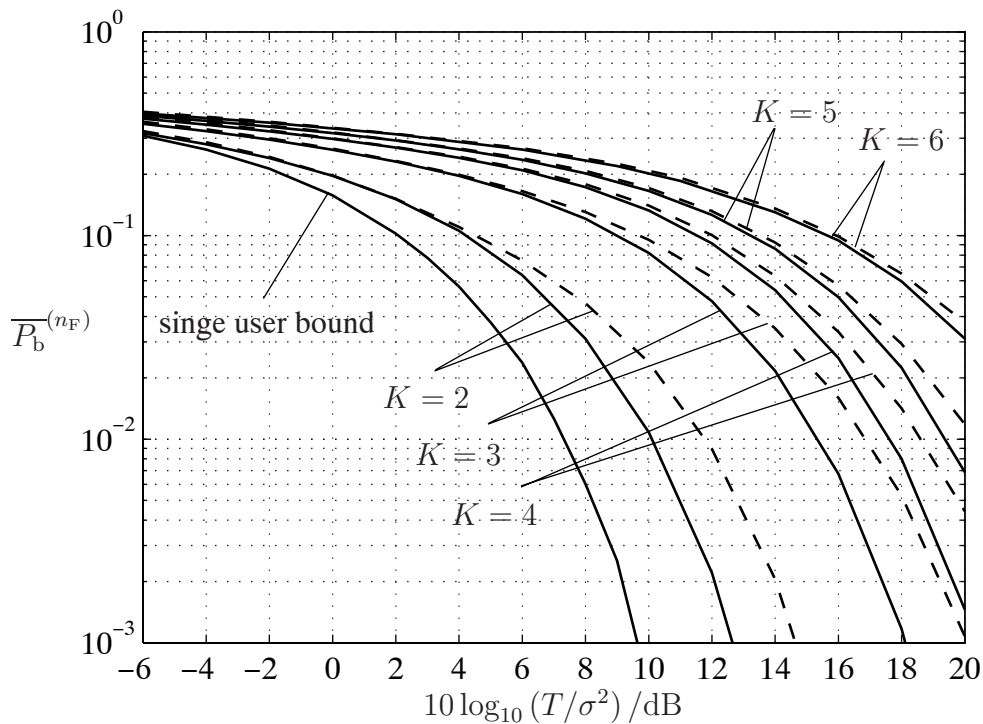
Figure 7.7. Average bit error probability $\overline{P}_\mathrm{b}^{(n_\mathrm{F})}$ for optimum JT, with variable transmit energy (solid lines) and fixed transmit energy (dashed lines); Parameters: $K_\mathrm{B} = 8$, $K = 2\ldots 6$

The investigation of the influence of the two transmit energy strategies on the performance of optimum JT is the target of the simulations of Fig. 7.7. From Fig. 7.7 it can be seen that approximately $2\,\mathrm{dB}$ of T/σ^2 at a bit error probability $\overline{P}_\mathrm{b}^{(n_\mathrm{F})} = 10^{-2}$ are gained by the use of optimum JT with the variable energy strategy as compared to when optimum JT with the fixed energy strategy is used. However, by increasing the number K of MTs and by constant number K_B of APs, the gain in terms of T/σ^2 slowly vanishes. Moreover, if the system load K/K_B

remains constant, Fig. 7.7 shows that for low T/σ^2 only small differences in the achieved bit error probability $\overline{P}_{\mathrm{b}}^{(n_{\mathrm{F}})}$ for given T/σ^2 exist between the two transmit energy strategies.

7.2.4 Bit error probability of iterative joint transmission

In Section 5.4 an iterative JT scheme is introduced, as an alternative to TxZF JT of Section 5.3. It is shown that in the DL transmission of SA-based systems intra-SA interference is mitigated in an iterative manner by iterative JT and that iterative JT of Section 5.3 in the DL is dual to iterative JD with transparent data estimate refinement of Section 4.4.2 in the UL. In the present Section, the performance of iterative JT in terms of the bit error probability $P_{\mathrm{b}}^{(k,n_{\mathrm{F}})}$ is assessed.

Figs. 7.8 and 7.9 depict the bit error probability $P_{\mathrm{b}}^{(1,1)}$ of iterative JT for the following parametrization

- $K = 4$ MTs,

- $K_{\mathrm{B}} = 4$ APs,

- single subcarrier,

- single snapshot of the MIMO parametric channel model,

- no FEC coding,

- $P = 5$ iterations,

- forward path matrix $\underline{\mathbf{F}} = \left(\mathrm{diag}\left(\underline{\mathbf{H}}^*\underline{\mathbf{H}}^{\mathrm{T}}\right)\right)^{-1}$, and

- reverse path matrix $\underline{\mathbf{R}} = \overline{\mathrm{diag}}\left(\underline{\mathbf{H}}^*\underline{\mathbf{H}}^{\mathrm{T}}\right)$.

If

$$\rho = 0.1 \tag{7.21}$$

holds, Fig. 7.8 shows that iterative JT converges towards TxZF JT, which needs a $0.4\,\mathrm{dB}$ higher T/σ^2 than the reference system in order to achieve a bit error probability $P_{\mathrm{b}}^{(1,1)} = 10^{-3}$. In the case of

$$\rho = 0.15, \tag{7.22}$$

shown in Fig. 7.9, iterative JT converges towards TxZF JT, which needs a $1\,\mathrm{dB}$ higher $T^{(1,1)}/\sigma^2$ than the reference system in order to achieve a bit error probability $P_{\mathrm{b}}^{(1,1)} = 10^{-3}$. As compared to Fig. 7.8, convergence of iterative JT towards TxZF JT in Fig. 7.9 takes place at a lower speed.

Taking advantage of the duality between iterative JT and iterative JD with transparent data estimate refinement outlined in Section 5.4, the results concerning convergence of iterative JD can be directly applied to iterative JT. In particular, it can be shown that the matrix product $\underline{\mathbf{F}}\,\underline{\mathbf{R}}$ of dimension $KN_{\mathrm{F}} \times KN_{\mathrm{F}}$ has the spectral radius

$$\lambda_{\max}\left(\underline{\mathbf{F}}\,\underline{\mathbf{R}}\right) = (K-1)\frac{2\rho + (K-2)\rho^2}{1 + (K-1)\rho^2}, \tag{7.23}$$

with which it can be shown that iterative JT in the case of the MIMO parametric channel model converges if

$$\rho < \frac{1}{K-3}\left(\sqrt{2\frac{K-2}{K-1}} - 1\right) \tag{7.24}$$

holds. In the specific case of

$$K = 4 \tag{7.25}$$

(7.24) yields

$$\rho < 0.155. \tag{7.26}$$

7.3   Transmission efficiency

7.3.1   The transmission efficiency as performance measure

With the aid of the transmission efficiency, the efficiency by which JT in the DL of SA-based systems converts the available transmit energy $T^{(k,n_{\mathrm{F}})}$ into receive energy $R^{(k,n_{\mathrm{F}})}$ is assessed. The assessment of the said efficiency is based on a comparison of $\left(R^{(k,n_{\mathrm{F}})}/T^{(k,n_{\mathrm{F}})}\right)_{\mathrm{JT}}$ with the maximum possible ratio $\left(R^{(k,n_{\mathrm{F}})}/T^{(k,n_{\mathrm{F}})}\right)_{\mathrm{ref}}$ corresponding to the reference system, i.e., the transmission efficiency of JT is defined as [TWMB01]

$$t^{(k,n_{\mathrm{F}})} = \frac{\left(R^{(k,n_{\mathrm{F}})}\big/T^{(k,n_{\mathrm{F}})}\right)_{\mathrm{JT}}}{\left(R^{(k,n_{\mathrm{F}})}\big/T^{(k,n_{\mathrm{F}})}\right)_{\mathrm{ref}}}. \tag{7.27}$$

Due to the suboptimum conversion of the transmit energy $T^{(k,n_{\mathrm{F}})}$ into receive energy $R^{(k,n_{\mathrm{F}})}$, the transmission efficiency $t^{(k,n_{\mathrm{F}})}$ of (7.27) takes the values $t^{(k,n_{\mathrm{F}})} \in [0,1]$.

Figure 7.8. Bit error probability $P_{\mathrm{b}}^{(1,1)}$ of iterative JT and of TxZF JT; Parameters: $K = 4$, $K_{\mathrm{B}} = 4$, no FEC coding, MIMO parametric channel model with $\rho = 0.1$

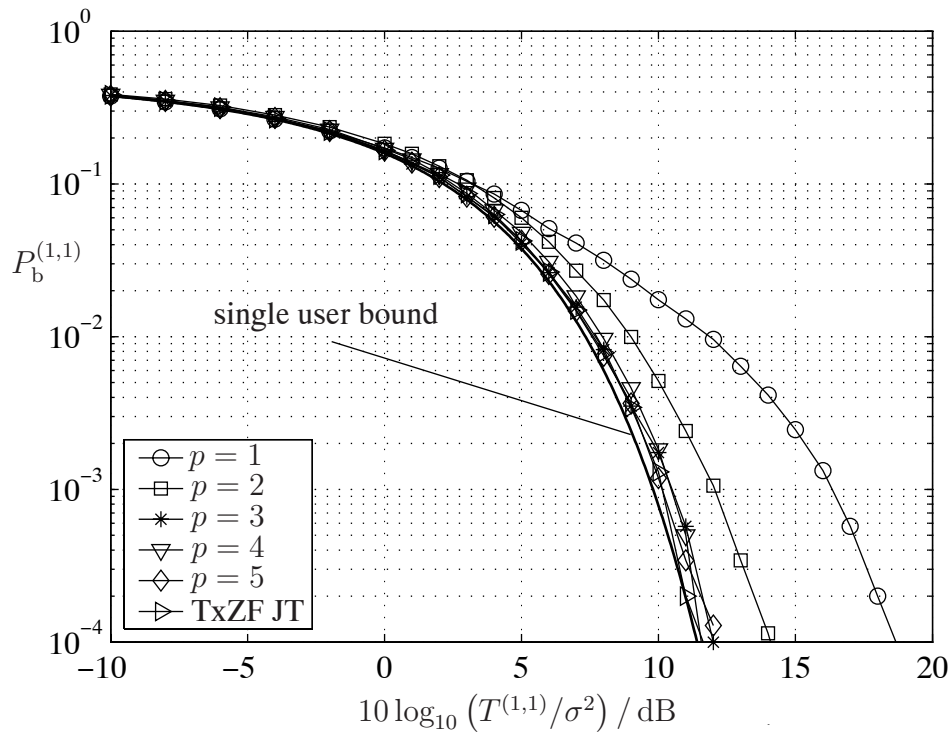Figure 7.9. Bit error probability $P_{\mathrm{b}}^{(1,1)}$ of iterative JT and of TxZF JT; Parameters: $K = 4$, $K_{\mathrm{B}} = 4$, no FEC coding, MIMO parametric channel model with $\rho = 0.15$
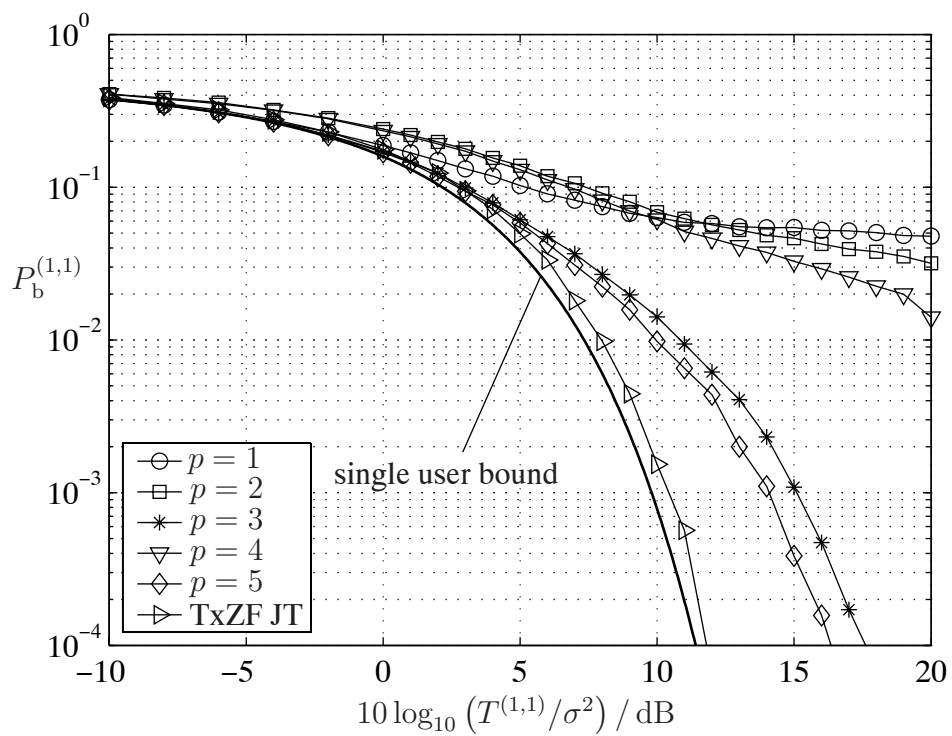
In the case of TxZF JT as described in (5.40), with the transfer matrix $\underline{\mathbf{H}}^{(n_{\mathrm{F}})\mathrm{T}}$ and using (7.1) and with the modulator matrix $\underline{\mathbf{M}}_{\mathrm{TxZF}}^{(n_{\mathrm{F}})}$ of (5.40),

$$
\left(\frac{R^{(k,n_{\mathrm{F}})}}{T^{(k,n_{\mathrm{F}})}}\right)_{\mathrm{JT}} = \frac{\dfrac{1}{2}\mathrm{E}\left\{|\underline{d}^{(k,n_{\mathrm{F}})}|^2\right\}}{\dfrac{1}{2}\mathrm{E}\left\{|\underline{d}^{(k,n_{\mathrm{F}})}|^2\left[\underline{\mathbf{M}}_{\mathrm{TxZF}}^{(n_{\mathrm{F}})\,*\mathrm{T}}\underline{\mathbf{M}}_{\mathrm{TxZF}}^{(n_{\mathrm{F}})}\right]_{k,k}\right\}}
$$
$$
= \frac{1}{\left[\left(\underline{\mathbf{H}}^{(n_{\mathrm{F}})\mathrm{T}}\underline{\mathbf{H}}^{(n_{\mathrm{F}})*}\right)^{-1}\right]_{k,k}} \tag{7.28}
$$

follows for the ratio $\left(R^{(k,n_{\mathrm{F}})}/T^{(k,n_{\mathrm{F}})}\right)_{\mathrm{JT}}$. As far as the reference system is concerned, with the transmit energy $T^{(k,n_{\mathrm{F}})}$ of (7.4) and the receive energy $R^{(k,n_{\mathrm{F}})}$ of (7.6), follows

$$
\left(\frac{R^{(k,n_{\mathrm{F}})}}{T^{(k,n_{\mathrm{F}})}}\right)_{\mathrm{ref}} = \left[\underline{\mathbf{H}}^{(n_{\mathrm{F}})\mathrm{T}}\underline{\mathbf{H}}^{(n_{\mathrm{F}})*}\right]_{k,k}. \tag{7.29}
$$

Hence, with $\left(R^{(k,n_{\mathrm{F}})}/T^{(k,n_{\mathrm{F}})}\right)_{\mathrm{JT}}$ of (7.28) and $\left(R^{(k,n_{\mathrm{F}})}/T^{(k,n_{\mathrm{F}})}\right)_{\mathrm{ref}}$ of (7.29), the transmission efficiency $t^{(k,n_{\mathrm{F}})}$ of (7.27) becomes

$$
t_{\mathrm{TxZF}}^{(k,n_{\mathrm{F}})} = \left(\left[\left(\underline{\mathbf{H}}^{(n_{\mathrm{F}})\mathrm{T}}\underline{\mathbf{H}}^{(n_{\mathrm{F}})*}\right)^{-1}\right]_{k,k}\left[\underline{\mathbf{H}}^{(n_{\mathrm{F}})\mathrm{T}}\underline{\mathbf{H}}^{(n_{\mathrm{F}})*}\right]_{k,k}\right)^{-1}. \tag{7.30}
$$

The transmission efficiency $t_{\mathrm{TxZF}}^{(k,n_{\mathrm{F}})}$ of (7.30) expresses the fact that, given a receive energy $R^{(k,n_{\mathrm{F}})}$, a higher transmit energy $T^{(k,n_{\mathrm{F}})}$ is required by TxZF JT as compared to the reference system in order to render the partial received signal corresponding to MT k orthogonal to the useful received signals of the other MTs of the SA.

7.3.2 Statistics of the transmission efficiency of transmit zero-forcing joint transmission

In this Section TxZF JT is assessed on the basis of the transmission efficiency $t_{\mathrm{TxZF}}^{(k,n_{\mathrm{F}})}$ of (7.30). In Section 7.3.1 it is shown that the transmission efficiency $t^{(k,n_{\mathrm{F}})}$ of (7.27) assesses the efficiency of the conversion of the transmit energy $T^{(k,n_{\mathrm{F}})}$ into receive energy $R^{(k,n_{\mathrm{F}})}$ by JT, when compared to a reference system. According to an alternative interpretation of (7.27), the transmission efficiency $t^{(k,n_{\mathrm{F}})}$ measures the increase in the transmit energy $T^{(k,n_{\mathrm{F}})}$ required by JT relative to the reference system in order to achieve a given bit error probability $P_{\mathrm{b}}^{(k,n_{\mathrm{F}})}$. Moreover, in the case of TxZF JT the transmission efficiency $t_{\mathrm{TxZF}}^{(k,n_{\mathrm{F}})}$ of (7.30) does not depend on the power σ^2 of the noise at the MTs. Hence, a duality is revealed between the transmission efficiency $t_{\mathrm{TxZF}}^{(k,n_{\mathrm{F}})}$ of (7.30) of TxZF JT in the DL and the asymptotic multiuser efficiency $\eta_{\mathrm{RxZF}}^{(k,n_{\mathrm{F}})}$ of (6.33) of RxZF JD in the UL, i.e., both $t_{\mathrm{TxZF}}^{(k,n_{\mathrm{F}})}$ and $\eta_{\mathrm{RxZF}}^{(k,n_{\mathrm{F}})}$ express the price to be paid for the intra-SA interference elimination.
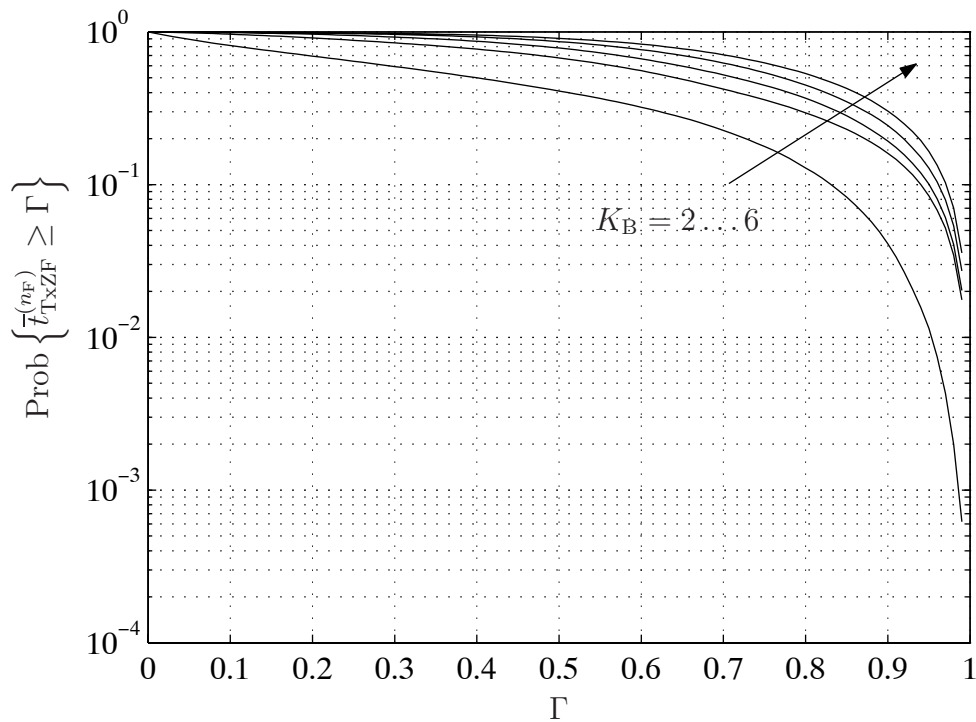
Figure 7.10. CCDF of $\overline{t}_{\mathrm{TxZF}}^{(n_{\mathrm{F}})}$; Parameters: $K = 2$, $K_{\mathrm{B}} = 2\ldots 6$, single subcarrier, geometric indoor channel model, $r_{\mathrm{B}} = 5\lambda$, $x_{\max} = 40\lambda$, $y_{\max} = 40\lambda$

Figure 7.11. CCDF of $\overline{t}_{\mathrm{TxZF}}^{(n_{\mathrm{F}})}$; Parameters: $K = 3$, $K_{\mathrm{B}} = 3\ldots 6$, single subcarrier, geometric indoor channel model, $r_{\mathrm{B}} = 5\lambda$, $x_{\max} = 40\lambda$, $y_{\max} = 40\lambda$
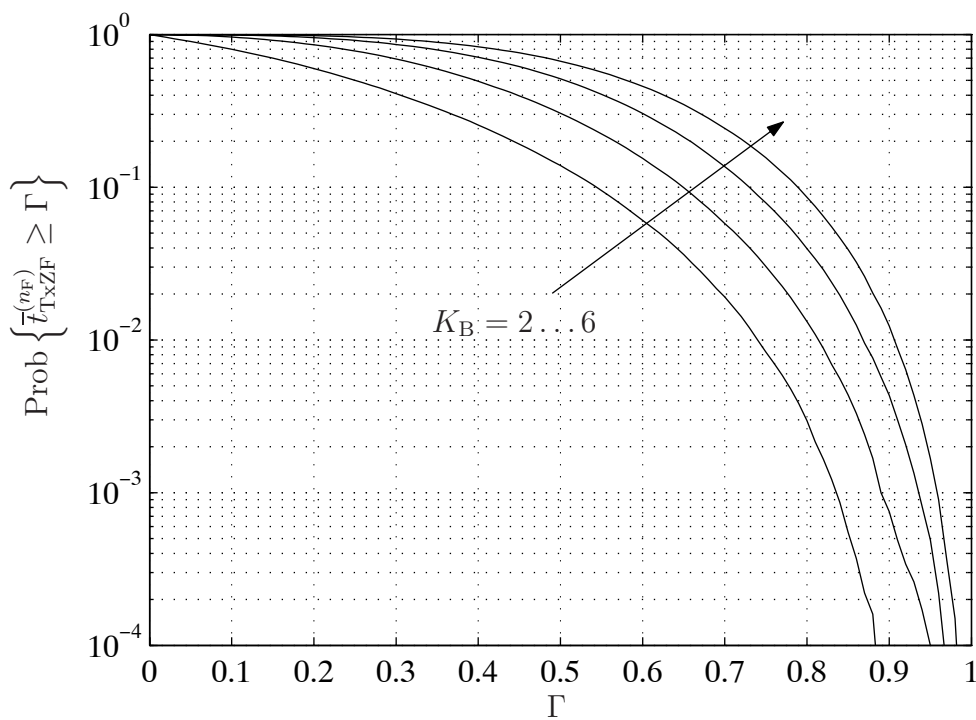
The said duality is further confirmed by the simulation results of the bit error probability $P_{\mathrm{b}}^{(k,n_{\mathrm{F}})}$ of TxZF JT of Section 7.2.2. It is shown that relative to the corresponding reference systems, the increase in the transmit energy $T^{(k,n_{\mathrm{F}})}$ required by TxZF JT in order to achieve a given bit error probability $P_{\mathrm{b}}^{(k,n_{\mathrm{F}})}$ relative to the reference system is equal to the increase in the receive energy $R^{(k,n_{\mathrm{F}})}$ required by RxZF JD in order to achieve the same bit error probability $P_{\mathrm{b}}^{(k,n_{\mathrm{F}})}$ relative to the corresponding reference system of Section 6.1. In order to further confirm that the results and conclusions regarding the average asymptotic multiuser efficiency $\eta_{\mathrm{RxZF}}^{(k,n_{\mathrm{F}})}$ of RxZF JD in the UL are directly applicable to the case of TxZF JT in the DL, Figs. 7.10 and 7.11 depict the CCDF of $\bar{t}_{\mathrm{TxZF}}^{(n_{\mathrm{F}})}$ of TxZF JT for

$$K = 2 \tag{7.31}$$

and

$$K = 3 \tag{7.32}$$

MTs respectively, for the following parameters:

- Indoor geometric channel model,

- single subcarrier,

- $r_{\mathrm{B}} = 5\lambda$,

- $x_{\max} = 40\lambda$, and

- $y_{\max} = 40\lambda$.

For the case of (7.31), Fig. 7.10 shows that a transmission efficiency $\bar{t}_{\mathrm{TxZF}}^{(n_{\mathrm{F}})}$ of at least 0.6 is achieved with probability of 0.3 with 2 APs. With $3, 4, 5$, or 6 APs the corresponding probability $\mathrm{Prob}\left\{\bar{t}_{\mathrm{TxZF}}^{(n_{\mathrm{F}})} \geq 0.6\right\}$ becomes 0.55, 0.65, 0.75, and 0.85, respectively.

If (7.32) holds, according to Fig. 7.10 a minimum average transmission efficiency $\bar{t}_{\mathrm{TxZF}}^{(n_{\mathrm{F}})}$ of 0.6 is obtained with a probability of 0.06 in the case of full system load $K/K_{\mathrm{B}} = 1$. An increase of the number K_{B} of APs to $4, 5$, or 6 results in an increase of the probability $\mathrm{Prob}\left\{\bar{t}_{\mathrm{TxZF}}^{(n_{\mathrm{F}})} \geq 0.6\right\}$ to 0.15, 0.3, and 0.45, respectively.

By comparing of Figs. 7.10 and 7.11 to Figs. 6.10 and 6.11 the conclusion is drawn that the transmission efficiency $\bar{t}_{\mathrm{TxZF}}^{(n_{\mathrm{F}})}$ of TxZF JT in the DL is characterized by the same CCDF as the asymptotic multiuser efficiency $\bar{\eta}_{\mathrm{ZF}}^{(k,n_{\mathrm{F}})}$ of RxZF JD in the UL. Hence, all results and conclusions regarding the asymptotic multiuser efficiency $\eta_{\mathrm{RxZF}}^{(k,n_{\mathrm{F}})}$ of RxZF JD in Chapter 6 hold also for the transmission efficiency $t_{\mathrm{TxZF}}^{(n_{\mathrm{F}})}$ of TxZF JT.

8 Performance assessment of service area based systems

8.1 Introduction

The main advantageous characteristic of SA-based systems in comparison to state-of-the-art cellular systems is that the intercell interference which disturbs the transmissions in cellular systems can be combated by interference mitigation techniques in SA-based systems offering the potential of an increased spectrum capacity η_c of (1.1). As it is shown in Chapters 4 and 5, there exists freedom of choice with respect to the employment of techniques for the mitigation of intra-SA interference in the UL and in the DL transmission. Among the various techniques described in Chapters 4 and 5, RxZF JD and TxZF JT are of special interest due to the fact that by their use unbiased data transmission is achieved in the SA. RxZF JD and TxZF JT are subcases of the general class of linear unbiased data transmission techniques. Target of the present Chapter is to derive a unified data transmission model for UL and DL as well as the corresponding performance measures for linear unbiased data transmission techniques for SA-based systems. Moreover, system layer aspects of SA-based systems employing unbiased linear data transmission are investigated. In order to provide insight into the motivation of the investigations of the present Chapter, first a brief overview of the dominant characteristics of RxZF JD and TxZF JT is performed.

In the UL of SA-based systems, the received signals available to the CU are comprised of K partial received signals, each corresponding to one of the K MTs of the SA. As the K partial received signals are in general not orthogonal to each other, the estimation of the data symbol $\underline{d}^{(k,n_F)}$ sent by MT k by RxZF JD consists in using only the part of the useful received signal corresponding to MT k, which is orthogonal to the partial received signals of the other $K-1$ MTs of the SA. Due to the fact that only a part of the useful received signal of each MT is used, RxZF JD is suboptimum with respect to the use of the corresponding receive energy $R^{(k,n_F)}$ in comparison to a reference system which uses the whole useful received signal of MT k. The aforementioned suboptimum use of the receive energy $R^{(k,n_F)}$ by RxZF JD is quantified by the asymptotic multiuser efficiency $\eta_{ZF}^{(k,n_F)}$ of (6.33) of RxZF JD.

Likewise in the DL of SA-based systems, the received signal at each MT k is in general a superposition of K partial received signals and the partial received signal intended for MT k is the useful received signal of MT k. Equivalently, a partial received signal corresponding to MT k is received by all K MTs of the SA. In order to eliminate intra-SA interference in the DL transmission, TxZF JT uses for data symbol $\underline{d}^{(k,n_F)}$ an increased transmit energy $T^{(k,n_F)}$ as compared to a single user reference system in order to render the partial received signals

corresponding to data symbol $\underline{d}^{(k,n_{\mathrm{F}})}$ orthogonal to the useful received signal of every other MT in the SA, resulting into a lower receive energy $R^{(k,n_{\mathrm{F}})}$ at MT k as compared to the single user reference system. The aforementioned suboptimum transformation of the transmit energy $T^{(k,n_{\mathrm{F}})}$ into receive energy $R^{(k,n_{\mathrm{F}})}$ with respect to the reference system is quantified by the transmission efficiency $t_{\mathrm{TxZF}}^{(k,n_{\mathrm{F}})}$ of (7.30) of TxZF JT.

Using the more general terms transmitter and receiver instead of CU and MTs to characterize a SA-based system independently of whether UL or DL transmission is considered, it can be deduced that the price to be paid for the elimination of intra-SA interference by JD and JT is that in a SA suboptimum use is made of a given transmit energy $T^{(k,n_{\mathrm{F}})}$ as compared to the single user reference system. The latter conclusion is further verified by the simulation results of Chapter 7, which reveal that the same energy loss compared to the single user reference system has to be paid for the intra-SA interference elimination by RxZF JD and TxZF JT. This commonality between RxZF JD and TxZF JT is treated with in detail in the present Chapter. Moreover, a unified performance assessment method of linear unbiased data transmission for UL and DL is presented.

8.2   Dualities between uplink and downlink

8.2.1   Model of general unbiased linear data transmission

In this Section, a generalized transmission model for unbiased linear data transmission is presented. With respect to the nomenclature of Chapter 3 regarding OFDM-based MIMO systems, a SA-based system in which intra-SA interference is eliminated in the UL transmission is a MIMO system in which the transmitters employ no pre-processing whereas linear post-processing is performed by the receiver. On the other hand, in the DL transmission the transmitter employs linear pre-processing and no post-processing is performed by the receivers. Hence, the UL and DL transmission in a SA-based system employing linear pre- and post-processing are subcases of a generalized unbiased data transmission with linear pre- and post-processing stages, i.e., of an unbiased data transmission in which the transmit vector $\underline{s}^{(n_{\mathrm{F}})}$ is a linear function of the data vector $\underline{d}^{(n_{\mathrm{F}})}$ and the estimated data vector $\hat{\underline{d}}^{(n_{\mathrm{F}})}$ is a linear function of the received vector $\underline{e}^{(n_{\mathrm{F}})}$, as shown in Fig. 8.1. As linear processing can be performed in a subcarrierwise fashion, the model depicted in Fig. 8.1 models transmission and estimation at a single subcarrier n_{F} of the SA-based system. Nevertheless, the presented transmission model is also more generally valid for flat fading MIMO channels. It is assumed that each MT and each AP is equipped with a single antenna and that no spreading is employed.

$$\mathbf{n}^{(n_\mathrm{F})}$$
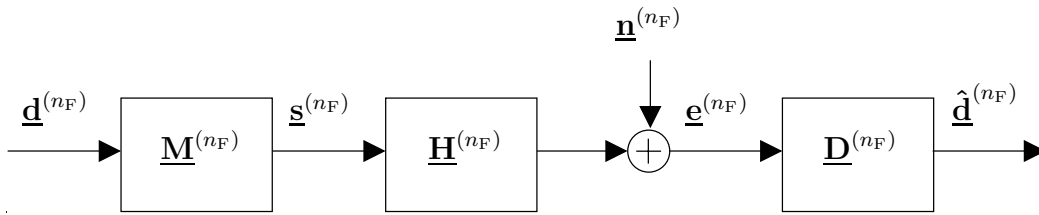
Figure 8.1. Model of general subcarrierwise linear data transmission

At the considered system of Fig. 8.1 pre-processing is linear, i.e., a modulator matrix $\underline{\mathbf{M}}^{(n_\mathrm{F})}$ of dimension $K_\mathrm{I} \times K$ can be used to describe the generation of the transmit vector

$$\underline{\mathbf{s}}^{(n_\mathrm{F})} = \underline{\mathbf{M}}^{(n_\mathrm{F})}\underline{\mathbf{d}}^{(n_\mathrm{F})} \tag{8.1}$$

of dimension K_I from the data vector $\underline{\mathbf{d}}^{(n_\mathrm{F})}$ of dimension K. In the case of the UL in the considered SA-based system, $\underline{\mathbf{M}}^{(n_\mathrm{F})}$ of (8.1) is a diagonal matrix, due to the fact that the K MTs are spatially separated.

With the transmit vector $\underline{\mathbf{s}}^{(n_\mathrm{F})}$, and using the $K_\mathrm{O} \times K_\mathrm{I}$ transfer matrix $\underline{\mathbf{H}}^{(n_\mathrm{F})}$ and the noise vector $\underline{\mathbf{n}}^{(n_\mathrm{F})}$ of dimension K_O, the received vector

$$\underline{\mathbf{e}}^{(n_\mathrm{F})} = \underline{\mathbf{H}}^{(n_\mathrm{F})}\underline{\mathbf{s}}^{(n_\mathrm{F})} + \underline{\mathbf{n}}^{(n_\mathrm{F})} \tag{8.2}$$

of dimension K_O is obtained. Regarding $\underline{\mathbf{n}}^{(n_\mathrm{F})}$ of (8.2), it is assumed that it contains uncorrelated complex elements with Gaussian distributed real and imaginary parts of variance σ^2.

At the receiver side linear post-processing is performed, which means that estimation can be described by a demodulator matrix $\underline{\mathbf{D}}^{(n_\mathrm{F})}$ of dimension $K \times K_\mathrm{O}$ with the aid of which the estimated data vector

$$\hat{\underline{\mathbf{d}}}^{(n_\mathrm{F})} = \underline{\mathbf{D}}^{(n_\mathrm{F})}\underline{\mathbf{e}}^{(n_\mathrm{F})} \tag{8.3}$$

of dimension K is obtained from the received vector $\underline{\mathbf{e}}^{(n_\mathrm{F})}$ of dimension K_O of (8.2). Due to the spatial separation of the MTs, in the DL $\underline{\mathbf{D}}^{(n_\mathrm{F})}$ of (8.3) is a diagonal matrix.

(8.1), (8.2), and (8.3) model a generalized linear data transmission scheme. The said data transmission is unbiased, if the restriction

$$\underline{\mathbf{D}}^{(n_\mathrm{F})}\underline{\mathbf{H}}^{(n_\mathrm{F})}\underline{\mathbf{M}}^{(n_\mathrm{F})} = \mathbf{I}_K \tag{8.4}$$

holds for the modulator matrix $\underline{\mathbf{M}}^{(n_\mathrm{F})}$ and the demodulator matrix $\underline{\mathbf{D}}^{(n_\mathrm{F})}$.

8.2.2   Energy efficiency

As shown by the simulation results of Chapters 6 and 7, RxZF JD and TxZF JT are characterized by the same energy loss with respect to the corresponding reference system. In this Section, a performance measure is derived, quantifying the common energy loss in UL and DL by RxZF JD and TxZF JT, respectively.

In a first step, the reference system is defined, in which only a single data symbol $\underline{d}^{(k,n_\mathrm{F})}$ is transmitted. However, unlike the reference systems used for the investigations in Chapters 6 and 7, the chosen reference system for the generalized unbiased linear data transmission utilizes all K_I inputs and all K_O outputs due to the need for application on both UL and DL. The reference system is optimum with respect to the use of the transmit energy

$$T^{(k,n_\mathrm{F})} = \frac{1}{2}\,\underline{\mathbf{s}}^{(n_\mathrm{F})*\mathrm{T}}\underline{\mathbf{s}}^{(n_\mathrm{F})} \tag{8.5}$$

per data symbol. In order to achieve the said optimum use, the transmit vector $\underline{\mathbf{s}}^{(n_\mathrm{F})}$ in the reference system is the eigenvector corresponding to the eigenvalue of $\underline{\mathbf{H}}^{(n_\mathrm{F})*\mathrm{T}}\underline{\mathbf{H}}^{(n_\mathrm{F})}$ with the largest magnitude. With the spectral radius $\lambda_{\max}\left(\underline{\mathbf{H}}^{(n_\mathrm{F})*\mathrm{T}}\underline{\mathbf{H}}^{(n_\mathrm{F})}\right)$ of $\underline{\mathbf{H}}^{(n_\mathrm{F})*\mathrm{T}}\underline{\mathbf{H}}^{(n_\mathrm{F})}$ [Sch88b], the maximum possible receive energy

$$E_{\mathrm{b,opt}}^{(k,n_\mathrm{F})} = \frac{1}{2}\,T^{(k,n_\mathrm{F})}\lambda_{\max}\left(\underline{\mathbf{H}}^{(n_\mathrm{F})*\mathrm{T}}\underline{\mathbf{H}}^{(n_\mathrm{F})}\right) \tag{8.6}$$

and the minimum possible bit error probability

$$P_{\mathrm{b,opt}}^{(k,n_\mathrm{F})} = \frac{1}{2}\mathrm{erfc}\left(\sqrt{\frac{1}{2\sigma^2}\,T^{(k,n_\mathrm{F})}\lambda_{\max}\left(\underline{\mathbf{H}}^{(n_\mathrm{F})*\mathrm{T}}\underline{\mathbf{H}}^{(n_\mathrm{F})}\right)}\right) \tag{8.7}$$

for each bit in the QPSK data symbol $\underline{d}^{(k,n_\mathrm{F})}$ are obtained [Pro95] given the transmit energy $T^{(k,n_\mathrm{F})}$ of (8.5).

SA-based systems with linear pre- and post-processing are suboptimum with respect to the use of the transmit energy $T^{(k,n_\mathrm{F})}$, due to the following two reasons:

- Due to the spatial separation of the MTs, the eigenvector corresponding to the eigenvalue of $\underline{\mathbf{H}}^{(n_\mathrm{F})*\mathrm{T}}\underline{\mathbf{H}}^{(n_\mathrm{F})}$ with the largest magnitude cannot be used as the transmit vector, which means that the transmit energy $T^{(k,n_\mathrm{F})}$ cannot be converted in receive energy $R^{(k,n_\mathrm{F})}$ as efficiently as in the reference system and

- only a part of the receive energy $R^{(k,n_\mathrm{F})}$ is used, in contrast to the reference system.

The above mentioned reasons hold due to the multiuser nature of the SA-based system. In contrast to the reference system, more than one data symbols have to be transmitted and the eigenvector corresponding to the maximum eigenvalue of $\underline{\mathbf{H}}^{(n_{\mathrm{F}})*\mathrm{T}}\underline{\mathbf{H}}^{(n_{\mathrm{F}})}$ cannot be used for all the data symbols $\underline{d}^{(k,n_{\mathrm{F}})}$, $k = 1 \dots K$. The corresponding suboptimum conversion of $T^{(k,n_{\mathrm{F}})}$ into $R^{(k,n_{\mathrm{F}})}$ is quantified by the transmission efficiency [WSLW03, TWMB01]

$$
t^{(k,n_{\mathrm{F}})} = \frac{\left[\underline{\mathbf{M}}^{(n_{\mathrm{F}})*\mathrm{T}}\underline{\mathbf{H}}^{(n_{\mathrm{F}})*\mathrm{T}}\underline{\mathbf{H}}^{(n_{\mathrm{F}})}\underline{\mathbf{M}}^{(n_{\mathrm{F}})}\right]_{k,k}}{\lambda_{\max}\left(\underline{\mathbf{H}}^{(n_{\mathrm{F}})*\mathrm{T}}\underline{\mathbf{H}}^{(n_{\mathrm{F}})}\right)\left[\underline{\mathbf{M}}^{(n_{\mathrm{F}})*\mathrm{T}}\underline{\mathbf{M}}^{(n_{\mathrm{F}})}\right]_{k,k}}
\tag{8.8}
$$

of generalized unbiased linear data transmission.

At the receiver side, in contrast to the reference system, in which the whole $E_{\mathrm{b}}^{(k,n_{\mathrm{F}})}$ is used, only a part of the receive energy $R^{(k,n_{\mathrm{F}})}$ and thus of the receive energy $E_{\mathrm{b}}^{(k,n_{\mathrm{F}})}$ per bit in the QPSK data symbol $\underline{d}^{(k,n_{\mathrm{F}})}$ is used, due to the need for the elimination of intra-SA interference. The said suboptimum use of $E_{\mathrm{b}}^{(k,n_{\mathrm{F}})}$ is measured by the asymptotic multiuser efficiency [WSLW03, Ver98]

$$
\eta^{(k,n_{\mathrm{F}})} = \frac{1}{\left[\underline{\mathbf{M}}^{(n_{\mathrm{F}})*\mathrm{T}}\underline{\mathbf{H}}^{(n_{\mathrm{F}})*\mathrm{T}}\underline{\mathbf{H}}^{(n_{\mathrm{F}})}\underline{\mathbf{M}}^{(n_{\mathrm{F}})}\right]_{k,k}\left[\underline{\mathbf{D}}^{(n_{\mathrm{F}})}\underline{\mathbf{D}}^{(n_{\mathrm{F}})*\mathrm{T}}\right]_{k,k}}
\tag{8.9}
$$

of generalized unbiased linear data transmission.

Both the transmission efficiency $t^{(k,n_{\mathrm{F}})}$ of (8.8) and the asymptotic multiuser efficiency $\eta^{(k,n_{\mathrm{F}})}$ of (8.9) are heavily influenced by the spatial separation of the MTs in the SA which is expressed in a diagonal form of the modulator matrix $\underline{\mathbf{M}}^{(n_{\mathrm{F}})}$ or the demodulator matrix $\underline{\mathbf{D}}^{(n_{\mathrm{F}})}$ in the UL or the DL transmission, respectively. Moreover, as $t^{(k,n_{\mathrm{F}})}$ of (8.8) measures the suboptimum conversion of the transmit energy $T^{(k,n_{\mathrm{F}})}$ to receive energy $R^{(k,n_{\mathrm{F}})}$ and $\eta^{(k,n_{\mathrm{F}})}$ of (8.9) the suboptimum use of the available receive energy $R^{(k,n_{\mathrm{F}})}$, the energy efficiency

$$
\begin{aligned}
\varepsilon^{(k,n_{\mathrm{F}})} &= t^{(k,n_{\mathrm{F}})}\eta^{(k,n_{\mathrm{F}})} \\
&= \frac{1}{\lambda_{\max}\left(\underline{\mathbf{H}}^{(n_{\mathrm{F}})*\mathrm{T}}\underline{\mathbf{H}}^{(n_{\mathrm{F}})}\right)\left[\underline{\mathbf{M}}^{(n_{\mathrm{F}})*\mathrm{T}}\underline{\mathbf{M}}^{(n_{\mathrm{F}})}\right]_{k,k}\left[\underline{\mathbf{D}}^{(n_{\mathrm{F}})}\underline{\mathbf{D}}^{(n_{\mathrm{F}})*\mathrm{T}}\right]_{k,k}}
\end{aligned}
\tag{8.10}
$$

collectively expresses the suboptimum use of the transmit energy $T^{(k,n_{\mathrm{F}})}$ by both transmitter and receiver sides together. With $\varepsilon^{(k,n_{\mathrm{F}})}$ of (8.10), and using (8.8) and (8.9), and with $E_{\mathrm{b,opt}}^{(k,n_{\mathrm{F}})}$ of (8.6), the bit error probability

$$
\begin{aligned}
P_{\mathrm{b}}^{(k,n_{\mathrm{F}})} &= \frac{1}{2}\operatorname{erfc}\left(\sqrt{\frac{E_{\mathrm{b,opt}}^{(k,n_{\mathrm{F}})}\varepsilon^{(k,n_{\mathrm{F}})}}{\sigma^2}}\right) \\
&= \frac{1}{2}\operatorname{erfc}\left(\sqrt{\frac{T^{(k,n_{\mathrm{F}})}}{2\sigma^2\left[\underline{\mathbf{M}}^{(n_{\mathrm{F}})*\mathrm{T}}\underline{\mathbf{M}}^{(n_{\mathrm{F}})}\right]_{k,k}\left[\underline{\mathbf{D}}^{(n_{\mathrm{F}})}\underline{\mathbf{D}}^{(n_{\mathrm{F}})*\mathrm{T}}\right]_{k,k}}}\right)
\end{aligned}
\tag{8.11}
$$

of each bit in the QPSK data symbol $\underline{d}^{(k,n_\mathrm{F})}$ is calculated [Pro95]. As (8.11) shows, $P_\mathrm{b}^{(k,n_\mathrm{F})}$ depends on the matrices $\underline{\mathbf{M}}^{(n_\mathrm{F})}$ and $\underline{\mathbf{D}}^{(n_\mathrm{F})}$, i.e., on the linear processing in the transmitter and receiver side, and implicitly also on the transfer matrix $\underline{\mathbf{H}}^{(n_\mathrm{F})}$ due to the requirement for unbiased linear data transmission of (8.4).

Hence, in the case of unbiased linear data transmission in SA-based systems, independently of whether UL or DL is considered, the energy efficiency $\varepsilon^{(k,n_\mathrm{F})}$ of (8.10) expresses the suboptimum use of the transmit energy $T^{(k,n_\mathrm{F})}$ by the transmitter and receiver sides in the generalized unbiased linear data transmission, as compared to the reference system. In particular, if a certain transmit energy is required by the reference system in order to achieve a given a target bit error probability $P_\mathrm{b}^{(k,n_\mathrm{F})}$, a SA-based system employing unbiased linear data transmission requires an transmit energy $T^{(k,n_\mathrm{F})}$ increased by the factor $1\left/\varepsilon^{(k,n_\mathrm{F})}\right.$ to obtain the same bit error probability $P_\mathrm{b}^{(k,n_\mathrm{F})}$ as compared to the reference system, and this increase of the required transmit energy $T^{(k,n_\mathrm{F})}$ is the price to be paid for the elimination of the intra-SA interference in the generalized unbiased linear transmission. In what follows, $\varepsilon^{(k,n_\mathrm{F})}$ of (8.10) is determined for UL and DL of SA-based systems.

In the UL transmission of SA-based systems, the spatial separation of the MTs results in the modulator matrix

$$\underline{\mathbf{M}}_{\mathrm{UL}}^{(n_\mathrm{F})} = \mathbf{I}_K. \tag{8.12}$$

Due to the said spatial separation of the MTs, the K inputs to the $K_\mathrm{B} \times K$ MIMO channel of the SA are not jointly available as it is the case in the reference system. With the modulator matrix $\underline{\mathbf{M}}_{\mathrm{UL}}^{(n_\mathrm{F})}$ according to (8.12) and the transfer matrix $\underline{\mathbf{H}}_{\mathrm{UL}}^{(n_\mathrm{F})}$ valid for the UL, the aforementioned fact results in a decreased transmission efficiency

$$t_{\mathrm{UL}}^{(k,n_\mathrm{F})} = \frac{\left[\underline{\mathbf{H}}_{\mathrm{UL}}^{(n_\mathrm{F})}\underline{\mathbf{H}}_{\mathrm{UL}}^{(n_\mathrm{F})*\mathrm{T}}\right]_{k,k}}{\lambda_{\max}\left(\underline{\mathbf{H}}_{\mathrm{UL}}^{(n_\mathrm{F})*\mathrm{T}}\underline{\mathbf{H}}_{\mathrm{UL}}^{(n_\mathrm{F})}\right)}. \tag{8.13}$$

Linear post-processing is performed by the CU at the receiver side. With the use of the demodulator matrix

$$\underline{\mathbf{D}}_{\mathrm{UL}}^{(n_\mathrm{F})} = \left(\underline{\mathbf{H}}_{\mathrm{UL}}^{(n_\mathrm{F})*\mathrm{T}}\underline{\mathbf{H}}_{\mathrm{UL}}^{(n_\mathrm{F})}\right)^{-1}\underline{\mathbf{H}}_{\mathrm{UL}}^{(n_\mathrm{F})*\mathrm{T}} \tag{8.14}$$

according to the RxZF principle [Kle96, SWC$^+$02, WMS$^+$02], all intra-SA interference is cancelled. Due to the need for intra-SA interference elimination, only the orthogonal parts of the partial received signals are used. With (8.9) and using the demodulator matrix $\underline{\mathbf{D}}_{\mathrm{UL}}^{(n_\mathrm{F})}$ of (8.14) and the transfer matrix $\underline{\mathbf{H}}_{\mathrm{UL}}^{(n_\mathrm{F})}$, the said suboptimum use of the available receive energy $R^{(k,n_\mathrm{F})}$ in the UL is quantified by the asymptotic multiuser efficiency

$$\eta_{\mathrm{UL}}^{(k,n_\mathrm{F})} = \frac{1}{\left[\left(\underline{\mathbf{H}}_{\mathrm{UL}}^{(n_\mathrm{F})*\mathrm{T}}\underline{\mathbf{H}}_{\mathrm{UL}}^{(n_\mathrm{F})}\right)^{-1}\right]_{k,k}\left[\underline{\mathbf{H}}_{\mathrm{UL}}^{(n_\mathrm{F})*\mathrm{T}}\underline{\mathbf{H}}_{\mathrm{UL}}^{(n_\mathrm{F})}\right]_{k,k}}. \tag{8.15}$$

With $t_{\mathrm{UL}}^{(k,n_{\mathrm{F}})}$ of (8.13) and $\eta_{\mathrm{UL}}^{(k,n_{\mathrm{F}})}$ of (8.15) follows from (8.10) the energy efficiency

$$\varepsilon_{\mathrm{UL}}^{(k,n_{\mathrm{F}})} = \frac{1}{\lambda_{\max}\left(\mathbf{\underline{H}}_{\mathrm{UL}}^{(n_{\mathrm{F}})*\mathrm{T}}\mathbf{\underline{H}}_{\mathrm{UL}}^{(n_{\mathrm{F}})}\right)\left[\left(\mathbf{\underline{H}}_{\mathrm{UL}}^{(n_{\mathrm{F}})*\mathrm{T}}\mathbf{\underline{H}}_{\mathrm{UL}}^{(n_{\mathrm{F}})}\right)^{-1}\right]_{k,k}} \tag{8.16}$$

of the UL transmission.

In the DL transmission of SA-based systems, he spatial separation of the MTs in the DL is expressed by the diagonal demodulator matrix

$$\mathbf{\underline{D}}_{\mathrm{DL}}^{(n_{\mathrm{F}})} = \mathbf{I}_K. \tag{8.17}$$

Because each MT uses the whole available received energy $R^{(k,n_{\mathrm{F}})}$, an asymptotic multiuser efficiency

$$\eta_{\mathrm{DL}}^{(k,n_{\mathrm{F}})} = 1 \tag{8.18}$$

follows from (8.9) for the DL transmission.

At the transmitter side, the modulator matrix

$$\mathbf{\underline{M}}_{\mathrm{DL}}^{(n_{\mathrm{F}})} = \mathbf{\underline{H}}_{\mathrm{DL}}^{(n_{\mathrm{F}})*\mathrm{T}}\left(\mathbf{\underline{H}}_{\mathrm{DL}}^{(n_{\mathrm{F}})}\,\mathbf{\underline{H}}_{\mathrm{DL}}^{(n_{\mathrm{F}})*\mathrm{T}}\right)^{-1} \tag{8.19}$$

is used according to the TxZF principle [MBW^{+}00, WMS^{+}02]. Because a part of the available transmit energy $T^{(k,n_{\mathrm{F}})}$ is devoted to eliminate intra-SA interference, from (8.8) and using $\mathbf{\underline{M}}_{\mathrm{DL}}^{(n_{\mathrm{F}})}$ of (8.19) and the transfer matrix $\mathbf{\underline{H}}_{\mathrm{UL}}^{(n_{\mathrm{F}})}$, the suboptimum use of $T^{(k,n_{\mathrm{F}})}$ in the DL transmission is is quantified by the transmission efficiency

$$t_{\mathrm{DL}}^{(k,n_{\mathrm{F}})} = \frac{1}{\lambda_{\max}\left(\mathbf{\underline{H}}_{\mathrm{DL}}^{(n_{\mathrm{F}})}\mathbf{\underline{H}}_{\mathrm{DL}}^{(n_{\mathrm{F}})*\mathrm{T}}\right)\left[\left(\mathbf{\underline{H}}_{\mathrm{DL}}^{(n_{\mathrm{F}})}\mathbf{\underline{H}}_{\mathrm{DL}}^{(n_{\mathrm{F}})*\mathrm{T}}\right)^{-1}\right]_{k,k}}. \tag{8.20}$$

With $t_{\mathrm{DL}}^{(k,n_{\mathrm{F}})}$ of (8.20) and $\eta_{\mathrm{DL}}^{(k,n_{\mathrm{F}})}$ of (8.18), follows from (8.10) for the DL transmission the energy efficiency

$$\varepsilon_{\mathrm{DL}}^{(k,n_{\mathrm{F}})} = \frac{1}{\lambda_{\max}\left(\mathbf{\underline{H}}_{\mathrm{DL}}^{(n_{\mathrm{F}})}\mathbf{\underline{H}}_{\mathrm{DL}}^{(n_{\mathrm{F}})*\mathrm{T}}\right)\left[\left(\mathbf{\underline{H}}_{\mathrm{DL}}^{(n_{\mathrm{F}})}\mathbf{\underline{H}}_{\mathrm{DL}}^{(n_{\mathrm{F}})*\mathrm{T}}\right)^{-1}\right]_{k,k}}. \tag{8.21}$$

Given that TDD is employed and that the channels of UL and DL are reciprocal,

$$\mathbf{\underline{H}}_{\mathrm{DL}}^{(n_{\mathrm{F}})} = \mathbf{\underline{H}}_{\mathrm{UL}}^{(n_{\mathrm{F}})\mathrm{T}} \tag{8.22}$$

holds for the transfer matrices of UL and DL. Moreover, for a square matrix $\underline{\mathbf{X}}$

$$\lambda_{\max}\left(\underline{\mathbf{X}}^{\mathrm{T}}\right) = \lambda_{\max}\left(\underline{\mathbf{X}}\right) \tag{8.23}$$

holds [ZF86].

Using (8.22) and (8.23), the comparison of $\varepsilon_{\mathrm{UL}}^{(k,n_{\mathrm{F}})}$ of (8.16) and $\varepsilon_{\mathrm{DL}}^{(k,n_{\mathrm{F}})}$ of (8.21) yields

$$\varepsilon_{\mathrm{UL}}^{(k,n_{\mathrm{F}})} = \varepsilon_{\mathrm{DL}}^{(k,n_{\mathrm{F}})} \tag{8.24}$$

and for the corresponding bit error probabilities

$$P_{\mathrm{b,UL}}^{(k,n_{\mathrm{F}})} = P_{\mathrm{b,DL}}^{(k,n_{\mathrm{F}})} \tag{8.25}$$

holds.

(8.24) expresses an important characteristic of SA-based systems. According to (8.24), with the transfer matrix $\underline{\mathbf{H}}^{(n_{\mathrm{F}})}$ valid for the UL transmission, UL and DL are characterized by the same energy efficiency

$$\varepsilon^{(k,n_{\mathrm{F}})} = \frac{1}{\lambda_{\max}\left(\underline{\mathbf{H}}^{(n_{\mathrm{F}})*\mathrm{T}}\underline{\mathbf{H}}^{(n_{\mathrm{F}})}\right)\left[\left(\underline{\mathbf{H}}^{(n_{\mathrm{F}})*\mathrm{T}}\underline{\mathbf{H}}^{(n_{\mathrm{F}})}\right)^{-1}\right]_{k,k}}. \tag{8.26}$$

In other words, the price to be paid for intra-SA interference elimination is the same for RxZF JD and TxZF JT. Consequently, investigations regarding the energy efficiency $\varepsilon^{(k,n_{\mathrm{F}})}$ in the case of unbiased linear data transmission in SA-based systems can be carried out jointly for UL and DL.

8.3   System layer aspects

The energy efficiency $\varepsilon^{(k,n_{\mathrm{F}})}$ as defined in (8.24) is an energy related measure. As such, it is useful also in investigations concerning the system layer of SA-based systems with unbiased linear data transmission, in which not the structure of the signals, but the transmit and receive energies play a role. For this reason, the energy efficiency $\varepsilon^{(k,n_{\mathrm{F}})}$ as defined in (8.24) is used in this Section to provide an insight in issues regarding the system layer of SA-based systems, i.e., in issues related to inter-SA interference.

The energy efficiency $\varepsilon^{(k,n_{\mathrm{F}})}$ as defined in (8.24) quantifies the efficiency of the use of the transmit energy $T^{(k,n_{\mathrm{F}})}$. An energy efficiency $\varepsilon^{(k,n_{\mathrm{F}})}$ smaller than unity means that a higher transmit energy $T^{(k,n_{\mathrm{F}})}$ is required by the SA-based system than by the reference system in

order to achieve a given bit error probability $P_\text{b}^{(k,n_\text{F})}$, and that higher energy is radiated towards the neighboring SAs causing inter-SA interference. Equivalently, for given transmit energy $T^{(k,n_\text{F})}$ lower receive energy $R^{(k,n_\text{F})}$ is achieved relative to the reference system, which means that the sensitivity of the receivers in a SA to noise, i.e., to inter-SA interference is increased. Hence, the energy efficiency $\varepsilon^{(k,n_\text{F})}$ of (8.24) is a measure for the inter-SA interference caused from the transmitters of a SA to neighboring SAs or equivalently, for the sensitivity of the receivers in a SA to inter-SA interference stemming from neighboring SAs.

An important aspect of interest to system level considerations is the dependence of the energy efficiency $\varepsilon^{(k,n_\text{F})}$ of (8.24) on the number K of MTs and the number K_B of APs. Fig. 8.2 depicts the average energy efficiency $\overline{\varepsilon}^{(n_\text{F})}$ of unbiased linear data transmission in a SA for fixed system load K/K_B. The transfer matrix $\underline{\mathbf{H}}^{(n_\text{F})}$ used consists of independent and identically distributed complex random variables, each having a magnitude following the Rayleigh distribution. As
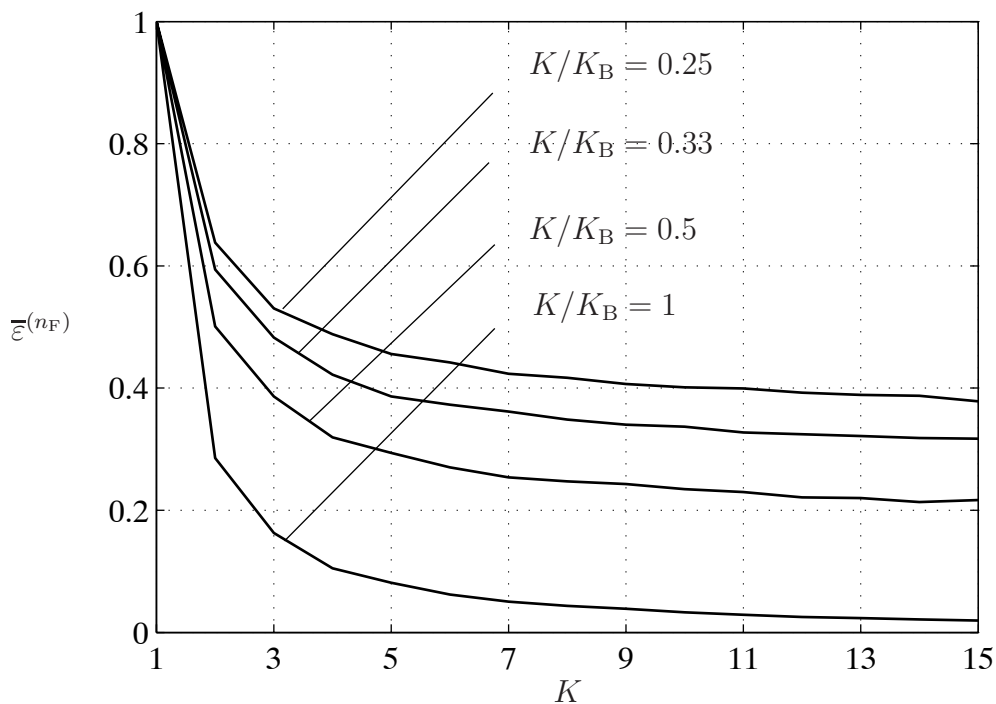
Figure 8.2. Average energy efficiency $\overline{\varepsilon}^{(n_\text{F})}$ of a SA employing unbiased linear data transmission for Rayleigh fading

can be seen from Fig. 8.2, the energy efficiencies $\overline{\varepsilon}^{(n_\text{F})}$ are unity for $K = 1$ MT, for all system loads K/K_B, as expected from theory. The energy efficiency $\overline{\varepsilon}^{(n_\text{F})}$ initially decreases for increasing number of MTs K, and for large K converges to a constant value. The said limiting value of $\overline{\varepsilon}^{(n_\text{F})}$ could be computed analytically with the aid of random matrix theory [Meh91]. Ultimately, Fig. 8.2 shows that for a large number K of MTs, the energy efficiency $\overline{\varepsilon}^{(n_\text{F})}$ is a function only of the system load K/K_B and is independent of the number K of MTs.

The transmit energy used by the reference system in which a single data symbol is transmitted is antiproportional to the number K_B of employed APs, i.e., of the number of antennas jointly available in the SA [God97a, God97b]. Therefore, due to the fact that the average energy efficiency $\overline{\varepsilon}^{(n_F)}$ is a function of the system load K/K_B only, the transmit energy used in a SA for a single data symbol $\underline{d}^{(k,n_F)}$ is also antiproportional to the number K_B of APs for given system load K/K_B. From the latter observation follows directly that the total transmit power in a SA is a function of the system load K/K_B only and independent of the number K of MTs. Hence, the inter-SA interference induced from a SA to its neighboring SAs in a SA-based system for a given system load K/K_B does not depend on the number K of MTs. Equivalently, if the system load K/K_B is kept constant, the number K of MTs in a SA of a SA-based system employing unbiased linear data transmission can be increased without any increase in the inter-SA interference.

With respect to the spectrum capacity η_c of (1.1), it follows that a decisive increase in the spectrum capacity η_c is achievable in SA-based systems as compared to state-of-the-art mobile radio systems based on the cellular air interface architecture. For this reason, the choice of the SA air interface architecture is especially attractive for application on beyond 3G mobile radio systems, on which the demand for high spectrum capacity η_c is posed.

9 Summary

9.1 Summary in English

The present thesis deals with a novel air interface concept for beyond 3G mobile radio systems. Signals received at a certain reference cell in a cellular system which originate in neighboring cells of the same cellular system are undesired and constitute the intercell interference. Due to intercell interference, the spectrum capacity of cellular systems is limited and therefore the reduction of intercell interference is an important goal in the design of future mobile radio systems. In the present thesis, a novel service area based air interface concept is investigated in which interference is combated by joint detection and joint transmission, providing an increased spectrum capacity as compared to state-of-the-art cellular systems.

Various algorithms are studied, with the aid of which intra service area interference can be combated. In the uplink transmission, by optimum joint detection the probability of erroneous decision is minimized. Alternatively, suboptimum joint detection algorithms can be applied offering reduced complexity. By linear receive zero-forcing joint detection interference in a service area is eliminated, while by linear minimum mean square error joint detection a trade-off is performed between interference elimination and noise enhancement. Moreover, iterative joint detection is investigated and it is shown that convergence of the data estimates of iterative joint detection without data estimate refinement towards the data estimates of linear joint detection can be achieved. Iterative joint detection can be further enhanced by the refinement of the data estimates in each iteration. For the downlink transmission, the reciprocity of uplink and downlink channels is used by joint transmission eliminating the need for channel estimation and therefore allowing for simple mobile terminals. A novel algorithm for optimum joint transmission is presented and it is shown how transmit signals can be designed which result in the minimum possible average bit error probability at the mobile terminals. By linear transmit zero-forcing joint transmission interference in the downlink transmission is eliminated, whereas by iterative joint transmission transmit signals are constructed in an iterative manner.

In a next step, the performance of joint detection and joint transmission in service area based systems is investigated. It is shown that the price to be paid for the interference suppression in service area based systems is the suboptimum use of the receive energy in the uplink transmission and of the transmit energy in the downlink transmission, with respect to the single user reference system. In the case of receive zero-forcing joint detection in the uplink and transmit zero-forcing joint transmission in the downlink, i.e., in the case of linear unbiased data transmission, it is shown that the same price, quantified by the energy efficiency, has to be paid for interference elimination in both uplink and downlink. Finally it is shown that if the system load is fixed, the number of active mobile terminals in a SA and hence the spectrum capacity can be increased without any significant reduction in the average energy efficiency of the data transmission.

9.2   Summary in German

Die vorliegende Dissertation befaßt sich mit einem neuartigen Konzept für die Luftschnittstelle von Mobilfunksystemen jenseits der dritten Generation. In einer Referenzzelle eines zellularen Mobilfunksystems empfangene Signale, die in Nachbarzellen des selben Mobilfunksystems abgestrahlt wurden, sind unerwünscht und bilden die Interzellinterferenz. Wegen der Interzellinterferenz ist die spektrale Kapazität zellularer Systeme begrenzt und daher ist die Reduktion der Interzellinterferenz ein wichtiges Ziel beim Entwurf zukünftiger Mobilfunksysteme. In der vorliegenden Dissertation wird ein neuartiges Luftschnittstellenkonzept auf der Basis von Service Gebieten, in dem Interferenz mittels Joint Detection und Joint Transmission bekämpft wird und dadurch eine höhere spektrale Kapazität als in zellularen Mobilfunksystemen gemäß dem Stand der Technik erzielt werden kann, untersucht.

Eine Vielfalt von Algorithmen, mit deren Hilfe die Intraserviceareainterferenz unterdrückt werden kann, werden untersucht. In der Aufwärtsstrecke wird die Wahrscheinlichkeit der Fehlentscheidung mittels optimalem Joint Detection minimiert. Alternativ kann durch geringere Komplexität gekennzeichnetes suboptimales Joint Detection eingesetzt werden. Mit linearem Zero-Forcing Joint Detection wird die Interferenz innerhalb eines Service Gebietes eliminiert und lineares Minimum Mean Square Error Joint Detection bildet einen Kompromiss zwischen Interferenzelimination und Rauschenverstärkung. Zusätzlich wird Iteratives Joint Detection untersucht und es wird gezeigt, daß Konvergenz der Datenschätzungen von Iterativem Joint Detection ohne Schätzwertverbesserung und linearem Joint Detection erreicht werden kann. Iteratives Joint Detection kann man verbessern, indem man die Datenschätzungen in jeder Iteration verbessert. Für die Abwärtsstrecke wird die Reziprozität zwischen den Kanälen der Auf- und Abwärtsstrecke von Joint Transmission ausgenutzt. Somit wird die Notwendigkeit einer Kanalschätzung in der Abwärtsstrecke eliminiert und die Komplexität der Mobile Terminals gering gehalten. Ein neuartiges Verfahren für optimales Joint Transmission wird eingeführt und der Entwurf von Sendesignalen, die zu minimaler Bitfehlerwahrscheinlichkeit an den Mobile Terminals führen, beschrieben. Mit Hilfe von linearem Joint Transmission kann Interferenz in der Abwärtsstrecke eliminiert werden und mit Iterativem Joint Transmission werden die Sendesignale iterativ konstruiert.

In einem nächsten Schritt wird die Performanz von Joint Detection und Joint Transmission in auf Service Gebieten basierenden Systemen untersucht. Es wird gezeigt, daß das suboptimale Nutzen der Empfangsenergie in der Aufwärtsstrecke und der Sendeenergie in der Abwärtsstrecke im Vergleich zum Referenzsystem der für die Unterdrückung der Interferenz zu zahlende Preis ist. Es folgt, daß im Fall von linearem Zero-Forcing Joint Detection und linearem Transmit Zero-Forcing Joint Transmission der selbe Preis für die Interferenzunterdrückung zu zahlen ist, der sich mit der Energieeffizienz quantitativ beschreiben läßt. Schließlich wird gezeigt, daß bei konstanter Systemlast in einem Service Gebiet die Anzahl der Mobile Terminals beliebig erhöht werden kann, ohne daß die Energieeffizienz der Datenübertragung merklich abnimmt.

Appendix A

Frequently used abbreviations and symbols

A.1 Abbreviations

AP	access point
BPSK	binary phase shift keying
BS	base station
BU	bad urban
CCDF	complemetary cumulative distribution function
CDMA	code division multiple access
COST	european cooperation in the field of science and technology
CU	central unit
dB	decibel
DL	downlink
FEC	forward error correcting
HT	hilly terrain
JD	joint detection
JT	joint transmission
LOS	line of sight
MAP	minimum a posteriori
MF	matched filter
ML	maximum likelihood
MIMO	multiple input multiple output
MMSE	minimum mean square error
MT	mobile terminal
OFDM	orthogonal frequecy division multiplexing
QPSK	quadrature phase shift keying
RA	rural area
RxZF	receive zero - forcing
SA	service area
SNR	signal to noise ratio
TDD	time division duplexing
TU	typical urban
TxMF	transmit matched filter
TxZF	transmit zero - forcing
UL	uplink
ZF	zero - forcing

A.2   Symbols

A	area covered by the mobile radio system
$\underline{b}_{n_\mathrm{F},n_\mathrm{S}}^{(k_\mathrm{I},k_\mathrm{O})}(t)$	combined time continuous impulse response between input k_I and output k_O of the MIMO mobile radio channel, (3.12)
B	system bandwidth
c_0	speed of propagation of electromagnetic waves in the vacuum
$\underline{c}_\mathrm{r}(t)$	basic receive signature in the analysis filter bank, (3.17)
$\underline{c}_{\mathrm{r},n_\mathrm{F},n_\mathrm{S}}(t)$	impulse response of each filter in the analysis filter bank at subcarrier n_F and symbol slot n_S, (3.18)
$\underline{c}_\mathrm{t}(t)$	basic transmit signature, (3.9)
$\underline{c}_{\mathrm{t},n_\mathrm{F},n_\mathrm{S}}(t)$	transmit signature at subcarrier n_F and symbol slot n_S, (3.10)
$\underline{d}^{(k,n_\mathrm{F})}$	data symbol of MT k sent at subcarrier n_F , (3.38)
$\underline{\hat{d}}^{(k,n_\mathrm{F})}$	estimated data symbol of MT k at subcarrier n_F
$d_m^{(k)}$	m-th coded bit of MT k
$\hat{d}_m^{(k)}$	m-th estimated coded bit of MT k
$\underline{\mathbf{d}}$	total data vector, (3.41)
$\underline{\hat{\mathbf{d}}}$	total estimated data vector, (3.43)
$\underline{\hat{\mathbf{d}}}(p)$	total estimated data vector by iterative JD at iteration p
$\underline{\hat{\hat{\mathbf{d}}}}(p)$	total refined estimated data vector by iterative JD at iteration p
$\mathbf{d}^{(k)}$	coded bit vector of MT k, (4.3)
$\hat{\mathbf{d}}^{(k)}$	estimated coded bit vector of MT k, (4.47)
$\underline{\mathbf{d}}^{(n_\mathrm{F})}$	data vector at subcarrier n_F, (3.40)
$\underline{\hat{\mathbf{d}}}^{(n_\mathrm{F})}$	estimated data vector at subcarrier n_F, (3.42)
$\mathbf{d}_v$	effective data vector
$\mathbf{d}_v^{(n_\mathrm{F})}$	effective data vector at subcarrier n_F
D	cardinality of the data symbol alphabet $\mathbb{D}$
$\mathbb{D}$	data symbol alphabet
$\mathbb{D}^K$	set of data vectors $\underline{\mathbf{d}}$
$\mathbb{D}_\mathrm{eff}^K$	set of effective data vectors $\underline{\mathbf{d}}_v$, (5.9)
$\underline{\mathbf{D}}^{(n_\mathrm{F})}$	demodulator matrix of linear JD at subcarrier n_F
$\underline{\mathbf{D}}_\mathrm{DL}^{(n_\mathrm{F})}$	demodulator matrix in the DL of the generalized linear data transmission, (8.17)
$\underline{\mathbf{D}}_\mathrm{MMSE}^{(n_\mathrm{F})}$	demodulator matrix of MMSE JD at subcarrier n_F, (4.25)
$\underline{\mathbf{D}}_\mathrm{ZF}^{(n_\mathrm{F})}$	demodulator matrix of RxZF JD at subcarrier n_F, (4.21)
$\underline{\mathbf{D}}_\mathrm{UL}^{(n_\mathrm{F})}$	demodulator matrix in the DL of the generalized linear data transmission, (8.14)
$\underline{e}^{(k,n_\mathrm{F})}$	receive value at MT k at subcarrier n_F at the downlink
$\underline{e}^{(k_\mathrm{B},n_\mathrm{F})}$	receive value at AP k_B at subcarrier n_F at the uplink
$\underline{e}^{(k_\mathrm{O})}(t)$	time-continuous received signal at output k_O of the MIMO mobile radio channel, (3.11)

$\underline{e}^{(k_\mathrm{O},n_\mathrm{F},n_\mathrm{S})}$	receive value at output k_I, subcarrier n_F and symbol slot n_S, (3.21)
$e_v^{(k,n_\mathrm{F})}$	effective received value by MT k at subcarrier n_F
$\underline{\mathbf{e}}$	total received vector
$\underline{\mathbf{e}}^{(k_\mathrm{O})}$	receive vector at output k_I, (3.3)
$\underline{\mathbf{e}}^{(n_\mathrm{F})}$	receive vector at subcarrier n_F
$\underline{\mathbf{e}}^{(n_\mathrm{F},n_\mathrm{S})}$	receive vector at subcarrier n_F and symbol slot n_S, (3.32)
$\mathbf{e}_v^{(n_\mathrm{F})}$	effective received vector, (5.31)
$\overline{E}_\mathrm{b}$	average received energy per bit
$E_\mathrm{b}^{(k,n_\mathrm{F})}$	received energy per bit in the data symbol $\underline{d}^{(k,n_\mathrm{F})}$
$E_\mathrm{b,opt}^{(k,n_\mathrm{F})}$	received energy per bit in the data symbol $\underline{d}^{(k,n_\mathrm{F})}$ in the single user reference system, (8.6)
$f_{\mathrm{D},w}$	doppler shift exhibited by path w of the mobile radio channel
F	subcarrier spacing in a multicarrier system
$\mathbf{F}$	forward path matrix of iterative JD (4.30) and iterative JT (5.49)
$\underline{h}^{(k,k_\mathrm{B},n_\mathrm{F})}$	transfer factor of the wireless channel between MT k, AP k_B at subcarrier n_F
$\underline{h}^{(k_\mathrm{I},k_\mathrm{O})}(t)$	time continuous channel impulse response between input k_I and output k_O of the MIMO mobile radio channel
$\underline{h}^{(k_\mathrm{I},k_\mathrm{O},n_\mathrm{F})}$	discrete transfer coefficient between input k_I and output k_O at subcarrier n_F, (3.26)
$\underline{H}(f)$	time invariant complex transfer function of the point to point mobile radio channel
$\underline{H}(f,t)$	time variant complex transfer function of the point to point mobile radio channel
$\underline{H}^{(k,k_\mathrm{B})}(f)$	time invariant complex transfer function of the point to point mobile radio channel between MT k and AP k_B
$\mathbf{H}$	total transfer function matrix of the uplink transmission, (4.7)
$\mathbf{H}^{(n_\mathrm{F})}$	transfer function matrix at subcarrier n_F of the uplink transmission
$\mathbf{H}^{(n_\mathrm{S},n_\mathrm{F})}$	transfer function matrix at subcarrier n_F and symbol slot n_S, (3.35)
k	index of MTs in the SA
k_B	index of APs in the SA
k_I	index of inputs of the MIMO channel
k_O	index of outputs of the MIMO channel
K	number of MTs in the SA
K_B	number of APs in the SA
K_I	number of inputs to the MIMO channel
K_O	number of outputs of the MIMO channel
L	number of bits corresponding to each MT k
M	number of outputs of a MIMO channel
M_B	number of receivers in an excerpt of a MIMO system
$\mathbf{M}$	total modulator matrix for TxZF JT
$\mathbf{M}^{(n_\mathrm{F})}$	modulator matrix of linear JT at subcarrier n_F
$\underline{\mathbf{M}}_\mathrm{DL}^{(n_\mathrm{F})}$	modulator matrix in the DL of the generalized linear data transmission, (8.19)

$\underline{\mathbf{M}}_{\mathrm{TxZF}}^{(n_{\mathrm{F}})}$	modulator matrix for TxZF JT at subcarrier n_{F}, (5.40)
$\underline{\mathbf{M}}_{\mathrm{UL}}^{(n_{\mathrm{F}})}$	modulator matrix in the UL of the generalized linear data transmission, (8.12)
$\underline{\mathbf{M}}_{\infty}$	linear modulator matrix, to which iterative JT converges (5.46)
$\underline{n}^{(k_{\mathrm{O}})}(t)$	noise at output k_{O}
$\underline{n}^{(k_{\mathrm{O}},n_{\mathrm{F}},n_{\mathrm{S}})}$	noise value at output k_{O}, subcarrier n_{F} and symbol slot n_{S}, (3.22)
$\tilde{n}_{\mathrm{d}}$	noise value disturbing the coded bit $d_m^{(k)}$
n_{F}	subcarrier index
n_{S}	symbol slot index
$\underline{\mathbf{n}}$	total noise vector
$\underline{\mathbf{n}}^{(n_{\mathrm{F}})}$	noise vector at subcarrier n_{F}
$\underline{\mathbf{n}}^{(n_{\mathrm{F}},n_{\mathrm{S}})}$	noise vector at subcarrier n_{F} and symbol slot n_{S}, (3.33)
N	number of inputs of a MIMO channel
N_0	one-sided power spectral density of the noise $\underline{n}^{(k_{\mathrm{O}})}(t)$
N_{B}	number of transmitters in an excerpt of a MIMO system
N_{F}	number of subcarriers
N_{S}	number of symbol slots
p	index of iterations of iterative JD and iterative JT
P	number of iterations of iterative JD and iterative JT
$P_{\mathrm{b}}^{(k,n_{\mathrm{F}})}$	bit error probability of data symbol $\underline{d}^{(k,n_{\mathrm{F}})}$
$\overline{P}_{\mathrm{b}}^{(n_{\mathrm{F}})}$	bit error probability averaged over the V effective data vectors $\underline{\mathbf{d}}_v^{(n_{\mathrm{F}})}$, $v = 1 \ldots V$, (5.35)
$\overline{P}_{\mathrm{b},v}^{(n_{\mathrm{F}})}$	average bit error probability of the effective data vector $\underline{\mathbf{d}}_v^{(n_{\mathrm{F}})}$, (5.34)
$P_{\mathrm{b,ref}}^{(k,n_{\mathrm{F}})}$	bit error probability of data symbol $\underline{d}^{(k,n_{\mathrm{F}})}$ in the single user reference system
$P_{\mathrm{b,RxZF}}^{(k,n_{\mathrm{F}})}$	bit error probability of data symbol $\underline{d}^{(k,n_{\mathrm{F}})}$ in RxZF JD, (6.27)
$P_{\mathrm{b},v}^{(k,n_{\mathrm{F}})}$	bit error probability of data symbol $\underline{d}^{(k,n_{\mathrm{F}})}$ in the effective data vector $\underline{\mathbf{d}}_v^{(n_{\mathrm{F}})}$
$P_{\mathrm{b},v,\mathrm{opt}}^{(k,n_{\mathrm{F}})}$	bit error probability of data symbol $\underline{d}^{(k,n_{\mathrm{F}})}$ in the effective data vector $\underline{\mathbf{d}}_v^{(n_{\mathrm{F}})}$ in optimum JT
$P_{\mathrm{b},v,\mathrm{TxZF}}^{(k,n_{\mathrm{F}})}$	bit error probability of data symbol $\underline{d}^{(k,n_{\mathrm{F}})}$ in the effective data vector $\underline{\mathbf{d}}_v^{(n_{\mathrm{F}})}$ in TxZF JT
$r^{(k,k_{\mathrm{B}})}$	distance between MT k and AP k_{B} in the indoor geometric channel model, (2.3)
r_{B}	radius of the circular periphery on which the APs are positioned in the SA according to the geometric channel model
$\mathbf{r}$	output vector of matched filter bank in iterative JD, (4.26)
R	rate of the FEC code
$R^{(k,n_{\mathrm{F}})}$	receive energy corresponding to data symbol $\underline{d}^{(k,n_{\mathrm{F}})}$
$R_{\mathrm{ref}}^{(k,n_{\mathrm{F}})}$	receive energy corresponding to data symbol $\underline{d}^{(k,n_{\mathrm{F}})}$ in the single user reference system, (7.6)
$\underline{\mathbf{R}}$	reverse path matrix by iterative JD (4.31) and iterative JT (5.50)
$\underline{\mathbf{R}}_{\mathrm{n}}$	noise correlation matrix, (3.34)
$\underline{\mathbf{R}}_{\mathrm{dd}}^{(n_{\mathrm{F}})}$	data correlation matrix at subcarrier n_{F}, (4.24)

$\underline{s}^{(k_\mathrm{B},n_\mathrm{F})}$	transmit value from AP k_B at subcarrier n_F at the downlink
$\underline{s}^{(k_\mathrm{I},n_\mathrm{F},n_\mathrm{S})}$	transmit value at input k_I, subcarrier n_F and symbol slot n_S
$\underline{s}^{(k_\mathrm{I})}_{n_\mathrm{F},n_\mathrm{S}}(t)$	partial time continuous transmit signal corresponding to transmit value $\underline{s}^{(k_\mathrm{I},n_\mathrm{F},n_\mathrm{S})}$, (3.5)
$\underline{s}^{(k_\mathrm{I})}(t)$	time continuous transmit signal fed to the input k_I of the time continuous MIMO mobile radio channel, (3.6)
$\underline{\mathbf{s}}$	total transmit vector
$\underline{\mathbf{s}}(p)$	total transmit vector at iteration p of iterative JT, (5.43)
$\underline{\mathbf{s}}^{(k_\mathrm{I})}$	transmit vector at input k_I, (3.2)
$\underline{\mathbf{s}}^{(n_\mathrm{F},n_\mathrm{S})}$	transmit vector at subcarrier n_F and symbol slot n_S, (3.31)
$\underline{\mathbf{s}}^{(n_\mathrm{F})}$	transmit vector at subcarrier n_F
$\mathbf{s}^{(n_\mathrm{F})}_\mathrm{opt}$	transmit vector of optimum JT
$\mathbf{s}^{(n_\mathrm{F})}_v$	effective transmit vector corresponding to the effective data vector $\mathbf{d}^{(n_\mathrm{F})}_v$, (3.31)
$\mathbf{s}^{(n_\mathrm{F})}_{v,\mathrm{opt}}$	effective transmit vector corresponding to the effective data vector $\mathbf{d}^{(n_\mathrm{F})}_v$ of optimum JT
$\mathbf{s}^{(n_\mathrm{F})}_{0,v}$	normalized effective transmit vector corresponding to the effective transmit vector $\mathbf{s}^{(n_\mathrm{F})}_v$, (5.17)
$S\left(\tau,f_\mathrm{D}\right)$	scattering function of the mobile radio channel
$S_\mathrm{c}\left(0,f_\mathrm{D}\right)$	Doppler power spectrum of the mobile radio channel
$\mathbb{S}^{(n_\mathrm{F})}_\mathrm{eff}$	set of effective transmit vectors $\mathbf{s}^{(n_\mathrm{F})}_v$, (5.12)
$\mathbb{S}^{(n_\mathrm{F})}_\mathrm{opt}$	set of transmit vectors $\mathbf{s}^{(n_\mathrm{F})}_\mathrm{opt}$ of optimum JT
$\mathbb{S}^{(n_\mathrm{F})}_\mathrm{eff,opt}$	set of effective transmit vectors $\mathbf{s}^{(n_\mathrm{F})}_v$ of optimum JT
$\underline{\mathbf{t}}(p)$	transformed total data vector at iteration p of iterative JT, (5.42)
$t^{(k,n_\mathrm{F})}$	transmission efficiency of data symbol $\underline{d}^{(k,n_\mathrm{F})}$, (7.27)
$t^{(k,n_\mathrm{F})}_\mathrm{DL}$	transmission efficiency of data symbol $\underline{d}^{(k,n_\mathrm{F})}$ in the DL of the generalized unbiased linear data transmission, (8.20)
$t^{(k,n_\mathrm{F})}_\mathrm{TxZF}$	transmission efficiency of data symbol $\underline{d}^{(k,n_\mathrm{F})}$ in TxZF JT, (7.30)
$\overline{t}^{(n_\mathrm{F})}_\mathrm{TxZF}$	transmission efficiency averaged over the K data symbols $\underline{d}^{(k,n_\mathrm{F})}$, $k=1\ldots K$, in TxZF JT
$t^{(k,n_\mathrm{F})}_\mathrm{UL}$	transmission efficiency of data symbol $\underline{d}^{(k,n_\mathrm{F})}$ in the UL of the generalized unbiased linear data transmission, (8.13)
$t^{(n_\mathrm{F})}_v$	energy factor of effective transmit vector $\mathbf{s}^{(n_\mathrm{F})}_v$
T	transmit energy corresponding to a single data symbol
$T^{(k,n_\mathrm{F})}$	transmit energy corresponding to data symbol $\underline{d}^{(k,n_\mathrm{F})}$
T_h	time duration of the time continuous channel impulse response $\underline{h}^{(k_\mathrm{I},k_\mathrm{O})}(t)$
T_s	time duration of an OFDM symbol slot
$T^{(k,n_\mathrm{F})}_\mathrm{ref}$	transmit energy corresponding to data symbol $\underline{d}^{(k,n_\mathrm{F})}$ in the single user reference system, (7.4)
$T^{(n_\mathrm{F})}_\mathrm{tot}$	total transmit energy of JT at subcarrier n_F, (5.39)
$T^{(n_\mathrm{F})}_\mathrm{tot,v}$	energy of effective transmit vector $\mathbf{s}^{(n_\mathrm{F})}_v$, (5.14)

$\overline{T}_{\text{tot},v}^{(n_\text{F})}$ transmit energy averaged over all V effective transmit vector $\mathbf{s}_v^{(n_\text{F})}$, (5.15)

$\mathbf{u}^{(k)}$ bit vector corresponding to MT k, (3.1)

$\hat{\mathbf{u}}^{(k)}$ estimated bit vector corresponding to MT k, (3.4)

$u_l^{(k)}$ l-th bit corresponding to MT k

$\hat{u}_l^{(k)}$ l-th estimated bit corresponding to MT k

v index of effective data vectors

V cardinality of the set $\mathbb{D}_\text{eff}^K$ of effective data vectors $\underline{\mathbf{d}}_v$, (5.11)

W number of paths of the mobile radio channel

x_max horizontal dimension of the SA in the indoor geometric channel model

$x_\text{AP}^{(k_\text{B})}$ horizontal coordinate of AP k_B in the indoor geometric channel model

$x_\text{MT}^{(k)}$ horizontal coordinate of MT k in the indoor geometric channel model

y_max vertical dimension of the SA in the indoor geometric channel model

$y_\text{AP}^{(k_\text{B})}$ vertical coordinate of AP k_B in the indoor geometric channel model

$y_\text{MT}^{(k)}$ vertical coordinate of MT k in the indoor geometric channel model

$\gamma_\text{ref}^{(k,n_\text{F})}$ SNR corresponding to data symbol $\underline{d}^{(k,n_\text{F})}$ of the single user reference system in the UL (6.6)

$\gamma_\text{RxZF}^{(k,n_\text{F})}$ SNR corresponding to data symbol $\underline{d}^{(k,n_\text{F})}$ in RxZF JD (6.26)

$\delta_\text{RxZF}^{(k,n_\text{F})}$ SNR degradation of data symbol $\underline{d}^{(k,n_\text{F})}$ in RxZF JD (6.35)

$\overline{\varepsilon}^{(k,n_\text{F})}$ average energy efficiency in the generalized unbiased linear data transmission

$\varepsilon^{(k,n_\text{F})}$ energy efficiency of data symbol $\underline{d}^{(k,n_\text{F})}$ in the generalized unbiased linear data transmission (8.26)

$\varepsilon_\text{DL}^{(k,n_\text{F})}$ energy efficiency of data symbol $\underline{d}^{(k,n_\text{F})}$ in the DL of the generalized unbiased linear data transmission (8.21)

$\varepsilon_\text{UL}^{(k,n_\text{F})}$ energy efficiency of data symbol $\underline{d}^{(k,n_\text{F})}$ in the UL of the generalized unbiased linear data transmission (8.16)

θ_w null phase angle of path w of the mobile radio channel

$\theta_v^{(n_\text{F})}$ angles for the representation of the energy factors $t_v^{(n_\text{F})}$, $v = 1 \ldots V$, in the generalized coordinate system, (5.30)

$\eta^{(k,n_\text{F})}$ asymptotic multiuser efficiency of data symbol $\underline{d}^{(k,n_\text{F})}$, (6.25)

$\eta_\text{DL}^{(k,n_\text{F})}$ asymptotic multiuser efficiency of data symbol $\underline{d}^{(k,n_\text{F})}$ in the DL of the generalized unbiased linear data transmission, (8.18)

$\eta_\text{UL}^{(k,n_\text{F})}$ asymptotic multiuser efficiency of data symbol $\underline{d}^{(k,n_\text{F})}$ in the UL of the generalized unbiased linear data transmission, (8.15)

η_c spectrum capacity, (1.1)

$\eta_\text{e}^{(k,n_\text{F})}(\sigma^2)$ multiuser efficiency of data symbol $\underline{d}^{(k,n_\text{F})}$, (6.24)

$\eta_\text{RxZF}^{(k,n_\text{F})}$ asymptotic multiuser efficiency of data symbol $\underline{d}^{(k,n_\text{F})}$ in RxZF JD, (6.33)

$\overline{\eta}_\text{RxZF}^{(n_\text{F})}$ asymptotic multiuser efficiency averaged over the K data symbols $\underline{d}^{(k,n_\text{F})}$, $k = 1 \ldots K$, in RxZF JD

λ system wavelength

$\lambda_\text{max}(\underline{\mathbf{X}})$ spectral radius of matrix $\underline{\mathbf{X}}$, (4.32)

$\underline{\lambda}_q$ eigenvalue q, $q = 1 \ldots Q$, of a complex matrix

$\underline{\rho}$ parameter of the MIMO parametric channel model, (2.6)

$\underline{\rho}_{kk_\mathrm{B}}$	parameter of the extended MIMO parametric channel model, describing the transfer factor between MT k and AP k_B, (2.7)
$\rho_\mathrm{T}(\tau,0)$	delay power spectrum of the mobile radio channel
σ^2	variance of real and imaginary parts of the noise $\underline{n}^{(k_\mathrm{O})}(t)$
σ_d^2	variance of the noise value $\tilde{n}_\mathrm{d}$ disturbing the coded bit $d_m^{(k)}$
$\hat{\sigma}_\mathrm{d}^2$	estimated variance of the noise value $\tilde{n}_\mathrm{d}$ disturbing the coded bit $d_m^{(k)}$
τ_w	delay of path w of the mobile radio channel
$\varphi_v^{(k_\mathrm{B},n_\mathrm{F})}$	angles for the representation of the normalized effective transmit vector $\mathbf{s}_{0,v}^{(n_\mathrm{F})}$ in the generalized coordinate system, (5.29)
$\varphi_{v,\mathrm{opt}}^{(k_\mathrm{B},n_\mathrm{F})}$	angles corresponding to optimum JT in the generalized coordinate system
$\varphi_{v,\mathrm{TxZF}}^{(k_\mathrm{B},n_\mathrm{F})}$	angles corresponding to TxZF JT in the generalized coordinate system

References

[AGR98]   Alexander, P. D.; Grant, A. J.; Reed, M. C.: Iterative detection in code-division multiple-access with error control coding. *European Transactions on Communications*, vol. 9, 1998, pp. 419–425.

[Ahl73]   Ahlswede, R.: Multi-way communication channels. *Proc. of International Symposium on Information Theory*, 1973, pp. 23–52.

[Ala98]   Alamouti, S.: Space block coding: A simple transmit diversity technique for wireless communications. *IEEE Journal on Selected Areas in Communications*, vol. 16, 1998, pp. 1451–1458.

[AMAS02]   Atarashi, H.; Maeda, N.; Abeta, S.; Sawahashi, M.: Broadband packet wireless access based on VSF-OFDM and MC/DS-CDMA. *Proc. IEEE 13th International Symposium on Personal, Indoor and Mobile Radio Communications (PIMRC'02)*, vol. 3, Lisabon, 2002, pp. 992–997.

[ARAS99]   Alexander, P. D.; Reed, M. C.; Asenstorfer, J. A.; Schlegel, C. B.: Iterative multiuser interference reduction: Turbo CDMA. *IEEE Transactions on Communications*, vol. 47, 1999, pp. 1008–1014.

[Bar02]   Baretto, A. N.: *Signal Pre-Processing in the Downlink of Spread–Spectrum Communication Systems*. Fortschrittberichte VDI, Reihe 10, no. 687. Düsseldorf: VDI-Verlag, 2002.

[BARY95]   Bach Andersen, J.; Rappaport, T.; Yoshida, S.: Propagation measurements and models for wireless communications channels. *IEEE Communications Magazine*, vol. 33, 1995, pp. 42–49.

[BBS97]   Baier, P. W.; Blanz, J. J.; Schmalenberger, R. M.: Fundamentals of smart antennas for mobile radio communications. Glisic, S.; Leppännen, P. (Eds.): *Proc. IEEE 8th International Symposium on Personal, Indoor and Mobile Radio Communications (PIMRC'97)*. pp. 345–376. Dordrecht: Kluwer Academic Publishers, 1997.

[BCJR74]   Bahl, L. R.; Cocke, J.; Jelinek, F.; Raviv, J.: Optimal decoding of linear codes for minimizing symbol error rate. *IEEE Transactions on Information Theory*, vol. 20, 1974, pp. 284–287.

[BDMP98]   Benedetto, S.; Divsalar, D.; Montorsi, G.; Pollara, F.: Serial concatenation of interleaved codes: Performance analysis, design, and iterative decoding. *IEEE Transactions on Information Theory*, vol. 44, 1998, pp. 909–926.

[Bel63]   Bello, P. A.: Characterization of randomly time-variant linear channels. *IEEE Transactions on Communications Systems*, vol. 11, 1963, pp. 360–393.

[BFKM93]   Baier, P. W.; Felhauer, T.; Klein, A.; Mämmelä, A.: Survey of linear block estimation algorithms for the detection of spread spectrum signals transmitted over frequency selective channels. *IEICE Transactions on Communications*, vol. 76, 1993, pp. 825–834.

[BG96]   Berrou, C.; Glavieux, A.: Near optimum error correcting coding and decoding: Turbo codes. *IEEE Transactions on Communications*, vol. 44, 1996, pp. 1261–1271.

[BGT93]   Berrou, C.; Glavieux, A.; Thitimajshima, P.: Near Shannon limit error-correcting coding and decoding: Turbo codes. *Proc. IEEE International Conference on Communications (ICC'93)*, vol. 2, Geneva, 1993, pp. 1064–1070.

[Bin91]   Bingham, J.: *ADSL, VDSL and Multicarrier Modulation*. New York: John Wiley & Sons, 1991.

[Bla98]   Blanz, J. J.: *Empfangsantennendiversität in CDMA-Mobilfunksystemen mit gemeinsamer Detektion der Teilnehmersignale*. Fortschrittberichte VDI, Reihe 10, no. 535. Düsseldorf: VDI-Verlag, 1998.

[BM96]   Benedetto, S.; Montorsi, G.: Iterative decoding of serially concatenated convolutional codes. *IEEE Electronics Letters*, vol. 32, 1996, pp. 1186–1187.

[BOS98]   *Joint Predistortion: A Proposal to Allow for Low Cost UMTS TDD Mode Terminals*. Technical Report ETSI SMG2 UMTS L1 82/98, Bosch, 1998.

[BR98]   Brüninghaus, K.; Rohling, H.: Verfahren zur Rahmensychronization in einem OFDM-system. *Proc. of 3. OFDM-Fachgespräch*, Braunschweig, 1998.

[Bro70]   Broyden, C. G.: The convergence of a class of double-rank minimization algorithms. *Journal of the Institute of Mathematics and its Applications*, vol. 6, 1970, pp. 76–90.

[Cal88]   Calhoun, G.: *Digital cellular radio*. Norwood: Artech House, Inc., 1988.

[CCB95]   Chow, P.; Cioffi, J.; Bingham, J.: A practical discrete multitone transceiver loading algorithm for data transmission over spectrally shaped channels. *IEEE Transactions on Communications*, vol. 43, 1995, pp. 773–775.

[Cim85]   Cimini, L.: Analysis and simulation of a digital mobile channel using orthogonal division frequency multiplexing. *IEEE Transactions on Communications*, vol. 33, 1985, pp. 665–675.

[Cos83]   Costa, M. H. M.: Writing on dirty paper. *IEEE Transactions on Information Theory*, vol. 29, 1983, pp. 439–441.

[COS88]   COST - European Cooperation in the field of Scientific and Technical research: *Digital land mobile radio-communications - action point 207*. Luxembourg: Office for Official Publications of the European Communities, 1988.

[CS00]   Caire, G.; Shamai, S.: On achievable rates in a multi-antenna broadcast downlink. *Proc. 38th Annual Allerton Conference on Communications, Control and Computing*, 2000, pp. 1188–1193.

[CT91]   Cover, T. M.; Thomas, J. A.: *Elements of Information Theory*. John Wiley & Sons, 1991.

[CTC91]   Chow, P.; Tu, J.; Cioffi, J.: Performance evaluation of a multichannel tranceiver system for ADSL and VHDSL services. *IEEE Journal on Selected Areas in Communications*, vol. 9, 1991, pp. 909–919.

[CWKS97]   Chow, P.; Widjada, I.; Kim, J.; Sakai, P.: IEEE 802.11 wireless local area networks. *IEEE Communications Magazine*, vol. 9, 1997, pp. 116–126.

[Dav59]   Davidon, W.: *Variable Metric Method for Minimization*. Technical Report ANL-5990, A.E.C. Research and Development Report, 1959.

[DB96]   David, K.; Benkner, T.: *Digitale Mobilfunksysteme*. Stuttgart: B. G. Teubner, 1996.

[DCGV02]   D. Chizhik, G. F.; Gans, M.; Valenzuela, R.: Keyholes, correlations, and capacities of multielement transmit and reveive antennas. *IEEE Transactions on Wireless Communications*, vol. 1, 2002, pp. 361–368.

[DJB$^+$95] Douillard, C.; Jézéquel, M.; Berrou, C.; Picart, A.; Didier, P.; Glavieux, A.: Iterative correction of intersymbol interference: Turbo-equalization. *European Transactions on Communications*, vol. 6, 1995, pp. 507–511.

[DSR98]   Divsalar, D.; Simon, M. K.; Raphaeli, D.: Improved parallel interference cancellation for CDMA. *IEEE Transactions on Communications*, vol. 46, 1998, pp. 258–268.

[ENS97]   Esmailzadeh, R.; Nakagawa, M.; Sourour, E. A.: Time-division duplex CDMA communications. *IEEE Personal Communications*, vol. 4, 1997, pp. 51–56.

[ETS96]   *Radio equipment and systems, high performance radio local area network (HIPERLAN) Type 1*. Technical Report EN 300–652, European Telecommunication and Standardization Institute (ETSI), 1996.

[ETS97a]   *Digital video broadcasting: Framing structure, channel coding, and modulation for digital terrestial television*. Technical Report EN 300–744, European Telecommunication and Standardization Institute (ETSI), 1997.

[ETS97b]   *Radio broadcasting systems; digital audio broadcasting (DAB) to mobile, portable and fixed receivers*. Technical Report EN 300–401, ed. 2, European Telecommunication and Standardization Institute (ETSI), 1997.

[ETS98]   *Universal Mobile Telecommunications System (UMTS); Concept groups for the definition of the UMTS Terrestrial Radio Access (UTRA)*. Technical Report TR 101 397, European Telecommunication and Standardization Institute (ETSI), 1998.

[ETS99]   *Broadband radio access networks (BRAN) HIPERLAN Type 2 technical specification Part 1 − physical layer*. Technical Report DTS/BRAN030003-1, European Telecommunication and Standardization Institute (ETSI), 1999.

[FCG$^+$03] Foschini, G. J.; Chizhik, D.; Gans, M. J.; Papadias, C.; Valenzuela, R. A.: Analysis and performance of some basic space-time architectures. *IEEE Journal on Selected Areas in Communications Special Issue on MIMO Systems*, vol. 21, 2003, pp. 303–320.

[FG98]   Foschini, G. J.; Gans, M. J.: On limits of wireless communication in a fading environment when using multiple antennas. *Wireless Personal Communications*, vol. 6, 1998, pp. 311–335.

[FH96] Fischer, R. F. H.; Huber, J. B.: A new loading algorithm for discrete multitone transmission. *Proc. IEEE Global Telecommunications Conference (GLOBECOM'96)*, vol. 783, London, 1996, pp. 724–728.

[Fis02] Fischer, R.: *Precoding and Signal Shaping for Digital Transmission*. New York: John Wiley & Sons, 2002.

[FK03] Fhazel, K.; Kaiser, S.: *Multi-Carrier and Spread Spectrum Systems*. Chichester: John Wiley & Sons, 2003.

[FKB94] Felhauer, T.; Klein, A.; Baier, P. W.: A low-cost method for CDMA and other applications to separate non orthogonal signals. *IEEE Transactions on Communications*, vol. 42, 1994, pp. 881–883.

[FL61] Franco, G. A.; Lachs, G.: An orthogonal coding technique for communications. *Proc. IRE*, vol. 9, 1961, pp. 126–133.

[FL96] Fleury, B. H.; Leuthold, P. E.: Radiowave propagation in mobile communications: An overview of European research. *IEEE Communications Magazine*, vol. 34, 1996, pp. 70–81.

[Fle70] Fletcher, R.: A new approach to variable metric algorithms. *Computer Journal*, vol. 13, 1970, pp. 317–322.

[Fos96] Foschini, G.: Layered Space-Time Architecture for Wireless communication in a Fading Environment when Using Multiple Antennas. *The Bell System Technical Journal*, vol. 1, 1996, pp. 41–59.

[FP63] Fletcher, R.; Powell, M. D. J.: A rapidly convergent descent method for minimization. *Computer Journal*, vol. 6, 1963, pp. 163–168.

[GFVW98] Golden, G.; Foschini, G.; Valenzuela, G.; Wolniansky, P.: V-BLAST: A high capacity space-time architecture for the rich-scattering wireless channel. *Proc. 5th Workshop on Smart Antennas in Wireless Mobile Communications*, Stanford Univ., 1998.

[GFVW99] Golden, G.; Foschini, G.; Valenzuela, G.; Wolniansky, P.: Detection algorithm and initial laboratory results using the V-BLAST space–time communications architecture. *IEEE Electronics Letters*, vol. 35, 1999, pp. 14–15.

[Gib99] Gibson, J. D. (Ed.): *The Mobile Communications Handbook*. 2. edition. Heidelberg: Springer-Verlag, 1999.

[God97a] Godara, L. C.: Applications of antenna arrays to mobile communications, part I: Performance improvement, feasibility, and system considerations. *Proceedings of the IEEE*, vol. 85, 1997, pp. 1031–1060.

[God97b] Godara, L. C.: Applications of antenna arrays to mobile communications, part II: Beam-forming and direction-of-arrival considerations. *Proceedings of the IEEE*, vol. 85, 1997, pp. 1195–1245.

[Gol70] Goldfarb, D.: A family of variable metric updates derived by variational means. *Mathematics of Computing*, vol. 24, 1970, pp. 23–26.

[GR00]   Grünheid, R.; Rohling, H.: Adaptive Modulation and Multiple Access for the
            OFDM Transmission Technique. *Wireless Personal Communications*, vol. 13,
            2000, pp. 5–13.

[Gra81]   Graham, A.: *Kronecker Products and Matrix Calculus with Appliations*. Chich-
            ester: Ellis Horwood Limited, 1981.

[GRC+01]   Galda, D.; Rohling, H.; Costa, E.; Haas, H.; Schulz, E.: Broadband OFDM-
            FDMA system for the uplink of a wireless LAN. *Proc. 3rd IEEE workshop on
            Wireless Local Area Networks (WLAN'01)*, vol. 2, Boston, 2001.

[GRC+02]   Galda, D.; Rohling, H.; Costa, E.; Haas, H.; Schulz, E.: A low complexity trans-
            mitter structure for the OFDM-FDMA uplink. *Proc. 55th semi–annual Vehicular
            Technology Conference (VTC)*, vol. 2, Birmingham, USA, 2002, pp. 575–579.

[GSM98]   *GSM specifications*. Technical Report, European Telecommunication and Stan-
            dardization Institute (ETSI), 1998.

[GW00]   Giannakis, G.; Wang, Z.: Wireless multicarrier communications. *IEEE Signal
            Processing Magazine*, 2000, pp. 29–48.

[Hag96]   Hagenauer, J.:   Forward error correcting for CDMA systems. *Proc. IEEE
            4th International Symposium on Spread Spectrum Techniques & Applications
            (ISSSTA'96)*, vol. 2, Mainz, 1996, pp. 566–569.

[Hag97]   Hagenauer, J.: The turbo principle: Tutorial introduction and state of the art.
            Proc. International Symposium on Turbo codes and Related Topics, Brest, 1997,
            pp. 1–11.

[HE97]   Házy, L.; El-Tanany, M.: Synchronization of OFDM Systems over frequency
            selective fading channels. *Proc. IEEE 47th Vehicular Technology Conference
            (VTC'97)*, vol. 3, Phoenix, Arizona, 1997, pp. 2094 – 2098.

[HH]   Hughes-Hartogs, D.: *Ensemble Modem Structure for Imperfect Transmission
            Media*. U.S. Patent No. 4679227 (1987); 4731816 (1988); 4833706 (1989).

[HL98]   Hui, A. L. C.; Letaief, K. B.: Successive interference cancellation for multiuser
            asynchronous DS/CDMA detectors in multipath fading links. *IEEE Transactions
            on Communications*, vol. 46, 1998, pp. 384–391.

[HM72]   Harashima, H.; Miyakawa, H.: Matched-transmission technique for channels
            with intersymbol interference. *IEEE Transactions on Communications*, vol. 20,
            1972, pp. 774–780.

[Hoe92]   Hoeher, P.: A statistical discrete-time model for the WSSUS multipath channel.
            IEEE Transactions on Vehicular Technology, vol. 41, 1992, pp. 461–468.

[HOP96]   Hagenauer, J.; Offer, E.; Papke, L.: Iterative decoding of binary block and con-
            volutional codes. *IEEE Transactions on Information Theory*, vol. 42, 1996, pp.
            429–445.

[HT02]   Holma, H.; Toskala, A.: *WCDMA for UMTS, 2nd Edition*. Chinchester: John
            Wiley & Sons, 2002.

[Hug00]   Hughes, B.: Differential space time modulation. *IEEE Transactions on Information Theory*, vol. 46, 2000, pp. 2567–2578.

[IEE99]   *IEEE standard for wireless LAN medium access control (MAC) and physical layer (PHY) specifications, High-speed Physical Layer (PHY) in the 5GHz Band.* Technical Report ISO/IEC 8802-11:1999/Amd 1:2000(E), IEEE, 1999.

[IEE03]   IEEE: *IEEE Standard for IT-Telecommunications and information exchange between systems LAN/MAN - Part II: Wireless LAN Medium Access Control (MAC) and Physical Layer (PHY) specifications Amendment 4: Further Higher Data Rate Extension in the 2.4 GHz Band.* IEEE Standard No. 802.11G-2003, no. SH95134-TBR. IEEE Press, 2003.

[INF01]   Irmer, R.; Nahler, A.; Fettweis, G.: On the impact of soft decision functions on the performance of multistage parallel interference cancelers for CDMA systems. *Proc. IEEE 53th Vehicular Technology Conference (VTC'01 Spring)*, vol. 2, Rhodes, 2001, pp. 1513–1517.

[IRF03]   Irmer, R.; Rave, W.; Fettweis, G.: Minimum BER transmission for TDD-CDMA in frequency-selective channels. *Proc. IEEE 14th International Symposium on Personal, Indoor and Mobile Radio Communications (PIMRC'03)*, vol. 2, Beijing, 2003, pp. 1260–1264.

[JG04]   Jafar, S. A.; Goldsmith, A. J.: Transmitter optimization and optimality of beamforming for multiple antenna systems. *IEEE Transactions on Wireless Communications*, vol. 3, 2004, pp. 1165–1175.

[JKG⁺02]   Joham, M.; Kusume, K.; Gzara, M. H.; Utschick, W.; Nossek, J. A.: Transmit Wiener filter for the downlink of TDD DS-CDMA systems. *Proc. IEEE 9th International Symposium on Spread Spectrum Techniques & Applications (ISSSTA'02)*, vol. 1, Prague, 2002, pp. 9–13.

[Jon95]   Jones, D.: Frequency domain echo cancellation for discrete multitone asymmetric digital subscriber lines tranceivers. *IEEE Transactions on Communications*, vol. 43, 1995, pp. 1663–1672.

[JUN01]   Joham, M.; Utschick, W.; Nossek, J.: On the Equivalence of Prerake and Transmit Matched Filter. *Proc. 10th Aachen Symposium on Signal Theory (ASST 2001)*, Aachen, 2001, pp. 313–318.

[JVG01]   Jafar, S. A.; Vishwanath, S.; Goldsmith, A. J.: Channel capacity and beamforming for multiple transmit and receive antennas with covariance feedback. *Proc. IEEE International Conference on Communications (ICC'01)*, vol. 7, Burbank, California, 2001, pp. 2266–2270.

[JVG02]   Jindal, N.; Vishwanath, S.; Goldsmith, A. J.: On the duality of Gaussian multiple access and broadcast channels. *Proc. of International Symposium on Information Theory*, Lausanne, 2002, p. 500.

[KB92]   Klein, A.; Baier, P. W.: Simultaneous cancellation of cross interference and ISI in CDMA mobile radio communications. *Proc. IEEE 3rd International Symposium on Personal, Indoor and Mobile Radio Communications (PIMRC'92)*, Boston, 1992, pp. 118–122.

[KB93]   Klein, A.; Baier, P. W.: Linear unbiased data estimation in mobile radio systems applying CDMA. *IEEE Journal on Selected Areas in Communications*, vol. 11, 1993, pp. 1058–1066.

[KIHP90]   Kohno, R.; Imai, H.; Hatori, M.; Pasupathy, S.: Combination of an adaptive array antenna and a canceller of interference for direct-sequence spread-spectrum multiple-access system. *IEEE Journal on Selected Areas in Communications*, vol. 8, 1990, pp. 675–682.

[KKKB94]   Klein, A.; Kaweas Kaleh, G.; Baier, P. W.: Equalizers for multi-user detection in code division multiple access mobile radio systems. *Proc. IEEE 44th Vehicular Technology Conference (VTC'94)*, vol. 2, Stockholm, 1994, pp. 762–766.

[KKKB96]   Klein, A.; Kawas Kaleh, G.; Baier, P. W.: Zero Forcing and Minimum Mean-Square-Error Equalization for Multiuser Detection in Code-Division Multiple-Access Channels. *IEEE Transactions on Vehicular Technology*, vol. 45, 1996, pp. 276–287.

[Kle96]   Klein, A.: *Multi-user detection of CDMA signals − algorithms and their application to cellular mobile radio*. Fortschrittberichte VDI, Reihe 10, no. 423. Düsseldorf: VDI-Verlag, 1996.

[KM00]   Kowalewski, F.; Mangold, P.: Joint predistortion and transmit diversity. *Proc. IEEE Global Telecommunications Conference (GLOBECOM'00)*, vol. 1, San Francisco, 2000, pp. 245–249.

[KZ89]   Kalet, I.; Zervos, N.: Optimized decision feedback equalization versus optimized orthogonal frequency division multiplexing, for high-speed data transmission over the local cable network. *Proc. IEEE International Conference on Communications (ICC'89)*, vol. 9, 1989, pp. 1080–1085.

[Lam00a]   Lampe, A.: An analytic solution to the performance of iterated soft decision interference cancellation for coded CDMA transmission over frequency selective fading channels. *Proc. IEEE 7th International Symposium on Spread Spectrum Techniques & Applications (ISSSTA'00)*, Parsippany, 2000, pp. 368–372.

[Lam00b]   Lampe, A.: Multiuser detection with iterated soft decision interference cancellation for multipath fading channels. *Archiv für Elektronik und Übertragungstechnik (AEÜ)*, vol. 54, 2000, pp. 285–292.

[Lee82]   Lee, W.: *Mobile communications engineering*. New York: McGraw–Hill, 1982.

[Lee89]   Lee, E. A.: Programmable DSP architectures: Part II. *IEEE ASSP Magazine*, vol. 1, 1989, pp. 4–14.

[LV89]   Lupas, R.; Verdú, S.: Linear multiuser detectors for synchronous code-division multiple-access channels. *IEEE Transactions on Information Theory*, vol. 35, 1989, pp. 123–126.

[LV90]   Lupas, R.; Verdú, S.: Near-far resistance of multiuser detectors in asynchronous channels. *IEEE Transactions on Communications*, vol. 38, 1990, pp. 496–508.

[Mas02]   Massey, J.: Turbo Codes, Space-Time Codes, what next? *Proc. IEEE International Telecommunications Symposium 2002 (ITS2002)*, Natal, 2002.

[MBW$^+$00]   Meurer, M.; Baier, P. W.; Weber, T.; Lu, Y.; Papathanassiou, A.: Joint Transmission, an advantageous Downlink Concept for CDMA Mobile Radio Systems using Time Division Duplexing. *IEEE Electronics Letters*, vol. 36, 2000, pp. 900–901.

[McD79]   McDonald, V.: The cellular concept. *The Bell System Technical Journal*, vol. 58, 1979, pp. 15–41.

[Meh91]   Mehta, M.: *Random Matrices*. New York: Academic Press, 1991.

[MH94]   Madhow, U.; Honig, M. L.: MMSE interference suppression for direct-sequence spread spectrum CDMA. *IEEE Transactions on Communications*, vol. 42, 1994, pp. 3178–3188.

[MH97]   Müller, R. R.; Huber, J. B.: Iterated soft decision interference cancellation for CDMA. *Proc. 9th Tyrrhenian International Workshop on Digital Communications*, Italy, 1997.

[MH99]   Marzetta, T. L.; Hochwald, B. M.: Capacity of a mobile multiple-antenna communication link in Rayleigh flat fading. *IEEE Transactions on Information Theory*, vol. 45, 1999, pp. 139–157.

[Mil88]   Milstein, L. B.: Interference rejection techniques in spread spectrum communications. *Proc. IEEE*, vol. 76, 1988, pp. 657–671.

[Moh98]   Moher, M.: An iterative multiuser decoder for near-capacity communications. *IEEE Transactions on Communications*, vol. 46, 1998, pp. 870–880.

[MW03]   Meurer, M.; Weber, T.: Generalized data estimate refinement techniques for iterative multiuser detection in TD-CDMA including higher order modulation. *Proc. 10th International Conference on Telecommunications (ICT'03)*, vol. 1, Papeete, 2003, pp. 781–787.

[MWS$^+$02]   Maniatis, I.; Weber, T.; Sklavos, A.; Liu, Y.; Costa, E.; Haas, H.; Schulz, E.: Pilots for joint channel estimation in multi-user OFDM systems. *Proc. IEEE 9th International Symposium on Spread Spectrum Techniques & Applications (ISSSTA'02)*, vol. 1, Prague, 2002, pp. 44 – 48.

[ntz00a]   Europäische Vergabeverfahren von UMTS-Lizenzen kritisiert. *Nachrichtentechnische Zeitschrift*, vol. 5, 2000, p. 16.

[ntz00b]   UMTS-Versteigerungsverfahren erzielte 99,3682 Mrd. DM. *Nachrichtentechnische Zeitschrift*, vol. 10, 2000, p. 16.

[Ost01]   Oster, J.: *Ein Beitrag zur Interzellinterferenzreduktion in zeitgeschlitzten CDMA-Systemen*. Dissertation, Lehrstuhl für hochfrequente Signalübertragung und -verarbeitung, Universität Kaiserslautern, 2001.

[Pap00]   Papathanassiou, A.: *Adaptive antennas for mobile radio systems using Time Division CDMA and joint detection*. Dissertation, Lehrstuhl für hochfrequente Signalübertragung und -verarbeitung, Universität Kaiserslautern, 2000.

[Par92]   Parsons, J. D.: *The Mobile Radio Propagation Channel*. London: Pentech Press, 1992.

[PH94]   Patel, P.; Holtzman, J.: Analysis of a simple successive interference cancellation scheme in a DS/CDMA system. *IEEE Journal on Selected Areas in Communications*, vol. 12, 1994, pp. 796–807.

[Poo00]   Poor, H. V.: Turbo multiuser detection: An overview. *Proc. IEEE 7th International Symposium on Spread Spectrum Techniques & Applications (ISSSTA'00)*, vol. 2, Parsippany, 2000, pp. 583–587.

[Pro95]   Proakis, J. G.: *Digital Communications*. New York: McGraw-Hill, 1995.

[RCLF89]   Rault, J.; Castelain, D.; Le Floch, B.: The coded orthogonal division multiplexing (COFDM) technique, and its application to digital radio broadcasting towards mobile receivers. *Proc. IEEE Global Telecommunications Conference (GLOBECOM'89)*, vol. 1, Dallas, 1989, pp. 428–432.

[RG97]   Rohling, H.; Grünheid, R.: Performance Comparison of Different Multiple Access Schemes for the Downlink of an OFDM Communications System. *Proc. IEEE 47th Vehicular Technology Conference (VTC'97)*, vol. 3, Phoenix, 1997, pp. 1365 – 1369.

[RGG01a]   Rohling, H.; Grünheid, R.; Galda, D.: OFDM - an Attractive Candidate for the Air Interface of the 4th Generation Mobile Communication System. *Proc. 39th Annual Allerton Conference on Communications, Control and Computing*, Urbana-Champain, Illinois, 2001.

[RGG01b]   Rohling, H.; Grünheid, R.; Galda, D.: OFDM Transmission Technique for the 4rth Generation of Mobile Communications Systems. *Proc. 6th International OFDM Workshop (InOWo'01)*, Hamburg, 2001, pp. 0–1 – 0–28.

[Roh95]   Rohling, H.: *Einführung in die Informations- und Codierungstheorie*. Stuttgart: B. G. Teubner, 1995.

[Roh00]   Rohling, H.: The golden future of OFDM. *Proc. 5th International OFDM Workshop (InOWo'00)*, Hamburg, 2000, pp. 0–1 – 0–8.

[RS95]   Russel, M.; Stüber, G.: Terrestrial digital video broadcasting for mobile reception using OFDM. *Wireless Personal Communications*, vol. 2, 1995, pp. 45–66.

[RSAA98]   Reed, M. C.; Schlegel, C. B.; Alexander, P. D.; Asenstorfer, J. A.: Iterative multiuser detection for CDMA with FEC: Near-single-user performance. *IEEE Transactions on Communications*, vol. 46, 1998, pp. 1693–1699.

[Sal67]   Saltzberg, B.: Performance of an efficient parallel data transmission system. *IEEE Transactions on Communications*, vol. 15, 1967, pp. 805–811.

[Sch88a]   Schulze, H.: Stochastische Modelle und digitale Simulation von Mobilfunkkanälen. *Kleinheubacher Berichte*, vol. 32, Miltenberg, 1988, pp. 473–483.

[Sch88b]   Schwarz, H. R.: *Numerische Mathematik*. 2. edition. Stuttgart: B. G. Teubner, 1988.

[Sha48]   Shannon, C. E.: A mathematical theory of communication. *The Bell System Technical Journal*, vol. 27, 1948, pp. 137–423, 623–656.

[Sha70]   Shanno, D. F.: Conditioning of quasi-newton methods for function minimization. *Mathematics of Computing*, vol. 24, 1970, pp. 647–656.

[SMW+01]   Sklavos, A.; Maniatis, I.; Weber, T.; Baier, P. W.; Costa, E.; Haas, H.; Schulz, E.: Joint Channel Estimation in Multi-User OFDM Systems. *Proc. 6th International OFDM Workshop (InOWo'01)*, Hamburg, 2001, pp. 3–1 – 3–4.

[Ste92]   Steele, R.: *Mobile Radio Communications*. London: Pentech Press, 1992.

[Sto83]   Stoer, J.: *Numerische Mathematik*. Berlin: Springer-Verlag, 1983.

[SW94]   Seshadri, N.; Winters, J.: Two schemes for improving the performance of frequency division (FDD) transmission systems using transmitter antenna diversity. *International Journal of Wireless Information Networks*, vol. 1, 1994, pp. 49–60.

[SWBC02]   Sklavos, A.; Weber, T.; Baier, P. W.; Costa, E.: Beyond 3G radio interface JOINT: Optimum uplink data detection when applying OFDM. *Proc. 7th International OFDM Workshop (InOWo'02)*, Hamburg, 2002, pp. 11 –15.

[SWC+02]   Sklavos, A.; Weber, T.; Costa, E.; Haas, H.; Schulz, E.: Joint Detection in multi-antenna and multi-user OFDM systems. Fhazel, K.; Kaiser, S. (Eds.): *Multi-Carrier Spread Spectrum & Related Topics*. pp. 191–198. Dordrecht: Kluwer Academic Publishers, 2002.

[Tel99]   Telatar, I. E.: Capacity of multi-antenna Gaussian channels. *European Transactions on Communications*, vol. 10, 1999, pp. 585–595.

[TIA00]   *Physical Layer Standard for cdma2000 Spread Spectrum Systems, Release A, Addendum 1*. Technical Report C.S0002-A-1, Telecommunications Industry Association (TIA), 2000.

[TJC99]   Tarokh, V.; Jafarkhani, H.; Calderbank, R.: Space–time block codes from orthogonal designs. *IEEE Journal on Selected Areas in Communications*, vol. 16, 1999, pp. 1456–1467.

[TL97]   Thibault, L.; Le, M.: Performance evaluation of COFDM for digital audio broadcasting part I: Parametric study. *IEEE Transactions on Broadcasting*, vol. 43, 1997, pp. 64–75.

[Tom71]   Tomlinson, M.: New automatic equalizer employing modulo arithmetic. *IEE Electronics Letters*, vol. 7, 1971, pp. 138–139.

[TR00]   Tan, P. H.; Rasmussen, L. K.: Linear interference cancellation in CDMA based on iterative techniques for linear equation systems. *IEEE Transactions on Communications*, vol. 48, 2000, pp. 2099–2108.

[TSC98]   Tarokh, V.; Seshadri, N.; Calderbank, R.: Space–time codes for high rate wireless communications. *IEEE Transactions on Information Theory*, vol. 44, 1998, pp. 744–765.

[TWMB01]   Tröger, H.; Weber, T.; Meurer, M.; Baier, P. W.: Performance Assessment of Joint Transmission (JT) Multi-User Downlinks with Multi-Element Transmit Antennas. *European Transactions on Telecommunications (ETT)*, vol. 12, 2001, pp. 407–416.

[VA90]   Varanasi, M. K.; Aazhang, B.:   Multistage detection in asynchronous code-division multiple-access communications. *IEEE Transactions on Communications*, vol. 38, 1990, pp. 509–519.

[VA91]   Varanasi, M. K.; Aazhang, B.:   Near-optimum detection synchronous code-division multiple-access systems.   *IEEE Transactions on Communications*, vol. 39, 1991, pp. 725–736.

[Var95]   Varanasi, M. K.:   Group detection for synchronous Gaussian code-division multiple-access channels. *IEEE Transactions on Information Theory*, vol. 41, 1995, pp. 1083–1096.

[Ver86a] Verdú, S.:   Minimum probability of error for asynchronous Gaussian multiple-access channels. *IEEE Transactions on Information Theory*, vol. 32, 1986, pp. 85–96.

[Ver86b] Verdú, S.:   Optimum multiuser asymptotic efficiency. *IEEE Transactions on Communications*, vol. 34, 1986, pp. 890–897.

[Ver98]   Verdú, S.: *Multiuser Detection*. Cambridge University Press, 1998.

[Vit91]   Viterbi, A. J.:   Wireless digital communication: A view based on three lessons learned. *IEEE Communications Magazine*, vol. 11, 1991, pp. 33–36.

[VJ98]   Vojčić, B.; Jang, W.: Transmitter precoding in synchronous multiuser communications. *IEEE Transactions on Communications*, vol. 46, 1998, pp. 1346–1355.

[VJG02]   Vishwanath, S.; Jindal, N.; Goldsmith, A.: On the capacity of multiple input multiple output broadcast channels. *Proc. IEEE International Conference on Communications (ICC'02)*, vol. 2, Rzeszów, 2002, pp. 1444–1450.

[VM01]   Visotsky, E.; Madhow, U.:   Space-time transmit precoding with imperfect feedback. *IEEE Transactions on Information Theory*, vol. 47, 2001, pp. 2632–2639.

[vNAM+99] van Nee, R.; Awater, G.; Morikura, M.; Takanashi, H.; Webster, M.: Near high-rate wireless LAN standards. *IEEE Communications Magazine*, vol. 12, 1999, pp. 82–88.

[vNP00]   van Nee, R.; Prasad, R.:   *OFDM for Wireless Multimedia Communications*. Boston: Artech House, 2000.

[vSB97]   van de Beek, J.; Sandell, M.; Börjesson, P.: ML estimation of time and frequency offsets in OFDM Systems. *IEEE Transactions on Signal Processing*, vol. 45, 1997, pp. 1800 – 1805.

[VT03]   Vishwanath, S.; Tse, D.: Sum capacity of the multiple antenna Gaussian broadcast channel. *IEEE Transactions on Information Theory*, vol. 48, 2003, pp. 1912–1921.

[VTA01]   Vishwanath, S.; Tse, D.; Anantharam, V.: Asymptotically optimal water-filling in vector multiple-access channels. *IEEE Transactions on Information Theory*, vol. 47, 2001, pp. 241–267.

[VW98]   Valenti, M. C.; Woerner, B. D.: Iterative multiuser detection for convolutionally coded asynchronous DS-CDMA. *Proc. IEEE 9th International Symposium on Personal, Indoor and Mobile Radio Communications (PIMRC'98)*, vol. 1, Boston, 1998, pp. 213–217.

[w3G99]   *Physical channels and mapping of transport channels onto physical channels (FDD)*. Technical Report 3GPP TS 25.211, 3rd Generation Partnership Project (3GPP), 1999.

[WE71]   Weinstein, S.; Erbert, P.: Data transmission by frequency–division multiplexing using the discrete Fourier transform. *IEEE Transactions on Communications*, vol. 5, 1971, pp. 628–634.

[Wes02]   Wesołowski, K.: *Mobile Communication Systems*. New York: John Wiley & Sons, 2002.

[Wit93]   Wittneben, A.: A new bandwidth efficient transmit antenna modulation diversity scheme for linear digital modulation. *Proc. IEEE International Conference on Communications (ICC'93)*, vol. 3, Geneva, 1993, pp. 1630–1634.

[WMS$^+$02] Weber, T.; Maniatis, I.; Sklavos, A.; Liu, Y.; Costa, E.; Haas, H.; Schulz, E.: Joint transmission and detection integrated network (JOINT), a generic proposal for beyond 3G systems. *Proc. 9th International Conference on Telecommunications (ICT'02)*, vol. 3, Beijing, 2002, pp. 479 – 483.

[WOWB02]   Weber, T.; Oster, J.; Weckerle, M.; Baier, P. W.: Turbo multiuser detection for TD-CDMA. *Archiv für Elektronik und Übertragungstechnik (AEÜ)*, 2002.

[WP99]   Wang, X.; Poor, V. H.: Iterative (turbo) soft interference cancellation and decoding for coded CDMA. *IEEE Transactions on Communications*, vol. 47, 1999, pp. 1046–1061.

[WR01]   Walke, C.; Rembold, B.: Joint detection and joint pre-distortion techniques for SD/TD/CDMA systems. *Frequenz*, vol. 55, 2001, pp. 204–213.

[WSLW03]   Weber, T.; Sklavos, A.; Liu, Y.; Weckerle, M.: The air interface concept JOINT for beyond 3G mobile radio networks. *Proc. Wireless Communications Conference WCC'03*, vol. 1, Calgary, 2003, pp. 25–33.

[WWR]   Wireless world research forum. *http://www.wireless-world-research.org*.

[XSR90]   Xie, Z.; Short, R. T.; Rushforth, C. K.: A family of suboptimum detectors for coherent multiuser communications. *IEEE Journal on Selected Areas in Communications*, vol. 8, 1990, pp. 683–690.

[YC01]   Yu, W.; Cioffi, J.: Trellis precoding for the broadcast channel. *Proc. IEEE Global Telecommunications Conference (GLOBECOM'01)*, vol. 2, San Antonio, 2001, pp. 1344 – 1348.

[YKI93]   Yoon, Y. C.; Kohno, R.; Imai, H.: A spread-spectrum multiaccess system with cochannel interference cancellation for multipath fading channels. *IEEE Journal on Selected Areas in Communications*, vol. 11, 1993, pp. 1067–1075.

[YRBC01] Yu, W.; Rhee, W.; Boyd, S.; Cioffi, J.: Iterative water-filling for Gaussian vector multiple access channels. *2001 International Symposium on Information Theory*, Washington, DC, 2001, p. 322.

[ZF86]   Zurmühl, R.; Falk, S.: *Matrizen und ihre Anwendungen*. vol. 2. 5. edition. Berlin: Springer-Verlag, 1986.

Tabellarischer Lebenslauf

Name:	Alexandros Sklavos
Adresse:	Hermann–Hesse–Straße 30
	67663 Kaiserslautern
Geburtsdatum:	15. Juli 1977
Familienstand:	ledig
Staatsangehörigkeit:	griechisch
Schulausbildung:	September 1983 – Juni 1989 Grundschule in Athen
	September 1989 – Juni 1992 Gymnasium in Athen
	September 1992 – Juni 1995 Lyzeum in Athen
Schulabschluß:	Abitur
Hochschulaufnahmenprüfung:	Juni 1995
Studium:	Oktober 1995 – Juli 2000
	Studium der Elektrotechnik
	an der Technischen Universität Athen
Studienabschluß:	Diplom
Berufstätigkeit:	September 2000 – Dezember 2000
	wissenschaftliche Hilfskraft
	am Lehrstuhl für hochfrequente Signalübertragung
	und –verarbeitung der Universität Kaiserslautern
	seit Januar 2001
	wissenschaftlicher Mitarbeiter
	am Lehrstuhl für hochfrequente Signalübertragung
	und –verarbeitung der Universität Kaiserslautern